



HAL
open science

From continental rifting to conjugate margins: insights from analogue and numerical modelling

Anouk Beniést

► **To cite this version:**

Anouk Beniést. From continental rifting to conjugate margins: insights from analogue and numerical modelling. Earth Sciences. Université Pierre et Marie Curie - Paris VI, 2017. English. NNT: 2017PA066289 . tel-01706702

HAL Id: tel-01706702

<https://theses.hal.science/tel-01706702>

Submitted on 12 Feb 2018

HAL is a multi-disciplinary open access archive for the deposit and dissemination of scientific research documents, whether they are published or not. The documents may come from teaching and research institutions in France or abroad, or from public or private research centers.

L'archive ouverte pluridisciplinaire **HAL**, est destinée au dépôt et à la diffusion de documents scientifiques de niveau recherche, publiés ou non, émanant des établissements d'enseignement et de recherche français ou étrangers, des laboratoires publics ou privés.

DOCTORAL THESIS OF THE UNIVERSITY OF PIERRE ET MARIE CURIE

Domain:
Geosciences

L'Institut des Sciences de la Terre de Paris (Paris)

Presented by:
Anouk BENIEST

To obtain the grade of:
DOCTOR of the University Pierre et Marie Curie

Thesis subject:
**From continental rifting to conjugate margins:
Insights from analogue and numerical modelling**

Supervised by:

Dr. William Sassi	IFP Energies nouvelles	Directeur de thèse
Dr. Sylvie Leroy	ISTeP, Université Pierre et Marie Curie	Co-directrice de thèse
Dr. Xavier Guichet	IFP Energies nouvelles	Promoteur IFPEn

Defended on the 8th of December 2017

Jury:

Prof. Claudio Rosenberg	Université Pierre et Marie Curie	Examineur
Dr. Mathilde Cannat	Institut Physique du Globe de Paris	Rapporteur
Prof. Claudio Faccenna	Universita degli Studi di Roma III	Rapporteur
Dr. Muriel Gerbault	Géosciences Environnement Toulouse	Examineur
Prof. Sierd Cloetingh	Universiteit Utrecht	Examineur
Prof. Sveva Corrado	Universita degli Studi di Roma III	Examineur
Dr. Alexander Koptev	Universität Tübingen	Invited

From continental rifting to conjugate margins: Insights from analogue and numerical modelling

Anouk Beniest

Université Pierre et Marie Curie/IFP Energies nouvelles

2017

*...We fight for the future of our nation
Let's come together and unite
Nothing's gonna stop us now...*

~ Nakatomi

Abstracts

ABSTRACT (English)

The South Atlantic conjugate margins are the product of continental rifting and break-up of Pangea, which was made up of different crustal features prior to rifting. This study investigates continental rift initiation and break-up of alternative lithospheric setups, consisting of large segments with different rheological strength, with the use of analogue and numerical modelling. The analogue models investigate the effect of far-field forces on a system that consist of multiple rheological segments, whereas the numerical models include thermal processes and focus on the impact of initial plume emplacement on such a setup.

Lithosphere-scale analogue models consisting of two different rheological compartments have been subjected to extensional forces, to understand effect of far-field forces on large rheological heterogeneities in a system within an extensional tectonic regime. The results show that in such a system, the weaker segment accommodates all the extension. At the contact between the two compartments no rift-initiation is observed. In the presence of a strong sub-Moho mantle, the rift evolution consists of two phases. The first phase is a wide or distributed rift event. Once the strong part of the upper mantle has sufficiently weakened, the rift localizes and a narrow rift continues to accommodate the extension. If extension would continue, break-up would happen at the location of the narrow rift, thereby breaking a rather homogenous part within a laterally heterogeneous system. This would result in asymmetric margins with hyperextended, weak crust on both margins.

The numerical results show that, in the case of plume-induced continental break-up, the classical ‘central’ mode of break-up, where the break-up centre develops above the plume-impingement point is not the only form of continental break-up. When the mantle anomaly is located off-set from the contact between rheological segments, a ‘shifted’ mode of break-up may develop. In this case, the mantle plume material rises to the base of the lithosphere and migrates laterally to the contact between two rheological segments where rifting initiates. Mantle material that does not reach the spreading centre and remains at lower crustal depths, resemble high density/high velocity bodies at depth found along the South Atlantic margin and providing geometric asymmetry.

Further investigation on the exact influence of the initial plume position with respect to the contact between the rheological compartments shows that there is a critical distance for which the system develops either ‘central’ (or ‘plume-induced’) continental break-up or ‘shifted’ (or ‘structural inherited’) continental break-up. For Moho temperatures of 500 – 600 °C, there is a window of ~50 km where the system creates two break-up branches. These results explain complex rift systems with both vertical penetration of plume material into the overlying lithosphere as well as reactivated inherited structures developing break-up systems both aided by the same mantle plume.

The analogue models provide an explanation for the formation of a-symmetric margins without the use of a mantle plume. The numerical model results show that in the presence of a mantle plume, several modes of continental break-up modes may occur and care should therefore be taken with the initial position of a thermal anomaly in a thermo-mechanical model. These results can be used to simulate in more detail the thermal evolution of conjugate margin basins. In absence of an anomaly, heat flow intensities are lower than when a mantle plume is present. The different heat transfer trends can be used in basin modelling programs to investigate a more varied heat flow on basin scale processes e.g. hydrocarbon maturation and generation.

Key words: rifting, continental break-up, South Atlantic, rheology, analogue modelling, thermo-mechanical modelling, lithosphere, mantle plume, crust, a-symmetry, conjugate margins

L'ABSTRACT (français)

Les marges conjuguées de l'Atlantique Sud sont le produit du rifting et de la rupture du continent Pangée. Ce continent présente une hétérogénéité crustale et lithosphérique importante, dont la prise en compte est un objectif de la thèse. Afin de comprendre la rupture continentale à l'échelle lithosphérique de systèmes de rhéologies préexistantes très différentes, nous avons effectué des modélisations, analogique et numérique. Les modèles analogiques s'attachent à montrer l'effet des forces externes sur un tel système hétérogène tandis que les modèles numériques, thermomécaniques, se concentrent sur l'impact des anomalies de fusion du manteau sur le rifting avec une telle configuration.

Avec la modélisation analogique, l'effet des forces aux limites sur un système composé de deux segments de rhéologies différentes a été testé à l'échelle de la lithosphère pour comprendre l'influence de l'hétérogénéité rhéologique dans un système en extension. Les résultats montrent que dans un système combiné, toute l'extension se produit dans le segment faible et que le contact entre les deux segments ne joue pratiquement aucun rôle dans l'initiation des failles. Lorsque le segment le plus faible contient une couche résistante dans le manteau supérieur, le rift évolue en deux phases. La première phase montre un système de failles larges où la déformation est distribuée. Une fois que la partie résistante du manteau supérieur est suffisamment affaiblie, l'extension se localise le long d'une zone de faille étroite. Si l'extension continuait, la rupture se produirait à cet emplacement, dans une partie plutôt homogène alors que le système est latéralement hétérogène. Le résultat de ce système extensif serait des marges asymétriques avec une croûte faible/hyper-étirée sur deux marges.

Les résultats numériques montrent que, dans le cas de la rupture continentale induite par un panache, le mode de rupture «central», où la rupture se localise au-dessus du point de l'impact du panache, est une forme de rupture continentale parmi d'autres. Ainsi, lorsque l'anomalie de fusion du manteau est localisée de manière décalée par rapport au contact entre les segments rhéologiques, un mode de rupture "décalé" peut se développer. Dans ce cas, le matériel du panache atteint la base de la lithosphère et s'écoule latéralement jusqu'au contact entre les deux segments rhéologiques où le rifting se localise *in fine*. La partie du matériel qui n'arrive pas au centre de la zone de rupture, se situe au niveau de la croûte inférieure ou bien plus profond, ressemblant aux corps de densité/vitesse élevées imagés le long des marges de l'Atlantique Sud. De plus, le mode «décalé» reproduit l'asymétrie des marges conjuguées.

Un deuxième exercice de modélisation numérique porte sur l'influence de la position initiale du panache par rapport au contact entre les segments de rhéologie différente. Il montre qu'il existe une distance critique pour laquelle le système développe une rupture continentale "centrale" ou "décalée" (ou structurellement héritée). Pour les températures de Moho de 500 à 600°C, il y a une fenêtre de ~ 50 km pour laquelle deux branches de rifts sont créées. Cela explique l'existence de systèmes de rifts complexes avec une ou plusieurs branches avortées, et également la pénétration de matériel mantellique dans la lithosphère sous-jacente associée à la réactivation des structures héritées. Cela permet le développement de deux zones de rupture avec un seul panache.

D'une part, les modèles analogiques donnent une nouvelle explication sur la formation des marges asymétriques sans l'intervention d'anomalies de fusion mantelliques. D'autre part, les résultats des simulations numériques montrent qu'il y a plusieurs façons pour aboutir à la rupture continentale avec l'aide d'un panache. Ainsi, la position d'une anomalie thermique dans un modèle thermomécanique est capitale et doit être considérée. Ces résultats pourront être utilisés pour simuler en détail l'évolution du flux de chaleur avec le temps pour les différents modes de rupture et pourront être intégrés dans les modèles de bassins afin d'examiner l'effet sur les processus à l'échelle du bassin, par exemple la maturation et la production d'hydrocarbures.

Mots de clés: rifting, la rupture continentale, Atlantic Sud, rhéologie, modélisation analogique, modélisation thermomécanique, anomalie mantellique, lithosphère, croûte, asymétrie, marges conjuguées

Samenvatting (Nederlands)

De tegenover elkaar liggende marges van de Zuid-Atlantische Oceaan zijn het product van de breking van Pangea, dat op dat moment uit verschillende stukken korst bestond. Deze studie onderzoekt het ontstaan van scheuren in de korst en het breken van continenten met alternatieve opbouw van de lithosfeer, dat wil zeggen bestaande uit grote fragmenten met verschillende sterkten, met behulp van analoge en numeriek methoden. De analoge modellen onderzoeken het effect van externe krachten op een heterogeen systeem terwijl de numerieke modellen zich richten op de invloed van mantelanomalieën op zo'n opstelling.

Het effect van externe krachten op een systeem dat bestaat uit twee verschillende reologische segmenten is getest met behulp van analoge modellen om de invloed van reologische heterogeniteit in een systeem dat onder extensie staat te begrijpen. Uit de resultaten blijkt dat in een gecombineerd systeem met een relatief 'zwak' en 'sterk' compartiment, het zwakke segment alle krachten opneemt en dat het contact vrijwel geen rol speelt bij de breking. Wanneer het zwakkere segment een sterke laag in de bovenmantel bevat, bestaat de brekingsevolutie uit twee fasen. De eerste fase is de vorming van een breed rift-systeem. Zodra het sterke deel van de bovenmantel voldoende verzwakt is, ontwikkelt zich een smal rift direct boven het verzwakte punt. Als de extensie door zou gaan, zou er op de plaats van het smalle rift breking plaatsvinden, waardoor een homogeen deel in een lateraal heterogeen systeem doormidden breekt. Het resultaat zouden asymmetrische marges zijn met een sterk verdunde, zwakke korst aan beide kanten van het spreidingscentrum.

Uit de numerieke resultaten blijkt dat in het geval van continentale breking beïnvloed door mantelanomalieën, de klassieke 'centrale' afbreekwijze, waar het brekingscentrum zich boven het inslagspunt ontwikkelt, slechts één vorm van continentale breking is. Wanneer de anomalie inslaat onder een homogeen deel van de lithosfeer, kan een 'verschoven' breukvorming ontstaan. Hierbij stijgt mantelpluim materiaal op naar de onderkant van de lithosfeer, waarna het vervolgens lateraal migreert naar het contact tussen twee reologische segmenten, waar het rift ontstaat. Mantelmateriaal dat niet in het spreidingscentrum terecht komt blijft op diepte van de onder-korst hangen, waar ze lijken op hoge dichtheids- / hoge snelheidslichamen die op diepte langs de Zuid Atlantische marge worden gevonden en die bijdrage aan de asymmetrie van de marges.

Verder onderzoek naar de exacte invloed van de aanvankelijke pluimpositie met betrekking tot het contact tussen reologische segmenten laat zien dat er een kritische afstand is waarbij het systeem 'centrale' of 'verschoven' continentale breking laat zien. Voor Moho-temperaturen van 500 tot 600 °C is er een marge van ~ 50 km waar het systeem twee verschillende brekings-armen ontwikkelt. Dit helpt de uitleg van complexe rif systemen met een of meer afgebroken armen met behulp van een combinatie tussen verticale penetratie van mantle materiaal in de overliggende lithosfeer en de reactiviteit van oude structuren die de breking accommoderen met behulp van slechts één mantle pluim.

De analoge modellen geven een nieuwe uitleg over het ontstaan van asymmetrische geometrieën zonder de invloed van een mantle pluim. De numerieke resultaten van dit werk laten zien dat er meer dan één vorm van continentale breking mogelijk is wanneer er een mantle pluim bij betrokken is. Er moet zorg gedragen worden voor de positie van de mantle pluim in thermo-mechanische modellen aangezien dit een cruciale factor is. De resultaten kunnen worden gebruikt om de warmteoverdracht door de tijd heen van de verschillende type breking te simuleren. Bekkenmodelleringsprogramma's kunnen deze tendensen gebruiken om het effect op van lithosfeer-schaal processen te onderzoeken op bekken-schaal, bijvoorbeeld voor olie- en gasontwikkeling.

Sleutelwoorden: rift, continentale breking, Zuid-Atlantische Oceaan, reologie, analoge modellen, thermo-mechanische modellen, mantle pluim, lithosfeer, korst, asymmetrie, tegenoverliggende marges.

CONTENT

Table of content

19	Foreword
23	Chapter 1. Introduction
	1.1. A short history on plate tectonics
	1.2. A journey through scales
	1.3. From rift to drift
	1.4. Analogue and numerical models
	1.5. The South Atlantic as a case study
	1.6. Objective and approach
55	Chapter 2. Extending the continental lithosphere
	2.1. Introduction
	2.2. Experimental setup
	2.3. Modelling results
	2.4. Implications for rift geodynamics
	2.5. Conclusion
75	Chapter 3. Numerical models for continental break-up
	3.1. Introduction
	3.2. Geological Setting
	3.3. Model Setup
	3.4. Model results
	3.5. Discussions
	3.6. Conclusions
103	Chapter 4. Two-branch rift systems by a single mantle plume
	4.1. Introduction
	4.2. Numerical model setup
	4.3. Experimental results
	4.4. Discussion and conclusion
121	Chapter 5. Discussion
	5.1 From continental rifting to break-up
	5.2 The thermal evolution of conjugate marginal basins
135	Chapter 6. Conclusions
141	Chapter 7. Future work and perspectives
145	References
157	Appendices
	I. Numerical model explication: FLAMAR
	II. Numerical model I3ELVIS and supplementary material chapter 4
	III. Report scientific cruise INGON
195	Acknowledgments
205	Curriculum Vitae
209	Peer-reviewed Articles

Foreword

This thesis project started in January 2015 and was a successful collaboration between IFP Energies nouvelles and the University Pierre et Marie Curie (UPMC) in France. The study focussed on rift initiation and continental break-up processes at lithosphere scale. An extensive literature study on geological and geophysical observations of the South Atlantic conjugate margins pointed to a crust and lithosphere consisting of different parts with various crustal thicknesses, thermal structure and acting forces (such as far-field forces and mantle anomalies). How do extensional forces work on a system consisting of multiple segments with different rheologies? Are rheological differences alone enough to explain features along the margins of the South Atlantic domain or are more complicated setups needed that include for example inherited structures and thermal anomalies? These questions were addressed by performing lithosphere scale continental rift initiation and break-up tests of alternative, more complex lithosphere setups using analogue models and 2D thermo-mechanical numerical models. The analogue models were used to investigate the impact of external forces on a rheological divers system. This was done at the TecLab of Utrecht University in The Netherlands for a period of 10 weeks (Chapter 2). The numerical modelling was done at IStEP, UPMC in France, using the SGI Ulysse cluster, to address the effect of thermal processes on the break-up of laterally varying lithosphere. The first exercise used the FLAMAR code (Chapter 3), written at UPMC, whereas the second exercise used the I3ELVIS code from the ETH Zürich (Chapter 4), Austria. The three chapters together show that the more complex a problem is, the more complex the results and solutions are. At least four different kind of rift initiation and continental break-up evolutions have been modelled. Altogether, they explain margin asymmetry in the South Atlantic domain as well as one of the possible reasons why petroleum systems are dissimilar in conjugate basins sets along the margins in the South Atlantic (Chapter 5). As part of enhancing the skills on geophysical data acquisition a six-week cruise on the Indian Ocean organised by the Alfred Wegner Institute and the University of Bremerhaven, Germany, was part of the program (appendix III).

CHAPTER 1. Introduction

...I was so busy making maps I let them argue...

There's some truth to the old cliché

That a picture is worth a thousand words and that seeing is believing...

~ Marie Tharp, Geologist

1.1. A short history on plate tectonics

1.1.1. On the origin of plate tectonics

Early recognition of plate movements were known as continental drift, first proposed by von Wegener (1912). He noticed the perfect jigsaw-fit between South-America and Africa and concluded that the two continents had been in close contact at some point in time (Fig. 1.1). Unfortunately he lacked a mechanism to support his theory and so he went with the ‘pole-fleeing force’ theory that used the earth’s centrifugal force. He later included gravitational forces of the sun and the moon to explain the movement of continents. These mechanisms were quickly rejected by the scientific community, but despite the lack of evidence, he did have supporters for his theory of ‘moving plates’. One of them was Arthur Holmes who proposed that the movement of the earth’s continents could be due to convection currents that worked as conveyer belts, transporting the continents around the globe, breaking them apart and bringing them back together (Holmes, 1929). Unfortunately for him, at that time there was no evidence of a once existing supercontinent that could support his theory. Alexander Du Toit was also in favour of the continental drift theory and came with supporting evidence for a former supercontinent. He studied the structural geology and paleontology of the Karoo region in South Africa and compared this with data he obtained from Argentina, Paraguay and Brazil. He found remarkable similarities on both continents and proposed the existence of two supercontinents (Laurasia and Gondwana) that collided to form Pangea (Du Toit, 1937), the last supercontinent on earth.

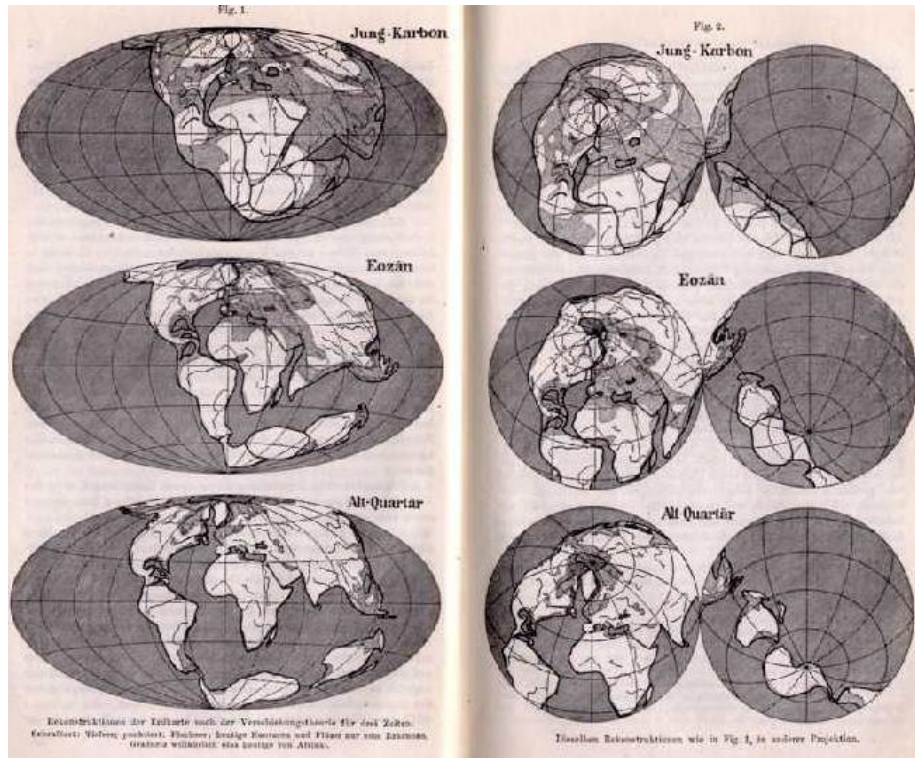


Figure 1.1. Copy of a figure of Alfred von Wegener’s proposition of continental drift from the Carboniferous to present-day (von Wegener, 1912).

The concept of continental drift altered significantly after the release of global echo-sound data acquired by research vessels after World War II, during the Cold War. Marie Tharp, an oceanographer and geologist, got the task to draw a bathymetric map of the ocean floor, starting with the Atlantic Ocean, using the echo-sound data acquired by research vessels. In 1953 she finished her first map of the North Atlantic Ocean (Fig. 1.2). Her results showed a large mountain range in the middle of the Atlantic Ocean with a deep trough at its centre. Initially she thought it was a flaw in the data but her exceptional knowledge of the ocean floor made her realise one of the most revolutionary discoveries in geosciences of the last century. The feature, now known as the Atlantic Mid Oceanic Ridge, was a plate boundary. Her ideas were originally dismissed by her colleague, prof. Heezen, but she kept her ground convincing him. Eventually he still ran off with her idea and created a shock wave through the geological community when he published Tharp's ideas in 1956, excluding her name (Heezen, 1956). Few years later, her work was credited and a new concept for plate tectonics was born (Heezen et al., 1959).



Figure 1.2. Marie Tharp's first bathymetric map, based on echo-sound data acquired by research vessels after World War II, during the Cold War. At the centre of the ocean, there is a clear feature visible, which is nowadays known as the Atlantic Mid Oceanic Ridge (Heezen et al., 1959).

1.1.2. The principles of plate tectonics

During the 60's and 70's the for that time controversial idea of oceanic crust being formed at the centre of the ocean, was discussed in a series of papers that eventually disproving the mechanism behind continental drift as von Wegner had proposed. The 'spreading sea-floor theory' was based on the acceptance of large-scale convection cells operating in the mantle. The 'crustal layers' were different for oceanic and continental crust, considering the strength of the crust and Holmes' conveyor belt theory was discarded (Dietz, 1961).

The high heat flow of the oceanic ridge together with equal divergence rate on both sides of the ridge, were arguments in favour of seafloor spreading (Hess, 1962). Hess (1962) also gave a first age constrained on the oldest oceanic crust on earth, not more than 100 Myr. Another key-argument in favour of the seafloor spreading theory was the observation that magnetic anomalies had similar patterns on both sides of an oceanic ridge (Vine and Matthews, 1963). As a result of this, a whole field developed in magnetic data reconstruction, solemnly investigating the magnetic fabric of oceanic and continental crust, including the construction of a global polarity timescale (GPTS, (Gradstein et al., 2012)). It took only until the 1965 for a first quantitative attempt to fit together the two continents that von Wegner had recognised as the perfect jigsaw-fit (South America and Africa), using a numerical approach of least square fit for the whole Atlantic ocean (Fig. 1.3, Bullard et al., 1965). Even though computers have become much faster and the reconstruction gap between South America and Africa has diminished significantly since this first numerical approach, up until today, the puzzle has not yet been completely solved as the most tide fits, still contain some error (e.g. Aslanian et al., 2009; Eagles, 2007; Jackson et al., 2000; Moulin et al., 2010; Nürnberg and Müller, 1991; Torsvik et al., 2009; Unternehr et al., 1988; Vink, 1982). Finally, when plate tectonics as a scientific theory was accepted, the Wilson Cycle theory was developed, which stated that every 300 to 500 million years all the earth's continents aggregate into one big supercontinent, the most recent one being Pangea (Wilson, 1966). Trying to fit the continents together by correlating geometries and magnetic anomalies eventually led to the question why Gondwanaland and Pangea broke apart in the first place. This is still a major questions in plate tectonics and geodynamics and this thesis contributes to better understanding of continental rift initiation and break-up.

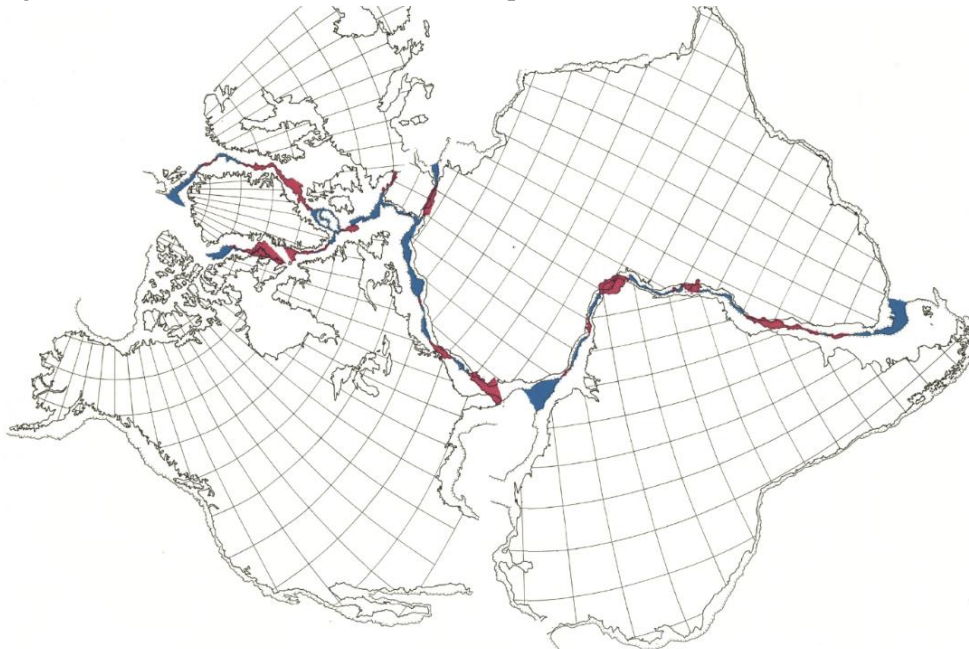


Figure 1.3. Example of the first quantitative approach, based on least square fit approximation, fitting all continents around the Atlantic at 500 finite contour transverse Mercator projection (Bullard et al., 1965).

1.2. A journey through scales

1.2.1. The crust

The crust is the upper-most part of the lithosphere and is separated by the mantle through the Moho, a seismic discontinuity signal that can be traced all around the globe, discovered in 1910 by the Croatian seismologist Andrija Mohorovičić. The Moho is interpreted as a mineralogical transition that separates the earth's crust from its mantle (Fig. 1.4). This discovery led to the understanding that the Earth was not a homogeneous solid but instead consisted of several compositional and physical phases.

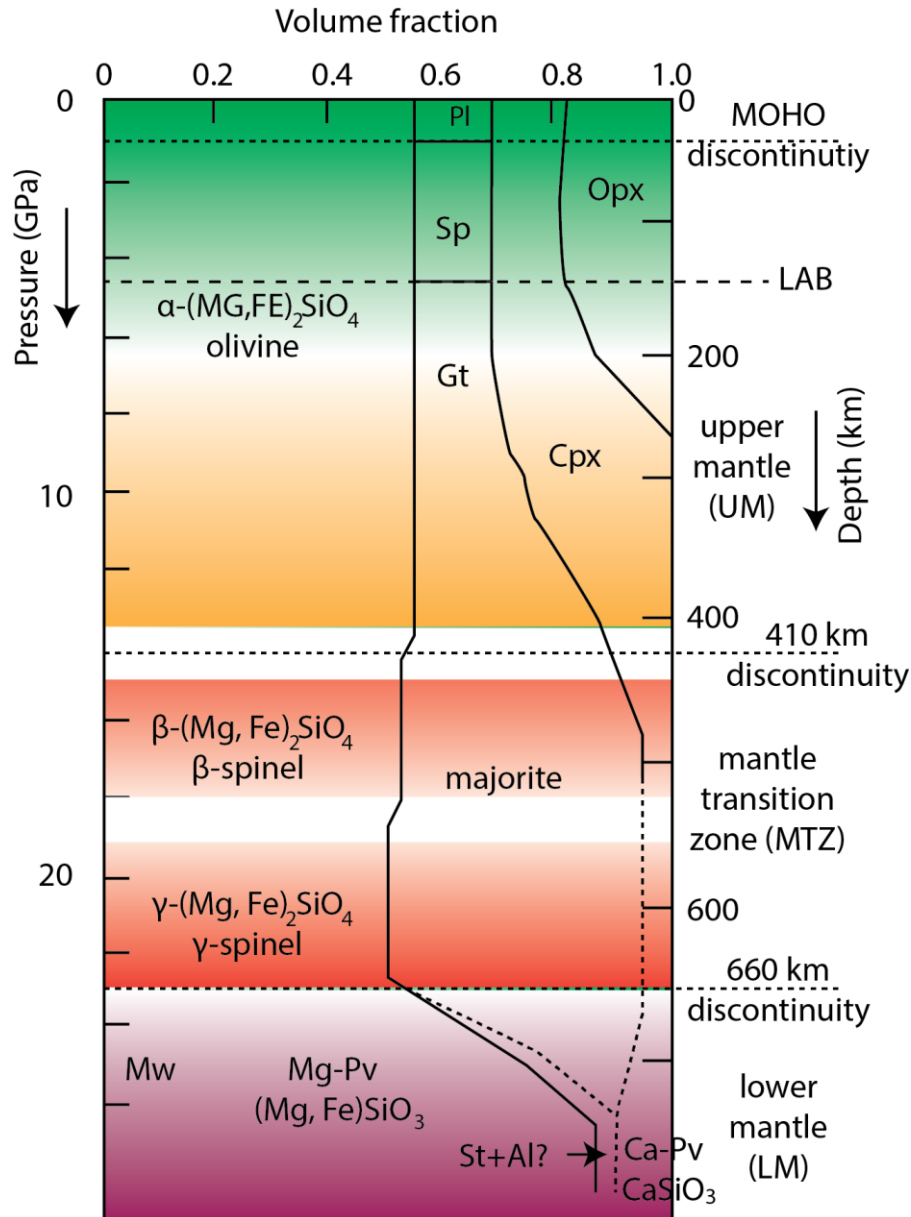


Figure 1.4. Phase diagram of phase transformations versus pressure and depth. The Moho and LAB are variable with depth. At 410 km and 660 km depth major phase changes occur defining the mantle transition zone (after Ringwood, 1991).

Not only are there vertical variations in the earth as a result of different mineral phases, there is also a large difference in composition and behaviour between oceanic and continental crust. For example, oceanic crust is normally between 5 and 9 km thick and has a more mafic composition, whereas continental crust can be as thick as 100 km and contains more felsic minerals. Also within continental crust itself, large variations exist as it consists sometimes of old, heavy crust (cratons), but can also be made of younger, lighter crust. Deformation styles in the crust depend greatly on differences such as mineral composition, inherited structures, pressure and temperature (Passchier and Trouw, 1996) and thus oceanic crust and continental crust respond very differently to forces acting upon it.

Isostasy and gravity studies are used to describe the earth's topography and understand the structure of the crust. These kind of studies describe the state of the earth in gravitational equilibrium. They require accurate numbers of the density of the crust. Early models describing the relation between topography and the structure of the crust were developed in the mid-19th century. John Henry Pratt stated that different masses of rocks caused topography, more mass, meant higher topography than less mass (Fig. 1.5a). Another possibility was proposed by George Biddell Airy, who dictated topography changes to different density's (Fig. 1.5b). Later 'Dynamic Topography' was introduced, an new concept stating that topography is induced on the surface by buoyancy differences in the earth's mantle (Hager and Richards, 1989). Another version of dynamic topography is flexural isostasy (proposed by Vening Meinesz) which calculates the response of the lithosphere to a certain load, (Allen and Allen, 2013), for example a seamount or glaciation (Fig. 1.5c). Gravity studies were than introduced to work out the mass and density of crustal structures. This can be estimated by measuring gravitational deflections to the normal gravity, which is the free-fall acceleration of an object to the earth. There are two main types of estimating the gravitational force of an object. The free-air anomaly is the observed (or measured) gravity minus the normal gravity. The Bouguer anomaly assumes a plate of a certain thickness and indefinite length that takes into account the gravity of the plate itself. Any gravitational deflections to this 'standard' are anomalies and tell something about the crustal structure and the density of different crustal bodies.

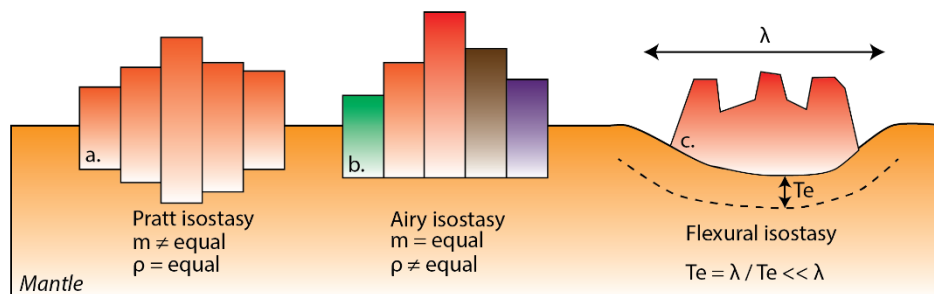


Figure 1.5. Three types of isostasy. a) Pratt isostasy assumes an equal density and unequal mass for different crustal sections. b) Airy isostasy predicts topography after different densities of crustal sections with an equal mass. c) Flexural isostasy calculates the lithosphere compensation to a certain load, where T_e is the flexural rigidity of the lithosphere and λ the flexural wavelength. After (Watts, 2001)

When the crust with all its heterogeneities is put under tensional or extensional stress, its initial behaviour is elastic until it breaks or starts to flow. In general, brittle structures like faults develop in the upper crust and faults and shearzones form at depth in the ductile regime or lower crust. At a larger scale this results in orogens or basins. In this thesis we focus on marginal basins, although basins can form in different tectonic settings (Fig. 1.6). In a purely compressional setting accommodation space is created through tectonic processes in back-arc basins (Fig. 1.6a), e.g. the Aegean region (Jolivet et al., 2015), or accretion wedges (Fig. 1.6b), e.g. the Calabrian wedge, one of the many accretionary wedges that resulted from the Alpine orogeny (Minelli and Faccenna, 2010). In a purely extensional setting basins can develop intra-cratonically (Fig. 1.6c), for example the Paris Basin (Averbuch and Piromallo, 2012) or along passive margins (Fig. 1.6d), for example the South Atlantic basins (Marcano et al., 2013). Also in strike-slip setting accommodation space forms in pull-apart basins, e.g. the pull-apart basins in Western and Central Africa (Guiraud and Maurin, 1992).

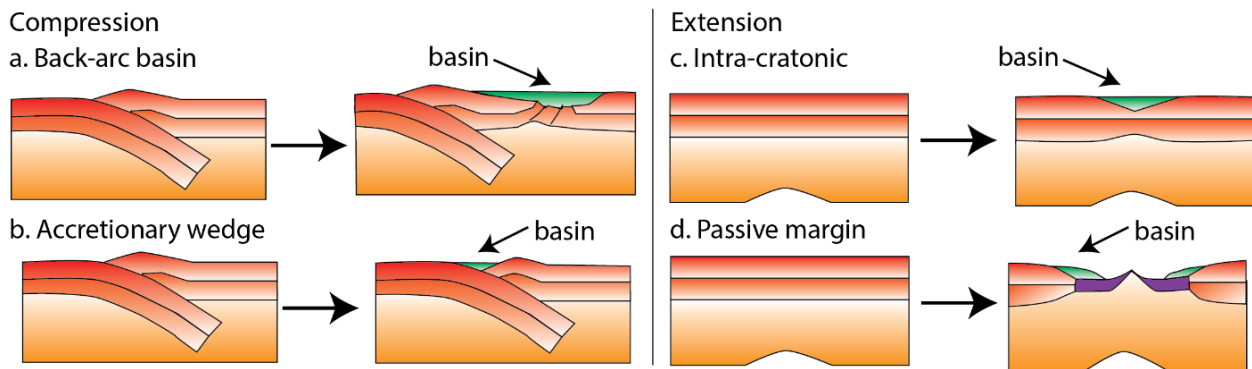


Figure 1.6. Different tectonic settings where basins or accommodation space is formed in both compressional (a and b) and extensional settings (c and d).

1.2.2. The lithosphere

The word ‘lithosphere’ comes from the Greek words ‘λίθος (lithos)’, meaning ‘rock’ and ‘σφαίρα (sphaira)’, meaning ‘sphere’, in other words, ‘the rocky sphere’. The lithosphere is the solid, buoyant, outermost-layer of the earth that cools through conduction. There are two types of lithosphere: continental lithosphere and oceanic lithosphere. The continental lithosphere has a thermal thickness between 150 - 350 km for Archaean and Proterozoic rocks (Artemieva and Mooney, 2001), whereas the oceanic lithosphere is thinner between 100-125 km (Burov, 2011). The lithosphere is separated from the underlying less viscous asthenosphere. The asthenosphere transports heat on geological timescales through convection (e.g. Sleep, 2005). The boundary between the lithosphere and asthenosphere is known as the Lithosphere-Asthenosphere Boundary (LAB). There are five main physical and chemical ways to define the lithosphere (Fig. 1.7). It can be described as 1) a mechanical boundary layer, marked by a decoupling layer shown as a sudden increase in strain-rate with depth (Fig. 1.7a). The LAB can be defined by 2) its thermal structure.

The thermal thickness of the lithosphere corresponds to the 1330 °C mantle adiabat and the temperature gradient of the Moho varies between 500 and 800 °C depending on its age (Fig. 1.7b, Artemieva and Mooney, 2001). The LAB can also be explained using 3) seismic velocities where high velocities (characteristic for more ‘solid’ parts) represent the lithosphere and low velocities the underlying asthenosphere (Fig. 1.7c, Eaton et al., 2009). Also 4) anisotropy can be used to identify the LAB. Examples of rock’s anisotropy are, seismic anisotropic changes such as the change from anisotropic cratonic lithosphere to isotropic asthenosphere, also known as the Lehmann discontinuity (Gaherty and Jordan, 1995) or a directional change in anisotropy (Debayle and Kennett, 2000, Fig. 1.7d). The 5) electrical resistivity, which decreases drastically below the LAB (Fig. 1.7e, Eaton et al., 2009), can also be used to detect the LAB.

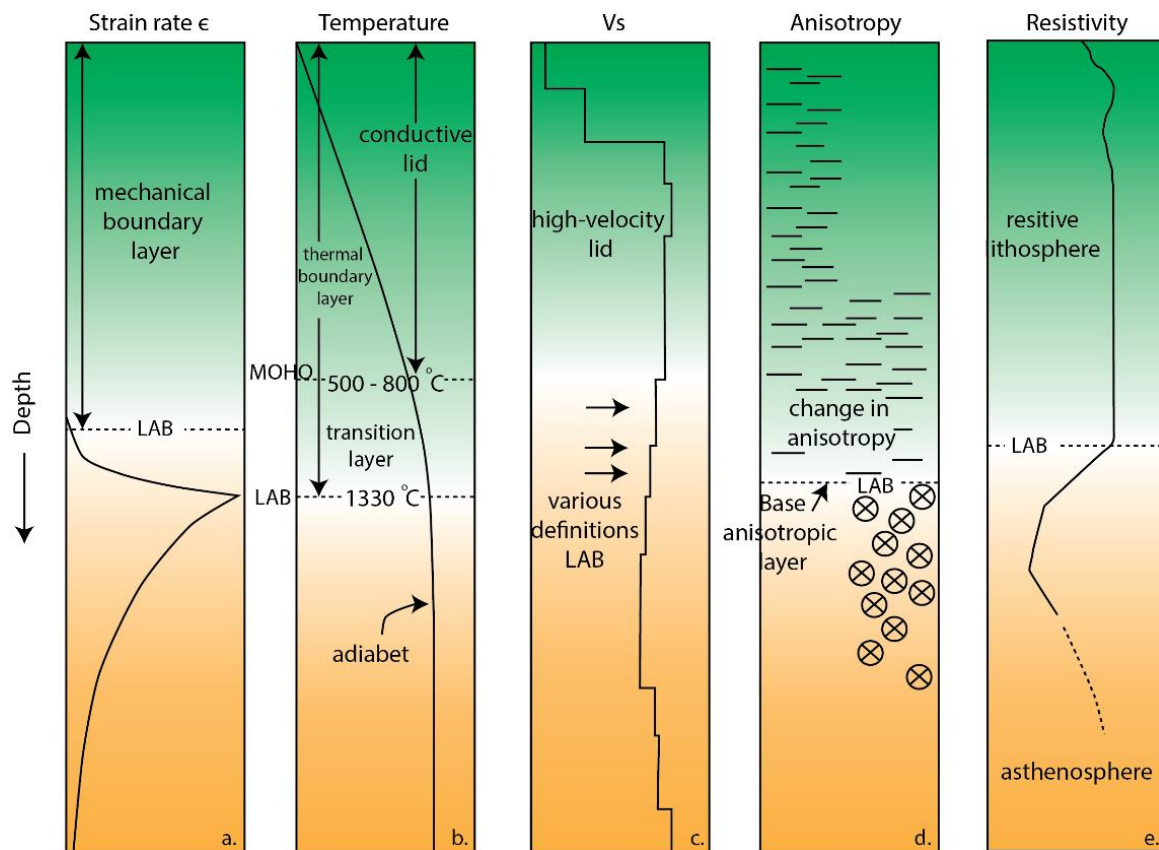


Figure 1.7. Five ways to physically describe the lithosphere-asthenosphere-boundary (LAB). a) mechanical (strain rate), b) thermal, c) seismic velocities, several velocity transitions can be interpreted as the LAB d) anisotropic variations and e) electrical resistivity (after Eaton et al., 2009).

Changes in mineral phases are a petrological way to determine the LAB (Fig. 1.4). For example, when more rigid and depleted peridotite (the mantle lithosphere) reaches the liquidus and becomes partially melted, hydrated and enriched peridotite (the mantle asthenosphere) (Hirth and Kohlstedt, 1996), the LAB has been crossed. The LAB depth ranges from roughly 80 km for oceanic lithosphere to a maximum of 250 km for

old, cratonic lithosphere. At 410 km depth another seismic discontinuity is observed, which marks the top of the mantle transition zone. At this point, olivine minerals change into spinel and this process contributes to a distinctive seismic discontinuity. This zone is 250 km thick and separates the upper mantle from the lower mantle (Fig. 1.4). At 660 km depth, spinel changes to magnesium-perovskite and the lower mantle has been reached (Ringwood, 1991). These phase transformations have been determined with experimental and petrological studies that mimic bulk chemical composition of the upper mantle (pyrolite) conditions at 800 km depth (Ringwood, 1991). Most of the experimental studies use pressures up to 30 GPa, which corresponds to approximately 800 km depth (Dorfman, 2016), some studies investigated pressure up to 50 GPa (Tange et al., 2009) and only few studies have investigated ultra-high pressures of more than 100 GPa (Yamazaki et al., 2014).

1.2.3. The thermo-mechanical lithosphere

The boundaries or discontinuities within the crust and lithosphere result from thermo-mechanical properties of the system, which are also known as the ‘rheology’. The word ‘rheology’ is also deduced from the Greek language with ‘ $\rho\epsilon\omega$ (reo)’ meaning ‘flow’ and ‘ $\lambda\omicron\gamma\iota\alpha$ (logia)’ meaning ‘study’, or, in other words ‘the study of flow’. The most important parameters that define the rheology are pressure, temperature, strain, strain rate, strain history, grain size, the chemical activity of mineral components, fluid content, pore fluid pressure, and volatile fugacities (Burov, 2011; Evans and Kohlstedt, 1995; Keefner et al., 2011).

The strength of a lithospheric plate varies laterally and vertically and depends thus on the rheological properties and the thermal state of the lithosphere and also the geodynamic setting (Burov, 2011). The elastic thickness of the lithosphere is the strong part of the lithosphere. This thickness diminishes significantly at 100-180 km depth for continental lithosphere and 20-60 km for oceanic lithosphere and the oceanic lithosphere is largely dependent on the age of the lithosphere.

The lithosphere consists of brittle and ductile parts that, when described separately, comply with different physical laws. The brittle rock strength is calculated using Byerlee’s law (Byerlee, 1978). The strength of the layer is a function of pressure and depth and behaves as Mohr-Coulomb plasticity. From Byerlee’s law, it has also been demonstrated that the angle of internal friction for almost all rock types is between 30° and 33° and this is thus the value for internal friction adopted in numerical models. Ductile rock strength on the contrary depends heavily on the type of rock and a multitude of parameters such as grain size, macro- and microstructures, temperature, strain rate, fluid content, etc. (Burov, 2011). Ductile rock strength can be described as a function of strain rate, not of strain itself as is the case for brittle material. When the rock strength is linearly dependent on strain rate, deformation is Newtonian viscous. When this dependency is non-linear the rock’s viscosity is non-Newtonian.

A brittle-ductile layered system has an elastic response when a force acts on it for a very short time, for example a seismic wave. The material returns to its original state after being subjected to this force. When the layers react inelastically, the force exerted on the system has deformed the material in such a way that it cannot go back to its original state. This can happen in a brittle way, where the Mohr-Coulomb criterion best expresses brittle deformation or in a ductile manner where stress is a function of strain rate and not dependent on strain itself.

In natural systems, brittle and ductile layers form one system and they are thus subjected to the same force. This makes both brittle and viscous material strain rate dependent. To account for that, different constitutive models (e.g. Maxwell or Kelvin) describe the relationship between elastic and viscous strain and stresses (Burov, 2011). Goetze and Evans (1979) combined these rheological laws into yield-stress-envelopes (YSE), to calculate the strength of the whole system. An YSE is a vertical profile that calculates the maximum differential stress of the lithosphere before deforming (Fig. 1.8) based experimental data being extrapolated to geological time scales. They provide the elastic thickness of the lithosphere. For oceanic lithosphere, YSE are well established, but for continental lithosphere it is more complicated as continental crust is thicker, its structures and properties may vary for different regions and it contains fluids that might weaken the YSE at depth (Jackson, 2002).

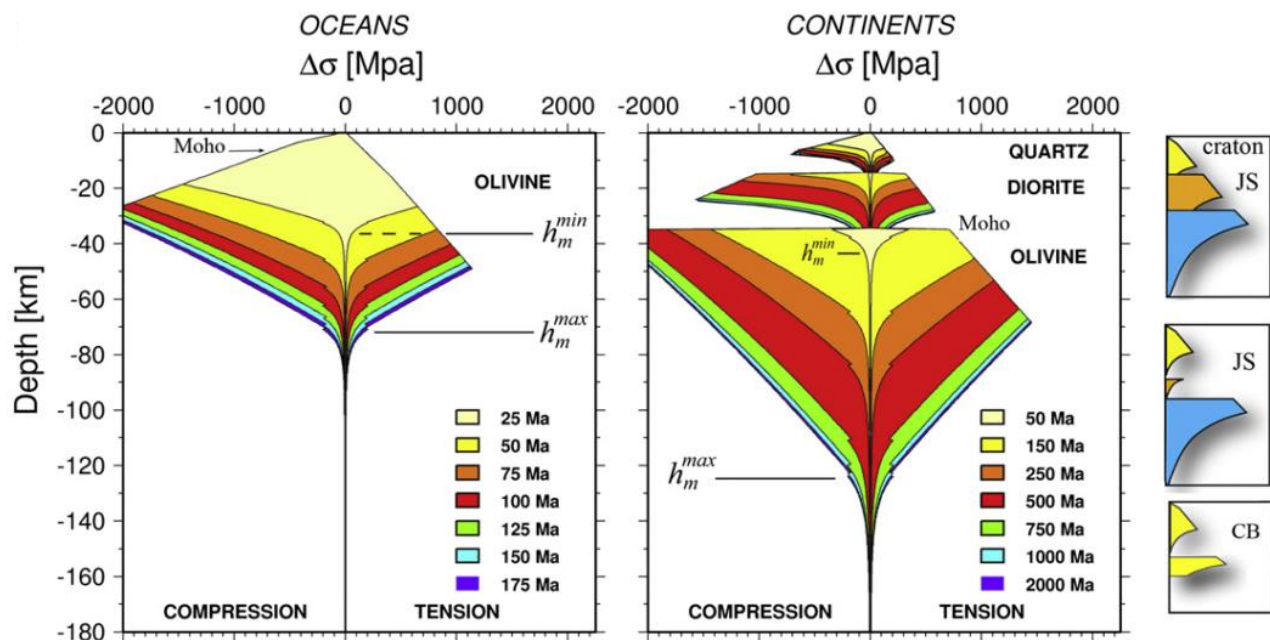


Figure 1.8. Rheological yield stress envelopes for a) oceanic lithosphere and b) continental lithosphere. The major difference lies in the multi-layer structure and thickness of the continental crust and compared to the one layered and thin oceanic crust. The right examples (c) give different variations and commonly used rheological yield stress envelopes for craton (jelly-sandwich, JS) and hot lithosphere (crème-brûlée, CB) (Burov, 2011).

An YSE depends on so many different properties that there is an infinite amount of possibilities to describe the strength of the lithosphere. To be able to do quantitative research some ‘end-member’ YSE’s have been proposed. For example, the ‘crème brûlée’ YSE describes young, hot (continental) lithosphere, with a thin brittle crust overlying a hot, viscous mantle, where the crust and mantle are coupled. A ‘jelly-sandwich’ YSE on the contrary, describes cold and cratonic lithosphere (Burov, 2011) of several brittle and ductile layers, that result in decoupling between the different layers (Brun, 2002).

Apart from material properties, another way to describe the lithosphere is in terms of temperature and thermal state (Eaton et al., 2009) where the change from convective to conductive mode of heat transfer defines the LAB. The surface heat calculated on earth is a result of two primary heat producing mechanisms: 1) radiogenic heat production by radioactive decay of atoms in the crust and 2) the primordial heat residing in the earth. Only $8.7 \times 10^{-2} \text{ W/m}^2$ accounts for the surface heat produced by these two processes (Fowler, 1990), compared to $4.0 \times 10 \text{ W/m}^2$ that comes from heat generated by the sun that is reflected back to outer space (Jaupart and Mareschal, 2010). The total heat budget of the earth is estimated at approximately 47 TW (Davies and Davies, 2010).

Heat transfer through convection takes place by moving material (mass) around and is the dominant mechanism of heat transfer in the Earth’s mantle. Heat transfer through conduction occurs through the interaction between atoms or molecules of two connecting, solid media that differ in temperature causing heat to transfer from the warmer body to the colder body. This happens in the solid inner core and in the lithosphere.

The main body through which the earth loses heat is the oceanic crust with an estimate of 510 mW/m/yr^2 (Pollack et al., 1993) and a total heat flux of 32 TW compared to an average of only 65 mW/m^2 for the continental crust (Jaupart and Mareschal, 2010) and a total heat flux of 12 TW (Davies and Davies, 2010). Oceanic lithosphere loses heat solemnly through cooling of the crust formed at spreading centres which is linearly dependent on age until the crust is 80 Myr old (Burov, 2011; Jaupart and Mareschal, 2010). The continental crust loses heat through cooling of the earth and in addition has its own resource through radiogenic heat production by the decay of radioactive elements (Furlong and Chapman, 2013). This heat producing mechanism is limited to the upper continental crust (9-10 km) and is depleted in mafic rocks (Jaupart and Mareschal, 2010). In addition, the crust is very heterogeneous with thicker and thinner crust and different rock types. Zones of higher heat flows are for example tectonically active regions and continental margins that are not in a steady thermal state. Zones of extension have a high heat flux ($72 - 125 \text{ mW/m}^2$) (Morgan, 1983). Zones of lower thermal gradients are cratons or compressional orogens (Jaupart and Mareschal, 2010).

The rate at which heat transfers with conduction through a solid medium (e.g. the lithosphere) is measured with gradients: the difference in temperature per unit length. The thermal conductivity ($\text{W/m/}^\circ\text{C}$) is an

important property of rocks as it describes how fast a material transfers heat. The accompanying heat flow (Q) is measured in W/m^2 flows in the opposite direction of the temperature that increases with depth. The thermal conductivity varies per rock type and vary between $3.0 W m^{-1} °C^{-1}$ for granitic upper crustal rocks to $2.6 W m^{-1} °C^{-1}$ as an average for lower crustal rocks (Cemark and Rybach, 1982; Furlong and Chapman, 2013). It depends on the composition of the rock, temperature and also to some extent on pressure (Furlong and Chapman, 2013).

To calculate a reasonable geotherm the surface temperature is often set at 0 km depth with a temperature range between $-50 °C$ for polar regions and 30 degrees for equatorial regions. Also, close to the lithosphere base, geotherms should approach melting conditions to be consistent with shear wave velocities observed in the Earth's asthenosphere and lastly, xenolith samples and or exhumed metamorphic rocks, should be used to classify geotherm families (Furlong and Chapman, 2013).

There are many reservations in describing the rheology of the earth's lithosphere. For starters, experimental rock mechanics data brings uncertainties. For faulting and fracturing values, Byerlee's law is valid for brittle deformation of homogeneous systems, but it is questionable if it works for extensive fault zones (Chester, 1995) and whether it works at depths below 30 – 50 km (e.g. Kirby et al., 1996). Ductile rock mechanics have complex problems due to the extrapolation of the results to geological time scales (Burov, 2011). Experimental temperatures and strain rates for ductile deformation are higher than in nature, samples are much smaller and rather homogeneous compared to natural rocks, there might be water in the system that is not accounted for by the experiments and thermodynamic reactions and P-T conditions are different than in nature. The second uncertainties results from calculating synthetic yield stress envelopes where vertical and horizontal strain rate variations are not coherent with the background strain rate given by the initial YSE (e.g. Burov and Poliakov, 2001; Kuszniir et al., 1991). Also ductile materials have a strong reaction to small temperature changes, e.g. due to increasing geotherm or radioactive heat production (Burov, 2011). Third, elastic-viscous-plastic deformation mechanisms are not completely understood. There are for example secondary factors like frictional heating, pressure, fluid content, partial melting and metamorphic phase changes that have a great influence on the system, but are not always taken into account. Lastly, these analytical and numerical methods need to be compared to observations to parametrize the rheology for geological time scales (Burov, 2011).

Passive margins are located between oceanic and continental crust and have a complex crustal structure. Despite these uncertainties on the rheology and the thermal state, thermo-mechanical modelling and analogue modelling provide valuable insight in the interaction between physical forces, the thermal state and material behavior of the lithosphere. They are the main methods used in this PhD to investigate the initiation of continental rifting and break-up.

1.3. Rift-to-spreading systems

1.3.1. Classifying extension systems

The first classification of extensional systems was made during the 70's with a distinction between 'active' and 'passive' systems (Fig. 1.9a, Olsen and Morgan, 1995; Sengör and Burke, 1978). An 'active' extensional system develops as a reaction to thermal upwelling (Bott and Kusznir, 1979; Dewey and Burke, 1974), for example a rising mantle plume. A 'passive' extensional system is the result of far-field forces caused by plate-pull (McKenzie, 1978a). This specific way of classifying rift systems (active versus passive) has continuously developed and the most recent version takes into account the geodynamical setting. There are 1) active intra-continental rifts that develop on continental lithosphere (e.g. the Rhine Graben or the East African Rift), 2) active intra-oceanic rifts that form on oceanic lithosphere but that are tightly connected to the continent (e.g. the Red Sea or the Gulf of California) rifts and 3) inactive rifts such as paleo-rifts (e.g. Labrador Sea) or aborted arms (e.g. Central North Sea) (Cloetingh et al., 2013).

A second way of grouping extensional systems was designed in the 80's when rift geometries were linked according to shear settings (Fig. 1.9b). The 'pure shear' setting is characterized by listric faults, extensive horst and graben structures, symmetry and is largely influenced by the thermal state of the system (McKenzie, 1978a). The 'simple shear' setting is marked by basin development bounded by low angle detachment faults, asymmetry and a lower thermal regime (Wernicke, 1985). Of course these are two extreme version so rather quickly an intermediate extension setting was introduced, known as the 'delamination' setting (Lister et al., 1986). Here, the system consists of low-angle detachment faults, asymmetry and thermally subsiding basins that are offset from the thinning centre.

The division of extensional systems by geometry soon became related to tectonic processes and the rheology at lithosphere scale (Fig. 1.9c). Rift systems can be 'narrow', which is a sign for a strong continental lower crust, extension concentrated in the mantle of the lithosphere and a low thermal gradient. Rift systems can also be 'wide', which is the result of a weak continental lower crust, thinning that is uniformly distributed over the mantle and lithosphere (Buck, 1991) and an intermediate thermal gradient. A last type of extension mode within this classification system is the 'core-complex' type of extension system, where the lower crust is exhumed through extension that localised in the upper crust and a high thermal gradient.

A fourth categorisation of extensional systems was based on the tectonic setting, e.g. extension vs. contraction. The category 'Atlantic'-type of system points to rift-to-break-up systems that form in an extensional setting. It is comparable to the 'active' category from the first classification system (Fig. 1.9a) but it is not necessarily the result of a thermal anomaly at the base of the system. This type goes through the entire rift-to-spreading cycle, eventually reorganising the mantle convection system (Ziegler, 1993). The 'Atlantic'-type rifts are accompanied by failed horst and graben structures that might be re-used later in the tectonic cycle. The 'back-arc'-type of rift develops in an overarching contractional regime (e.g. the Aegean

Sea) and is comparable to the ‘passive’ classification (Fig. 1.9b), although ‘far-field forces’ that result from slab-pull of the subducting slab are only one parameter that can cause this setting. This type of rifting also forms when the convergence rate of plates changes or when young colliding orogens stop diverging. When the convergence rate changes, the heavier subducting slab sinks, becomes steeper and allows mantle material to well-up, weakening the crust (Okay et al., 1994; Uyeda and McCabe, 1983). When young orogens stop to collide, deviatoric stresses can change, making the area more prone to back-arc formation.

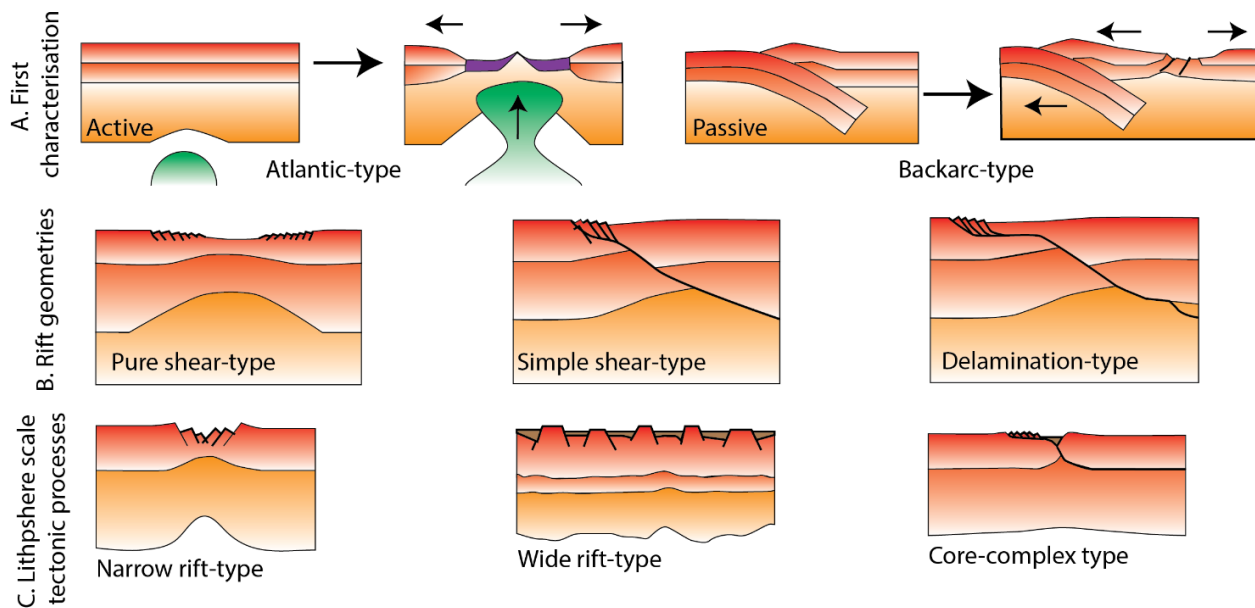


Figure 1.9. Different rift classification systems. a) The first classification system is based on ‘active’ as the result of thermal upwelling and ‘passive’ rifting as a result of far-field forces. These are comparable with the Atlantic-type system and the back arc-type systems that take into account the tectonic setting (overall extension or contraction). b) Rifts can also be described based on their geometry, resulting in ‘pure-shear’, ‘simple shear’ and an intermediate ‘delamination-type’ rift-system classification. Lastly, c) are rift systems where lithosphere scale tectonic processes result in ‘narrow’, ‘wide’, or ‘core-complex’ type rift systems.

One of the difficulties with all these classification systems is that they are all based on different characteristics. They show overlap but there is no over-arching system that includes all modes. Most rift-systems do fit in more than one box and are both influenced by thermal processes as far-field forces. Also, there is still a large debate whether thermal anomalies in the mantle are essential for producing a successful rift-to-spreading centre or not. Some back-arc basins might eventually lead to oceanic crust formation and are then suddenly of Atlantic-type of system. The pure shear and simple shear end-member geometries are not observed on earth as such and can only be reproduced with analogue and numerical models. The challenge with the classification is to deal with the large heterogeneity of the lithosphere which makes it extremely difficult for a coherent, comprehensive classification system. In the above classification systems, crustal processes such as like erosion, sediment deposition and water-content are not taken into account, but their impact on rift formation processes is beyond the scope of this work and thus the existing rift

classification systems are used. Processes that initiate crustal thinning, rupture and the formation of oceanic crust are still debated (Rosenbaum et al., 2008; Rosendahl et al., 2005) and the more factors taken into consideration, the more complex continental rifting and conjugate margin formation becomes.

1.3.2. From rift to drift

A rift-system goes through several phases before it enters the post-rift phase and either stops extending (resulting in a failed rift) or becomes a successful spreading centre (Fig. 1.10). The first phase is the pre-rift phase, where the initial conditions of a rift-to-drift system are generated. This is followed by a rift or syn-rift phase, then break-up and exhumation of the lower crust and mantle and finally a post-rift, drift or spreading phase with an oceanic ridge at the centre.

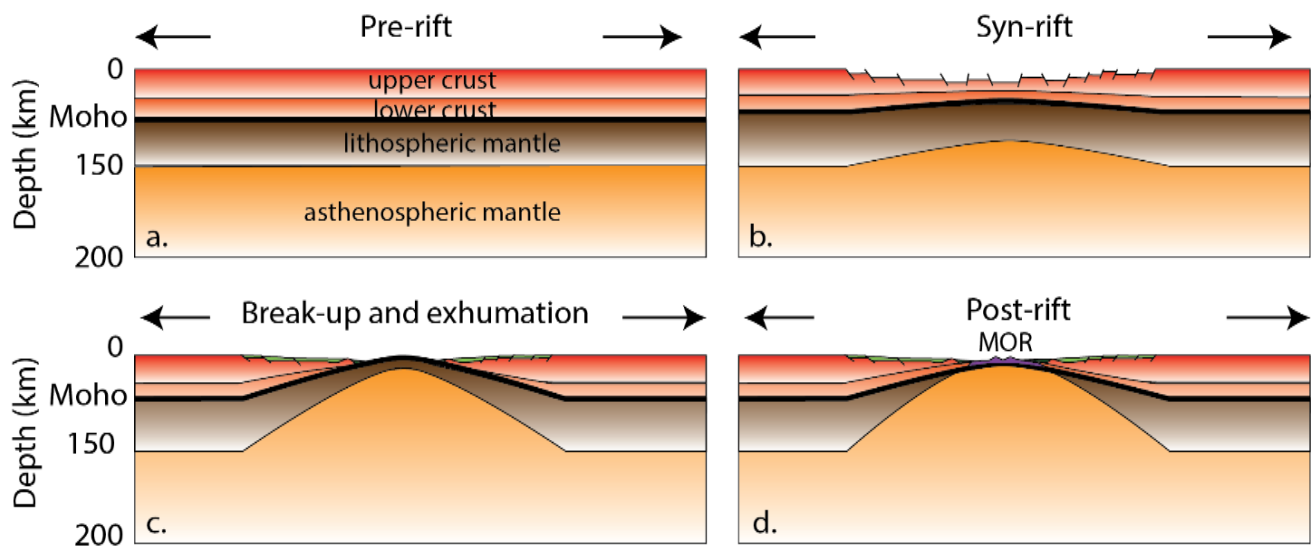


Figure 1.10. Schematic representation of the three major phases of a rift-to-break-up system. a) The pre-rift phase b) the syn-rift phase, c) the break-up and exhumation phase and d) the (early) post-rift phase. MOR = Mid-Oceanic Ridge.

The shift from a stable pre-rift situation to a syn-rift phase is the result of changing thermal and/or mechanical conditions. The strength of the lithosphere is a key-parameter for the likelihood of a rift system to develop (Burov, 2011; Cloetingh et al., 2013). Especially its compositional layers (e.g. Brun et al., 1999; Buck, 1991; Huismans and Beaumont, 2011, 2008), their individual thicknesses (Burov and Diament, 1995), the lateral variation in rheology (e.g. Geoffroy, 2005; Ziegler et al., 1995) and the total effective elastic thickness of the lithosphere (Huismans and Beaumont, 2008; Watts, 2001) are very important. Inherited weak zones (Manatschal et al., 2015), such as ancient sutures or large shearzones and pre-existing anisotropy (e.g. Rosendahl, 1987; Younes and McClay, 2002) also play a significant role in localizing extension and initiating rifting. The thermal state (Carter and Tsenn, 1987; Davis and Kusznir, 2004; Goetze and Evans, 1979; Ranalli and Murphy, 1987), including the presence or absence of hotspots (e.g. Brozena and White,

1999; Feighner and Richards, 1995; Ito et al., 1996; Mittelstaedt et al., 2008; Ribe, 1996), the occurrence or enriched or depleted mantle (Hirth and Kohlstedt, 1996; Lee et al., 2005; Pollack, 1986) and the presence or absence of magma (Ebinger and Casey, 2001; Geoffroy, 2005; Stab et al., 2016), are crucial factors for controlling the thermal conditions. Also strain rate (Allemand and Brun, 1991; Ranalli, 1995) and the width of extension (Davis and Kusznir, 2004) should not be ignored.

One of the oldest, and well-established models, to explain the onset of rifting is the uniform stretching model (McKenzie, 1978b). This model assumes instantaneous and uniform crustal thinning that changes both the gravitational and thermal regime (Fig. 1.11). The system adapts directly to the gravitational instabilities, developing syn-rift subsidence and basin infill. The thermal response has a longer wavelength and will only re-stabilize in the post-rift part. Driving forces behind this model are for example plate boundary stresses, frictional forces and tensional stresses. Plate boundary forces include slab pull, slab roll-back, ridge push and collisional resistance. Frictional forces hold the interaction of mantle convection with the lithosphere base leading to the movement of the overlying plate (Bott, 1993; Forsyth and Uyeda, 1975; Wessel and Muller, 2007; Ziegler, 1993), also known as mantle drag (Ziegler et al., 2001). Tensional stresses (Bott, 1993) are diverging forces that act on the plate, e.g. far-field forces. New concepts result from the interaction of the large-scale forces described above. An example is an evolutionary trajectory going from passive to active in which volcanism and seismic activity increasingly play bigger roles (Burov and Cloetingh, 1997; Cloetingh et al., 2013; Huisman and Beaumont, 2011; Huisman et al., 2001; Wilson and Guiraud, 1992).

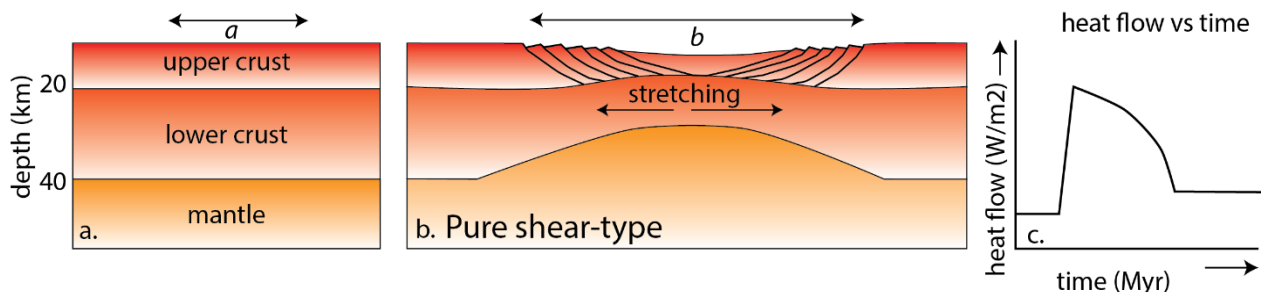


Figure 1.11. Schematic representation of the uniform stretching model (McKenzie, 1978b) where the β -factor can be calculated by dividing the width of the stretched domain (b , b) by the initial domain (a , a). It is then assumed that the vertical thinning is proportional to the horizontally stretched domain. The heat flow evolution corresponding to this stretching and thinning changes instantaneously, resulting in a heat flow peak at the syn-rift to post-rift phase transition. Only during subsidence does the system cool down over a long period of time after which it stabilizes during the post-rift phase (c).

This simplified uniform stretching model was initially build for the North Sea (McKenzie, 1978b) to explain the onset of rifting and subsequent syn-rift evolution. He identified a β -factor, or stretching factor, defined by 'b/a' where 'a' is the initial width of the stretched domain and 'b' the width of the stretched domain (Fig. 1.11). The vertical thinning of the crust is assumed to be proportional to the thinning factor of the stretched domain. The heat flow evolution that corresponds to the stretching and thinning changes instantaneously,

which results in a heat flow peak at the syn-rift to post-rift phase transition. During subsidence the system cool down over a long period of time after which it stabilizes during the post-rift phase. When applied to different areas, this model posed problems and modified versions appeared including depth-dependent stretching (Royden and Keen, 1980), ‘active’ rifting (Huisman et al., 2001), erosion and deposition (Burov and Poliakov, 2001) and mineral transitions (Podladchikov et al., 1994; Simon and Podladchikov, 2008; Yamasaki and Nakada, 1997). Most of these studies are theoretical studies, based on numerical modelling. Even though they do not explain all observations made, these studies aid our understanding on the onset of rifting and its subsequent evolution.

During the early syn-rift phase the lithosphere is under extension. Depending on amongst others the rheology of the crust and lithosphere, distributed or localized rifts develop. When the crust and mantle are coupled, wide-spread or distributed rift geometries such as horst and graben structures and rift cells develop (Buck, 1991; Taylor et al., 1995). When the lithosphere is decoupled, it includes for example a strong sub-Moho mantle, the rift width can be much narrower (Brun, 1999). The effective elastic thickness of the crust depends on the depth of the lithospheric necking level (McKenzie, 1978a). Once the system has overstepped the elastic boundary, entering the plastic regime, deformation is irreversible. Deep mantle processes, including upwelling of the asthenosphere, thermal displacement of the LAB, thermal expansion and intrusion of melts in the lower crust (Turcotte and Emerman, 1983; van der Beek et al., 1994) highly effect the rift evolution. Shallow crustal inherited structures guide lithosphere deformation as these features already weakened the system, prior to rifting (Manatschal et al., 2015). Structures that form during the early stages of rifting (e.g. faulting or softening) only affect deformation localization to a minor extent. During the later rift evolution, these inhomogeneities could help to localize and distribute crustal strain and favor a certain tensional reactivation (Janssen et al., 1995; Ziegler et al., 2001), but this is not always the case and strongly depends on the thermal regime (Chapter 4, Beniest et al., 2017b). The upper crust behaves brittle or plastic whereas the lower crust is less viscous. Faults are allowed to cross-cut the upper crust bringing water into the weaker lower crust and underlying mantle. This process leads to serpentinization of the mantle (Pérez-Gussinyé and Reston, 2001) allowing hyperextended crust to form, reaching beta-factor from 3-4.

This extreme thinning of the crust leads to weakening of the crust. On one hand, this provides early subsidence basins and accommodation space to put more load on the lithosphere. On the other hand, when extension continues, the lithosphere eventually breaks. The break-up phase is important as it decides much of the margin geometry that will develop in the post-rift phase. For example, depending on where the crust break symmetric or a-symmetric margins may form in terms of extended width (Fig. 1.12, Huisman and Beaumont, 2007)), basin distribution or crustal thickness. Also in terms of volcanism, the margins can be grouped differently, the most common division being ‘volcanic’ or ‘non-volcanic’ margins (Fig. 1.12b, Franke, 2013)). Whether the mantle lithosphere or the crust will break first are two different views that give

two different results. When the mantle lithosphere breaks first, mantle material reaches shallow depths and the margins of the spreading system become ‘volcanic’. When the crust breaks first, the margins already develop while the mantle lithosphere is still intact and ‘non-volcanic’ margins form (Tugend et al., 2017). During the post-rift phase the basins that did not suffer break-up, undergo a thermal subsidence phase which eventually re-equilibrates the lithosphere, similar to the model proposed by McKenzie (1978) and Royden et al. (1980). During this phase accommodation space is created and sediments can deposit. For a rift-system that reaches break-up and eventual spreading, the margins suffer from vertical movements, partly from thermal subsidence, but also from isostatic rebound of the lithosphere after the crust has broken apart (Kusznir and Ziegler, 1992) or vertical movements due to folding of the lithosphere through compression that resulted from abrupt changes in lithosphere thicknesses between continental and oceanic lithosphere (Japsen et al., 2012).

Most recent advances on continental rifting and break-up studies, including integrated 3D models, impose as many of the above described parameters on the system when simulating rifting. These studies look for example at alternative lithosphere setups by comprising strong crustal blocks resembling cratons and other inherited structures (Koptev et al., 2016, 2015), or pushing the model through the complete pre-rift to spreading evolution (Koptev et al., 2017). In this spirit, two chapters of this manuscript have been developed where the effect of initial mantle anomaly location on a lateral rheological varying lithosphere has been tested (Chapter 3 and 4, Beniést et al., 2017a, 2017b)

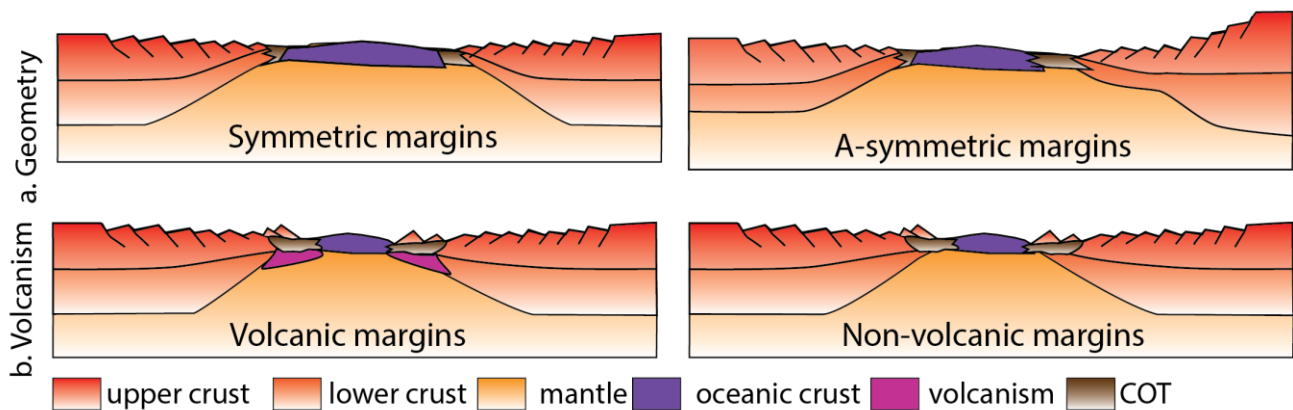


Figure 1.12. Schematic representation of the examples of types of margins that develop after continental break-up based on a) geometry (symmetric vs a-symmetric margins in terms of crustal thickness and margin width) and b) volcanism (volcanic vs non-volcanic margins). COT = continent-ocean-transition.

1.4. Analogue and numerical models

Analogue and numerical modelling methods are used to understand the plate tectonic processes. The advantage of analogue models is that resolution is higher and the models work in three dimensions per

definition. A drawback is the exclusion of thermal processes that are not accounted for in analogue experiments using silicon putty and sand that float on a liquid. For this, numerical models are more convenient because they can solve for temperature and displacement using physical principles. Appendix I and II provide the explanations of the numerical codes used in this project, the 2D thermo-mechanical FLAMAR code and a 2D version of the I3ELVIS code.

1.4.1. Analogue modelling

The first analogue models were performed by James Hall in the early 19th century, using sand layers with different colors to investigate how folding would develop under converging stresses. At the end of the 19th century other experiments developed with the aim to understand fracturing, folding and faulting of rocks, mainly in compression (Schellart and Strak, 2016). Analogue models investigating normal faulting and thus extensional processes occurred in the mid 20st century (e.g. Hubbert, 1951). From the 90's onwards a new wave of analogue models in extension occurred with a focus on lithosphere scale processes and the exhumation of the lower crust and mantle (e.g. Brun et al., 1994; Brun and Beslier, 1996). In contrast with earlier analogue models, these models used less viscous materials representing weaker parts of the crust and the upper mantle. With these type of analogue models extensional systems could be characterized in terms of width (“narrow” vs “wide” (Brun, 1999)) and geometry (“asymmetric” vs “symmetric” (e.g. Calignano et al., 2015a)).

The challenge with analogue models in extension using silicon putty, sand floating on a heavy liquid made of a glucose solution or polytungstate, is to localize the extension inside the model domain and not at the boundary. Weak zones are therefore often implemented in an overall lateral homogeneous setup to avoid model failure. These ‘weak zones’ can be formed by actively incorporating a weak material inside the model (e.g Corti et al., 2013, 2007; Tirel et al., 2006; Willingshofer et al., 2005). Other possibilities are simulating velocity discontinuities by a ‘box-in-box’ method, where a box half the width of the model box is attached to the moving wall (Allemand and Brun, 1991). The edges of the small box a discontinuity in the model at the desired place. Another possibility to provide displacement boundary conditions is the use of rubber sheets at the base of the model box (Withjack and Jamison, 1986).

The analogue models allow to investigate the rheological behavior of different materials in one system. The different layers as described in section 1.2 can be simulated with silicon (ductile material) and sand (brittle material). The decoupling of brittle layers by ductile layers has a major impact on the way rifting initiates in the system (Brun, 2002). Most analogue models are therefore vertically stratified but laterally homogeneous, except the implemented weak zone. As the earth's crust consists of many different types of rocks, the system cannot be seen a homogeneous system. Some recent studies attempted to include more variation in terms of crustal thickness (Bonini et al., 2007), various weak zones (Cappelletti et al., 2013)

and extension rate (Nestola et al., 2015). In chapter 2 of this manuscript the results of an analogue modelling exercise including different segments with different strength envelopes are presented.

Even though no thermal processes are taken into account with the analogue models presented in this manuscript, several attempts to understand for example plume geometries have been published (Davaille et al., 2005; Davaille and Vatteville, 2005). These models don't investigate the interaction between mantle plumes and overlying lithosphere, but the results of these analogue models can be compared to numerical models that do examine how the lithosphere reacts to thermal upwelling and plume-impingement.

1.4.2. Numerical modelling

Thermo-mechanical processes at lithosphere scale were initially tackled using a purely hydrodynamic approach (e.g. D'Acremont et al., 2003; Ribe and Christensen, 1994; Tackley, 2002, 1998). Later, thermo-mechanical models based on the FLAC algorithm were developed that could take into account non-linear elastic, brittle and ductile properties of the lithosphere (e.g. Burov and Diament, 1995; D'Acremont et al., 2003; Huisman et al., 2001; Le Pourhiet, 2004). These studies were dedicated to understand the behavior of the lithosphere in reaction to erosion and deposition of sediments (Burov and Cloetingh, 1997), lithospheric folding (Cloetingh et al., 1999) and thermal upwelling from the mantle (D'Acremont et al., 2003).

The FLAMAR code, used also in chapter 3 of this manuscript, proved to be very useful for questions that relate to changes in topography over time, as this code allows topography to develop freely. The 2D nature of the code makes it less time-consuming than many 3D numerical codes. Other exercises were performed to investigate for example the effect of strain-softening in the plastic-frictional domain (Huisman and Beaumont, 2002) or on deformation localization for various strength profiles (Huisman and Beaumont, 2007). After obtaining a better understanding of the influence different parameters have in thermo-mechanical modelling mineral phase changes that occurred when for example mantle material rises to shallower levels were incorporated in thermo-mechanical models, including mechanisms to account for fluid transport, as they heavily influence the results. Thermo-dynamic models such as *Perple_X* (Connolly, 2005) that uses experimentally acquired data to identify the state of the lithosphere when in thermodynamic equilibrium, were incorporated into the thermo-mechanical codes, including the (e.g. Mezri et al., 2015; Yamato et al., 2008).

With increasing computing power, more complex and powerful codes could be developed, leading to the rise of 3D numerical models that also take into account, e.g. *SLIM3D* (Popov and Sobolev, 2010) and *I3ELVIS* (Gerya, 2010; Gerya and Yuen, 2007), the latter being used for chapter 4 of this manuscript. Even though these models did not appear from scratch and they do include melt formation and phase changes, the 3D nature of these codes holds some limitations. Not only are 3D models time consuming in calculation

time, also the free surface, which proved to be very powerful for the 2D thermo-mechanical code is not so easily implemented in a 3D code.

Despite the limitations of either type of code, these numerical techniques are not only used by physicists and computer scientists. Geophysicists and geologists with numerical affiliation can be users of these codes and use them to explain geological observations. Some of the key-questions addressed in modelling extensional processes include the impact of inherited structures (e.g. Buiter and Tetreault, 2015; Manatschal et al., 2015), magmatic versus non-magmatic margin formation (e.g. Péron-Pinvidic and Manatschal, 2009), crustal break-up vs lithosphere break-up (e.g. Tugend et al., 2017), varying extension-rates (Brune et al., 2016, 2014) and symmetry and asymmetry in extensional settings (Brune et al., 2014; Huismans and Beaumont, 2003; Unternehr et al., 2010). The most recent thermo-mechanical models addressing extensional tectonic systems include complex lithosphere model setups that include the interaction of mantle anomalies (Beniest et al., 2017a, 2017b, Koptev et al., 2017, 2016, 2015) or investigate the effect of the presence of melts in the spreading centre on the spreading rate (Lavecchia et al., 2017).

1.5. The South Atlantic as a case study

1.5.1. Pre-rift

The pre-rift tectonic setting of the South Atlantic started with supercontinent Pangea that existed during the Permian (250 Ma). Pangea broke apart into two smaller super-continent Laurasia and Gondwanaland during the Triassic and Jurassic. South America and Africa were part of Gondwanaland, which was discovered by comparing Mesozoic lithologies and structures on both continents (Du Toit, 1937; Frimmel et al., 2011; Konopásek et al., 2016; Macdonald et al., 2003). Pre-break-up times, South-America and Africa were occupying a region ranging between 60 °S – 30 °N.

On Gondwanaland, tectonic ‘pre-rift inherited’ features were present that possibly guided rift initiation. These structures separated an amalgamation of Archaean and Proterozoic cratons (Fig. 1.13 from Frimmel et al. (2011)) through Pan-African fold-and-thrust belts and fore-land basins that could have worked as shearzones along which deformation during the syn-rift phase took place (Burke, 1996; Nürnberg and Müller, 1991; Torsvik et al., 2009, Jackson et al., 2000; Martin and Hartnady, 1986; Martin et al., 1981; Moulin et al., 2010; Rabinowitz and Labrecque, 1979; Talwani and Eldholm, 1973; Torsvik et al., 2009). Example of pre-break-up features that are now located on both continent are the Congo-São Francisco craton (Frimmel et al., 2011) and the Dom Feliciano-Damara belt (Konopásek et al., 2016).

Using data of the present-day structure of the South Atlantic margins a reconstruction of the pre-rift crustal structure of Gondwanaland can be made. Deep reflection seismic data provides Moho depth and crustal thickness (Pindell et al., 2014), refraction and reflection seismic data gives the crustal structure (Bauer et al., 2000; Blaich et al., 2011; Gladczenko et al., 1998; Mello et al., 2013). Gravity data is used to identify

different densities of bodies in the crust. Along the margins of the South Segment anomalous high-density bodies are observed at lower crustal depth. They have been interpreted in different ways, e.g. feeder dykes (Blaich et al., 2011) or heavily intruded continental crust (Cornwell et al., 2006; Schnabel et al., 2008) in the form of Seaward Dipping Reflectors (SDR's) or magmatic underplating and voluminous magmatism (White et al., 2008; White and Smith, 2009). In some parts, high-velocity-high-density bodies are only observed along the South American margin (Blaich et al., 2009; Franke et al., 2006) not along the South-African side. Here, these bodies could be inherited from Paleozoic accretion of bodies on the former SW-side of Gondwana (Ramos, 2004; Ramos et al., 1996) and therefore contribute to the heterogeneous pre-rift state of Gondwanaland.

The orientation of the basins along the South American margin in the South Segment of the South Atlantic is perpendicular to the present-day orientation of the spreading axis (Fig. 1.14), whereas on the African margin their orientation is parallel to the spreading axis. This difference in orientation suggests an earlier phase of extension for the South American side, before the opening of the South Atlantic ridge along former inherited structures (Franke et al., 2006; Pángaro and Ramos, 2012; Urien et al., 1981; Urien and Zambrano, 1973). This extension phase was perpendicular or obliquely oriented to the extension phase (Franke et al., 2006; Keeley and Light, 1993; Tankard et al., 1995; Urien et al., 1995) that caused the opening of the South Atlantic. This pre-spreading event (Autin et al., 2013) might have weakened the lithosphere in such a way that during the rift phase that would eventually form the South Atlantic, this weakened crust developed the break-up centre (Chapter 3, Beniest et al., 2017a). The perpendicular oriented basins are considered failed rift branches (Asmus and Baisch, 1983; Franke et al., 2002; Urien et al., 1995).

The thermal structure of the pre-rift lithosphere and underlying mantle is more questionable and evidence can only be derived with modelling based on thermal principles. What is interesting to note though is that there is a Large Low Shear Velocity Province (LLSVP) located below the western shores of the present-day south West African margin at lower mantle depths. Modelling has shown that these LLSVP's, do not move and evolve very fast, making its presence at the time of Gondwanaland rather likely (Bull et al., 2014). Around this LLSVP hot spot trails are observed (Hassan et al., 2015). Since the LLSVP remains rather stable and the hotspot trails are evidence for mantle anomalies. There is discussion if the Tristan Plume, the only rooted mantle plume in the South Atlantic domain, located slightly to the east of Mid Oceanic Ridge in the South Segment, has aided and perhaps even caused the break-up of Gondwanaland (e.g. Geoffroy et al., 2015; O'Connor and Duncan, 1990). If thermal anomalies or plumes exist (there are more than 50 definitions for this phenomenon (Lustrino, 2016)), they can be described in terms of composition and/or thermal state and/or origin in the crust (e.g. lower mantle vs upper mantle) with respect to the surrounding material. In this thesis we regard a plume or mantle anomaly as such: a body, less viscous than its surroundings, with an anomalous thermal state and/or composition originating at mantle depth.

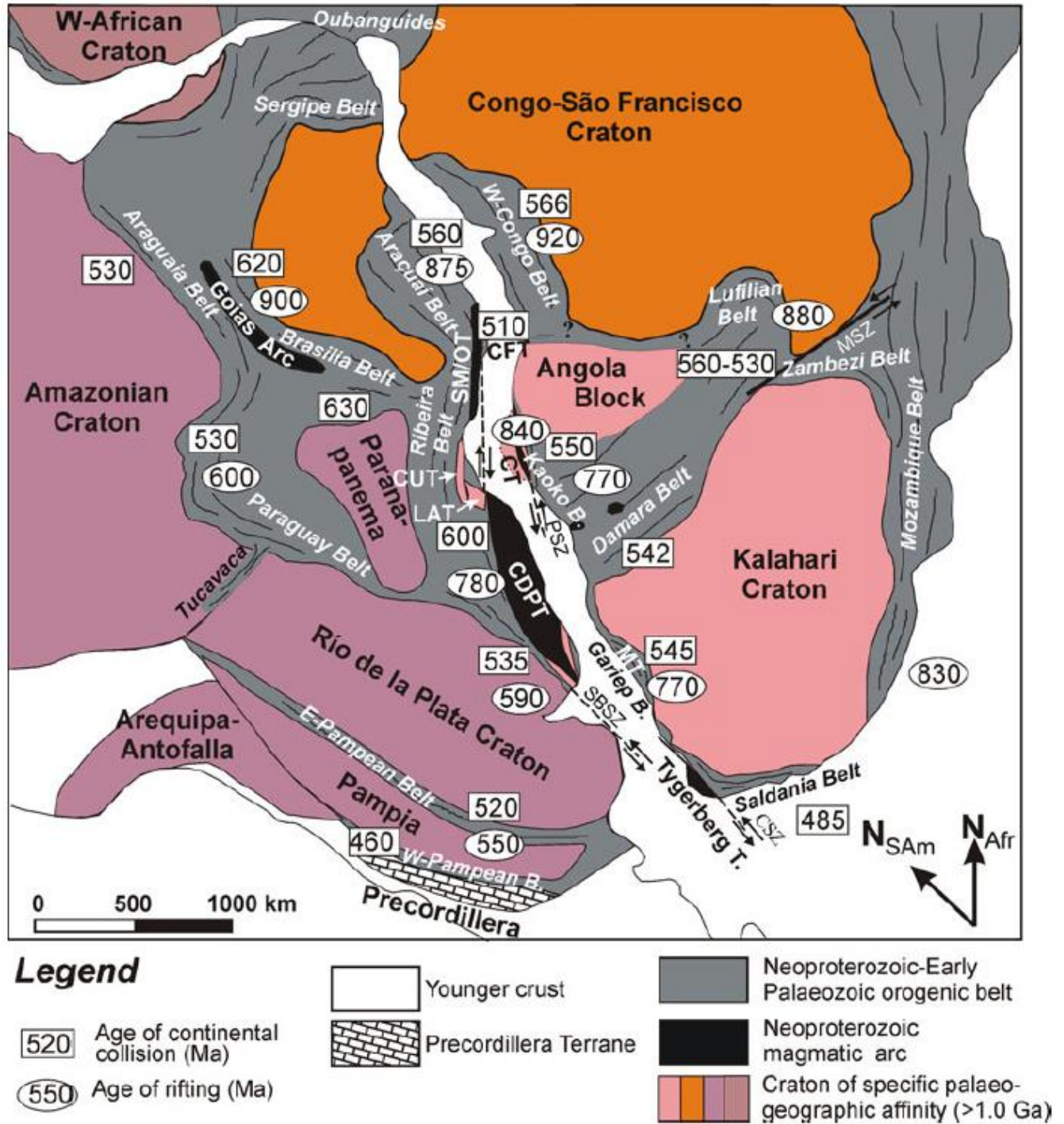


Figure 1.13. Paleogeographic map of the cratons, basins and fold-and-thrust belts of Gondwanaland from Frimmel et al. (2011). CDPT = Cuchilla Dionsio-Pelotas Terrane, CFT = Cabo Frío Terrane, CT = Coastal Terrane, CUT = Curitiba Terrane, LAT = Luis Alves Terrane, MT = Marmora Terrane, SM/OT = Serra do Mar-Oriental Terrane, PSZ = Purros Shear Zone, SBSZ = Sierra Ballena Shear Zone, CSZ = Colenso Shear Zone.

How these anomalous mantle features guide crustal deformation has been investigated since the 1990's early 2000's with thermo-mechanical models (Burov et al., 2001; Burov and Poliakov, 2001; Huisman and Beaumont, 2011; Huisman et al., 2001; Poliakov et al., 1993). Early plume-lithosphere interacting models showed that large-scale topographic changes could result from these rising bodies (e.g. Burov and Guillou-Frottier, 2005; D'Acromont et al., 2003; Guillou-Frottier et al., 2007).

One approach to better understand the role of mantle anomalies (or plumes) in rift initiation and continental break-up is forward thermo-mechanical modelling. Different scenarios have been modelled throughout the years that show that plumes can rise quickly to the base of the lithosphere (D'Acromont et al., 2003), they can cause topographic uplift prior to break-up (Burov et al., 2007; Burov and Cloetingh, 2009; Burov and Gerya, 2014), when extension rates are rather low, plumes help to localize rifting (Koptev et al., 2017), when the lithosphere is heterogeneous, plumes even assist continental break-up off-set from their impingement location (Chapter 3, Beniest et al., 2017a; Koptev et al., 2015) and they are capable of opening two rift branches in heterogeneous systems (Chapter 4, Beniest et al., 2017b).

1.5.2. Syn-rift and continental break-up

A combination of extensional forces (slab-roll back) and thermal weakening (mantle plume) of the lithosphere resulted in rift-initiation and break-up of Gondwanaland (Will and Frimmel, 2017). Extension was accommodated by shearzones and inherited features that separated the domains of Gondwanaland. The South Atlantic oceanic domain originates around 134 Ma (Channell et al., 1995) when continental break-up and spreading migrated from south to north until the northernmost segment, the Equatorial segment opened between 110-104 Ma (Eagles, 2007; Moulin et al., 2010; Nürnberg and Müller, 1991).

The first and strongest extensional pull was felt along the present-day Agulhas- Falkland Fracture Zone (AFFZ, Fig. 1.14) that was initially considered a moderate strike-slip boundary between rigid, continental blocks (Martin and Hartnady, 1986). The Agulhas part of the fracture zone is located on the African Plate, whereas the Falkland side is located on the South-American Plate (Ben-Avraham et al., 1997). On satellite-derived gravity maps (Sandwell and Smith, 2009) large movements/displacements of 500 km have been observed along the intraplate boundaries in South-America between 180 – 160 Ma (Torsvik et al., 2009). Further north, roughly 175 km of dextral movement occurred between 150 – 126 Ma and between Amazonia and Paraná, along the Florianopolis Fault Zone (FFZ, also known as Paraná-Etendeka Fracture Zone (PEFZ) or the Rio Grande – Walvis Ridge Fracture Zone) (Fig. 1.14, Torsvik et al. (2009)). During the syn-rift phase and perhaps also during the early post-rift phase, this fracture zone worked as a barrier with the South Segment to allow a thick sequence of salt to be deposited during the Aptian (Fig. 1.14, Antonio et al., 1981; Torsvik et al., 2009). Between 132 and 129 Ma the syn-rift phase ends in the South Segment when the lithosphere breaks and oceanic spreading starts (Ernesto et al., 1999; Raposo et al., 1998; Renne et al., 1996;

Torsvik et al., 2009). This was possibly aided by the arrival of the Tristan Plume that leaves two volcanic lineaments in the South Segment the Rio Grande Rise and the Walvis Ridge (O'Connor and Duncan, 1990). From ~126 Ma South-America behaved as a rigid single plate. In the Central Segment, the diverging continents thin the crust until 112 Ma when it breaks apart in two continents (Torsvik et al., 2009). The Romanch Fracture Zone separates the Central Segment from the Equatorial Segment and suffered two phases of transpressionally driven deformation. The first phase between 108-92 Ma and a second between 65-52 Ma. The first phase is possibly due to a 9° change in divergence direction between the two continents, which would have resulted in a convergence component across this fracture zone (Nemcok et al., 2013).

In older publications, the margins of the South Segment are considered 'volcanic' margins, because of the large number of melt occurrences in the form of SDR's, flood basalts and high velocity/high density bodies in the lower crust that are widely distributed in the north of the South segment, close to the Tristan Plume. These volcanic bodies were emplaced during the syn-rift phase when the system was under extension or during the early post-rift phase. Towards the south of the margins, the volume of melt decreases (Blaich et al., 2013), which adds to the question if the margins are really volcanic or not. The influence of the Tristan Plume is too far away in this region (further than 2000 km as proposed by White and McKenzie, 1989) to have caused the massive igneous occurrence in the central and south of the South Segment. Here, the volcanic occurrences originate from pulsed or episodic events that allowed melts to accumulate. The crust got heated after which volcanic rocks extruded along large or prominent transfer faults bordering the different segments (Blaich et al., 2013).

Some authors do not agree with the volcanic interpretation of the SDR and assign their existence to high-grade metamorphic crustal rocks, serpentinized material, or a mixture of mafic and ultramafic material (Contrucci et al., 2004; Moulin et al., 2005). To make it more complicated, the deep crustal structures (including the SDR's) are partially covered by a thick package of sediment. This makes it very difficult to distinguish intruded and underplated continental crust and oceanic crust (Ebinger and Casey, 2001). The SDR are also interpreted as proto-oceanic crust (Talwani and Abreu, 2000).

The half-graben systems along the margins are filled, either with pre-rift/syn-rift sedimentary rocks or basalt flows (Talwani and Abreu, 2000). A half-graben system on the South African margin extending landwards is observed and is possibly filled with post-rift/syn-rift sediments or basalt flows (Bauer et al., 2000). The Mesozoic (syn-rift) package is much thicker on the African side than on the South American side. The basin axes of the African basins are parallel to the coastline which implies they are formed along the same stresses as the Mid-Atlantic Ridge during the syn-rift phase. Some authors consider that the syn-rift deposits are not coeval and that a Mesozoic rifting phase occurs before the final opening of the South Atlantic (Macdonald et al., 2003). These authors propose that early rifting was oblique (NE-SW extension), which created basins at high angle to the trend of the ocean on the Argentine margin (Autin et al., 2013).

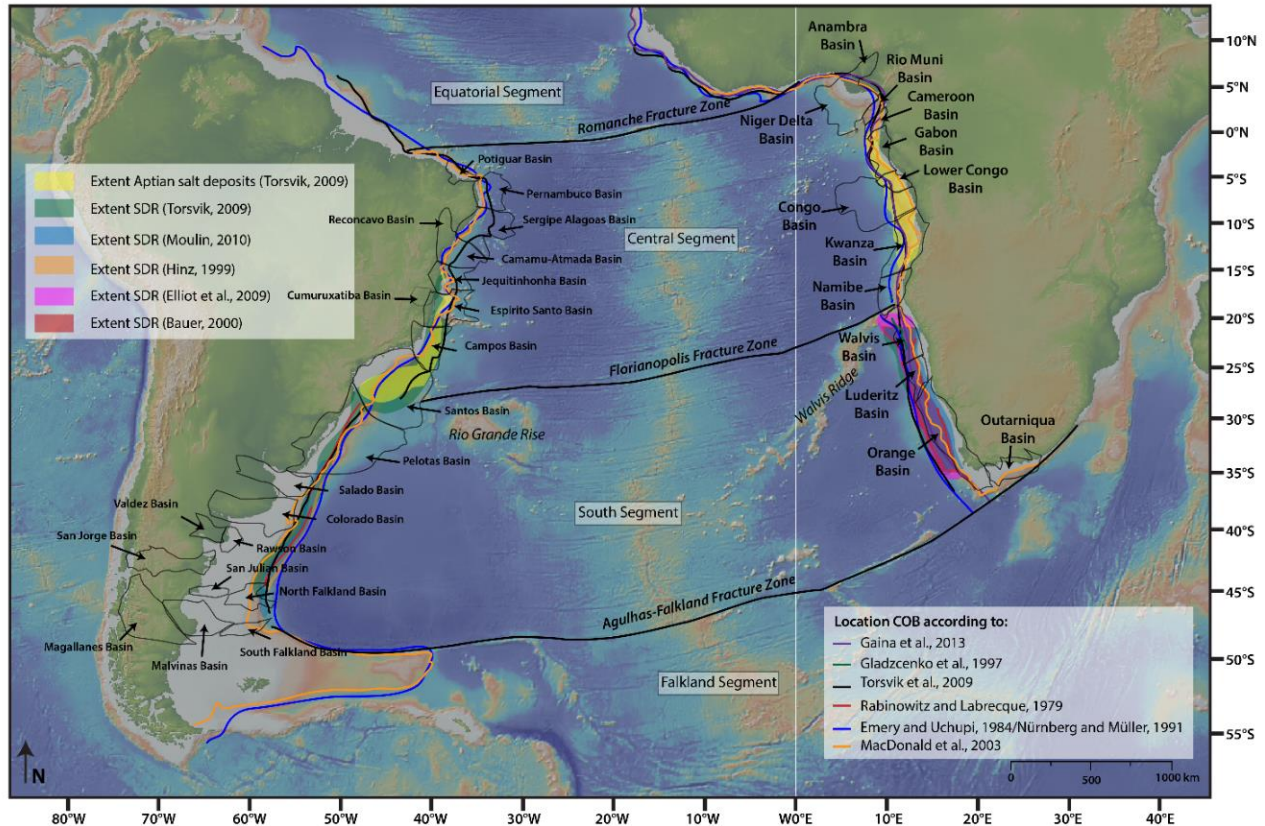


Figure 1.14. Bathymetric map of the South Atlantic domain showing the different segments and examples of continent-ocean boundary locations (COB), seaward-dipping-reflectors areas (SDR) and the outline of the marginal basins.

1.5.3. Post-rift

Magnetic anomalies have helped to determine the age of the oceanic crust and also to onset of spreading and thus the timing of continental break-up (e.g. Moulin et al., 2010; Nürnberg and Müller, 1991; Torsvik et al., 2009). The magnetic signal of oceanic crust is being captured by shipboard profiles and aeromagnetic profiles. The variations in magnetic strength of magnetic minerals of the Earth's crust can be mapped over large distances and are best captured in full oceanic crust (Fig. 1.15). In the South Atlantic domain, the oldest magnetic anomaly in full oceanic crust is of Aptian age and is called Chron M-0. Hence, seafloor spreading started at least during the Early Cretaceous (Channell et al., 1995). The M0-anomaly is also known as the 'magnetic quiet zone' or the 'Cretaceous superchron', between 108 Ma to 92 Ma. This period has been adopted in the Global Polarity Time Scale (GPTS) (Gradstein et al., 2012), the standard timescale based on paleomagnetic research and nanofossils. That the South Atlantic started spreading during the magnetic quiet zone, makes it very difficult to determine the exact timing of opening. Recent studies have identified two long wavelength magnetic wiggles within Chron M-0. These can be globally correlated to better constrain the magnetic quiet zone (Granot and Dyment, 2015). The most prominent magnetic anomaly recognized early on in magnetic studies is the so-called 'G magnetic anomaly' (Fig. 1.15) (Rabinowitz and

Labrecque, 1979). This very dominant anomaly has been interpreted as an edge-effect between the continent-ocean-boundary (COB) (Rabinowitz and Labrecque, 1979) or as the result of SDR's (Blaich et al., 2009; Hinz et al., 1999). The Large Marginal Anomaly (LMA) has a clear magnetic signal and includes the G-anomaly and two minor magnetic anomalies in the Early Cretaceous (M9 and M11), because these two are not clearly observed separately on magnetic data along the margins (Moulin et al., 2010). The LMA is very wide along the South African margin, with a double branch in the Orange basin. The LMA is less wide along the South American margin. The asymmetry between anomalies is also observed in the Northern Atlantic, where it can be explained by asymmetric sea-floor spreading (Larsen and Saunders, 1998) or stretched and intruded continental crust (White and Smith, 2009). The regularity of the magnetic anomalies facilitated the calculation of the age of the oceanic crust (Müller et al., 2008) and also the spreading rate (Colli et al., 2014).

The South Atlantic is divided into several segments. The segmentation is largely based on the subsurface margin (a)symmetry of the Continent-Ocean-Boundary (COB), its Continent-Ocean-Transition (COT), the presence or absence of volcanism and Seaward Dipping Reflectors (SDR) (Fig. 1.14 and 1.15). The term 'continent-ocean transition' (COT) is used for the part that separates clearly identifiable stretched continental crust and the fully developed oceanic crust (Blaich et al., 2011). Whether the COB is located towards the landwards edge or the seawards edge of the COT is still a matter of debate due to several factors such as the masking effects of the evaporitic sequences (Central Segment), the exhumed continental mantle (South Segment), depth-dependent stretching (Davis and Kusznir, 2004) and the different interpretations of SDR's (Torsvik et al., 2009). The COB, the location of the SDR's and the Aptian salt occurrences have been used to reconstruct the pre-break-up configuration, just before spreading started (Torsvik et al., 2009). Along the African margin, the COT is often mapped as a very narrow band of SDR's in the South Segment (Gladchenko et al., 1997). This correlates well with the integrated geophysical study of (Bauer et al., 2000). On the South American side there are three possibilities for the COT based on large volcanic activity (Gladchenko et al., 1997), the presence of SDR's and voluminous extrusive units (Chang et al., 1992; Mohriak et al., 1990) and residual isostatic gradients (Torsvik et al., 2009). The location of the COT in the Central Segment is more complicated due to the presence of salt (which is absent in the South Segment margins) and is often based on seismic data and less on gravimetry for example (Contrucci et al., 2004; Dupré et al., 2007; Moulin et al., 2005).

Gravity modelling is the most used method to identify the COB (Fig. 1.14). The positive gravity anomaly is interpreted as a broad Moho uplift in the footwall of Early Cretaceous extensional faults. Anomalies further offshore correlate well with a volcanic ridge, interpreted as a failed rift/spreading centre (Meisling et al., 2001). The COB is fairly well established north of the Santos Basin, due to well defined features in gravity data (Torsvik et al., 2009).

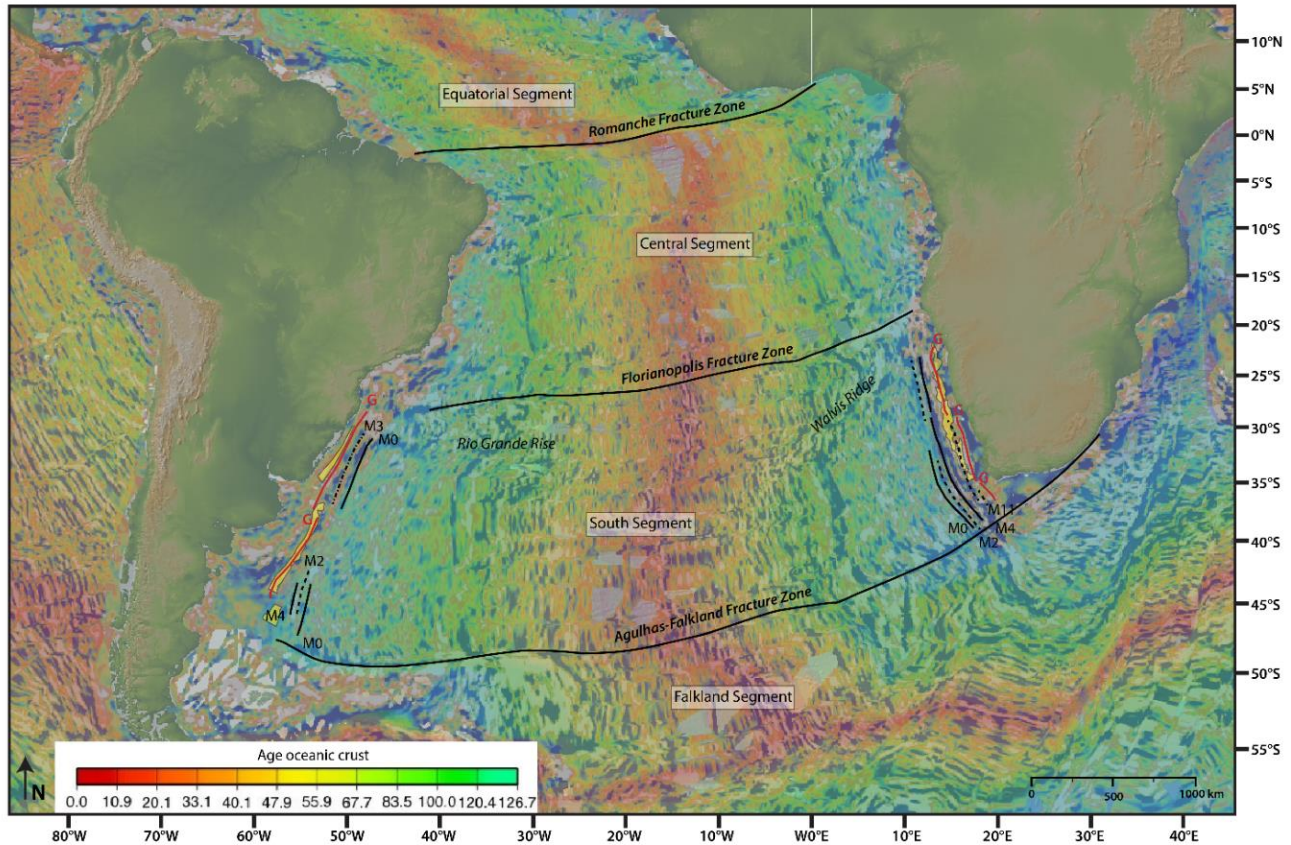


Figure 1.15. Map of the South Atlantic domain with four large segments, the magnetic anomalies (the most important anomalies are highlighted: Large-Marginal Anomaly after Moulin et al., 2013; M0, M2, M3, M4, M11 and G after Rabinowitz and Labrecque, 1979) and the age of the oceanic crust (Müller et al., 2008).

A second group of authors put the COB along the Brazilian coast further landwards (Macdonald et al., 2003; Müller et al., 1997). Arguments against this are the long distance of post-break-up salt flow that is needed to reach the current setting which are unrealistically high (Torsvik et al., 2009), even after correction of the landward COB (Müller et al., 2008).

The geometries of the margins differ too. Along the South Segment, the African margin is roughly 200 km wide, compared to 300 km on the South American side. (Blaich et al., 2009). In the Central Segment, the African margin is 400 km wide compared to 300 for the South American margin (Blaich et al., 2011). Also basin width, orientation and quantity is not the equally divided in the South Segment (Fig. 1.14). On the African side the basins are 75 – 150 km wide along the Namibian-South African margin (Bauer et al., 2000; Gladzenko et al., 1997), compared to 160 – 180 km off the Congo-Angolan margin (Moulin et al., 2005) and 120 km wide of the Gabon margin (Watts and Stewart, 1998). There are only three basins along the South Segment margins, all oriented parallel to the present-day spreading axis. On the South American side there are 10 basins, all oriented perpendicular to the Mid-Oceanic Ridge or with a more circular geometry. The sediment infill of the South America and African marginal basins contains syn-rift sedimentation and

they show that they have been affected by post-rift subsidence and uplift events (Marcano et al., 2013). In addition, the South American basins of the South Segment contain older sediments and a thick package of Mesozoic sediments, which is not the case for the African basins (Blaich et al., 2011) and implying a previous deformation phase.

1.6. Objective and approach

Ever since the Map of the Ocean Floor from Marie Tharp, the numerical studies of Bullard et al. (1965) and the Plate Tectonic Cycle of Richard Wagner were accepted, questions arose about the reasons for why continents break apart. The conceptual concepts of Mckenzie (1978) and Lister et al. (1986) and variations there-off were used for decades to explain rift-to-drift systems. However, the heterogeneous lithosphere and the numerous processes acting on it, drastically increased the complexity of lithosphere-scale processes in extension and the theoretical concepts for continental rifting and break-up.

There has long been a debate whether rifting originated from far-field stresses (e.g. ‘passive’ rifting) or thermal upwelling of mantle material (e.g. active rifting) (Olsen and Morgan, 1995; Sengör and Burke, 1978). In the case of the South Atlantic, where, at the time of rift initiation Gondwanaland consisted of an amalgamation of crustal blocks, the varied nature of the lithosphere, or its rheology is also extremely important. For that reason analogue modelling was performed at the tectonics laboratory at Utrecht University. The analogue modelling approach allowed to investigate in detail the response of extensional forces on a complex lithosphere, consisting of several segments, for example an amalgamation of crustal blocks or cratons, as no thermal processes are taken into account. Here, the objective was to understand what the effect is of far-field forces on complex lithospheric setups. Is it possible to reproduce features observed along the margins with just the interaction of far-field forces and rheological differences? Does such a system break at the contact between two different segments, the ‘inherited structure’, or not? Silicon-putty and sand models with lateral varying rheological segments were put under extensional forces. The results of this exercise can be read in Chapter 2.

In the South Atlantic domain a deep-rooted mantle anomaly is present and might have influenced rift initiation and continental break-up. Interestingly, the plume is located not exactly beneath the ridge and also the margins show dissimilar crustal thicknesses, orientation of basins and high velocity/high density bodies are present at depth. Since analogue modelling does not include thermal processes, 2D thermo-mechanical modelling has been performed to understand the influence of thermal processes on these complex lithosphere setups, consisting of different segments.

The first thermo-mechanical modelling exercise investigated the influence of far-field forces and plume locations on a lithosphere consisting of two different segments including different thicknesses of the segments and geometries between these segments. The objective was to understand how a laterally

heterogeneous lithosphere responds to different combinations of far-field forces, thermal anomalies and rheological setups. Does the ‘classical’ break-up mode always develop or are there other options? Is it possible reproduce margin asymmetry and lower crustal high density/high velocity bodies as observed along the margins of the South Atlantic? The 2D thermo-mechanical code FLAMAR is used for this exercise. The results can be found in Chapter 3 and a detailed explanation of the model can be found in appendix I.

The location of the plume turned out to be a key-parameter for rift initiation and final break-up location. However, the model design of the previous exercise did not allow a qualitative review of the impact of the plume location on continental break-up. For this reason, a set of models was designed that investigated in detail the location of the plume in combination with far-field forces, thermal gradients and, again, a complex rheological setup with a lithosphere consisting of two different segments. This time, a 2D version of the 3D thermo-mechanical code I3ELVIS was used. The results can be found in Chapter 4, with a detailed description of the model in in appendix II.

The analogue and numerical studies presented here help to explain geological and geophysical observations. They also provide a new hypotheses and ideas on the formation of asymmetric margins and plume-induced continental break-up that need verification by geological and geophysical observations. A detailed discussion about the impact of these exercises on geodynamic concepts in extensional tectonics, the formation of surface features and the implications for deeper structures is given in Chapter 5. Conclusions and perspectives provide ideas for follow-up work using of the results of this work to understand basin-scale processes. During the PhD, a scientific cruise on the acquisition of geophysical data (seismic reflection and refraction, gravity and magnetic data), which might eventually provide information on the formation of asymmetric margins and also the deeper crustal structure and the sub-Moho mantle, was held on the Indian Ocean during the summer of 2017. A report on this acquisition through Magnetometer and Ocean Bottom Seismometers deployment and recovery is provided in appendix III.

Main questions:

- What is the effect of far-field forces on a rheologically segmented lithosphere without taking thermal processes into account? Is it possible to reproduce features observed along the margins with just the interaction of far-field forces and lateral rheological variations? (Chapter 2)
- Can margin asymmetry and lower crustal high density/high velocity bodies be reproduced when including thermal processes through adding mantle plumes to the equation? (Chapter 3)
- What is the qualitative effect of pre-rift plume location on the final break-up style? (Chapter 4)
- How does conjugate margin asymmetry and thermal history vary with break-up mode? (Chapter 5)

Chapter 2: Extending the continental lithosphere: influence of lateral strength variations on deformation mode and geometry

Summary

Prior to break-up Gondwanaland consisted of an amalgamation of cratons, fold-and-thrust belts and basins. These different features have different internal properties and thus different strengths. If this system of amalgamated blocks is regarded as a whole, the question is how this complex setup reacts to extensional far-field forces. In the case of the opening of the South Atlantic these horizontal, far-field forces result from the slab roll-back of the subducting slab below the Andes, on the western side of the South American Plate. To investigate the effect of far-field forces on a more complex lithosphere (consisting of domains with different strengths) analogue modelling experiments have been performed at Utrecht University. The advantage of analogue models over numerical models in this specific case is that the models provide a higher resolution, they work in 3D and because there is no interaction with temperature anomalies purely the effect of extension can be tested on setups that contain large segments with different strength.

The model setups combine two large segments of equal size with different strength on which extension is applied on one side of the model by displacing a moving wall away from the model. The justification for only applying extension on one side of the model box results from the notion that the South American plate is moving fast towards the west as a result of the subducting slab that exerts horizontal far-field forces on this complex system. Africa remains rather stationary and thus the assumption is that extensional forces only act on the South American side, but they can be felt throughout the system.

The results of these analogue models show that in a complex setup with several domains with different strength, extension is accommodated in the weak zone only and not, as would be expected at the contact between the different segments. In case the crust and mantle are decoupled the strong upper mantle also accommodates extension, although initially rifting is distributed and wide rift geometries develop. When at some point the strong mantle breaks, a weak zone develops that then starts to accommodate all extension leading to extreme thinning of the lithosphere, developing a narrow rift zone. If extension would continue, this narrow rift domain is where the system would eventually break.

Margin geometries that result from this are comparable to the South Atlantic margins. When only taking into account the rifted domain, the margins appear to have been formed in a pure shear fashion, developing symmetric geometries comparable to the margins of the Central Segment. In case the initial system is looked at, including the strong part that has not suffered any extensional deformation, the geometries are asymmetric because the strong part has now a part of the thinned, weak lithosphere attached to it. This is comparable to margins of the South Segment where the crust is thicker and thins abruptly on the African side, whereas the South American side has a thinner crust in general. Also the basin distribution is comparable with more basins of the South American side than on the African side, although this is highly dependent on the location of failure of the strong part of the upper mantle.

Abstract

The South Atlantic domain is the result of continental rifting and break-up of supercontinent Pangea. Supercontinents consist of an amalgamation cratons, fold-and-thrust belts and basins before they break apart. These different features vary in lithosphere strength and respond differently to extensional forces. It is important to understand how the ensemble of a system that contains of a variety of lithospheric strengths responds to extensional forces because this might influence the rift localization location and final margin geometries. With lithosphere-scale analogue modelling the rift structure and evolution in response to extension of complex lithospheric setups has been studied. The experiments include two equally sized segments of continental lithosphere with a lateral strength variation. The results show that deformation by extension always localizes in the relatively weaker section and not at the contact between the lithospheres where the strength contrast is highest. When the weak segment consists of three layers (brittle crust, ductile crust and ductile mantle) a wide-rift develops due to ductile coupling of the lower crust and upper mantle. In case the weaker lithosphere includes a very resistant upper mantle layer, the system undergoes a two-phase evolution. First, a rift, with a 25% narrower width compared to the 3-layer experiment, develops under decoupled conditions. This mode of rifting persists until the mechanically strong upper mantle loses strength and the weak lower crust and weak upper mantle become a coupled system (phase two). The coupling results in immediate narrow-rift deformation localization that is symmetric in the mantle lithosphere, but asymmetric within the crust. This two-phased extension can explain different margin geometries depending on the scale the final system is looked at. When only the rifted domain is taken into consideration to describe margin geometries, the system develops in a pure-shear fashion, resulting in rather symmetric margins in terms of crustal thicknesses, comparable to the Central Segment of the South Atlantic. When the initial system as a whole is regarded, the system still developed in a pure-shear fashion. In this case though, the margin's geometry is asymmetric in terms of crustal thickness and unequal basin distribution on either side of the margin, because the 'stronger' segment has now a thin sliver of weak lithosphere attached to it. This asymmetry is comparable to the margins along the South Segment of the South Atlantic. The asymmetric basin distribution is highly dependent on the location of failure of the strong upper mantle. With this two-phased extension evolution we provide an alternative view on rift asymmetry based in the absence of lithosphere-scale detachments.

Reference: Beniést, A., Willingshofer, E. Sokoutis, S., Sassi, W. Extending the continental lithosphere: influence of lateral strength variations on deformation mode and geometry. In preparation.

2.1. Introduction

The last supercontinent, Pangea, consisted of amalgamated cratons, fold-and-thrust belts and basins prior to its break-up (Will and Frimmel, 2017). The East African rift and the South Atlantic domain are both results of the disintegration of Pangea. Different to the East African rift, the South Atlantic rift system did not always follow inherited tectonic contacts like suture zones for rift-localization and break-up, but also cross-cuts these contacts, e.g. the Gondwana Fold and Thrust Belt (Fig. 2.1, Cobbold et al., 1992). In some cases even, other crustal units broke apart rather, that can be found now on both sides of the Atlantic Ocean, e.g. the Dom Feliciano Gariép belts or former back-arc basins (Engelmann de Oliveira et al., 2016; Konopásek et al., 2016; Will and Frimmel, 2017). The localization of deformation and the geometry of rift structures can be explained by inherited structures, strain softening and complex brittle-ductile rheology and stratification (e.g. Balázs et al., 2017; Brun and Beslier, 1996; Manatschal et al., 2015; Philippon et al., 2014). The extensional deformation modes that eventually cause the break-up of continents and create rift geometries highly depend on first-order parameters such as temperature and strain rate that influence the rheological state of the lithosphere at the onset of rifting (eg. Buck 1991, Brun, 1999, Burov and Gerya, 2014). The difference in rift localization observed between the East African Rift and the South Atlantic might thus be a result of different interaction between the first order parameters and the rheological state of the lithosphere at the onset of rifting.

Analogue and numerical models are used to investigate the structural style that develops during plate rupture. In analogue modelling rheological weak zones are often implemented in lateral homogenous, but vertically layered model setups to simulate variations in strength (Chenin and Beaumont, 2013; Zwaan et al., 2016). These studies provide valuable insight in controls on strain localization and rift geometry. We know for example that weak zones in the lower crust impact rift localization more than weak zones in the lithospheric mantle (Sokoutis et al., 2007) and that different weak zones at lower crust impact along margin segmentation (Cappelletti et al., 2013). The effect of large lateral strength variations, that possibly interfered with the break-up of Gondwana into the South American and African plates (Will and Frimmel, 2017), can however, not be addressed with these kind of models. Experimental work using wide domains with significant rheological contrasts in extensional setting are scarce. An example could be the one from Corti et al. (2013) where a large weak segment is implemented at the centre of the model. However, even though the strength contrast is large in this study, the weak and strong domains cannot be compared to an amalgamation of strong crustal features present in supercontinents. The strength of the lithosphere is also impacted by thickness (Burov and Diament, 1995) which has been tested by Bonini et al. (2007) with small-scale analogue models. Here, deformation was mainly accommodated at the boundary between the two types of lithosphere or at an inherited structure, but not in either the thin or thick lithosphere segment.

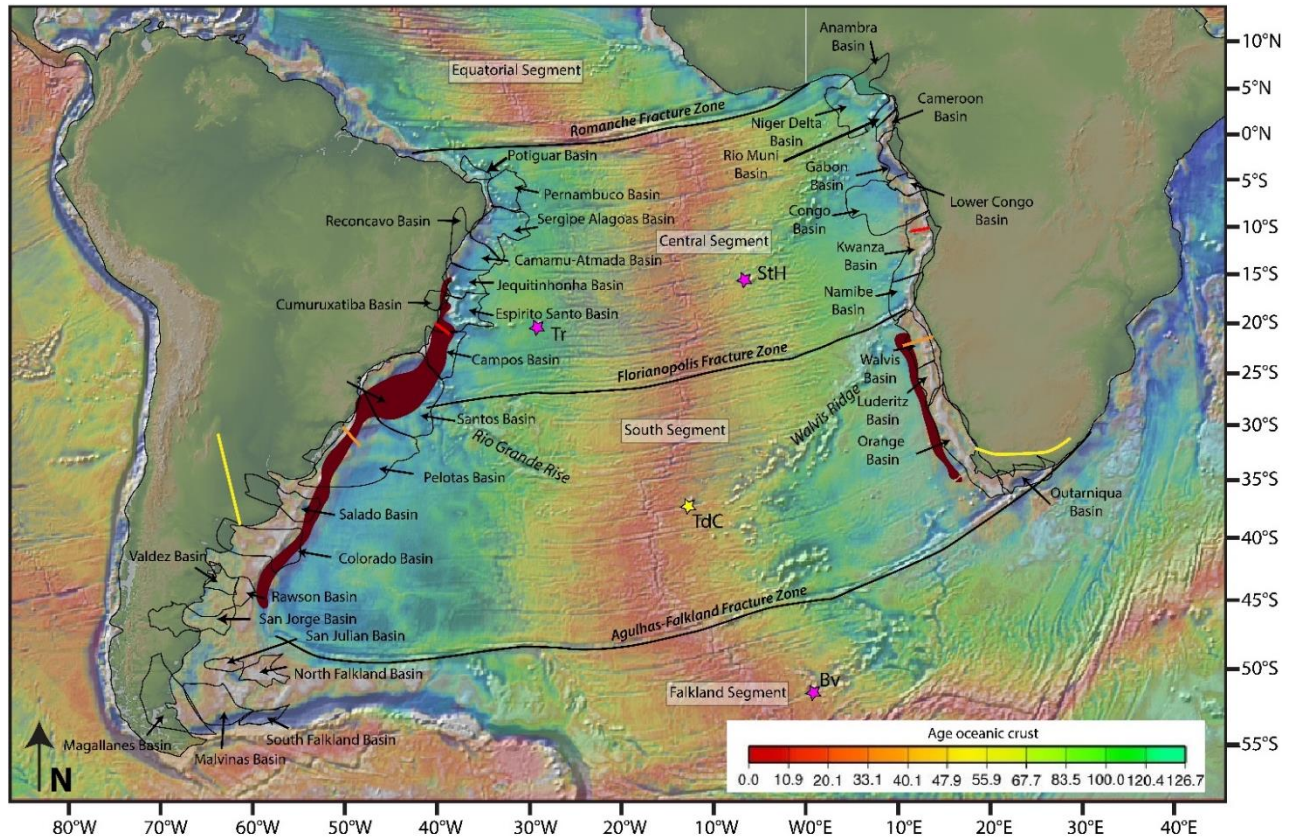


Figure 2.1. Map of the South Atlantic domain showing the outline of the basins along the margins in the Central and South Segment as well as the locations of the cross-section given in Fig. 5. (red lines: Fig. 5g, orange lines Fig. 5h). The extend of the SDR (after Torsvik et al., 2009) is also provided. Note the presence of one rooted mantle plume in the South Segment (TdC = Tristan da Cunha Plume) and two hotspots in the Central Segment (Tr = Trinidad hotspot) and StH = Saint Helena hotspot). The age of the oceanic crust (Müller et al., 2008) is overlying the bathymetry map (Ryan et al., 2009). The yellow line represents the Cape fold and thrust belt that partly runs on the African continent and the South American continent.

In numerical modelling up until recently, the strength profiles of model setups were mainly laterally homogeneous and vertically stratified. Weak seeds or thermal perturbations, not necessarily based on observations, are implemented to localize deformation within the model and not at its borders (e.g. Brune et al., 2014; Huismans and Beaumont, 2007). Combining two different rheological segments to test the effect of far-field forces on a laterally heterogeneous system has only been performed numerically (Beniest et al., 2017a, 2017b; Koptev et al., 2015, 2016), but always with the presence of a mantle plume. These studies have shown that in a system with lateral strength variations, several modes of break-up can occur depending on the thermal regime and far-field forces. These modes include break-up at lithospheric contacts (or inherited structures) but also in homogeneous parts of a lithospheric segment (Beniest et al., 2017a, 2017b), which could be the case for the South Atlantic (Engelmann de Oliveira et al., 2016). Also the implementation of large, strong crustal blocks in numerical models offsets the break-up centre significantly

from the plume impingement point (Koptev et al., 2016, 2015) thereby explaining the geometries observed in the East Africa Rift.

Not all extensional systems develop with the presence of a mantle plume. The Central Segment of the South Atlantic for example, does not have a rooted mantle plume below the Mid Oceanic Ridge. The influence of extensional forces on a system with large lateral strength variations without the inclusion of mantle anomalies have not been modelled up until today. The advantage of modelling this with analogue experiments is the high-resolution and the 3D nature of the models that allow for a good comparison with margin geometries in the South Atlantic domain. We address the question whether large lateral strength variations within the continental lithosphere can direct deformation localization and the evolution of rift structures and geometries. Our aim is to understand why, like in the case of the South Atlantic, localization of deformation is not solemnly controlled by inherited structures but also affected more homogeneous parts of a larger system containing lateral strength variations. The results of our study add to our understanding of the influence of strength variations in the lithosphere on complex rift systems.

2.2. Experimental setup

2.2.1. Analogue models setup

Lithosphere-scale analogue models have been performed, at the Tectonic Laboratory (TecLab) of Utrecht University. First, two reference models with no lateral strength variations consist of weak (model 1, M1, Fig. 2.2a) and intermediate strength (model 2, M2, Fig. 2.2b) profiles. Next, two equally sized compartments with weak and strong lithosphere (model 3, M3, Fig. 2.2c) and intermediate and strong lithosphere (model 4, M4, Fig. 2.2d) are combined. Lateral strength variations are achieved by increasing the thickness of the brittle layers in expense of the ductile layers across vertical boundaries. There is no weak zone added between the two lithospheric segments, but by placing these domains in direct contact a discontinuity in the system arises naturally. In our experiments, dry granular material such as feldspar and quartz sand represents the brittle crust and brittle mantle, whereas mixtures of Rhodorsil Gomme GSIR (RG) silicone with fillers embody the viscous layers (ductile crust and ductile mantle lithosphere; see table 1 for the material properties and scaling parameters).

The weakest strength profile (S1, Fig. 2.2e) consists of three layers, representing, from bottom to top, the strong part of the lithospheric upper mantle, the ductile lower crust and the brittle upper crust (Willingshofer et al., 2005). The stronger part of the upper mantle is represented by ductile Rhodorsil-gum layer with a density of 1503 kg/m^3 and an almost Newtonian viscosity (2 cm thickness), a second ductile Rhodorsil-gum layer with a density of 1407 kg/m^3 and an almost Newtonian viscosity represents the ductile lower crust (1 cm thickness). A brittle feldspar layer with a density of 1300 kg/m^3 with Mohr-Coulomb criteria represents the upper crust (1 cm thickness). The strength peak of this profile resides in the brittle upper crust. The

middle and strongest strength profiles (S2 and S3, Fig. 2.2f and 2.2g) both consist of four layers, a ductile Rhodorsil-gum layer (1.6 cm thick for S2 and 1.2 cm thick for S3) at the bottom of the model with a density of 1503 kg/m^3 , followed by a quartz sand layer with Mohr-Coulomb criteria and a density of 1503 kg/m^3 (0.4 cm thick for S2 and 0.8 cm thick for S3) that represent the strong part of the lithospheric mantle. The ductile lower crust is featured by a second Rhodorsil-gum layer with a density of 1.407 kg/m^3 and an almost Newtonian viscosity (thickness of 1.2 cm for S2 and 0.8 cm thickness for S3). The top layer depicts the upper crust and consists of feldspar sand with Mohr-Coulomb criteria and a density of 1300 kg/m^3 , the thickness being 0.8 cm for S2 and 1.2 cm for setup S3. The intermediate and strong strength profiles have two strength peaks, one in the brittle crust and another in the brittle mantle lithosphere (e.g. Brun, 1999).

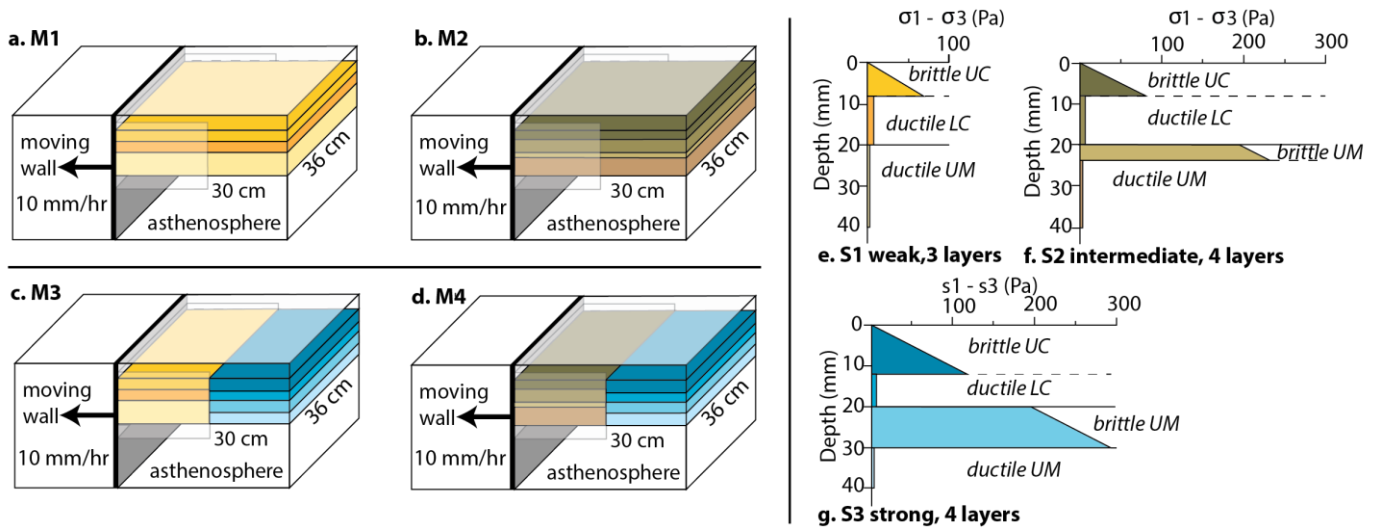


Figure 2.2. Experimental setup of the four analogue models (a-d) with rheological strength envelopes (e-g). a) Model 1 (M1), lateral homogeneous stratified strength profile S1 (weak, three layers, e). b) Model 2 (M2), lateral homogeneous stratified strength profile S2 (intermediate, four layers, f). c) Model 3, lateral variation in strength profile combining vertically stratified strength profile S1 (weak, three layers, e) and S3 (strong, four layers, g) and d) Model 4, lateral variation in strength profile combining vertically stratified strength profile S2 (intermediate, three layers, e) and S3 (strong, four layers, g). The black arrow indicates the direction of the moving wall (10 mm/hr, constant rate) that also holds the box-in-box. The layered lithosphere floats on a low viscosity high density fluid within the Plexiglas box. UC = upper crust, LC = lower crust, UM = upper mantle.

All models float on a heavy liquid consisting of a polytungstate-glycerol mixture, normally used for separating materials, with a density of 1600 kg/m^3 , to avoid the model from subducting (Fig. 2.2). This fluid represents the asthenosphere as well as the very weak part, with the least strength of the lithospheric mantle (Willingshofer et al., 2005). The used tank is transparent with one moving wall giving the model the dimension 36 x 30 cm. The total thickness of the lithosphere was kept the same at 4 cm for all models at the onset of extension, although strength variations may also be associated with thickness variations in nature (Burov and Diament, 1995). Following Allemand and Brun (1991), extension of the lithosphere was

implemented by a box-in-box construction. A small box that measured half of the model box' width was attached to the moving wall creating a velocity discontinuity at the long sides of the Plexiglas box (Fig. 2.2). One half of the box was attached to a wall that was pulled at constant rate of 1 cm/hr, which corresponds to 1.45 cm/yr in nature, perpendicular to the contact between lithosphere segments of variable strength (Fig. 2.2). During the experiments, top view photos were being made every 10 minutes. Models ran for a variety of time (3 to 8.5 hours).

2.2.2. Analogue model scaling

Analogue models are comparable with natural examples when three scaling criteria are fulfilled: geometric, dynamic and kinematic criteria.

For geometric scaling the modelled length ratios need to be equal in all directions (x (length), y (width) and z (depth), i.e. $X_m/X_n = Y_m/Y_n = Z_m/Z_n$). The reference models M1 and M2 consist of a lateral homogeneous setup of 36 x 30 x 4 cm. M3 and M4 consist of two types of strength profiles, with equal thicknesses (4 cm), widths (36 cm) and lengths (16 cm). With a scale-factor of 6.67×10^{-7} , this would represent 540 km x 480 km x 60 km in nature, or 1 cm is 15 km.

Dynamic scaling of the model with a natural example can be accomplished by respecting the stress-scale factor which includes of stress distribution, rheologies and densities (Hubbert 1937, Ramberg, 1981, Brun, 1999, Sokoutis, et al. 2005), $\sigma^*/L^* + \rho^* \times g^* - \rho^* (\varepsilon^*/t^*) = 0$, when conserving mass. The following conditions apply for the model:

$$\sigma^* = L^* \times \rho^* \times g^* \quad (\text{eq. 1})$$

$$\varepsilon^* = g^* \times (t^*)^2 \quad (\text{eq. 2})$$

where σ refers to stress, L to length, ρ to density, g to gravitational acceleration, ε strain and t to time. The asterisk indicates that the number is unit-less representing the ratio between the model and nature.

Experiments are carried out under normal gravity and therefore the gravity ratio (g^*) is equal to 1. The densities for the model and the natural example are in the same order of magnitude (e.g. 1300 kg/m^3 for the model and 2800 kg/m^3 for the natural example), hence the density ratio (ρ^*) is more or less equal to 1. This simplifies eq. 1 to:

$$\sigma^* = L^* \quad (\text{eq. 3})$$

or in other words, the ratio between the stresses and the length of the model and natural example need to be roughly equal (Davy and Cobbold, 1991). The last scaling criteria is the kinematic scaling, where the model and the natural example abide a timescale that is proportional to the changes in shape and/or position in both the model and natural example (so $t_m/t_n = t_{m2}/t_{n2} = t_{mx}/t_{nx}$ etc.). Since velocity is given by length/time, the model can be scaled with respect to the prototype with the following equation:

$$V_n = V_m \times ((L_n \times t_m) / (L_m \times t_n)) \quad (\text{eq. 4})$$

Table 2.1. Physical properties for experimental material and comparison of lithosphere and experiments.

Layer	Analogue material	Density		Layer thickness model (m)	Layer thickness nature (m)	Friction coefficient μ	Cohesion C (Pa)	Viscosity		Power $\dot{\eta}$	Rm model	Rm nature
		ρ (kg/m ³) model	ρ (kg/m ³) nature					η (Pa s) model	η (Pa s) nature			
Upper crust	Feldspar sand	1300	2700	0.012	2.20E+04	0.4-0.7	15-35					
		0.008		0.008	1.47E+04	0.4-0.7	15-35					
		0.006		0.006	1.10E+04	0.4-0.7	15-35					
Lower crust	Rhodorsil gum mixed with PDMS	1407	2900	0.012	2.20E+04			2.35E+04	1.00E+21	9.70E-01	3.04E+01	3.02E+01
				0.008	1.47E+04			2.35E+04	1.00E+21	9.70E-01	1.35E+01	1.36E+01
Brittle mantle lithosphere	Quartz sand	1500	3100	0.008	1.47E+04	0.6	30-70					
				0.004	7.34E+03	0.6	30-70					
High viscous mantle lithosphere	Rhodorsil gum mixed with PDMS	1503	3100	0.02	3.67E+04			1.88E+04	1.00E+22	1.9159	1.13E+02	2.15E+01
				0.016	2.94E+04			1.88E+04	1.00E+22	1.9159	4.07E+01	3.23E+00
				0.012	2.20E+04			1.88E+04	1.00E+22	1.9159	7.23E+02	6.12
Asthenosphere	Sodium polytungstate	1600	3200									

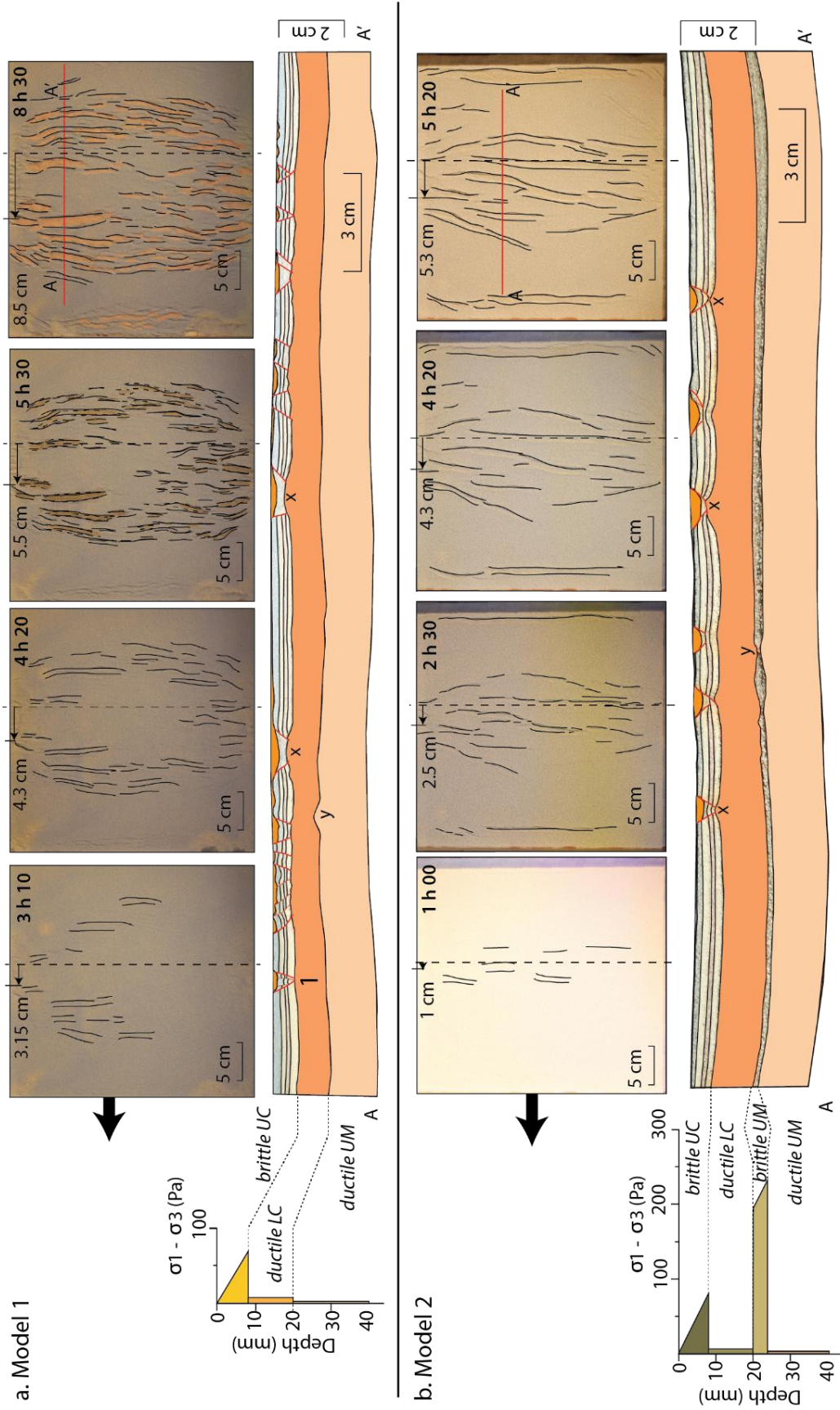
where V_n is velocity in nature, V_m is velocity in the model, L_n is length in nature, L_m is length in the model, t_n is time in nature and t_m is time of the model. With a modelled 1 cm/hr extension rate (V_m) the natural velocity is 1.45 cm/yr, which is comparable to the average extension rate in the South Atlantic domain (Müller et al., 2008). Table 1 lists all the properties of experimental materials and a comparison to lithosphere properties.

2.3. Modelling results

The results of the four analogue experiments with varying continental lithospheric strengths are presented here. The models with laterally uniform strength profiles have extended for 8.5 cm (127.5 km in nature, M1, Fig. 2.3a) and 5.3 cm (79.5 km in nature, M2, Fig. 2.3b). Both show that the brittle crust accommodates extension through normal faults that outline horst and graben, half-graben and tilted fault block geometries. Faults grow either through laterally propagating graben structures or by coalescence of individually developed fault segments to form structures features that span the entire width of the models (map views, Fig. 2.3a and Fig 2.3b). Asymmetric structures such as tilted blocks, half grabens or slightly asymmetric grabens exist on the scale of the brittle crust, but the overall deformation is symmetric, both on the scale of the individual layers as well as the entire lithosphere. With reference to the moving wall, the extensional structures develop randomly, not in sequence. This shows that deformation is evenly distributed. None of the structures developed into a major rift that would eventually lead to a break-up system. One important observation are the pinch and swell structures that develop in the brittle mantle of M2. This shows that deformation is also accommodated by deeper, brittle layers. The most important difference observed on the cross-sections between the above described experiments is that grabens in M1 are distributed over a distinctly wider area as opposed to M2 (compare Figs. 2.3a and 2.3b).

The combined weak (S1) and strong lithospheres (S3) has accommodated 3.2 cm of extension (48 km in nature, M3, Fig. 4a). This model develops deformation exclusively in the weak lithosphere. The structural style is similar to M1 with graben and half graben in the brittle crust and flow dominated deformation in the ductile layers. The more pronounced exhumation of the lower crust to shallow levels (location x, Fig. 4a) and a more distinct Moho topography are the consequence of extension being focused within a less wide segment of lithosphere compared to M1.

Figure 2.3 (next page). Experimental results of models with one type of lithosphere a) Model 1 (M1) and b) Model 2 (M2). Wide rifts form in both models, M2 being 25% less wide than M1 due to the presence of a stronger sub-Moho mantle. Ductile lower crust is exhumed (positions x, M1 and M2). Moho topography shows subtle long wavelength undulations, generally not in phase with the graben structures indicating the flow of material. Pinch and swell structures form in the brittle lithospheric mantle of M2 (position y). BC = brittle crust, DC = ductile crust, BM = brittle mantle, DM = ductile mantle.



The finite lithosphere-scale geometry of the model is asymmetric as a consequence of thinning of the weak lithosphere (S1) from 4.0 cm to 2.6 cm (35% thickness decrease). The combined intermediate (S2) and strong (S3) lithosphere has accommodated 6.2 cm of extension (93 km in nature, M4, Fig. 4b), also developed deformation structures solely within the relatively weaker (S2) lithosphere (Fig. 4b).

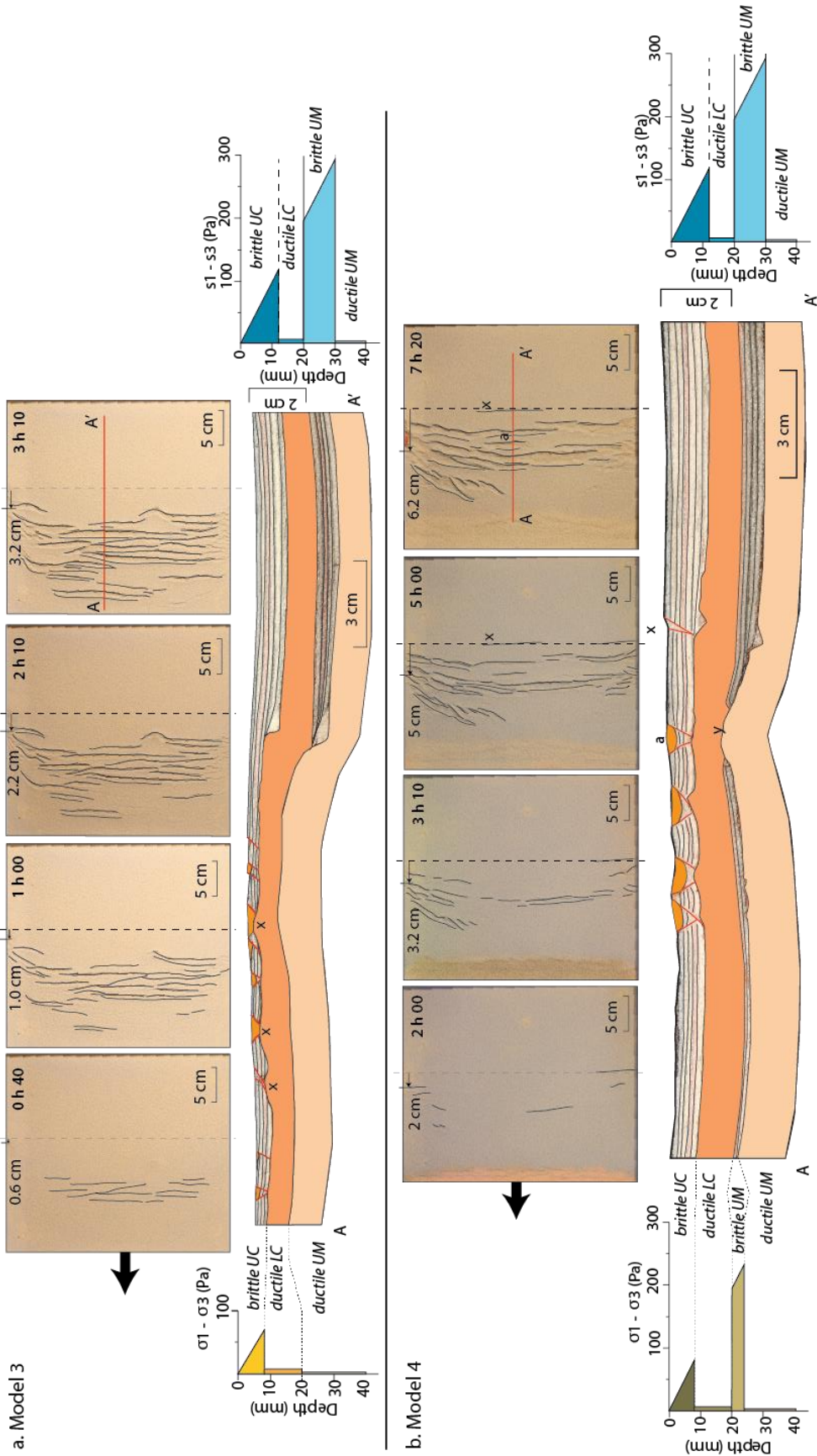
Deformation in the brittle crust is symmetric with a series of grabens that exhume lower crust material. Faulting affects the brittle layers in M4 until the boundary between the two lithosphere segments (Fig. 4d, position x). Different to M3, extension in M4 led to necking of the mantle lithosphere and exhumation of the ductile mantle layer where the brittle mantle broke and got separated (Fig. 4b, position y). This region of maximum thinning of the mantle lithosphere is only matched by the location of one of the grabens within the crust that developed late in the evolutionary sequence (graben a, Fig. 4b). Overall, narrow and localized deformation within the mantle lithosphere is compensated by distributed deformation within the crust. Besides thinning at the area of necking (4.0 cm to 2.6 cm, 35% thickness decrease), minor thickness change occurred within the mantle lithosphere of the intermediate-strength (S2) lithosphere (4.0 cm to 3.6 cm, 10% thickness decrease). For both M3 and M4 the strong segment kept its original thickness.

2.4. Implications for rift geodynamics

2.4.1. Rheological control on the locus of extension in continental lithosphere with lateral strength variations

Our experiments consistently predict that extension of continental lithosphere with lateral strength variations will lead to stretching of the relatively weaker (S1 or S2) lithosphere (Fig. 4, M3 and M4). Unexpectedly, deformation never initiates at the location where the rheological contrast is largest (at the transition of the weaker to stronger lithosphere) but always starts within the weaker segment and never propagates into the stronger one. This behaviour is different to convergent settings where deformation tends to localize at transitions from stronger to weaker and vice versa crust or lithosphere (e.g. Calignano et al., 2015b; Munteanu et al., 2014; Willingshofer et al., 2005). However, in an orthogonal rifting setting, simulated with a centrifugal experimental apparatus, similar results have been modelled, where the cratonic, strong part of the model remains rather unreformed and in the weaker segment, wide rift structures are observed (Bonini et al., 2007).

Figure 2.4 (next page). Experimental results of homogeneous lithospheric setup a) Model 3 (M3) and b) Model 4 (M4). M3 and M4 show that all extension is accommodated in the weak segment. The thickness of the weak segment of M3 decreases with 35% in a distributed fashion. In the weak segment of M4 the sub-Moho mantle has lost its strength and thickness decreases with 35% at the necking domain (Fig 4b, position y). The original thickness of the strong domains of both models remains. BC = brittle crust, DC = ductile crust, BM = brittle mantle, DM = ductile mantle.



2.4.2. *Rift evolution during extension of continental lithosphere with laterally varying strength*

In our experiments extension affects large parts of the weaker lithosphere, whereby the width of deformation is regulated by the degree of coupling among the layers that constitute the lithosphere. The width of the deformed zone is wider when layers are coupled (M1, Fig. 3a, and M3, Fig. 4a) and narrower by 40-50% when layers are less well coupled (M2 and M4). This behaviour is consistent with analogue modelling studies by Brun (1999). During distributed extension the ductile mantle rises below the larger grabens, leading to significant exhumation of the mantle lithosphere (Brun and Beslier, 1996; Corti et al., 2011) as often observed along passive margins (Manatschal et al., 2015). Rift localization and architecture is controlled partly by the extension rate (Brun, 1999). We argue that the switch from distributed to localized deformation through time is also controlled by the strength of the sub-Moho mantle. This strength decreases during the initial distributed rifting phase (Fig. 5a-c) after which a localized weaker zone emerges (Fig. 5d) that develops into the necking domain (M4, Fig. 5e) and eventually exhumes lower crust and mantle (Fig. 5f).

2.4.3. *Final rift geometries*

The final rift and break-up geometry can be interpreted in two different ways, depending on the scale. If the final rift geometry is only regarded from the 'rifted domain' point of view (small black box Fig. 5), the margins have equal thicknesses and look rather symmetric. Only the basin distribution on both margins might be different, but this depends largely on location where the resistant upper mantle mantle fails, which does not have to be exactly in the centre of the initial distributed rift (see section 4.2). On this scale, the break-up results from pure-shear deformation and the margin geometries appear symmetric. If, on the other hand, the complete system is taken into account (big red box, Fig. 5) when observing the final rift geometry, the margins seem asymmetric, because the crustal thicknesses are quite different and the basin distribution is far from equal. The margins of the Central Segment have been interpreted as rather symmetric (Blaich et al., 2011) in terms of crustal thickness of the continent side of both margins as well as the width of the transition zone. The margins of the South Segment show more asymmetric features (Blaich et al., 2011) with the African side of the continent being thicker (40 km, Maystrenko et al., 2013) compared to the South American side (25-30 km, Schnabel et al., 2008). Also in terms of width of the transition zone does the African side show a much wide transition zone than the South American side (Blaich et al., 2011). Both the Central and South segments of the South Atlantic domain can be explained by the analogue model presented in this paper, depending on the scale the break-up system is looked at only the rifted zone or also outside of the rift zone.

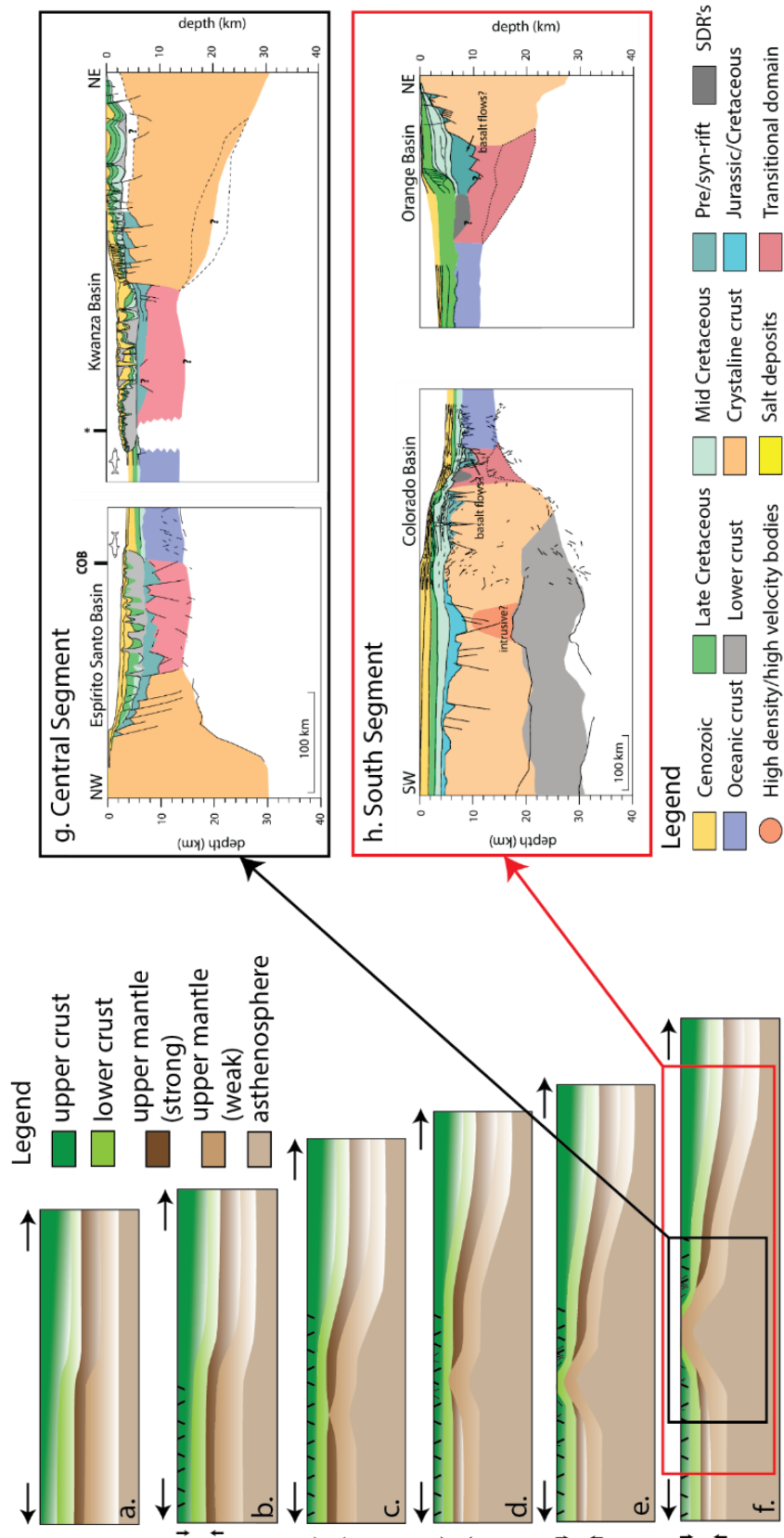


Figure 2.5 (previous page). Cartoon showing the two-phased conceptual evolution of continental break-up in a system consisting of two large lithosphere segments. Phase 1 (a-c): distributed rift formation, Phase 2 (d-e): localized deformation. Continuous extension will eventually lead to breakup above the necking point that formed during the second phase, resulting in asymmetric margins in terms of thickness and basin positioning. The scale on which the final results are regarded can be 'rift-wide' (red box), which has symmetric geometries and is comparable to the g) Central Segment continental margin in terms of crustal thickness or 'system-wide' (purple box) which gives asymmetric geometries and is comparable to the h) South Segment continental margins in terms of crustal thickness, width of transitional domain and basin distribution on either side of the margin.

2.5. Conclusion

We investigated the deformational response to extensional, far-field forces on continental lithosphere with lateral strength variations. Lithospheres with a lateral strength variation only develop deformation structures in the weaker lithosphere, not at the contact between the two segments. The weaker segment thins, whereas the strong segment preserves its original thickness, resulting in an asymmetric rift geometry. Models including a strong sub-Moho mantle develop a necking zone and their evolution is two-phased with 1) a distributed rift phase with normal fault systems throughout the weak segment and 2) a localized rift phase that forms once the strong sub-Moho mantle suffers strength failure and develops a necking zone. This two phase evolution forms asymmetric margins with different crustal thicknesses and lengths depending on the scale the system is looked at. When only taking into account the rifted domain, the margin geometries are symmetric and compare well with the margins of the Central Segment of the South Atlantic. When including the whole initial domain in the interpretation of margin geometries, asymmetry is observed which is coherent with observations along the South Segment margins of the South Atlantic domain. The unequal distribution of basins is highly dependent on the location of failure of the strong part of the upper mantle.

Highlights:

- Extension is accommodated in the rheological weak segment, not at the contact between two segments
- When a strong sub-Moho mantle is present the system develops in two phases
- Final margin geometries would be asymmetric in terms of crustal thickness and basin distribution if extension continues.

Chapter 3: Numerical models for continental break-up: implications for the South Atlantic

Summary

The results from the previous chapter explain well the difference in geometry observed along the margins of Central Segment and South Segment the South Atlantic domain. The biggest drawback however is that thermal processes have not been taken into account. In the South Segment a deep rooted mantle plume is present which supposedly had some influence on the development of the margins in this segment, for example the presence of volcanic material (Seaward Dipping Reflectors (SDR's) which are absent along the margins in the Central Segment, as well as the presence of high velocity/high density bodies at depth.

The question that arises is therefore how do thermal perturbations in the mantle influence rift initiation and break-up and the development of margin geometries?

To address this problem the 2D thermo-mechanical FLAMAR code has been used that couples rheological parameters and the heat equation and solves for temperature and displacement. The drawback is the 2D nature of the code which includes the assumption of a cylindrical continuation of the model box in the third dimension to compare the results to nature. The code has the advantage that calculation times are moderate, it include complex geometries, the thermal state of the lithosphere and it allows topography to develop freely. An erosion coefficient also accounts for vertical lithosphere processes that are affected by the removal and deposition of material. Even though this version of the code does not include phase changes to account for the formation of oceanic crust, the break-up locations and margin evolution can be simulated and compared to data along the margins of the South Segment of the South Atlantic.

The rheological parameters chosen for this setup are based on work by previous authors and assumes that the upper crust consists of silica (quartz, dry or wet) the lower crust of diabase, which behaves in a less viscous manner and a mafic upper mantle (peridotite/olivine). In laboratories the rheological parameters have been quantified in more than one way. To arrive at a strength profile that was suitable for this exercise multiple yield-stress-envelopes have been calculated after which a relatively weak and strong profile have been chosen to account for the different strength of rheological segments. No weak seeds are included, the contact between the two lithospheric segments and the presence of the mantle plume are sufficient to let develop the model internally and not at the borders of the model box.

The results show that as soon as the thermal state of the lithosphere is taken into account and a mantle anomaly is added to a complex system consisting of multiple lithosphere segments with different rheological strength, not just one mode of break-up is possible but several different modes. This is highly dependent on the initial location of the mantle anomaly. It is thus extremely important to put a plume at the correct location in the model as this greatly influences the model results. For the margins of the South Segment, a plume location slightly offset from the contact between the lithospheric segments gives results that compare best to the present-day margin geometries.

Abstract

We propose a mechanism that explains in one unified framework the presence of continental break-up features such as failed rift arms and high-velocity and high-density bodies that occur along the South Atlantic rifted continental margins. We used 2D and 3D numerical models to investigate the impact of thermo-rheological structure of the continental lithosphere and initial plume position on continental rifting and breakup processes. 2D experiments show that break-up can be 1) “centred”, mantle plume-induced and directly located above the centre of the mantle anomaly, 2) “shifted”, mantle plume-induced and 50 to 250 km shifted from the initial plume location or 3) “distant”, self-induced due to convection and/or slab-subduction/delamination and 300 to 800 km off-set from the original plume location. With a 3D, perfectly symmetrical and laterally homogenous setup, the location of continental break-up can be shifted hundreds of km’s from the initial position of the mantle anomaly. We demonstrate that in case of shifted or distant continental break-up with respect to the original plume location, multiple features can be explained. Its deep-seated source can remain below the continent at one or both sides of the newly-formed ocean. This mantle material, glued underneath the margins at lower crustal levels, resembles the geometry and location of high velocity/high density bodies observed along the South Atlantic conjugate margins. Impingement of vertically up-welled plume material on the base of the lithosphere results in pre-break-up topography variations that are located just above this initial anomaly impingement. This can be interpreted as aborted rift features that are also observed along the rifted margins. When extension continues after continental break-up, high strain rates can relocalize. This relocation has been so far attributed to rift jumps. Most importantly, this study shows that there is not one, single rift mode for plume-induced crustal break-up.

Reference: Beniést, A., Koptev, A., Burov, E., 2017. Numerical models for continental break-up: implications for the South Atlantic. Earth and Planetary Sciences Letters, 461, p. 176-189.

3.1. Introduction

Over the last decades a large variety of rift features have been recognised and explained with different methods and different concepts. These features include for example aborted rift structures, anomalous topography or anomalously high velocity/high density bodies located in the lower crust. Explanations for anomalous features often link one mechanism with one observed rift feature. For example, on plume impingement, a stratified lithospheric rheology (e.g. D’Acremont et al., 2003; Burov et al., 2007;) would result in topographic uplift, as has been modelled with thermo-mechanical modelling. Forward modelling shows that magmatic underplating can cause topographic variations (Hirsch et al., 2010). Anomalously high velocity/high density bodies have been observed on tomographic images below the continents, implying that in some regions magmatic processes dominate rifting (Cornwell et al., 2006). The latter is also suggested by gravity modelling that revealed the presence of anomalously high-density bodies in e.g. the South Atlantic domain, implying that volcanic activity played a key role in margin development (Blaich et al., 2011; Maystrenko et al., 2013b).

Review papers combine all these studies on one specific topic. Examples are the role of the Moho in extensional settings (Cloetingh et al., 2013), the effect of volcanism in rifting and continental break-up (Franke, 2013) or the dynamic processes that control rifting (Ziegler and Cloetingh, 2004).

With this study we demonstrate how one break-up mechanism can explain a multitude of features. We use the South Atlantic break-up as our case study for plume-induced continental break-up. Since the South Atlantic developed diachronously and it is a very complex region requiring a 3D approach, we have not the intention to reproduce the South Atlantic evolution as such, including along-axis northward break-up propagation to close to the plume (Franke, 2013), but rather to address general observations on continental break-up. Our fully coupled lithospheric-grade 2D and 3D models have an explicit elasto-visco-plastic rheology that accounts for realistic deformation of the lithosphere and a slip free surface that can calculate vertical motions. The 2D model has proven to be very useful to investigate plume-lithosphere interactions (e.g. d’Acremont et al., 2003; Burov et al., 2007). We take it one step further by developing one scenario to explain multiple anomalous features, such as high-velocity/high-density bodies and anomalous topographic variations with one single model. The 3D model is used to include the lateral component in a very simple, completely lateral homogeneous setting (Koptev et al., 2016).

3.2. Geological and geophysical setting

3.2.1. South Atlantic opening

Initial extension between Africa and South America was accommodated along a former fold-and-thrust belt (present-day location see Fig. 3.1), known as the Gondwana Fold Belt (GFB) or the Cape Fold Belt (CFB). This fold-and-thrust-belt was reactivated during the Early Mesozoic as a strike-slip system before the

opening of the South Atlantic (Cobbold et al., 1992). During this reactivation it weakened the South American plate prior to the development of the Atlantic Mid-Oceanic Ridge, forming a first set of extensional basins (Autin et al., 2013), their axes oriented obliquely to the present-day orientation of the spreading centre (Fig. 3.1).

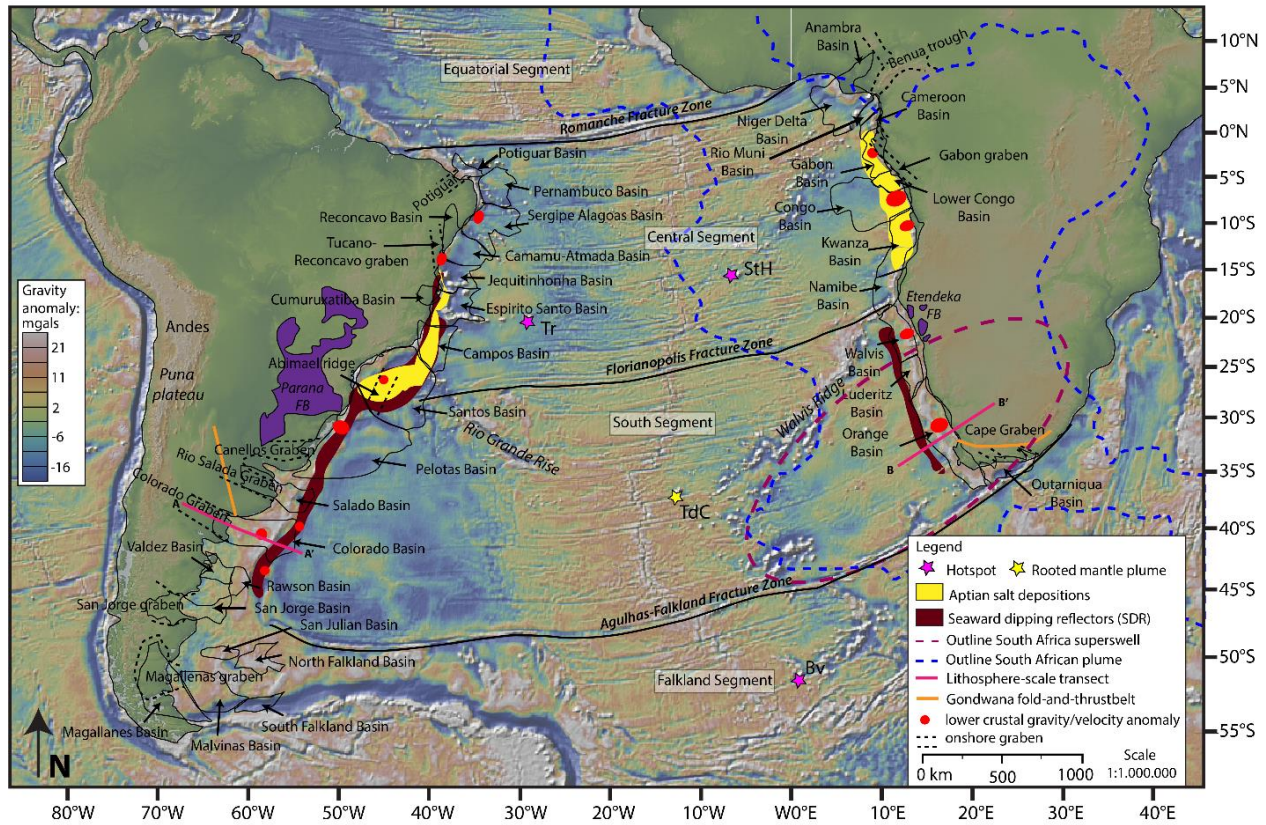


Figure 3.1. Map of the South Atlantic domain with the location of large fracture zones, high velocity bodies (red ellipsoids), onshore graben structures (black dashed lines), the outline of the African Super Plume (dashed green line, after Davaille et al. (2015)) and the African superswell (dashed red line, after Nyblade and Robinson, 1994). Also shown are the extent of the Seaward Dipping Reflectors (SDR's, blue after Moulin et al., 2010 and green after Torsvik et al., 2009) and the Aptian salt (yellow, after Torsvik et al., 2009) deposits. The orange line gives the location of the Gondwana Fold-and-Thrust-Belt. Pink solid lines mark locations of the lithosphere-scale cross-sections (South America: A-A'; South Africa: B-B', Fig. 3.2). Hotspots (red stars): Tr = Trinidad hotspot; StH = Saint Helena hotspot; Bv = Bouvet (Meteor) hotspot; Deep-rooted mantle plume (yellow star): TdC = Tristan deep-rooted hotspot.

Several extensional pulses caused the opening of the South Atlantic between 134 Ma and 113 Ma (e.g. Torsvik et al., 2009; Moulin et al., 2010). Voluminous volcanic activity, recognised on seismic reflection profiles as 'Seaward Dipping Reflectors' (SDR's) in the form of aerial flood basalts (extrusive) and/or underplating (intrusive) accompanied an episode of extension that created the South Segment (Fig. 3.1), starting between 134 Ma and 132 Ma (Moulin et al., 2010). Another pulse contributed to the formation of

the Central Segment, starting around 112 Ma (Moulin et al., 2010) and is marked by massive salt deposits that have not been found along the margins of the South Segment (Fig. 3.1, Torsvik et al., 2009). Only minor volcanic activity has been recorded in this segment as the typical SDR's are mostly absent, except just north of the Rio Grande Rise (Franke, 2013). The opening of the South Atlantic and formation of the Mid-Atlantic Ridge is considered to be due to a combination of passive far-field forces (Husson et al., 2012) and the presence of different hotspots (Torsvik et al., 2009). A major far-field stress component that enhanced the growth of the South Atlantic domain during the Mesozoic is the subducting and 'pulling' Nazca plate to the west of the South American continent, which also resulted in the faster west-ward migration of the South American plate with respect to the almost stationary African plate (e.g. Husson et al., 2012). The South-African super plume rises from the core-mantle boundary (CMB) to below the mantle transition zone (Hassan et al., 2015) which is reflected in present-day topography by a "superswell" at the margins of the south-west African continent (Nyblade and Robinson, 1994; Davaille et al., 2005). As shown by amongst others Lithgow-Bertelloni and Silver (1998), this excess of topography elevation is dynamically supported by upwelling flow of buoyant material through the mantle. From this large-scale, lower mantle low-velocity anomaly, the hotspots and their tracks (e.g. the Bouvet (Meteor), the Trinidad and St Helena Hotspots (Torsvik et al., 2006,2009)) and the only deep rooted Tristan plume (Fig. 3.1, Torsvik et al. (2009) and references therein) might develop over a long period of time (~200 Myr).

3.2.2. *Lithosphere structure margins*

The selected profile for our 2D model connects the offshore southwest Africa Orange Basin and its conjugate with the Colorado basin on the South American side (pink line, Fig. 3.1). The Tristan hotspot lies actually in the middle of the two transects (Fig. 3.1). The present-day crustal and lithosphere structure of these margins is constrained by combining published work on deep seismic refraction data, tomography, gravity and magnetic studies (Fig. 3.2). On the African side of the transect (Fig. 3.2a) the lithosphere thickness ranges from 120 km below the oceanic crust to 200 km below the continent (Fishwick, 2010). With gravity modelling and seismic interpretation the Moho-depth has been estimated to be less than 10 km below the oceanic crust of the Orange basin and over 40 km below the continent (Maystrenko et al., 2013b). Even though crustal movements have been observed in central Africa, the southern African plate is considered relatively stable with a strong rheology (Heine et al., 2013).

On the South American side the lithosphere-asthenosphere boundary (LAB) reaches depths of 160km below the stable continent in Eastern Brazil and 120 km in below the continent in Central Argentina (Heit et al., 2007). The Moho depth varies between 70 km below the plateau in the Andean orogeny to 25-35 km below the flat continent (Van Der Meijde et al., 2013). For the Colorado basin specifically, deep refraction seismic studies reveal a crustal thickness of the margins of 30 km (Franke et al., 2006).

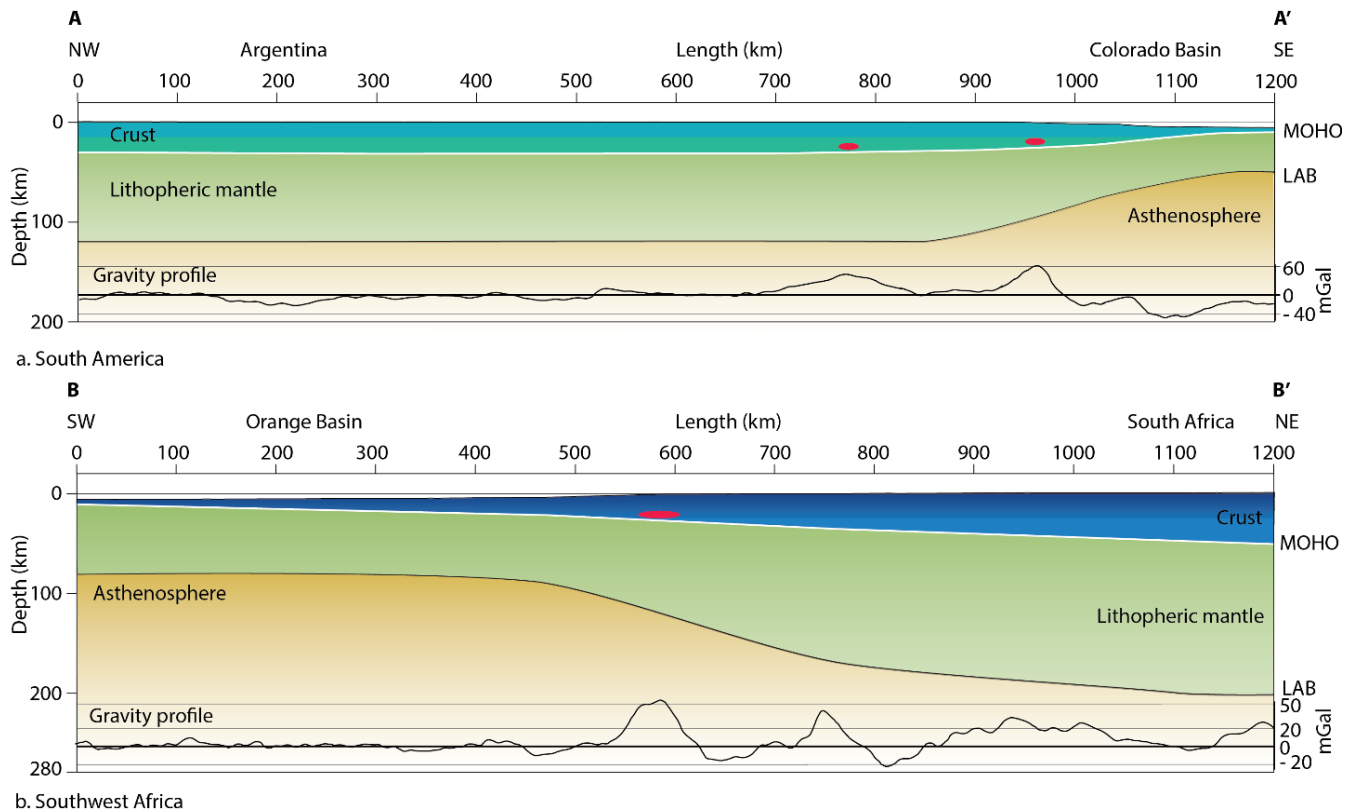


Figure 3.2. Lithosphere scale cross-sections of present-day South Atlantic margins. The Moho depth varies from 10 to 30 km on the South American side from ocean to continent (Schnabel et al., 2008). On the African side the depth varies from less than 10 km to over 40 km, ocean to continent (Maystrenko et al., 2013b). The lithosphere-asthenosphere boundary (LAB) varies from 50 km to 120 km, ocean to continent for Colorado basin on the Argentinean margin (Heit et al., 2007). The Orange Basin on the South African margin has a LAB depth ranging between 80 km and 200 km from ocean to continent (Fishwick, 2010). The location of anomalous bodies is depicted (in green) for the Colorado Basin (Schnabel et al., 2008) and the Orange Basin (Maystrenko et al., 2013b). The gravity profile has been extracted from the global marine gravity map of Sandwell and Smith v18.1 (Sandwell and Smith, 2009).

We assume that before continental break-up, the lithosphere thickness of the South American plate was similar to that of the African plate. However, the South American plate underwent an earlier deformation phase prior to the formation of the South Atlantic domain (Autin et al., 2013). Extensional deformation does result in lithospheric thinning and weakening (Ziegler and Cloetingh, 2004). We, therefore, adopt a weaker strength compared to the African plate and a thickness of 180 km, which is the mean between the 200 km of the African lithosphere and the present-day 160 km South American lithosphere, to account for this earlier deformation phase.

3.2.3. *High velocity/high density bodies and aborted rift structures*

Along the South Atlantic conjugate margins high velocity/high density bodies have been described at lower crustal depths below the continent and the margin (Fig. 3.1) using seismic data and gravity modelling. Anomalous gravity and velocity bodies have been noted in the Central segment on the African side from Gabon (Dupré et al., 2007) to the Lower Congo (Contrucci et al., 2004) and the Kwanza Basin (Blaich et al., 2011) and on the South American side from the Sergipe-Alagoas Basin (Mohriak et al., 2000), to the Camamu-Atmada basin (Blaich et al., 2011) and the Santos basin (Blaich et al., 2011). In the South segment on the African side these bodies have been observed in the Walvis Basin (Blaich et al., 2011) and the Orange Basin (Dressel et al., 2015) and on the South American side in the Colorado basin, along the Uruguayan margin (Clerc et al., 2015) and in the deep Argentina Basin (Franke et al., 2006; Schnabel et al., 2008). These bodies differ from the seaward-dipping reflectors (SDR) as they are situated at the base of the lithosphere or at lower crustal levels and do not necessarily have a magmatic origin. They could be serpentinized mantle or mafic and ultramafic crustal rocks (Fig. 3.2, Blaich et al., 2011).

Graben structures or aborted rift structures onshore along the whole South American margin of the South Atlantic domain (Burke, 1976), are located near the anomalously high velocity/high density bodies. In the South Segment, graben structures and failed rift structures are less-abundant along the African margin, where they appear mainly along the south South-African margin and in the Central segment along the Gabon and Benin margins. On the South American side of the South Segment, the basins oriented perpendicular to the present-day ridge extend onshore as aborted rift features (Burke, 1976). Another failed rift feature is observed in the southwestern part of the Santos Basin, where the now aborted Abimael ridge is located parallel to the present-day Mid Oceanic Ridge (Heine et al., 2013).

3.3. Model setup

The 2D thermo-mechanical numerical code FLAMAR, based on the FLAC-Para(o)voz algorithm (Cundall, 1989; Poliakov et al., 1993) has been used to investigate the effect of plume location on continental break-up using the South-Atlantic as an example of a fully developed rift-to-spreading system. We built our case on the continuation of earlier parametric studies on the rheology of the lithosphere and plume-continental lithosphere interactions (D'Acremont et al., 2003; Burov et al., 2007). Where needed, we adjust the parameters according to the geological and geophysical evidence described above. A symmetric simulation that is not area-specific are carried out with the 3D viscous-plastic numerical code 3DELVIS (Gerya and Yuen, 2007). All mechanical and thermo-rheological parameters are listed in table 3.1. We have performed a series of 36 experiments. Controlling parameters and principal results are summarized in table 3.2.

Thermal parameters	Thermal property	Value	Unit	Ref.
	Surface temperature	10	°C	1
	Temperature at the base of the thermal lithosphere	1330	°C	
	Temperature at the base of the upper mantle	1400	°C	
	Temperature mantle anomaly	1700	°C	
	Thermal conductivity crust	2.5	W/m °C	
	Thermal conductivity mantle	3.5	W/m °C	
	Radiogenic heat production at the surface	1.5e-9	W/kg	
	Radius radiogenic heat	10	km	
	Thermo-tectonic age of the lithosphere	500	myr s	
	Surface heat flow	40	mW/m ²	
	Mantle heat flow	15	mW/m ²	
Mechanical parameters	Mechanical property	Value	Unit	Ref.
Strong upper crust <i>Dry quartz</i>	Density	2600	kg/m ³	2
	Viscosity parameter N	3		
	Viscosity parameter A	6.8e-6	MPa ⁻ⁿ s ⁻¹	
	Viscosity parameter E	1.56e5	J/mol	
Strong lower crust <i>Strong diabase</i>	Density	2850	kg/m ³	3
	Viscosity parameter N	3.05		
	Viscosity parameter A	6.3e-2	MPa ⁻ⁿ s ⁻¹	
	Viscosity parameter E	2.76e5	J/mol	
Weak upper crust <i>Wet quartz</i>	Density	2500	kg/m ³	2
	Viscosity parameter N	2.3		
	Viscosity parameter A	3.2e-4	MPa ⁻ⁿ s ⁻¹	
	Viscosity parameter E	1.54e5	J/mol	
Weak lower crust <i>Weak diabase</i>	Density	2750	kg/m ³	4
	Viscosity parameter N	4.7		
	Viscosity parameter A	1.9e2	MPa ⁻ⁿ s ⁻¹	
	Viscosity parameter E	4.85e5	J/mol	
Lithospheric mantle <i>Peridotite</i>	Density	3330	kg/m ³	2
	Viscosity parameter N	3.5		
	Viscosity parameter A	2.5e4	MPa ⁻ⁿ s ⁻¹	
	Viscosity parameter E	5.32e5	J/mol	
Asthenosphere <i>Olivine</i>	Density	3310	kg/m ³	3
	Viscosity parameter N	3.2		
	Viscosity parameter A	7.0e3	MPa ⁻ⁿ s ⁻¹	
	Viscosity parameter E	5.1e5	J/mol	
Plume <i>Olivine</i>	Density	3250	kg/m ³	3
	Viscosity parameter N	3.5		
	Viscosity parameter A	5.e14	MPa ⁻ⁿ s ⁻¹	
	Viscosity parameter E	5.2e5	J/mol	
	Friction angle	30	°	
	Lamé elastic constant $\lambda = G$	25	GPa	
	Cohesion	20	MPa	
	Erosion coefficient (a)	500	m ² /yr	5

Table 3.1. Summary of the thermal and mechanical parameters used for this study. 1) Turcotte and Schubert (2002), 2) Ranalli (1995); 3) d'Acromont et al. (2003) and references therein; 4) Tsen and Carter (1987); 5) Burov and Poliakov (2001).

3.3.1. 2D numerical model

The FLAMAR code has been updated and modified over the last 20 years (Burov and Diament, 1995; Burov and Poliakov, 2001; Le Pourhiet et al., 2004; Yamato et al., 2008). For the sake of coherency with previously published papers we only describe the main features and essentials of the model used for this study. Detailed descriptions of the code can be found in Appendix I of this manuscript and in other studies that have tested the code for many different geological cases (D'Acremont et al., 2003; Le Pourhiet et al., 2004; Yamato et al., 2008). FLAMAR is a fully explicit, finite element/finite difference code based on a Cartesian coordinate frame. It has a 2D strain formulation with a Lagrangian mesh that consists of quadrilateral elements consisting of two couples of triangular sub-elements containing tri-linear shape functions. It uses a large-strain, time-marching scheme. The code solves for full Newtonian equations of motions in a continuum mechanics approximation (3.1)

$$\langle \rho \ddot{\mathbf{u}} \rangle - \nabla \sigma - \rho \mathbf{g} = 0 \quad (3.1)$$

where ρ , $\ddot{\mathbf{u}}$, σ and \mathbf{g} stands for density, acceleration of the object, stress and acceleration due to body forces or gravity, respectively.

It is coupled with constitutive laws (3.2) to quantify viscous, elastic and plastic characteristics by the heat transfer equation (3.3), where the heat advection term ($\dot{\mathbf{u}} \nabla T$) is included in the Lagrangian derivative (DT/Dt). Erosion and sedimentation is accounted for using a linear diffusion equation assuming conservation of mass (3.4).

$$\frac{D\sigma}{Dt} = F(\sigma, \mathbf{u}, \dot{\mathbf{u}}, \nabla \dot{\mathbf{u}}, T) \quad (3.2)$$

$$\rho C_p DT/Dt - k \nabla^2 T - \sum_i^n H_i = 0; \quad \rho = f(P, T) \quad (3.3)$$

$$\frac{dh}{dt} = a \nabla^2 h \quad (3.4)$$

In this case, t stands for time, \mathbf{u} is the displacement vector, and T is temperature. The heat transfer equation relies on C_p for the specific heat, k for thermal conductivity respectively and H for the internal heat production, including radiogenic heat and frictional heat dissipation. P stands for pressure that become negative for compression. The linear diffusion equation uses a constant a and the height or thickness of the sediments h .

The code is capable of calculating realistic visco-elasto-plastic rheologies explicitly. Pressure-dependent deformation is maintained through the Mohr-Coulomb criteria for the plastic regime and the non-linear viscous flow law at depth. The free surface upper boundary condition calculates high-resolution topographic changes due to deformation of the lithosphere.

Controlling parameters and principal results of the experiments.

Exp. No.	Controlling parameters				Mantle plume properties				Results								
	Boundary conditions		Extension rate (right)		Plume location		Density (kg/m^3)		Initial geometry		Break-up point		Break-up above center anomaly		Break-up mechanism		Figure
	Extension rate (left)	Extension rate (right)	Extension rate (left)	Extension rate (right)	Plume location	Diameter (km)	Density (kg/m^3)	Diameter (km)	Setup	Break-up point	Break-up above center anomaly	Break-up mechanism	Figure				
1	12.5 mm/yr	12.5 mm/yr	12.5 mm/yr	12.5 mm/yr	800 km	230	3250	230	Setup 1a	800 km	yes	Central	5a				
2	12.5 mm/yr	12.5 mm/yr	12.5 mm/yr	12.5 mm/yr	1000 km	230	3250	230	Setup 1a	1500 km	no	Distant					
3	12.5 mm/yr	12.5 mm/yr	12.5 mm/yr	12.5 mm/yr	1200 km	230	3250	230	Setup 1a	1200 km	yes	Central					
4	12.5 mm/yr	12.5 mm/yr	12.5 mm/yr	12.5 mm/yr	800 km	230	3250	230	Setup 1b	800 km	yes	Central					
5	12.5 mm/yr	12.5 mm/yr	12.5 mm/yr	12.5 mm/yr	1000 km	230	3250	230	Setup 1b	1000 km	yes	Central					
6	12.5 mm/yr	12.5 mm/yr	12.5 mm/yr	12.5 mm/yr	1200 km	230	3250	230	Setup 1b	1200 km	yes	Central	4a				
7	12.5 mm/yr	12.5 mm/yr	12.5 mm/yr	12.5 mm/yr	800 km	230	3250	230	Setup 2a	850 km	no	Shifted					
8	12.5 mm/yr	12.5 mm/yr	12.5 mm/yr	12.5 mm/yr	1000 km	230	3250	230	Setup 2a	800 km	no	Shifted	5e				
9	12.5 mm/yr	12.5 mm/yr	12.5 mm/yr	12.5 mm/yr	1200 km	230	3250	230	Setup 2a	1200 km	yes	Central	5b				
10	20 mm/yr	5 mm/yr	5 mm/yr	5 mm/yr	800 km	230	3250	230	Setup 2a	750 km	no	Shifted					
11	20 mm/yr	5 mm/yr	5 mm/yr	5 mm/yr	1000 km	230	3250	230	Setup 2a	800 km	no	Shifted	5d				
12	20 mm/yr	5 mm/yr	5 mm/yr	5 mm/yr	1200 km	230	3250	230	Setup 2a	1000 km	no	Shifted	4b/7				
13	12.5 mm/yr	12.5 mm/yr	12.5 mm/yr	12.5 mm/yr	800 km	230	3250	230	Setup 2b	1600 km	no	Distant					
14	12.5 mm/yr	12.5 mm/yr	12.5 mm/yr	12.5 mm/yr	1000 km	230	3250	230	Setup 2b	1450 km	no	Distant	5g				
15	12.5 mm/yr	12.5 mm/yr	12.5 mm/yr	12.5 mm/yr	1200 km	230	3250	230	Setup 2b	xxx	xxx	No break-up					
16	20 mm/yr	5 mm/yr	5 mm/yr	5 mm/yr	800 km	230	3250	230	Setup 2b	1200 km	no	Distant					
17	20 mm/yr	5 mm/yr	5 mm/yr	5 mm/yr	1000 km	230	3250	230	Setup 2b	1000 km	yes	Central	5c				
18	20 mm/yr	5 mm/yr	5 mm/yr	5 mm/yr	1200 km	230	3250	230	Setup 2b	1700 km	no	Distant					
19	12.5 mm/yr	12.5 mm/yr	12.5 mm/yr	12.5 mm/yr	800 km	230	3250	230	Setup 3a	1200 km	no	Distant					
20	12.5 mm/yr	12.5 mm/yr	12.5 mm/yr	12.5 mm/yr	1000 km	230	3250	230	Setup 3a	1000 km	yes	Central					
21	12.5 mm/yr	12.5 mm/yr	12.5 mm/yr	12.5 mm/yr	1200 km	230	3250	230	Setup 3a	1200 km	yes	Central					
22	20 mm/yr	5 mm/yr	5 mm/yr	5 mm/yr	800 km	230	3250	230	Setup 3a	1200 km	no	Distant	5h				
23	20 mm/yr	5 mm/yr	5 mm/yr	5 mm/yr	1000 km	230	3250	230	Setup 3a	1300 km	no	Distant	4c				
24	20 mm/yr	5 mm/yr	5 mm/yr	5 mm/yr	1200 km	230	3250	230	Setup 3a	1250 km	yes	Shifted					
25	12.5 mm/yr	12.5 mm/yr	12.5 mm/yr	12.5 mm/yr	800 km	230	3310	230	Setup 3a	800 km	yes	Central					
26	12.5 mm/yr	12.5 mm/yr	12.5 mm/yr	12.5 mm/yr	1000 km	230	3310	230	Setup 3a	1150 km	no	Shifted					
27	12.5 mm/yr	12.5 mm/yr	12.5 mm/yr	12.5 mm/yr	1200 km	230	3310	230	Setup 3a	xxx	xxx	No break-up					
28	12.5 mm/yr	12.5 mm/yr	12.5 mm/yr	12.5 mm/yr	800 km	100	3310	100	Setup 3a	xxx	xxx	No break-up					
29	12.5 mm/yr	12.5 mm/yr	12.5 mm/yr	12.5 mm/yr	1000 km	100	3310	100	Setup 3a	1400 km	no	Distant					
30	12.5 mm/yr	12.5 mm/yr	12.5 mm/yr	12.5 mm/yr	1200 km	100	3310	100	Setup 3a	xxx	xxx	No break-up					
31	12.5 mm/yr	12.5 mm/yr	12.5 mm/yr	12.5 mm/yr	800 km	230	3250	230	Setup 3b	800 km	yes	Central					
32	12.5 mm/yr	12.5 mm/yr	12.5 mm/yr	12.5 mm/yr	1000 km	230	3250	230	Setup 3b	1000 km	yes	Central					
33	12.5 mm/yr	12.5 mm/yr	12.5 mm/yr	12.5 mm/yr	1200 km	230	3250	230	Setup 3b	1200 km	yes	Central					
34	20 mm/yr	5 mm/yr	5 mm/yr	5 mm/yr	800 km	230	3250	230	Setup 3b	850 km	no	Shifted	5f				
35	20 mm/yr	5 mm/yr	5 mm/yr	5 mm/yr	1000 km	230	3250	230	Setup 3b	1400 km	no	Distant	5i				
36	20 mm/yr	5 mm/yr	5 mm/yr	5 mm/yr	1200 km	230	3250	230	Setup 3b	1700 km	no	Distant					

Table 3.2. Controlling parameters and principal results of the experiments.

3.3.2. *Model geometries*

The model box is 2000 km wide and 400 km deep. The grid size is 400 x 80 elements, resulting in a resolution of 5 km x 5 km per element. We have tested three different lithospheric setups with diverse complexities (see 3.1.2, Fig. 3.3) and three different locations of a 1700°C thermal and compositional mantle anomaly at 400 km depth (D’Acremont et al., 2003). The initial locations vary laterally at the base of the model with the centre of the anomaly positioned 1) at the centre of the model (i.e. plume location at 1000 km, see table 3.2), 2) at 200 km to the right of the model box’s centre (i.e. plume location at 1200 km) and 3) at 200 km to the left of the model box’s centre (i.e. plume location at 800 km). Each location is tested in a separate calculation. Following previous studies the base of the anomaly lies at 400 km depth as the deeper mantle phase does not have a large impact on the crustal evolution (D’Acremont et al., 2003; Ribe and Christensen, 1994). The anomaly has a simplified, symmetric, spherical shape since at depth viscous bodies take a spherical shape and this follows the line of 2D and 3D numerical modelling experiments on plume-lithosphere interaction (a.o. D’Acremont et al., 2003; Burov and Gerya, 2014; Koptev et al., 2016). In most of the experiments, it has a diameter of 230 km. The effects of a mantle anomaly with a diameter of 100 km were tested in a limited number of models. The composition of the mantle anomaly is olivine with a density of 3250 kg/m³ (except for several models where it is 3310 kg/m³) which has been determined to be an intermediate plume in previous studies (Turcotte and Schubert, 2002; D’Acremont et al., 2003). No background density tests have been performed as the background density used for background calculations is the same for the plume as well as the surrounding mantle. The thermal contrast between the plume and the mantle varies as thermal exchanges happen between the plume and the mantle, decreasing the temperature of the plume. The mantle also cools as the plume rises to shallower depths.

3.3.3. *Density and rheological structure*

The 2D model consists of four horizontal rheological layers. For Setup 1 (Fig. 3.3a and Fig. 3.3b), a laterally homogeneous 40 km thick two-layered crust and a 160 km thick lithospheric mantle have been applied. We test the model’s sensitivity for two different rheological properties of the crust. We use a “weaker” rheological strength envelope (Setup 1a; Fig. 3.3a), composed of 1) a wet quartz upper crust with a density of 2500 kg/m³ and 2) a diabase lower crust with a density of 2750 kg/m³. Our second rheological strength envelope has the characteristics of a “strong”, cratonic crust that consists of: 1) a dry quartz upper crust with a density of 2600 kg/m³ and 2) a strong diabase lower crust with a density of 2850 kg/m³. The rheological differences of the two strength envelopes represent a “weaker” crust that has been subject to an earlier deformation phase, before the opening of the South Atlantic, which is the case for the South American side (Autin et al., 2013), and a “stronger” crust of cratonic nature that represents the stable southern African continent (after Burov and Diament, 1995). Dry olivine flow law has been assumed for both lithospheric

and sub-lithospheric mantle in all our experiments. The initial density of the mantle decreases from 3330 kg/m³ to 3310 kg/m³ at the lithosphere-asthenosphere boundary. Specific values of the rheological parameters used are given in table 3.1.

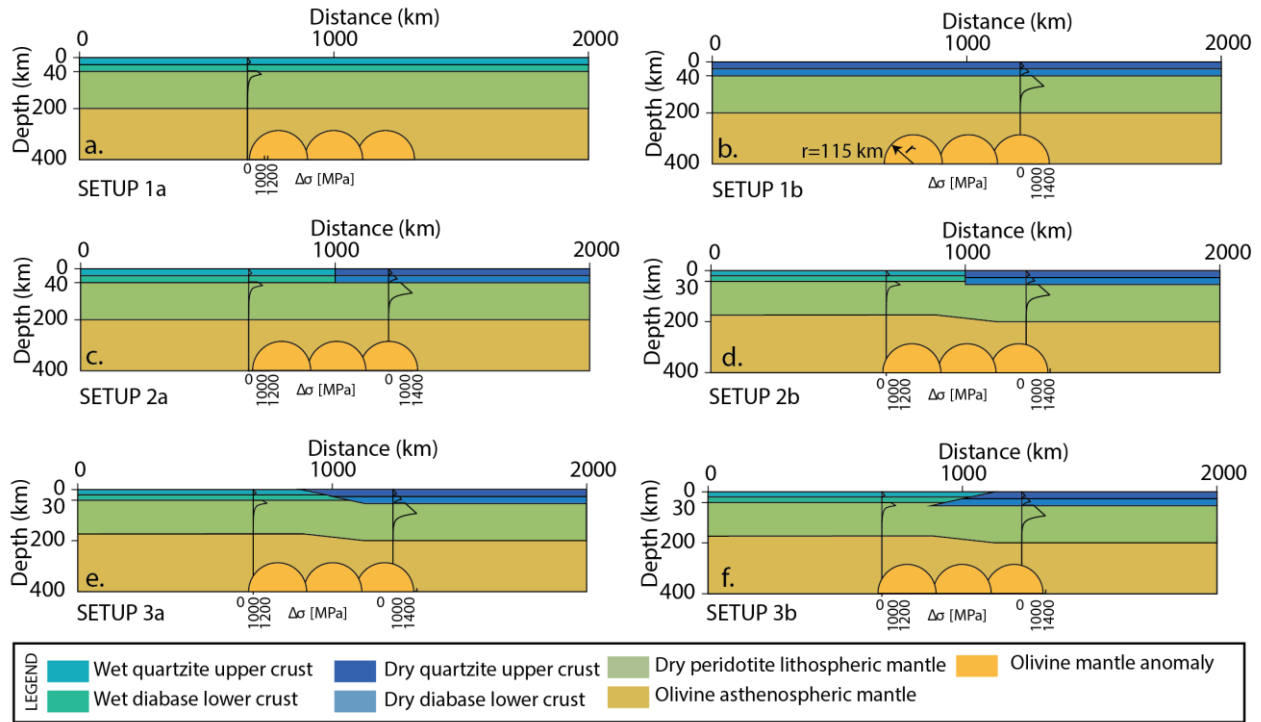


Figure 3.3. Six tested numerical setups. a) Setup 1a: 4-layered weak rheology, crust 40 km thick, lithosphere 200 km thick. b) Setup 1b: strong 4-layered rheology, crust 40 km thick, lithosphere 200 km thick. c) Setup 2a: combined rheological profiles (weak on the left side, strong on the right side), crust 40 km thick, and lithosphere 200 km (equal for both rheologies). d) Setup 2b: combined rheological strength envelopes, (weak on the left side, strong on the right side), crust 30 km thick on the right side and 40 km thick on the left side, lithosphere 180 km thick on the left side and 200 km thick on the right side, no complex contact geometries. e) Setup 3a: combined rheological strength envelopes, (weak on the left side, strong on the right side), crust 30 km thick on the right side and 40 km thick on the left side; lithosphere 180 km thick on the left side and 200 km thick on the right side. The contact between the two different crustal thicknesses is a low-angle geometry, dipping towards the right. f) Setup 3b: combined rheological strength envelopes, (weak on the left side, strong on the right side), crust 30 km on the right side and 40 km thick on the left side, lithosphere 180 km thick on the left side and 200 km thick on the right side. The contact between the two different crustal thicknesses is a low-angle geometry dipping towards the left.

For Setups 2 and 3 we apply a laterally non-homogeneous crustal rheology: a “weak” crustal rheology for the left half of the model and a “strong” crustal rheology for the right one (Fig. 3.3c-f). The crustal and lithospheric thicknesses are laterally homogeneous in Setup 2a: 20 km for upper crust, 20 km for lower crust and 160 km for lithospheric mantle (Fig. 3.3c). Setups 2b and 3 are characterized by laterally varying lithospheric layers, based on the lithospheric scale structure described in section 2.2: the “weaker” left half has a 15 km-thick upper crust, 15 km-thick lower crust and a 150 km-thick lithospheric mantle, whereas the “stronger” right half has a 20 km-thick upper crust, a 20-km thick lower crust and a 160 km-thick

lithospheric mantle (Fig. 3.3c-f). Three different contacts between the rheological strengths are tested. Setup 2b has a straight vertical contact. For Setup 3 we have adopted a geometry resembling the old suture zone that is reactivated during the first extensional phase. The suture is dipping either 40 degrees towards the ‘strong’, African rheology (Setup 3a) or towards the ‘weak’ South American rheology (Setup 3b). By the setups described above we have tested the following parameters: initial position of the plume, density of the mantle plume (limited to Setup 3a) and different half-rate velocity boundary conditions (see table 3.1).

3.3.4. *Mechanical and thermo-rheological boundary conditions*

We simulate tectonic forcing by applying a constant, time independent, extension rate along the vertical side of the box of 25 mm/yr. An equal half-rate velocity is applied on both sides of the box (12.5 mm/yr) to one set of models and 5 mm/yr on the right side and 20 mm/yr on the left side is applied to a second set of models (table 3.1). The half-rate velocities are adopted from (Müller et al., 2008). The bottom of the box is defined by hydrostatic pressure with free slip in all directions. The upper side of the box is a free surface boundary, implying a free stress and a free slip condition in all direction, allowing the lithosphere to develop freely. A moderate erosion by diffusion is applied ($a = 500 \text{ m}^2/\text{yr}$).

The upper and bottom thermal boundary condition is a fixed temperature 10 °C and 1400 °C respectively to represent a ‘cold’ geotherm. An old lithosphere of 500 Ma (Burov and Diament, 1995) has been assumed for the tectonic age used to represent the super-continent Pangea before break-up. The geotherm used for the models reaches 500 °C at Moho depth, 1330 °C at the lithosphere-asthenosphere boundary (LAB) after which it becomes adiabatic until it reaches 1400 °C at the base of the model at 400 km (Ribe and Christensen, 1994).

3.3.5. *3D numerical model*

A 3D model has been performed with the thermo-mechanical viscous-plastic 3DELVIS code (Gerya, 2010; Gerya and Yuen, 2007) that combines the finite difference method with a marker-in-cell technique. The 3D model box has the horizontal dimensions $1500 \times 1500 \times 635 \text{ km}$ and consists of $297 \times 297 \times 133$ nodes offering spatial resolution of ca. $5 \times 5 \times 5 \text{ km}$ per grid cell. Not area-specific initial setup consists of a stratified three-layer (upper/lower crust and lithospheric mantle) continental lithosphere underlain by an asthenosphere. The total thickness of the two-layer crust is 36 km; the depth of lithosphere-asthenosphere boundary is 150 km. The mantle plume has been seeded at the base of the modelled domain by a spherical thermal anomaly of 370 °C with a radius of 200 km. The initial geotherm is piece-wise linear with fixed temperatures at the surface (0°C), at the Moho (700°C), at the base of the lithosphere (1300°C), and at the bottom of the model box (1630°C). Weak tectonic forcing has been simulated by applying a constant ultra-slow divergent horizontal velocity of 3 mm/year along the sides of the model. More detailed information on

the 3D model setup and rheological and material properties used in our 3D experiments can be found in Burov and Gerya (2014) and Koptev et al. (2015, 2016).

3.4. Model results

3.4.1. 2D model results

Three types of model scenarios result from our set of experiments. “Centred” break-up, when the mantle anomaly moves vertically upwards and break-up happens directly above the original location of the centre of the mantle anomaly. “Shifted” break-up, when the mantle anomaly first migrates vertically and, once it reaches the base of the lithosphere, migrates laterally until break-up occurs with a 50 to 250 km offset with respect to the initial anomaly position. “Distant” break-up, when a mantle anomaly rises to the base of the lithosphere and remains there, while the location of break-up takes place more than 300 km away from the initial site of the anomaly.

Experiment 6, characterized by a “strong” homogenous lithosphere, is an example of “centred” break-up (Fig. 3.4a). The mantle anomaly reaches the base of the lithosphere rapidly within 2 Myr, after which it penetrates into the lithosphere. The rising flow of plume material is strong enough to break apart the overlying lithospheric mantle and crust between 7 and 8 Myr. The surface reacts by uplift, then subsidence and alternating positive and negative vertical movements of the margins and the rift centre. Although the initial position of break-up centre is situated directly above mantle plume, the continuous extensional evolution, including strain relocation and changing temperature distribution, suggest a post-rift lateral shift of the spreading axis. Note that after continental break-up mantle plume material reaches the surface where it contributes to the formation of new oceanic lithosphere.

The “shifted” mode of continental break-up is illustrated by Experiment 12 where the mantle plume anomaly has been seeded below a stronger lithosphere composing the right half of the model domain (Fig. 3.4b). As in the case of Experiment 6, the onset of rifting starts with a rapid rise of the anomaly, impinging the lithosphere not later than 2 Myr. Surface topography associated with localized crustal strain is formed around 3-4 Myr with small offset (<50 km) from the point directly above mantle plume impingement. Further upslope migration plume material leads to continental break-up between 7 and 10 Myr. A principal difference from the “centred” experiment 6 is the lateral shift (50 to 250 km) of the newly formed spreading axis with respect to the initial position of the mantle plume. Lateral migration of the plume head to this break-up axis leads to an asymmetrical distribution of the plume material: some of the material reaches the surface at the spreading centre, another part remains glued beneath the highly thinned lithosphere at depths between 200 and 10 km. Similar to Experiment 6, the final stage of the “shifted” system development is the strain relocation corresponding to 200 km-wide jump of the spreading axis.

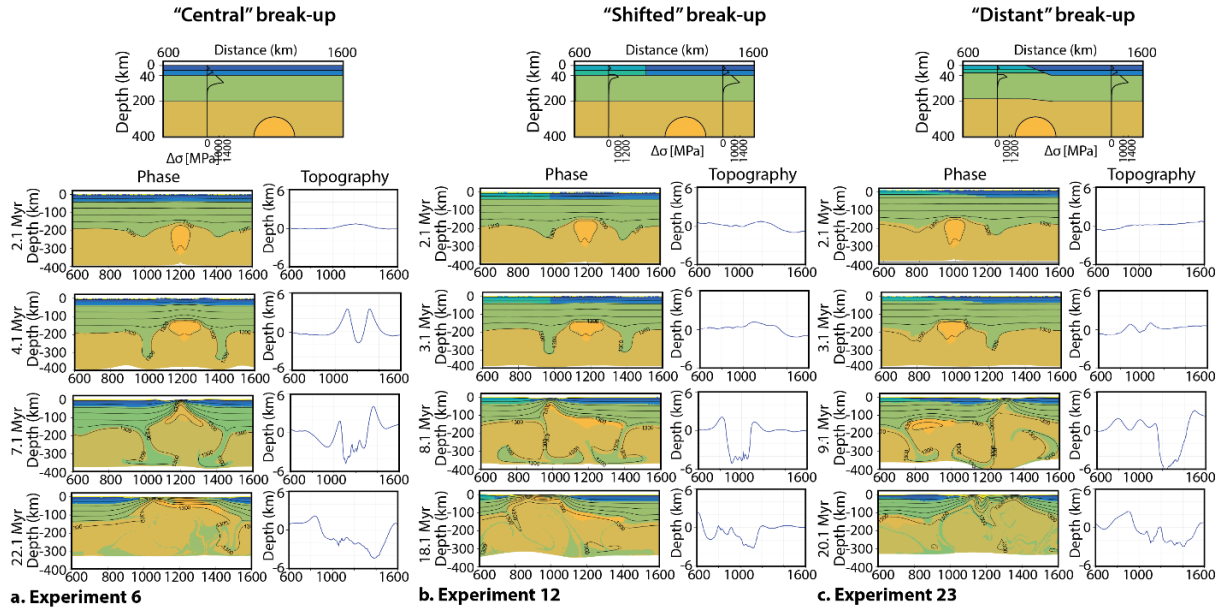


Figure 3.4. Models with different rheology and plume location showing the most representative examples of the three modes of continental break-up. a) “Centred”: Experiment 6, Setup 1, with a strong rheology and the anomaly located at 1200 km (200 km offset from the centre towards the right). At 2.1 Myr the first topographic response occurs. The break-up axis develops directly above the initial mantle plume position and mantle material reaches the surface. b) “Shifted”: Experiment 12, Setup 2, with a laterally varying rheology and the anomaly positioned in the centre at 1000 km. At 2.1 Myr the first topographic variation shows with a larger extend than the “centred” break-up model. The break-up axis develops offset from the original mantle plume location and mantle material migrates towards the spreading centre, reaching the surface. c) “Distant”: Experiment 23, Setup 3, has a laterally varying rheology and the anomaly is positioned in the centre at 1000 km. At 2.1 Myr minor topographic variation. The break-up axis develops far offset from the original mantle plume location and the mantle plume remains glued to the base of the lithosphere. The initial topographic variations remain visible after break-up.

Finally, experiment 16 illustrates the “distant” break-up mode that starts with a rapid uplift of the mantle plume to the bottom of the lithosphere, an observation typical for all performed models. This expectedly results in associated topography variations (Fig. 3.4c). In contrast with the two previously discussed break-up modes (experiments 6 and 12), mantle plume material remains glued beneath the base of the lithosphere without localized ascent towards the formed break-up centre. Lithosphere thinning that will result in break-up occurs at large distance (more than 500 km) from the plume impingement. This appears to be related to secondary mantle convection associated with plume-induced subduction of the lithospheric mantle that has developed upon plume upwelling to the lithosphere-asthenosphere boundary on both sides of the plume head. It is noteworthy that initial topographic changes created by the impingement of the plume remain visible throughout the model evolution. Given the lack of near-surface plume material, this “distant” mode cannot be considered as break-up directly induced by the impact of the mantle plume. Nevertheless, it might reflect the implicit influence of the upwelled plume on “distant” break-up processes via plume-induced subduction and mantle convection.

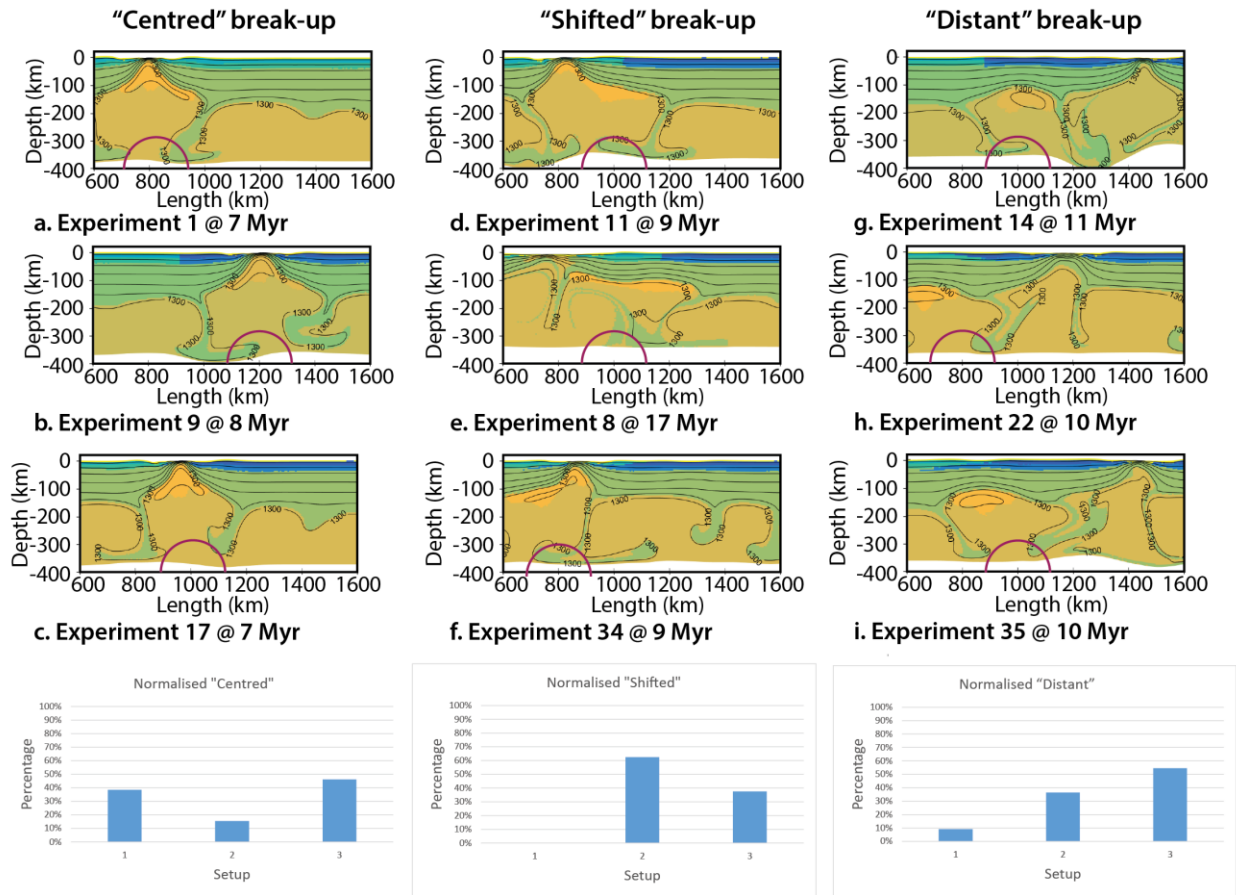


Figure 3.5. Examples of models with different setup, plume location rheological structure showing the different modes of break-up; a-c) “centred” examples, d-f) “shifted” examples, g-i) “distant” examples. In red the initial location of the mantle anomaly is drawn. The graphs below show the normalised, statistical likelihood of a mode (“centred”, “shifted” or “distant”) for a given setups.

“Centred” break-up preferably takes place using initial Setup 1, where the crust and lithospheric mantle are laterally homogeneous and no inherited structures are given (Fig. 3.4a, table 3.1), but other setups can also evolve according to this mode (Fig. 3.5a-c). Break-up occurs between 6 and 10 Myr, directly above the initial location of the mantle anomaly. Mantle material reaches the surface at the point of impingement that evolves into the break-up axis. Almost all plume material is involved in formation of new oceanic lithosphere. As a result, after continuous (more than 10 Myr) calculations, only little material remains below the thinned continental lithosphere. Note that, even though central located plumes are expected to develop to a symmetric or “central” mode, a central located plume evolves the least likely into “central” type of break-up (table 3.1). “Shifted” break-up is favoured by Setup 2a where the thickness of the lithospheric layers is laterally homogeneous but crustal rheology differs (Fig. 3.5d-f). The mantle anomaly rises and break-up also occurs between 6 and 10 Myr, but in this case it is shifted from the initial point of impingement. Most mantle material remains below the lithosphere, but through migration along the bottom

of the lithosphere some material still reaches the surface. This mode of break-up only occurs when the lithosphere properties (rheology and/or thickness) varies laterally, but it does not completely control “shifted” break-up, because not all laterally varying rheology experiments result in “shifted” break-up. Plume location is also not a controlling factor for the model to result in “shifted” break-up as all three plume locations can result in “shifted” break-up. The “distant” break-up experiments have a preference for Setup 2 and 3, where both the lithospheric layers’ thickness and the crustal rheology are laterally different (Fig. 3.5g-i). Crustal break-up happens slightly later compared to the “centred” and “shifted” experiments: between 9 and 12 Myr. Mantle anomaly material does not reach the surface, but remains completely glued to the bottom of the lithosphere. Most of the continental break-up modelled with the “distant” experiments occurs in the lithospheric segment that is characterized by a strong crust.

Almost half (12 out of 25) of the equal half-rate velocities boundary condition results in “centred” break-up. More than half (6 out of 11) of the unequal half-rate velocity boundary conditions result in “distant” break-up mode. The different velocity parameters do have a preference for a certain break-up style, but it is not a controlling factor.

The models that resulted in “shifted” break-up have a mantle anomaly that rises to the base of the lithosphere and upon arrival, migrates, in most cases, towards the weaker lithosphere to break through this less strong segment. This is in contrast with the “distant” model results that develop crustal break-up in the stronger lithosphere (11 out of 11 models) when the plume remains glued below the weaker lithosphere and does not break through. In case of “distant” break-up mode, the rheology is very important and strongly controls this mode of break-up.

3.4.2. 3D model results

Similarly to the 2D experiments, the 3D model shows a quick (<2 Myr) upwelling of the plume material up to lithosphere-asthenosphere boundary (Fig. 3.6a). After this, the plume head starts to spread laterally within lower part of lithospheric mantle (Fig. 3.6b-d). When the mantle plume impinges on the base of lithosphere, almost all plume material is partially melted (Fig. 3.6a). Following spreading and cooling expectedly leads to gradual solidification of the plume (Fig. 3.6b-c), which has been completed at 50 Myr (Fig. 3.6d).

The interplay between far-field forces and active mantle upwelling results in a “classical” single rift that crosses the entire model domain in the direction perpendicular to external extension (Fig. 3.6a). Continuous evolution shows the formation of a wide rift valley where localized brittle deformation is concentrated along the boundary fault (Fig. 3.6b-c). This rift basin opens rapidly (Fig. 3.6b) reaching a width of 600 km in less than 35 Myr while passive extension applied at the boundaries would result in only 200 km width (Fig. 3.6c). This highlights the important role of plume-related buoyancy forces in the context of studied “active-passive” rifting.

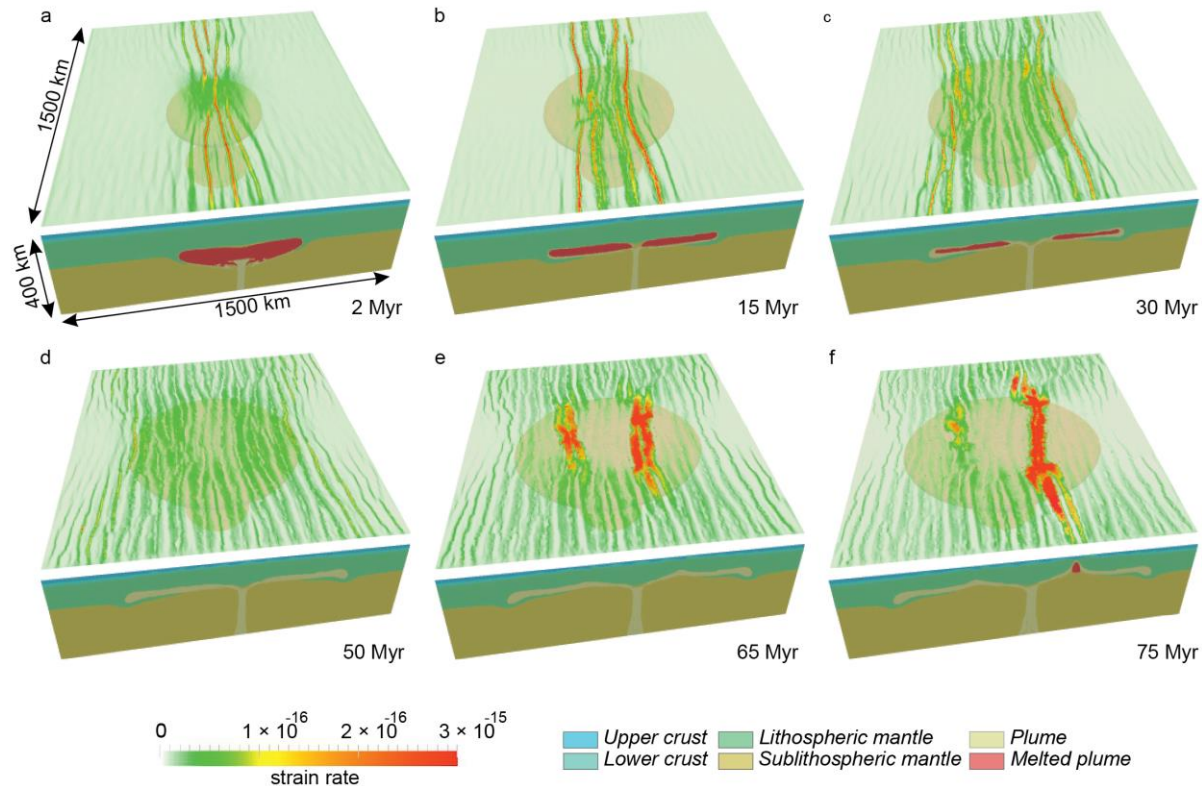


Figure 3.6. Evolution of 3D model a) rapid plume uplift leading to formation of linear extension-perpendicular rift at the crustal level; b-c) development of wide rift basin with localized crustal high strain along bounding normal faults; gradual cooling and solidification of plume head material; d) widely distributed rift above completely crystallized plume head ponding lithosphere-asthenosphere boundary; e) rapid transition from deformation localized in normal faults bounding wide rift valley to localized strain within narrow zones associated with localized plume ascent; f) breakup of the continental lithosphere along spreading zone considerably shifted from centre of the mantle plume. Bulk of plume material is shown in pale orange. Green to red colours indicate strain rate at the level of 10 km (i.e. within upper crust). Component distribution is shown for vertical cross-sections through central part of the model domain.

The next stage of the system evolution (65 Myr) is a quick switch of deformation localization from rift-bounding faults to narrow zones inside the rift valley (Fig. 3.6e). This change in rifting style is caused by initiation of localized upwelling of plume material along stretched zone(s) highlighted at the surface by localized high strain rates (Fig. 3.6e). Further localized plume ascent associated with decompression melting of plume material increases the rate of lithospheric thinning leading to continental break-up along a spreading axis that has shifted laterally outwards from the centre of the plume head (Fig. 3.6f). This asymmetrical position of the spreading zone arises spontaneously within initially symmetrical and laterally homogenous lithosphere and is likely controlled by melting and cooling processes into head of mantle plume. Thus, a lateral shift of plume-induced break-up centres with respect to initial plume impingement revealed in certain 2D experiments (see for example Experiment 6, Fig. 3.4a) appears to be an intrinsic characteristic of self-induced plume-related processes that do not necessary requires fast (>1 cm/y) external

extension nor any lateral lithospheric heterogeneity (see also Experiment 2 for a 2D example of “distant” break-up in the context of laterally homogenous lithosphere).

3.5. Discussions

3.5.1. General aspects

The results of our models are important in the context of ongoing discussion on plume-induced continental break-up. We show that continental break-up can be initiated by just one single mantle plume under different initial and boundary conditions. In most of our 2D models (32 out of 36) continental break-up takes place as a result of the direct (“centred” or “shifted” modes) or indirect (“distant” mode) impact of the mantle plume (Fig. 3.8). Four remaining models do not result in break-up. On one hand, the models that develop according to “centred” (Fig. 3.8b) or “shifted” (Fig. 3.8c) modes are directly induced by the plume anomaly which results in penetration of plume material up to the surface. On the other hand, the “distant” mode is characterized by secondary mantle convection associated with plume-induced *subduction* and/or *convection*. In this case, the mantle plume is not involved directly in break-up processes and remains glued at the base of adjacent unbroken lithosphere (Fig. 3.8d).

In a very early phase, strain rate localizes and topographic variations develop directly above the initial plume impingement location (Fig. 3.8a). They remain visible only in the “shifted” and “distant” models and can be interpreted as aborted rifts. It was commonly accepted and almost self-evident that in the case of plume-induced continental break-up, its axis should be situated directly above the initial plume impingement position (D’Acremont et al., 2003). However, observations such as failed rifts and deep-seated mantle sources beneath a strong continent that are significantly remote from the mid-oceanic ridge, actually imply that continental rifting and break-up are not a purely symmetric and “plume-centred” processes. Our modelling demonstrates that symmetric development of mantle material ascent and subsequent continental break-up are not a definite outcome. More than half of our models (19 out of 32) result in “shifted” and “distant” break-up modes, suggesting that these modes should also be expected in a wide range of initial and boundary conditions. Even so, our perfectly symmetric and lateral homogeneous 3D model shows that in a purely symmetric setting, with no lithospheric rheological heterogeneities, continental break-up shifted from the original centre of the mantle anomaly is possible. We argue here that “centred” symmetric continental break-up developed directly above mantle plume is only one particular case of possible evolutions of plume-induced break-up systems.

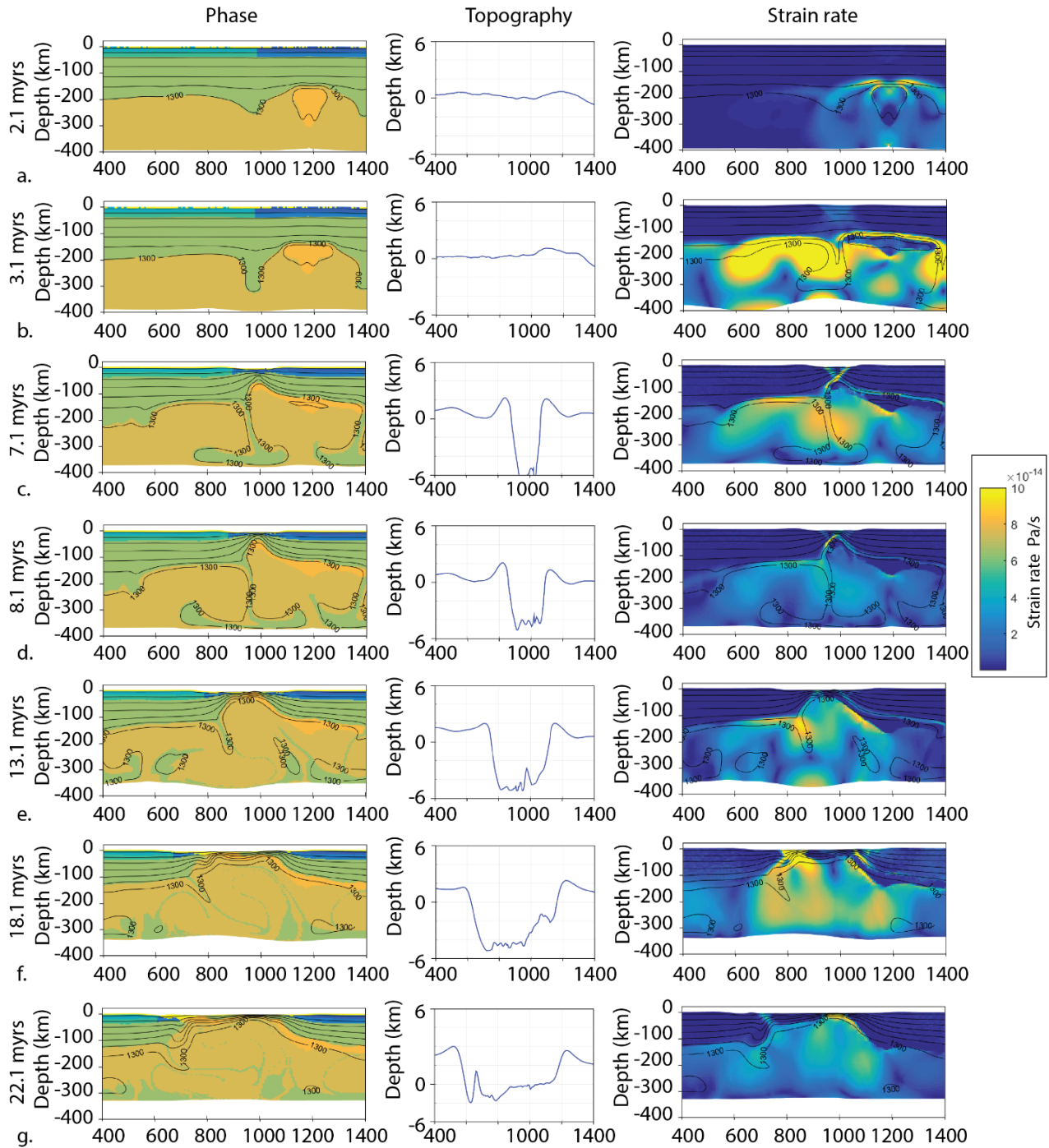


Figure 3.7. Detailed display of experiment 12. Setup 2 is the base for this experiment with a laterally varying rheology. The anomaly is positioned in the centre of the model at 1000 km. At 2.1 Myr the first topographic variation shows with a larger extent than the “centred” break-up model. Strain rate localizes slightly shifted from the plume impingement point at 3.1 Myr. Strain localizes, topography variations grow and crustal break-up occurs at 8.1 Myr. Mantle material slowly migrates towards the spreading centre reaching the surface until the material that remains below the lithosphere reaches thermal equilibrium around 22 Myr.

3.5.2. *The case of the South Atlantic*

The South Atlantic is considered to be a good example of plume-induced continental break-up (e.g. Torsvik et al., 2009). Some of the observations such as failed rifts (Heine et al., 2013) and high velocity bodies (e.g. Blaich et al., 2011) cannot be explained with conventional models, usually assuming a “centred”-like break-up style (e.g. Burov et al., 2007; D’Acromont et al., 2003). Yet, our experiments showing “shifted” break-up mode (Fig. 3.7; Fig. 3.8c) can be used to explain these features. In these models, initial crustal deformation associated with mantle plume impingement (Fig. 3.7a-b; Fig. 3.8a) are formed within the first 5 Myr. Significant topography variations developed during this initial stage of rift evolution (i.e. before break-up) can be interpreted as very early failed rift features (e.g. the failed Abimael rift in the southwest of the Santos Basin). The topographic plateaus that remain elevated long after break-up have also been observed with dynamic topography studies (Nyblade and Robinson, 1994). Next, localized strain becomes concentrated close to the boundary between strong and weak lithosphere that is laterally offset (~400 km) from the area of initial plume impingement (Fig. 3.7c). Transition from wide rift stage to lithospheric break-up is marked by narrowing a broad rift region (over 1000 km width) down to narrow rift valley (Fig. 3.7c-d) with the width of 10’s of kilometres between the two rift-shoulders. Associated lithospheric thinning leads to a separation of the two plates along a spreading centre corresponding to South Atlantic ridge (Fig. 3.7e; Fig. 3.8c). Part of strong crust that remains attached to the weaker lithosphere segment, could correspond to the Brazilian craton that was once bordering the African continent (Heine et al., 2013).

Simultaneously with thinning of the lithosphere below the future break-up centre, the plume material migrates along the base of the lithosphere and rises towards the deformed crust where it breaks through. This migration can go as far as 300 km from the plume impingement point and only ceases when the material that is still at the base of the lithosphere (at depths between 200 km and 10 km) reaches thermal equilibrium (in this case after 22 Myr). This confirms the hypothesis that one mantle anomaly (or plume) can flow laterally over significant distances below a slow-moving continent, after being risen to the base of the lithosphere (e.g. Sleep, 2006). When thermal equilibrium is reached, the mantle material glued to the base of the lithosphere at shallower depths corresponds geometrically and location-wise to high-velocity/high-density bodies observed on seismic data below the thinned continental lithosphere and the transition zone of the South Atlantic domain (Clerc et al., 2015). During migration, products of partial melting of the mantle material can move vertically to (shallow) lower crustal levels. They might resemble high density bodies observed at lower crustal levels inside continental crust with similar geometries observed with gravity modelling (Blaich et al., 2011). These processes cannot be reproduced by our 2D modelling, because no melt production and extraction have been simulated.

Note that our 2D study has not the intention to capture such 3D features like along-axis northward propagation of the break-up axis (Franke, 2013) up to the centre of the surface manifestation of Tristan plume activity – the Paraná-Etendeka continental flood basalts province.

After continental break-up, the mantle plume anomaly continues to play an important role in the spreading evolution of the system. Strain rate relocation takes place around 18 Myr, when the spreading axis shifts another 200 km towards the left from the original position of the break-up centre (Fig. 3.7f). This phenomenon could correspond to a rift-jump that have also been both observed and modelled (Brune et al., 2014) in the South Atlantic domain.

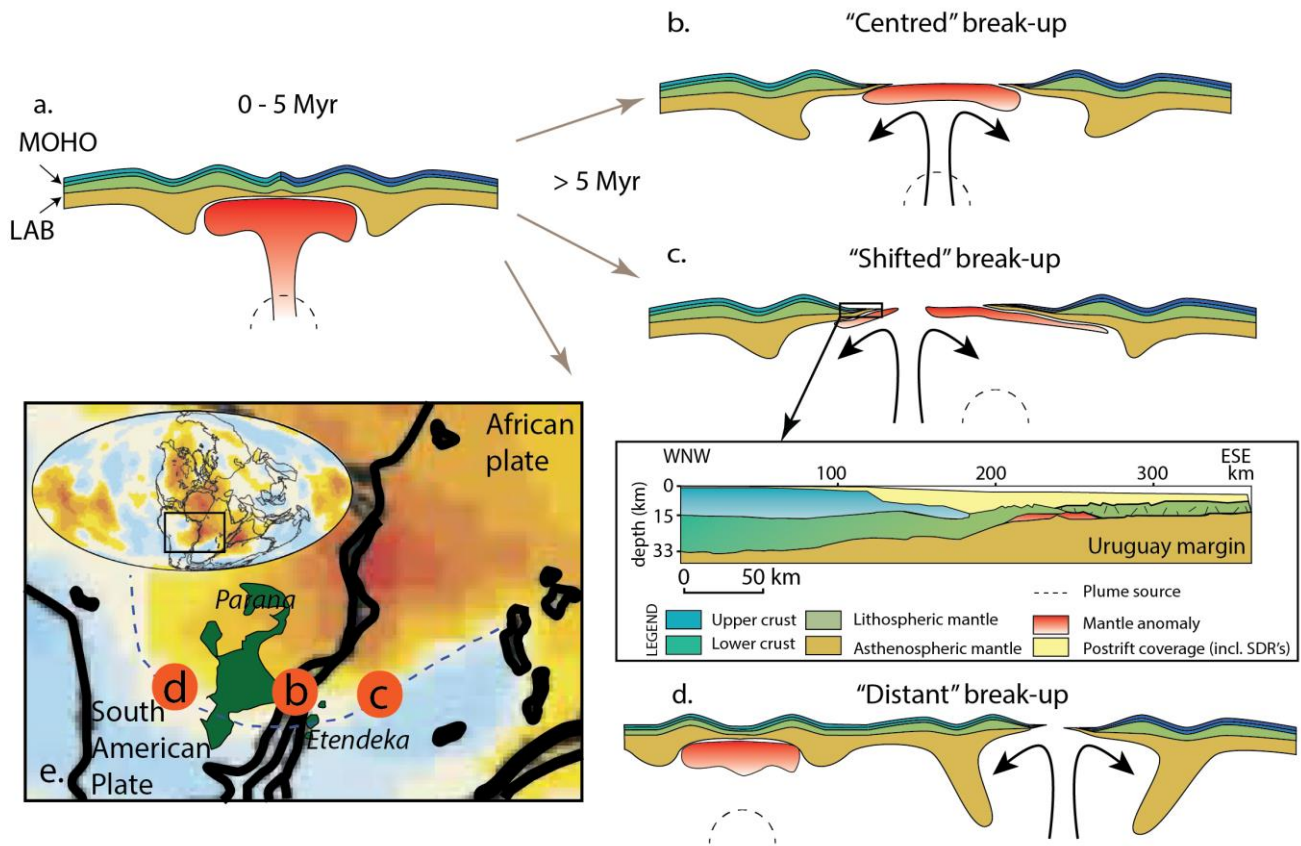


Figure 3.8. Schematic representation of the three modes of break-up. a) The very early phase of rifting (0 – 5 Myr) is very similar for all three modes after which they develop into b) “Centred”; c) “shifted” and d) “distant”. An example of a simplified interpretation of the Uruguayan margin (after Clerc et al., 2015) is used to demonstrate the resemblance of the “shifted” mode of break-up, like experiment 12, with the South Atlantic domain. e) Map showing the outline of the plate configuration at the moment of break-up between Africa and South America on the lower mantle low velocity zone (South African Super Plume) (from Davaille et al., 2005). The Paraná-Etendeka flood basalts are depicted in green (after Torsvik et al., 2009). The orange dots refer to the three possible principal locations of initial thermal anomaly at the upper/lower mantle boundary corresponding to the Tristan plume.

The question we raised about the initial position of the mantle plume anomaly responsible for continental break-up in the South Atlantic remains open. On Fig. 3.8e, we show a reconstructed configuration of the slow velocity anomaly (corresponding to the South African Super Plume) at the CMB based on present-day seismic tomography model (after Davaille et al., 2005). The orange dots refer to the three possible principal locations of initial thermal anomaly at the upper/lower mantle boundary corresponding to the Tristan plume. The central point refers to the most evident “centred” scenario (Fig. 3.8b) when the deep-seated thermal anomaly in the upper mantle is supposed to be located directly below its surface manifestation and hints to voluminous Paranà-Etendeka continental flood basalts province (Fig. 3.8e, e.g. Torsvik et al., 2009; Heine et al., 2013). This scenario, however, is not consistent with the commonly considered concept that plumes emerge from the edges of the large low-velocity anomalies at the CMB that has been confirmed by both numerical modelling (Hassan et al., 2015) and by empirically established correlation between downward projected plume-associated large igneous provinces and the margins of the large low shear velocity province beneath Africa (Torsvik et al., 2006). Moreover, with this ‘centred’ scenario we cannot explain additional features such as failed rift arms and anomalous bodies at lower crustal levels. The ‘distant’ break-up mode (Fig. 3.8d), where the initial plume centre is located below the South American section and remains there after “plume-independent” continental break-up, does not fit well with geological observations of the voluminous Paranà-Etendeka continental flood basalts that are supposed to be related with direct influence of the Tristan hot spot (Torsvik et al., 2009). Finally, initial plume position slightly moved to African side (right dot on Fig. 3.8e) refers to “shifted” scenario that seems to be preferable (Fig. 3.8c). The time length of the modelled rift phase (10 Myr +/- 3 Myr) is much shorter than has been inferred from geological and geophysical observations (160 Ma to 134 Ma, (Franke, 2013)) in the South Segment of the South Atlantic. Despite this, with the eastward offset initial position of the mantle plume with respect to a heterogeneous thermo-rheological lithospheric structure we are able to explain not only plume induced flood basalts but also a set of anomalous features such as failed rift systems, and deep crustal bodies.

3.6. Conclusion

Different lithospheric strengths comparable to the South American and African continental crust, inherited structures, boundary velocity conditions corresponding to average spreading rates, and initial location of a thermal mantle anomaly (i.e. plume) have been tested to investigate the dynamics of plume induced continental break-up. A set of 36 models shows that with only one anomaly three very different scenarios for continental break-up can be realized depending on the rheological structure, anomaly location and inherited structures. Continental break-up does not necessarily occur above the centre of the initial location of a mantle anomaly. As mentioned above, our models show three types of break-up 1) “centred” break-up, 2) “shifted” break-up and 3) “distant” break-up.

“Centred” and “shifted” break-up types of models refer to plume-induced type of break-up. For the first mode, mantle material rises vertically towards the bottom of the lithosphere after which it breaks through the crust and reaches the surface directly above the initial plume position. The “shifted” type of break-up shows continental break-up that is 50 to 200 km shifted from the initial location of the mantle anomaly. In this case, the mantle plume rises and impinges the lithosphere, after that it migrates laterally and cuts through the lithosphere reaching the surface at a break-up point considerably shifted from the area of initial, pre-break-up impingement. Some material remains glued underneath the lithosphere at depths between 200 and 10 km. These deep-seated bodies, at depths of 200 km, are not situated directly below the break-up centre, but are spread over a large area below the continental margins. The shallower bodies geometrically resemble high density/high velocity bodies detected by seismic profiling and gravity modelling along the margins of the South Atlantic domain and at lower crustal levels.

The “distant” break-up mode refers to continental rupture that is indirectly induced by the presence of the mantle plume ponding at the bottom of the weaker continental lithosphere, when “plume-independent” break-up of adjacent stronger lithosphere appears to be considerably (from 250 and 800 km) displaced from the location of plume-lithosphere interaction. In this case, laterally widely spread plume material remains glued below unbroken segments of the lithosphere.

Topographic changes that occur very early during initial rifting stage remain visible for a long period and can possibly be interpreted as failed rift systems (in the cases of “shifted” and “distance” modes). Strain relocation after continuous post-break-up extension could be interpreted as rift jumps. A simple 3D model has been built to illustrate that even in a fully symmetric setup, rift-to-break-up processes are not by default symmetric and can very well evolve asymmetrically.

There is no controlling parameter for one of the three types of rifting, with a combination of parameters determining the outcome, but the location of the mantle anomaly with respect to the rheology is the most essential. The most important result of this study is that there is not one single rift mode for plume-induced crustal break-up.

Highlights:

- Numerical models reveal several plume-induced crustal break-up modes
- Rift and spreading systems do not necessarily develop above the mantle plume
- Early plume impact results in topography that resembles failed rift features
- Material glued to the lithosphere-base resembles anomalous margin-features

**Chapter 4: Two-branch break-up systems by a single mantle plume: insights from numerical
modelling**

Summary

The results from chapter 3 showed that the initial plume location is a key-parameter for plume-related thermo-mechanical modelling. The results, however, did not show the qualitative impact of the initial plume-location for model setups with more complicated rheological setups. A second set of 47 numerical models was designed to investigate the impact of plume-location on complex lithospheric model setups. The model setups are similar to the setups in chapter 3, with two segments with different strengths. Not only the plume location was tested, of which the results can be found in this chapter, also the size of the plume, grid-cell size, temperature of the plume and the location of the plume below the weak lithosphere were investigated. These results can be found in appendix II. The results of this modelling exercise showed that the ‘shifted’ mode of break-up, modelled in chapter 3, is reproduced when the anomaly is located close enough to the contact between the two segments, this mode of break-up is called ‘structural inherited’ break-up as crustal break-up occurs at the contact or inherited structure between the two segments. When the plume is positioned further away, the ‘central’ mode of break-up modelled in chapter 3 is produced, which is here called ‘plume-centred’ mode of break-up. In this case the break-up centre develops directly above the plume-impingement point. This ‘plume-centred’ mode of break-up does not develop per definition when it is further away from the inherited structure or the contact between the two segments. This only occurs when the thermal gradient of the initial system is high enough, in this case 600 °C or more and the far-field forces are high enough, in this case over 10 mm/yr. When these conditions are met, the vertical penetration of plume material and thermal weakening of the crust in combination with far-field stresses have a stronger effect on the deformation of the system than deformation at the contact between the two segments. This has also been shown by Burov and Gerya (2014) who state that both thermal and displacement (e.g. extension rate) conditions should be present to localize deformation to eventually break- the crust. If one of the two is absent, no deformation localisation will occur in a vertically stratified and laterally homogeneous system. When in a complex system with two segments with different strength, the thermal and displacement constraints are in the order of magnitude to reproduce the ‘plume-centred’ break-up mode, then it is possible to reproduce not only the ‘plume-centred’ break-up mode, but also the ‘structural inherited’ break-up mode, creating two rift branches that can both develop into a spreading centre. This heavily depends on the initial location of the mantle plume in a system where the thermal and displacement conditions are favourable for extensional deformation localisation. The two-branch break-up results are not applicable to the South Atlantic. In the North Atlantic domain, several rift and spreading branches exist, that are considered to have somehow been influenced by the Iceland mantle plume. In this region, the two-branch break-up models might be applicable, showing that it is actually possible to create to break-up branches that both have been influenced by one, single mantle plume.

Abstract

Thermomechanical modelling of plume-induced continental break-up reveals that the initial location of a mantle anomaly relative to a lithosphere inhomogeneity has a major impact on the geometry and timing of a rift-to-spreading system. Models with a warmer Moho temperature are more likely to result in “plume-centred” mode, where the rift and subsequent spreading axis grow directly above the plume. Models with weak far-field forcing are inclined to develop a “structural-inherited” mode, with lithosphere deformation localized at the lateral lithospheric boundary. Models of a third group cultivate two break-up branches (both “plume-centred” and “structural inherited”) that form consecutively with a few million years delay. With our experimental setup, this break-up mode is sensitive to relatively small lateral variations of the initial anomaly position. We argue that one single mantle anomaly can be responsible for non-simultaneous initiation and development of two rift-to-spreading systems in a lithosphere with a lateral strength contrast.

Reference: Beniest, A., Koptev, A., Leroy, S., Sassi, W., Guichet, X., 2017. Two-branch break-up systems by a single mantle plume: insights from numerical modelling. Geophysical Research Letters, 44, pp. 1-9.

4.1 Introduction

Continental rifting is a complex process that depends on many factors such as the rheological structure of the crust and lithospheric mantle (Brun, 2002; Burov, 2011), thermal distribution in the lithosphere (Brune et al., 2014; Lavier and Manatschal, 2006)), the presence or absence of inherited structures (Chenin and Beaumont, 2013; Manatschal et al., 2015), far-field forces (e.g. Huisman et al., 2001) and mantle plume(s) (Burov and Gerya, 2014). To date, a variety of analogue and numerical models have examined plume-induced continental rifting and break-up. For example, these models are able to explain quite complex geometries of a plume itself (Davaille et al., 2005) and its diverse effects when interacting with a rheologically stratified lithosphere such as asymmetric short-wavelength topography (Burov and Cloetingh, 2010; Burov and Gerya, 2014), the reduction of lithospheric strength (Brune et al., 2013), the multiphase development of rifting with a quick transition from wide to narrow mode (Koptev et al., 2017) and the shifted position of the break-up centre with respect to the initial point of plume impingement (Beniest et al., 2017).

Single rift – plume interactions are well-investigated, but complex multi-branch continental rift and oceanic spreading systems are less well-understood even though they exist all around the world. The Labrador Sea between Greenland and mainland Canada (Chalmers et al., 1995; Saunders et al., 1997) and the Aegir Ridge between Greenland and Norway (Gaina et al., 2009) are two (non-active) spreading branches that developed consecutively in the North Atlantic region (Fig. 4.1a, for tectonic reconstruction see Skogseid et al. (2000)). The Abimael Ridge offshore south Brazil (Fig. 4.1b, for tectonic reconstruction see e.g. Torsvik et al. (2009) and Moulin et al. (2010)) corresponds to an abandoned part of the South Atlantic rift system (Mohriak et al., 2010). Another example is the Tasman Sea that is separated by the Dampier Ridge from the Lord Howe Rise and Middleton Basin, all part of the same rift system (Fig. 4.1c, for tectonic reconstruction see Gaina et al. (1998)). These ridges and branches differ significantly in terms of the width of newly formed oceanic lithosphere and the distance between active and aborted ridges. For example, the total width of the Norwegian-Greenland Sea reaches for some 1000 km (Fig. 4.1a, (Greenhalgh and Kusznir, 2007)) whereas both the Labrador and Tasman Sea only gained 100 of km's of oceanic crust width before abortion (Fig. 4.1a and 4.1c). The oceanic lithosphere associated with the Abimael ridge is even narrower than the Labrador Sea and the Tasman Sea, with a total width of a couple of 10's of kilometers only (Fig. 4.1b, (Mohriak et al., 2010)). The Lord Howe Rise and Middleton Basin (Fig. 4.1c) have only reached a rift phase (between 90 Ma and 84 Ma, Gaina et al. (1998)), not providing any evidence for oceanic crust formation, but they remain a separate branch of the break-up system of the Tasman Sea, where spreading initiated at 83 Myr (Gaina et al., 1998). The distance between the present-day location of the aborted and active rift- and spreading ridges can be as far away as over 5000 km's in the case of the Abimael ridge and the South Atlantic mid-ocean ridge (Fig. 4.1b) or as close by as only 200 km in case of the Aegir Ridge (Fig. 4.1a).

Despite these differences, such multi-branch systems have one important thing in common: they are underlain by a deep-rooted mantle anomaly with varying geometries that may have triggered their initiations and controlled their subsequent evolution. Present-day geometries of mantle anomalies can be visualized with mantle tomography. This method suggests that the Iceland plume (Fig. 4.1a, after (Zhao, 2007)) extends throughout the mantle to the core-mantle boundary (French and Romanowicz, 2015). The Tristan plume (Fig. 4.1b, (Zhao, 2007)) is rooted in the lower mantle and seems to be failing in the upper mantle nowadays, although it leaves an ancient hotspot trail behind (Schlömer et al., 2017). The Tasmantid (TasP) low velocity zone (Fig. 4.1c, (Zhao, 2007)) is currently confined to the upper mantle and transition zone with a lower mantle stem significantly distanced from the upper mantle part of the plume. Yet, up to five ancient hotspots could be the surface expressions of this mantle plume (Davies et al., 2015).

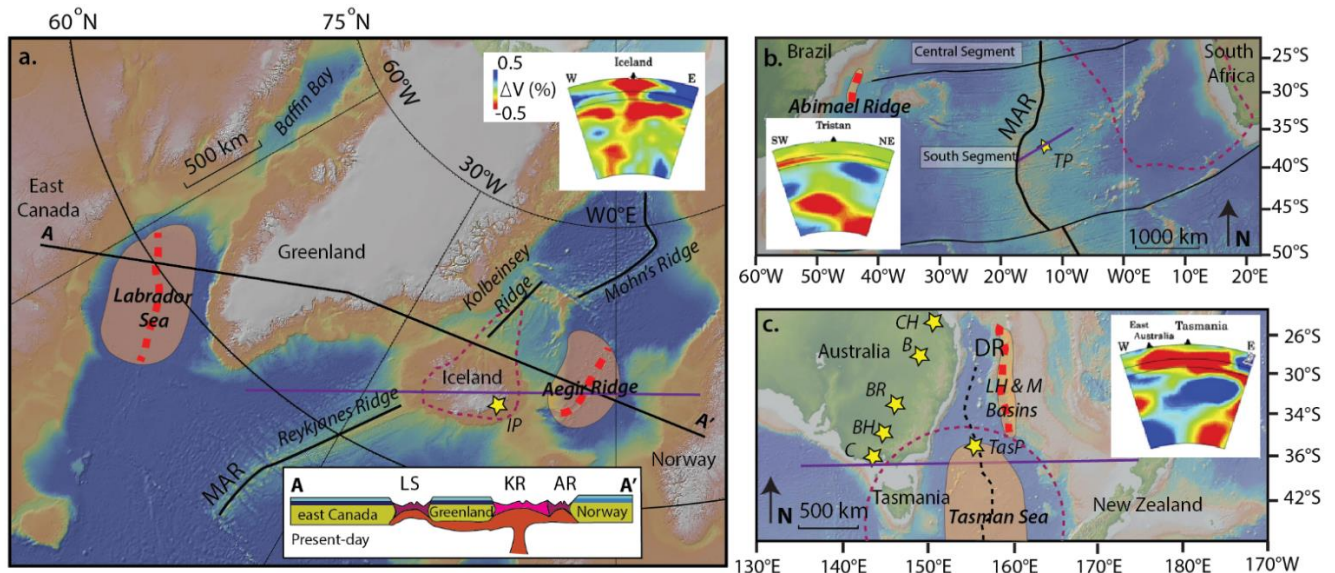


Figure 4.1. Three natural examples of a complex multi-branch spreading system associated with a single mantle plume: a) The Labrador Sea (Chalmers et al., 1995) and the Aegir Ridge (Greenhalgh and Kuszniir, 2007) developed consecutively in the North Atlantic region. The Iceland plume (dashed purple line) is now located directly below currently active mid-ocean ridge (Rickers et al., 2013). The black line represents a position of a schematic cross-section of the North Atlantic domain (for color-code see Figs. 4.2 and 4.4). b) The Abimael Ridge is a failed rift branch along which evidence for oceanic crust has been observed (e.g. Mohriak et al., 2010). The Tristan Plume associated to the African Superswell (dashed purple line) is located close to the South Atlantic mid-ocean ridge (Ernesto et al., 2002). c) The spreading axes of the Tasman Sea and rift axis of Lord Howe and Middleton Basins are part of the same system (Gaina et al., 1998). The Tasmantid (TasP) and Cosgrove (C) hotspots lay on the edge of the Tasmantid Plume (dashed purple line). The tomographic images are taken from Zhao [2007]. The purple lines show their approximate location. The yellow stars are asthenosphere hotspot locations. IP = Iceland Plume hotspot, LS = Labrador Sea, KR = Kolbeinsey Ridge, AR = Aegir Ridge, MAR = Mid-Atlantic Ridge, TP = Tristan Plume hotspot, BH = Begargo Hill hotspot, BR = Bokhara River hotspot, B = Buckland Hotspot, CH = Cape Hillsborough hotspot, DR = Dampier Ridge, LH&M Basins = Lord Howe and Middleton Basins. Australian hotspots after Davies et al. [2015].

Despite numerous numerical modelling exercises (Beniest et al., 2017; Brune et al., 2014; Burov and Gerya, 2014; Chenin and Beaumont, 2013; Huismans and Beaumont, 2008; Koptev et al., 2016; Lavecchia et al., 2017) no self-consistent numerical model has thus far explained how multi-branch break-up centres, separated in space and time, can result from the impact of the same mantle plume (Fig. 4.1). Here, we present the results of a 2D thermo-mechanical modelling study investigating the effect of the pre-rift position of a mantle plume anomaly on the rift-to-spreading evolution in a laterally heterogeneous lithosphere, with different initial Moho temperatures and various extension rates.

4.2. Numerical model setup

We use a 2D version of the viscous-plastic numerical code I3ELVIS (Gerya and Yuen, 2007) to study plume-induced rifting and continental break-up of a lithosphere with a lateral rheological contrast. This code combines a finite difference method on a staggered Eulerian grid with a marker-in-cell technique. For a detailed description of the code we refer to Gerya and Yuen (2007), Gerya (2010) and supplementary material 1.

The spatial dimensions of the model are 1500 km in length and 635 km in width. The model box contains 297 x 133 nodes, so that the grid cell size corresponds to 5 x 5 km. The model setup consists of a three-layered lithosphere (150 km), overlying the sub-lithospheric mantle (455 km). The crustal thickness is 40 km, equally divided in upper crust (20 km) and lower crust (20 km) (appendix II, supplementary Fig. 1.1). The homogenous upper crust has ductile properties of wet quartzite whereas the lower crust is characterized by a lateral contrast in rheological strength: a ‘strong’ left side, made of anorthite rheology, and a ‘weak’ right side, consisting of wet quartzite rheology (Bittner and Schmeling, 1995; Clauser and Huenges, 1995; Connolly, 2005; Kohlstedt et al., 1995; Ranalli, 1995; Turcotte and Schubert, 2002). The contact between these two rheologically different crustal segments represents a simplified inherited structure, located in the top-middle of the model box. The lithospheric and sub-lithospheric mantle uses dry olivine rheology whereas the mantle plume is simulated with wet olivine rheology (more detailed information on rheological and material properties of the crust can be found in appendix II, supplementary table 2.1). The initial mantle plume anomaly is positioned at the base of the model box and has a spherical shape with a radius of 200 km, which is in correspondence with previous work (e.g. Burov and Gerya, 2014; Koptev et al., 2015). We use a linear geotherm with 0 °C at the surface, 500 °C or 600 °C at the Moho (40 km), 1300 °C at the base of the lithosphere (150 km) and 1630 °C at the bottom of the model domain (635 km). The Moho temperature (500 °C and 600 °C) is one of the variable parameters of our study (appendix II supplementary table 3.1). The mantle anomaly has an initial temperature of 2000 °C corresponding to 300-370 °C contrast with surrounding mantle. The general thermal boundary conditions align with fixed temperatures at the top (0 °C) and bottom (1630 °C) of the model and zero heat flux is imposed on the vertical boundaries of the model

box. Far-field tectonic extension is applied on both vertical sides with a constant half-rate of 5 mm/yr or 10 mm/yr (appendix II supplementary table 3.1). The resulting horizontal forces along the border of the models are of the same order of magnitude (5×10^{12} N per unit length) as “ridge push” (e.g. Buck, 2007) and “slab-pull” forces (Schellart, 2004). Apart from the initial Moho temperature and the initial extension rate, our main changing parameter is the pre-rift plume location. In a previous study of Beniest et al. (2017a) the anomaly was positioned at three different locations with respect to the crustal rheological and geometrical variations. For this study, the mantle plume is initially placed directly below the rheological contact after which it is positioned further away from this contact below the ‘stronger’ half of the model with steps of 25-100 km. The maximum lateral shift of the plume with respect to its central location is 450 km. We performed 3 sets of 9 numerical experiments, resulting in 27 models total (appendix II supplementary table 3.1). The first set has a Moho temperature of 500 °C and an extension rate of 10 mm/yr, the second set has a Moho temperature of 600 °C and an extension rate of 10 mm/yr and the last set has a Moho temperature of 500 °C and an extension rate of 5 mm/yr. In addition, we performed 19 complementary models (supplementary material 3.2 and 4) to test the models sensitivity to certain parameters such as grid cell size (higher resolution), plume size (larger radius), plume temperature (1900 °C instead of 2000 °C), Moho isotherm (650 °C) and more complex structure of the lithospheric mantle (different thicknesses for “stronger” and “weaker” segments) and crustal geotherm (non-linear).

4.3. Experimental results

In all models the mantle plume rises rapidly, reaching the base of the lithosphere in less than 2 Myr. Plume material spreads laterally along the lowest part of the lithosphere flowing as far away as ~1000 km (similarly to previous 2D experiments of Burov and Cloetingh (2010) and 3D models of Koptev et al. (2017)). Unlike these models, our experiments develop different rift-to-break-up modes that can be divided into three major groups (Fig. 4.2 and appendix II, supplementary table 3.1).

The first group demonstrates continental break-up directly above the initial plume location (‘plume-centred’ break-up mode, model 8, Fig. 4.2d and appendix II supplementary Fig. 5.1d). This category corresponds to the classical plume models also shown by e.g. d’Acremont et al. (2003) and Burov and Cloetingh (2010). Despite initial deformation localization at the contact between the ‘weak’ and ‘strong’ segments (‘structural inherited’) (appendix II, supplementary Fig. 5.1d; 1 Myr), vertical ascent of hot plume material throughout the lithospheric mantle (Fig. 4.2d; 10 Myr) leads to a second ‘plume-centred’ zone of localized strain (appendix II supplementary Fig. 4.1d; 10 Myr). This zone becomes the dominant deformation domain (appendix II supplementary Fig. 4.1d; 13 Myr) at the moment of the continental break-up (Fig. 4.2d; 13 Myr). The initial ‘structural’ inherited’ deformation zone becomes eventually completely extinct (appendix II supplementary Fig. 4.1d; 21 Myr). Thus, the plume material flowing laterally at the base of the lithosphere

is unable to turn the distant ‘structural inherited’ rifting into a break-up centre (appendix II supplementary Fig. 5.1d).

The second category includes models showing rifting and subsequent break-up only at the contact between two rheological segments (‘structural inherited’ break-up mode). Here, due to the initial plume position being closer to the inherited structure, localized plume ascent coincides with the ‘structural inherited’ zone of the initial continental rifting. This leads to plume-induced (but ‘structural inherited’) break-up (model 3, Fig. 4.2a). Note that there is no evidence for strain localization within the stronger lithosphere above the initial plume location (appendix II supplementary Fig. 5.1a).

Models of the third group illustrate an intermediate behavior where two break-up centres form consecutively. These ‘two-branch’ experiments develop first the ‘structural inherited’ and then the ‘plume-centred’ break-up modes or vice-versa depending on the initial plume position (models 6 and 7, Figs. 4.2b and 3.2c). In both cases the first rifting phase is ‘structural inherited’ (appendix II supplementary Figs. 5b-c; 1 Myr), but the order in which the break-up centres develop, depends heavily on relatively small (< 30 km) lateral variation of the initial plume position with respect to the rheological boundary (Figs. 4.2b-c and appendix II supplementary Figs. 5b-c). When the initial thermal anomaly is situated further away from the rheological contact (at 375 km) ‘plume-centred’ break-up develops first, directly above the anomaly. This is due to the rapid, localized ascent of plume material through the mantle part of the stronger overlying lithosphere (Fig. 4.2c and appendix II supplementary Fig. 5.1c, 11-16 Myr). After that, hot plume material residing at the base of the lithosphere rises below the ‘structural inherited’ rift zone (Fig. 4.2c and appendix II supplementary Fig. 5.1c; 16 Myr) leading to complete rupture of the continent at the pre-imposed structural boundary (Fig. 4.2c and appendix II supplementary Fig. 5.1c; 22 Myr). When the mantle plume is positioned only 350 km away from the rheological contact ‘structural inherited’ break-up develops first, followed by a ‘plume-centred’ one (Fig. 4.2b; appendix II supplementary Fig. 5.1b). In both cases the time delay between these two continental break-ups is less than 10 Myr.

The ‘two-branch’ category results from the reference model setup that uses a relatively fast extension rate (half-rate 10 mm/yr) and colder Moho temperature (500 °C, models 1-9, Fig. 4.3a). In a different set of models where the extension rate is being kept at 10 mm/yr but the crustal geotherm is warmer (600 °C at the Moho, models 10-18), a similar ‘two-branch’ system is produced when the plume is shifted 300 km away from the rheological contact (Fig. 4.3b). Note, however, that in this model only the ‘plume-centred’ rift axis evolves into a spreading centre, whereas the ‘structural inherited’ branch does not reach this phase. For this set of model setups, the ‘plume-centred’ break-up mode is the dominant break-up mechanism when the anomaly is located 350 km or further away from the inherited structure (Fig. 4.3b).

A series of complementary experiments show that a further increase in the initial crustal geotherm (e.g. 650 °C, models 30-36) has no principal effect on the final continental break-up mode (compare Fig. 4.3b and

appendix II supplementary Fig. 4.2). Small variations in the initial temperature distribution, e.g. a non-linear crustal geotherm that takes into account radiogenic heat production (model 29, appendix II supplementary Fig. 4.1c), does not play a significant role neither. For the last set of models the thermal state is the same as for the reference model (500 °C Moho temperature) and the spreading rate is decreased to 5 mm/yr half-rate extension (models 19-27). For this model series, all models persistently cultivate ‘structural inherited’ break-up for all tested mantle plume emplacements (Fig 4.3c). Exactly the same behavior is observed in the complementary experiments that include non-uniform thicknesses of the lithosphere with a thicker “stronger” (150 km) segment and a thinner “weaker” (100 km) segment (models 43-46). Regardless the initial plume position and the type of transitional zone between the different rheological segments (vertical or slope), these models show only “structural inherited” break-up mode, without any evidence for “plume centred” rift initiation (appendix II supplementary Fig. 4.5). Without dismissing that such contrasts in the rheological and thermal structure are present not only at crustal level but also in the lithospheric mantle, our results provide new elements to evaluate the importance of the mantle inhomogeneities on the initiation and development of multi-branch rift systems.

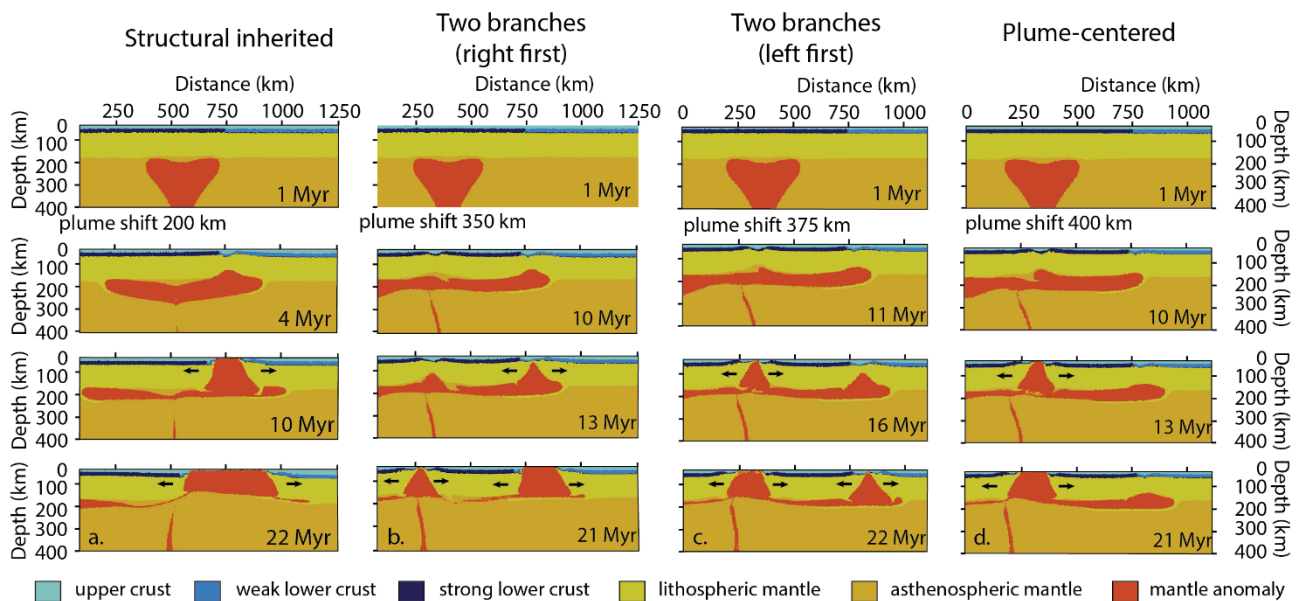


Figure 4.2. The most representative examples of the three different break-up modes (from the model series distinguished with a Moho temperature of 500 °C and half-rate extension of 10 mm/yr, see also Fig. 4.3a and appendix II and supplementary table 3.1): a) model 3 with an initial plume shift towards the stronger segment of 200 km: “structural inherited” mode; b-c) models 6 (plume shift of 350 km) and model 7 (plume shift of 375 km): “two-branch” mode; d) model 8 (plume shift of 400 km): “plume-centred” mode. Note that not only the initial position but also the initial size (models 37-38) and temperature (models 39-42) of the mantle anomaly (appendix II supplementary Figs. 4.3 and 4.4) might be critical for the final break-up mode.

4.4. Discussion and conclusion

Our results show that in case of a cold Moho (500 °C) and relatively fast (10 mm/yr) extension, three modes of break-up are possible, depending on the location of the mantle anomaly with respect to a rheological contact. With respect to this “reference model” set, a higher Moho temperature better facilitates deeper penetration of plume material into the lithosphere. This favors a vertical localized ascent up to the Moho ultimately leading to continental break up directly above initial plume emplacement. This “plume-centred” axis is situated closer to the rheological contact than in case of lower Moho temperature. A general example of this ‘plume-centred’ rifting, can be observed in for example the Afar depression where the formation of complex triple junction (e.g. McClusky et al., 2010) is linked to the arrival of the Afar plume (Bellahsen et al., 2003) at ~30 Ma (Hofmann et al., 1997; Coulié et al., 2003). In case extension rate is relatively low (5 mm/yr extension), the thermal impact of the mantle plume becomes less important, the system prefers deformation localization at the mechanical instability created by the rheological contact. This implies that external tectonic forcing is too weak to localize deformation outside of the pre-defined structural boundary even in presence of an active mantle anomaly that is considerably shifted with respect to this structure. This is generally consistent with numerical results done by Burov and Gerya (2014).

A natural example for ‘structural inherited’ break-up could be the South Atlantic domain where plume-induced break-up takes place at the boundary between stronger (African) and weaker (South-American) lithosphere segments despite possible eastward offset initial position of the mantle plume with respect to this boundary (see Beniest et al., (2017a) for more details).

When the anomaly is located at a position where both the impact of the mantle anomaly on the lithosphere and the predefined rheological contact of the system are competing for deformation localization, the ‘two-branch’ break-up mode develops. For our reference models set (Fig. 4.3a), a ‘two-branch’ system forms when the mantle anomaly has a lateral displacement of 350-375 km towards the stronger half of the model domain with respect to the rheological contact. The two branches develop consecutively, with roughly 10 Myr delay, with either ‘structural inherited’ break-up first, followed by ‘plume-centred’ (displacement 350 km, Fig. 4.2b) or the other way around (displacement 375 km, Fig. 4.2c). Slight offset to this specific dislocation converts the break-up mode to either ‘structural inherited’ or ‘plume-centred’ (Figs. 4.2, 4.3).

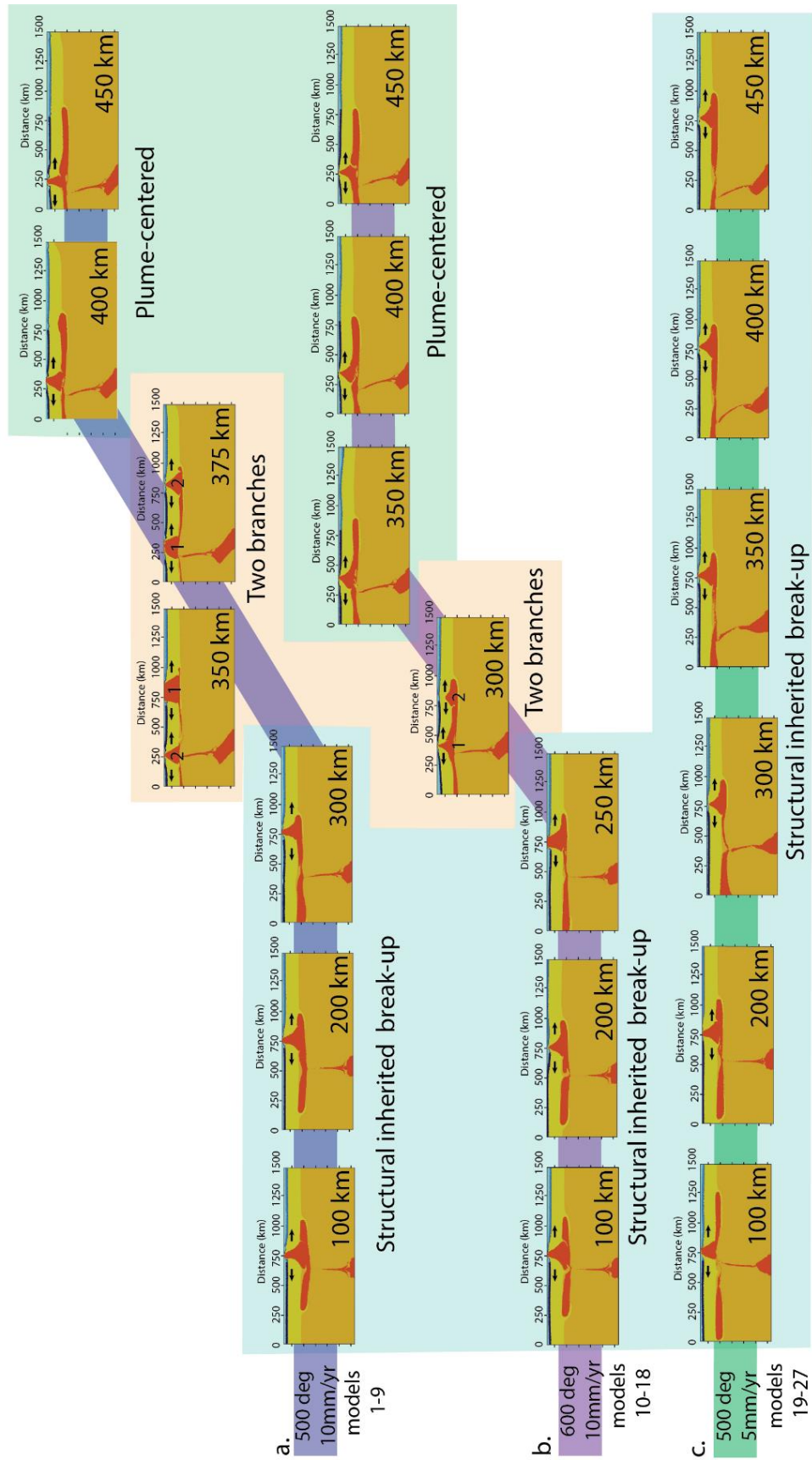


Figure 4.3 (previous page). Graph showing the results of the three sets of models (a. 500 °C Moho temperature and 10 mm/yr extension rate, b. 600 °C Moho temperature and 10 mm/yr extension rate and c. 500 °C Moho temperature and 5 mm extension rate) aligned with increasing distance between the initial anomaly location and the rheological contact. For the experiments with faster extension half-rate (10 mm/yr) there is a critical distance when the system changes from “structural inherited” to “plume-centred” break-up through a two-branch system. This distance is between 300 and 400 km for the Moho temperature of 500 °C (a) and between 250 and 350 km for Moho temperature of 600 °C (b). Closer to the rheological boundary the rift-to-spreading system develops uniquely above the structural inheritance, further away it evolves directly above the plume impingement point. Note that “plume-centred” mode of development does not exclude some localization of initial deformation at the rheological contact (“structural inherited” aborted rifting, see appendix II supplementary Fig. 5.1).

Both “plume-centred” and “structural inherited” modes of break-up have been modelled by Beniest et al., 2017a and Lavecchia et al., (2017). To model a “two-branch” system a particular position of the mantle plume anomaly with respect to rheological contrast at the crustal level should be determined. Only relatively narrow (25-50 km) range of initial plume locations can result in multi-branch systems associated with the direct impact of locally upwelled plume material. The thermal state appears to be of lesser importance (see Fig. 4.3a-b where two branches develop with both colder and hotter Moho temperatures), but far-field forcing should not be too weak (see Fig. 4.3c). Our ‘two-branch’ model with a plume location 375 km away from the rheological contact bears most similarities to the geodynamic history of the North Atlantic region (Fig. 4.4). Here, the old and rigid lithosphere of the Greenland craton (Kerr et al., 1997) was underlain by a single mantle anomaly (the Iceland mantle plume) before rifting started in the Labrador Sea (Lundin and Doré, 2002; Rogozhina et al., 2016). The old craton was subjected to plume-activated continental rifting in the Late Triassic or Jurassic (Peace et al., 2016) followed by seafloor spreading with the oldest accepted magnetic anomaly being of Danian (~64 Ma) age (Chalmers et al., 1995) (although older anomalies are still a matter of debate (Peace et al., 2016)). Note, however, that the opening of the mostly a-magmatic Labrador Sea might have started before the mantle plume impacted the lithosphere beneath West Greenland (Larsen and Saunders, 1998). A second axis of active spreading (the Aegir ridge) initiated at 57 Ma (i.e. 5-10 Myrs later) (Lundin and Doré, 2002) close to the adjacent Caledonian suture zone (Gaina et al., 2009; Abdelmalak et al., 2016), several 100’s of kilometers away from the area of the first plume impingement. Thus, both the position of the Iceland plume (e.g. Rogozhina et al. (2016) and references herein) near the western coast of Greenland (with a shift of several hundreds of kilometers with respect to the weaker Caledonian suture) at the moment of the initiation of the first spreading branch (even if the paleo-position of the Iceland hotspot remains debatable – see e.g. (Torsvik et al., 2015)) and the time delay of less than 10 Myr between “plume-induced” and “structural inherited” break-ups bear strong similarity with the key features of our “two-branch” model displayed in Fig. 4.2c and Fig. 4.4a-c.

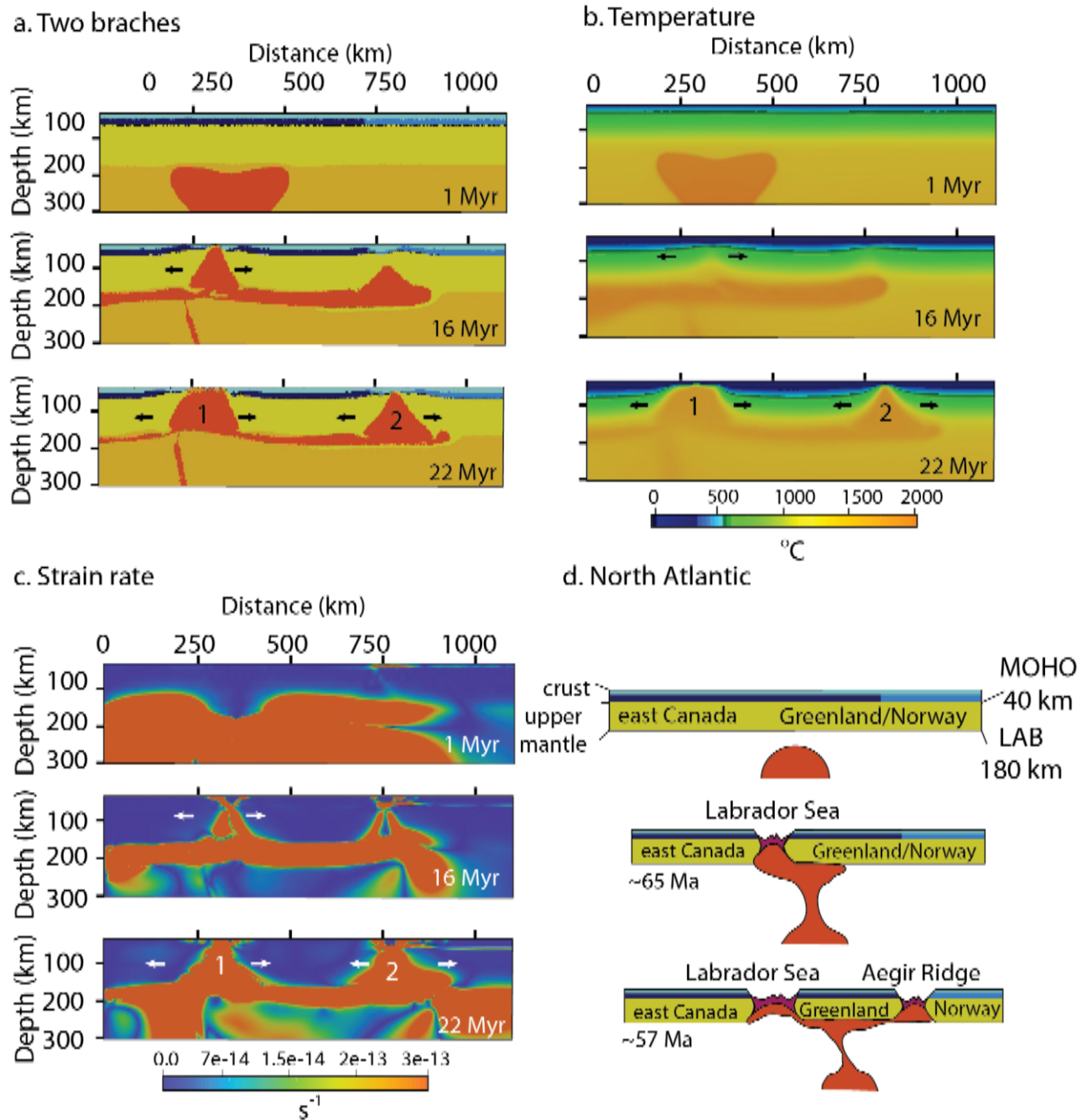


Figure 4.4. Phase (a), temperature (b) and strain rate (c) plots of model 7 (Moho temperature of 500 °C, extensional rate of 10 mm/y, plume shift of 375 km). This model develops a “two-branch” break-up mode and bears strong similarities with the geodynamical evolution in the North Atlantic domain (d, schematic representation) : 1) the first branch forms in the left part of the model, corresponding to the strong crust, similar to Greenland craton that will eventually separate Greenland and Canada (Peace et al., 2016); 2) the second branch forms 6 million years later close the inherited structure, comparable to the break-up of the Caledonian orogeny eventually separating Greenland and Norway (Lundin and Doré, 2002). The pink color on the schematic profiles refers to newly formed oceanic lithosphere.

In this case, the key-features refer to 1) lateral varying rheological contact resembling an inherited structure (the Caledonian Suture), 2) a relatively cool thermal structure comparable to a craton (West-Canada-Greenland craton), 3) the location of the mantle anomaly at 350-375 km away from the inherited structure, which would be well below the Greenland craton, and 4) the timing of the two break-up branches only 5-10 Myr apart in the model, that corresponds well to the 64 Ma for the Labrador Sea ('plume-centred' break-up branch) and 7 Myr later, at 57 Ma the Aegir Ridge ('structural inherited' break-up branch). We note that given the natural limitations of the used 2D approach, further explore the effect of plume on multi-branch systems with 3D tests would facilitate a more detailed comparison with observations in the North Atlantic.

Based on our modelling results and examples from nature, we note that rheological heterogeneities in the lithosphere, its thermal state and acting mechanical forces and the lithospheric structure are important parameters for the rift-to-break-up evolution of the system. In addition we show that, the initial location of the plume with respect to a laterally varying lithosphere is not only an important factor on rift and break-up modes and geometries, but also affects the timing and order of the development of the branches. We argue that, in combination with far-field forces and the thermal state of the system, the emplacement of the plume anomaly is a key parameter for plume-induced continental rifting and break-up numerical modelling.

Highlights:

- A single mantle plume can be responsible for two non-contemporaneous rift-to-spreading systems in a laterally nonhomogeneous lithosphere
- The pre-rift distance between a plume and a lateral lithospheric boundary between two segments controls rift-to-spreading systems
- The location of a plume with respect to lithosphere inhomogeneities is a key variable when modelling plume-induced continental break-up

Chapter 5: Discussion

If you know you are on the right track, if you have this inner knowledge,

Then nobody can turn you off. No matter what they say.

~ Barbara McClintock, Physiology and Medicine

5.1. From continental rifting to conjugate margins

The rift to spreading history of the break-up of Gondwanaland is recorded in the basins along the South Atlantic margins. The margins show dissimilarities in terms of crustal thickness, structure and basin sediment infill. These differences are not only latitudinal (between the Central and South Segment), but also exist between the conjugate margins (Fig. 5.1). The South Segment margins have massive SDR deposits that are mostly absent along the Central Segment margins (e.g. Blaich et al., 2011; Moulin et al., 2010; Torsvik et al., 2009). The basins along the Central Segment margins have massive salt deposits that are not observed in the basins along the Southern Segment (Blaich et al., 2011; Marcano et al., 2013).

The conjugate margins can be compared per segment as well. The South American margins of the Central Segment (e.g. Espírito-Santos basin) have transitional domains with similar widths (Blaich et al., 2011), although the whole African side (Kwanza basin) margin appears to be wider than the South American side (Fig. 5.1a). The crustal thicknesses of both margins are about 18 km thick (Blaich et al., 2011). In the South Segment, the margins of the South American side (e.g. in the Colorado basin) show extensional deformation features further land inwards, than on the African side (the Orange basin). The South American margin width is larger than its African conjugate (Fig. 5.1b). Also the crustal thickness varies as below the South American margin the thickness reaches 20 km compared to 30 below the African margin. Towards the ocean, crustal thicknesses become similar, roughly 10 km. For this reason the African margin appears to have thinned more than the South American.

Despite all these differences between the segments and conjugate margins of the South Atlantic domain, the final result is the same: the break-up of two continents. The compilation of rift-to-break-up models presented in Chapter 2, 3 and 4, show that there are indeed several ways to break-up a continent depending on the rheological differences in the lithosphere and the presence or absence of a mantle plume. Previous studies have already explained margin asymmetry and symmetry of the South Atlantic with numerical and analogue models. Some studies dedicate it to far-field forces that act on the system, for example as a result of non-linear extension velocities (Brune et al., 2016), steady-state rift migration of a system under continuous extension (Brune et al., 2014) or the oblique orientation of far-field forces to the spreading-centre (Brune et al., 2013). Others consider inherited structures as the main reason for the final geometry of the rift (Cappelletti et al., 2013) or the interplay between the rheology of the lithosphere and thermo-mechanical processes (Svartman Dias et al., 2015).

One thing that all these studies have in common is the rather homogeneous initial model setup. The contribution to this discussion on conjugate margin geometries that results from this thesis is the inclusion of more complex lithosphere initial model setup. The parameters tested with more homogenous models, have a different effect on the system once the system itself contains more *in-situ* variations. It's the combination between the initial state and these processes that define whether or not the crust will break at an inherited structure, in a 'pure-shear' mode or not at all.

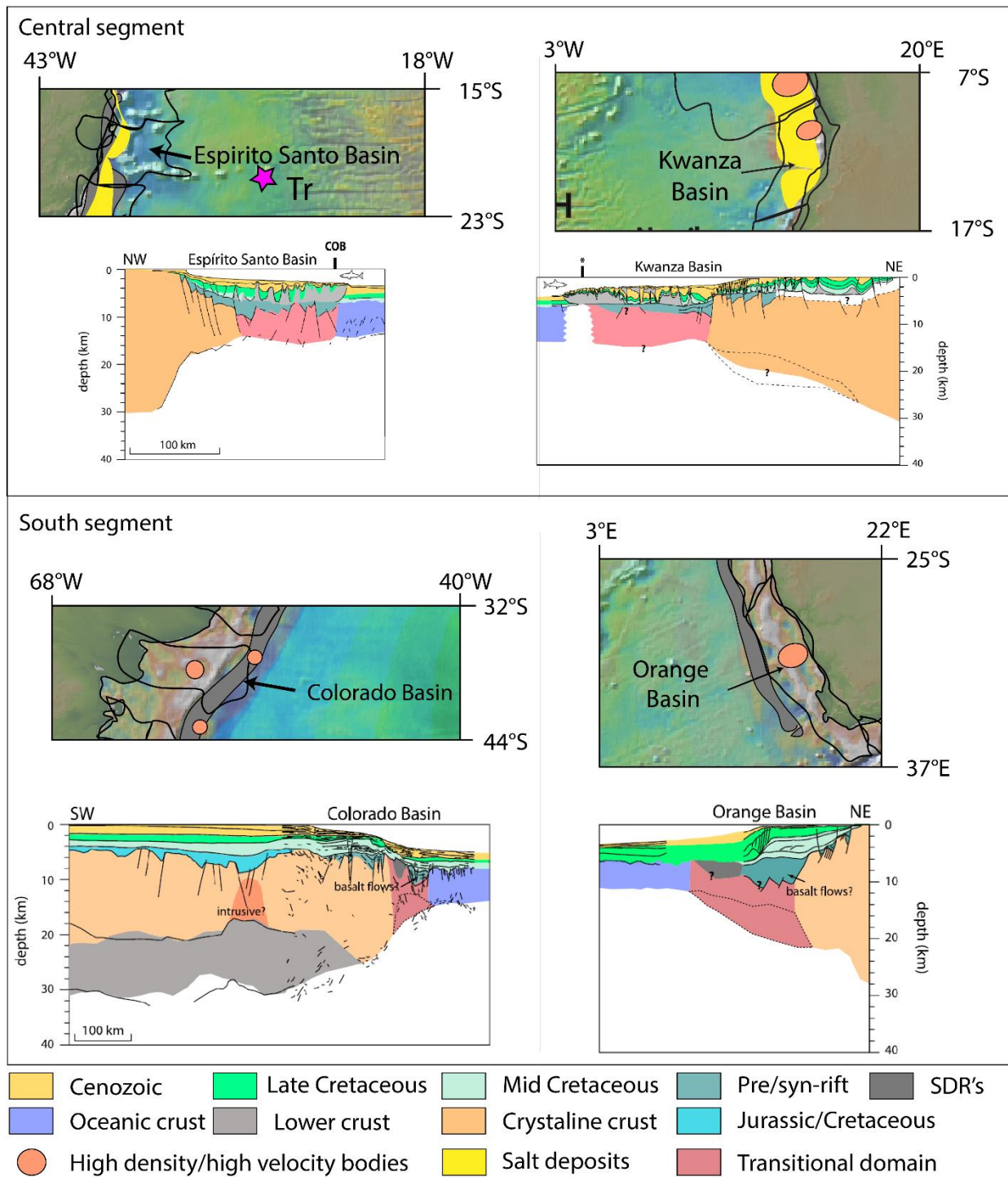


Figure 5.1. Two conjugate basin sets along the Central Segment (a) and the South Segment margins of the South Atlantic domain projected in map view (Beniest et al., 2017) and cross-sections (Blaich et al., 2013). Asymmetry is observed in crustal thickness, basin width, basin orientation, sediment thickness and the presence of high velocity/high density bodies observed on gravity.

Break-up of the central segment has resulted in rather symmetric transitional domain margin geometries, although the African margin is wider than the South American side. There is also no rooted mantle plume present in the Central Segment. Our analogue model results with two different lithosphere segments show that without the use of a thermal anomaly, break-up may occur in a 'pure-shear' way. The results are rather symmetric geometries close to the break-up point. This compares to e.g. the scale of the transitional domain in the Central Segment where transitional domain widths are rather similar. However, when taking into account the whole margin, including the strong segment, geometries become asymmetric, because the extension is accommodated only in the weak lithosphere, leaving the strong segment intact. Which is comparable to a larger scale of the Central Segment margins, including the continental and oceanic parts of the margin.

For the margins of the South Segment, including thermal processes is obligatory because of the presence of the Tristan Plume. Adding this parameter complicates rift initiation and increases the possibilities to arrive at continental break-up. In the case of the South Segment of the South Atlantic, positioning the plume slightly off-set below the stronger segment, results in asymmetric margin development, in terms of crustal thickness (similar to the margin geometries in Fig. 5.1b) and underplated material (comparable to the high density/high velocity bodies at lower crustal level that occur along the margins).

More specifically, depending on the thermal state and extensional forces acting on a system consisting of different rheological segments, it is possible to model two break-up branches, by just placing the mantle anomaly at a distance from the rheological contact. It is a rather sensitive parameter, as there is only a small window for which two-branch systems develop.

The location of the mantle anomaly with respect to rheological contacts is thus a key-parameter that has never been tested before in such detail with thermo-mechanical models. Here it has shown that its initial position plays a significant role in the formation of asymmetric margins, volcanism and anomalous bodies at lower crustal depth. This parameter should be used with care when performing thermo-mechanical modelling as it greatly influences the outcome. However, implementing a mantle anomaly in thermo-mechanical models and varying its initial plume-emplacment, increases the possibilities of geodynamic models for plume-induced continental break-up.

5.2. The thermal evolution of conjugate marginal basins

The different continental rift to break-up evolutions have implications for basin and petroleum systems that develop in the basins above these margins. As an example the focus will lie on the effect of thermal processes within a marginal basin.

The thermal state of the lithosphere and crust is often given as a geotherm that deviates from the mantle adiabat once it reaches that part of the system where conduction is the dominant way of heat transfer and not convection (Eaton et al., 2009). There are two ways to infer heat flow values. The first way is calculating heat flow from tectonic models, e.g. the 'pure-shear' extension model (McKenzie, 1978b) and variations thereof (e.g. Royden et al., 1980). Here, heat-flow increases sharply just before it reaches

the main thinning phase followed by a thermal relaxation period that can last millions of years (Fig. 1.11c). This way of estimating heat-flow works well for rift-systems, but is less adaptable for spreading systems, because the lateral component of heat transfer becomes higher and influences basins, especially when they are elongated and not too wide (Rosencrantz et al., 1988). Also the blanketing effect of sediments is not taken into account (Van Wees et al., 2009) which might result in both crustal cooling and heating depending on the sedimentation rate (ter Voorde and Bertotti, 1994). The second way of evaluating the heat flow overtime is by interpolating Vitrinite Reflection (VR) data. Vitrinite reflection data provides punctual data on the thermal state of a system at four point in time, when the system was 1) immature, 2) within the oil-window, 3) within the gas-window and 4) exhausted (Wangen et al., 2007). There are several approaches for interpolating these points to heat flow trends, e.g. simple linear trends between the points, Monte-Carlo best-fit solutions (Ferrero and Gallagher, 2002) or inverse modelling (Gallagher, 1998).

Both approaches for evaluating heat flows, weather the based on tectonic modelling or vitrinite reflection data neglect important factors. The models based on VR do not take into account tectonic processes, e.g. the time of a rift phase or a tectonic quiescence period, whereas the tectonic modelling often does not take into account radiogenic heat production and erosion and sedimentation processes (Van Wees et al., 2009), these processes have proven to affect the thermal history of basins (e.g. Wangen, 1995; Waples, 2001).

Thermo-mechanical modelling has also been used to investigate the thermal response of the crust to tectonic processes (ter Voorde and Bertotti, 1994; ter Voorde and Cloetingh, 1996). A similar approach has been adopted to investigate the heat flow trends that result from these different rift-to-break-up modes.

Both topography and heat flow are extracted from the thermo-mechanical models. Topography takes into account the sediments that are deposited in the basin through an erosion coefficient. The heat flow is calculated using a 1D heat equation Q (eq. 5.1)

$$Q = -k * A * \frac{\Delta T}{\Delta h} \quad (\text{eq. 5.1})$$

where k is the conductivity of the material, A the surface over which the heat flow is measured, which in this 1D approach equals 1, ΔT is the temperature difference between the bottom and the top of the layer, and Δh is the vertical thickness of the layer.

For the ‘central’ break-up mode, topography and heat flow values do not significantly differ between the margins (Figure 5.2a). A rather symmetric distribution and a ‘pure-shear’ style evolution is the result. The ‘shifted’ break-up mode has more variation along the margin both with topography and heat flow values (Fig. 5.2b). During the syn-rift and early spreading phase, there is a higher topography on the left margin compared to the right margin, this changes around 15 Myr. Heat flow values are systematically

higher on the right margin which is considered to be the result of the mantle plume impinging below the right margin before break-up. The “distant” mode is the only mode where no plume material reaches the spreading centre (Fig. 5.2c). The topographic and heat flow values are rather similar for both margins. This mode is also the only mode where a second depression and rise develop to the left side of the break-up centre, directly above the plume-impingement point. This is also reflected in the elevated heat flow on this side of the model. The heat flow values calculated with the models, falls within the range of heat flow measured along marginal basin (Davies, 2013; Davies and Davies, 2010). However, they should not be taken as fixed, because the heat flow calculation is only based on the vertical temperature differences, not taking into account lateral variations. Also crustal heterogeneities that are likely to occur in the Continent-Ocean-Transition zone, for example the change from underplated mafic rocks to more felsic basement rocks are not taken into account.

The values calculated with this model can be compared with for example the ‘pure-shear’ tectonic model (Fig. 5.3., Paton et al., 2007). Heat flow estimations using beta factors are in general higher than the ones calculated with the thermo-mechanical model. The trends of the thermo-mechanical model heat flow calculations show much more variation than the heat flow based on the ‘pure-shear’ tectonic model. The different modes of break-up, with or without the influence of a plume, result in different heat flow magnitude levels and also different intensities along the margins, depending on the presence or absence of a plume and the initial location of the plume (Fig. 5.4). When there is no plume involved, intensities remain rather low (e.g. the ‘distant’ break-up mode, Fig 5.3 and 5.4.a) but similar on both sides of the margin. In case there is a mantle plume involved and it develops into the ‘classical’ or ‘central’ break-up setting (Fig. 5.3 and 5.4b), intensities are higher, but still of equally intensity on both sides. Lastly, when the initial plume location is not directly below the final break-up centre and plume material has to migrate laterally along the base of the lithosphere (‘shifted’ break-up mode, Fig. 5.3 and 5.4c) the heat flow is significantly higher below the margin along which plume material has migrated compared to the other one.

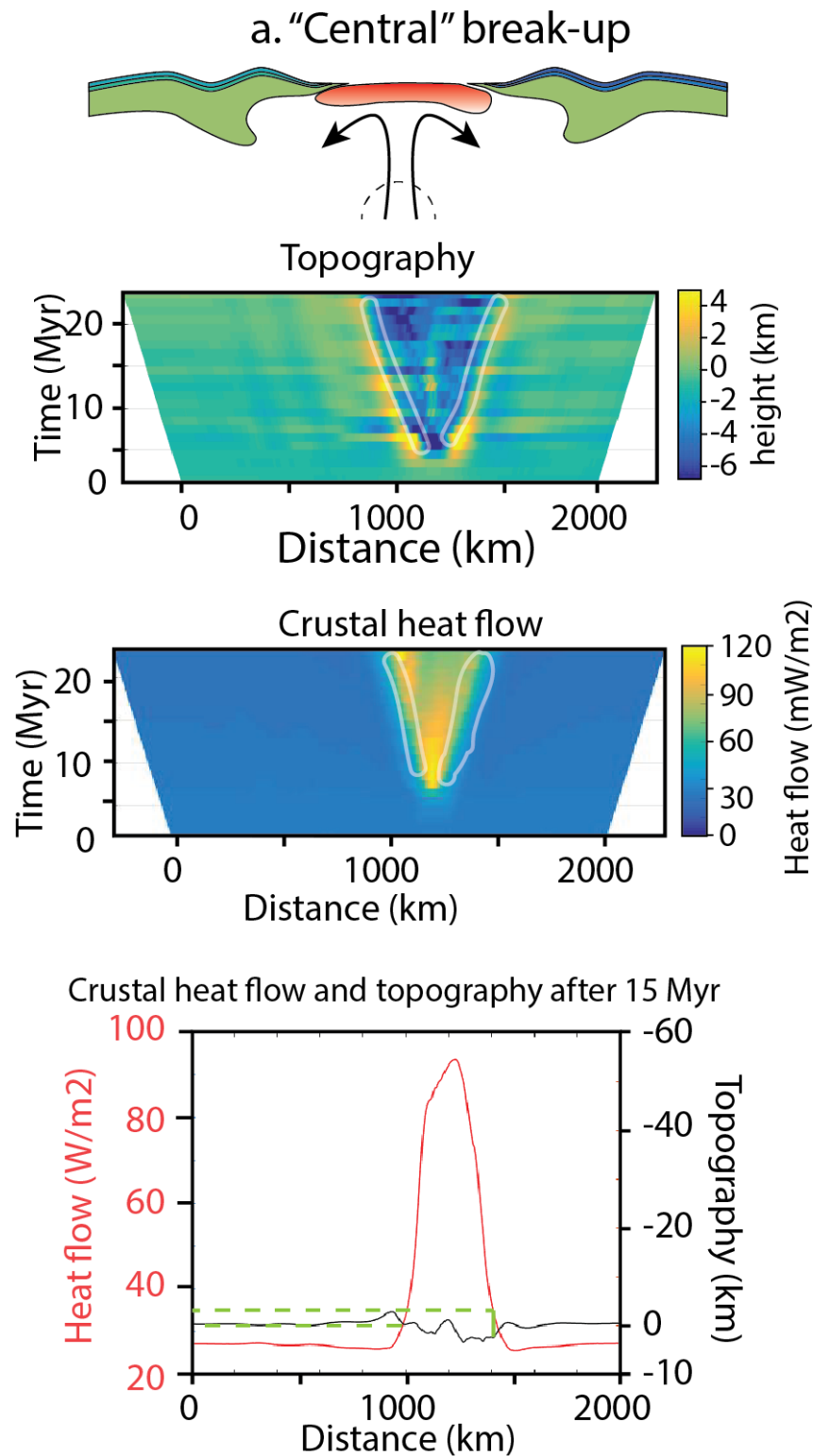


Figure 5.2a. Topographic and heat flow evolution of over time for the 'central' mode of break-up. The profiles show the topography and heat flow at 15 Myr, during the post-rift phase. The white outline shows the location of the conjugate basins. Both heat flow and topography show similar values true time, although just before break-up (around 7 Myr) the left margin has a higher heat flow value than the left margin.

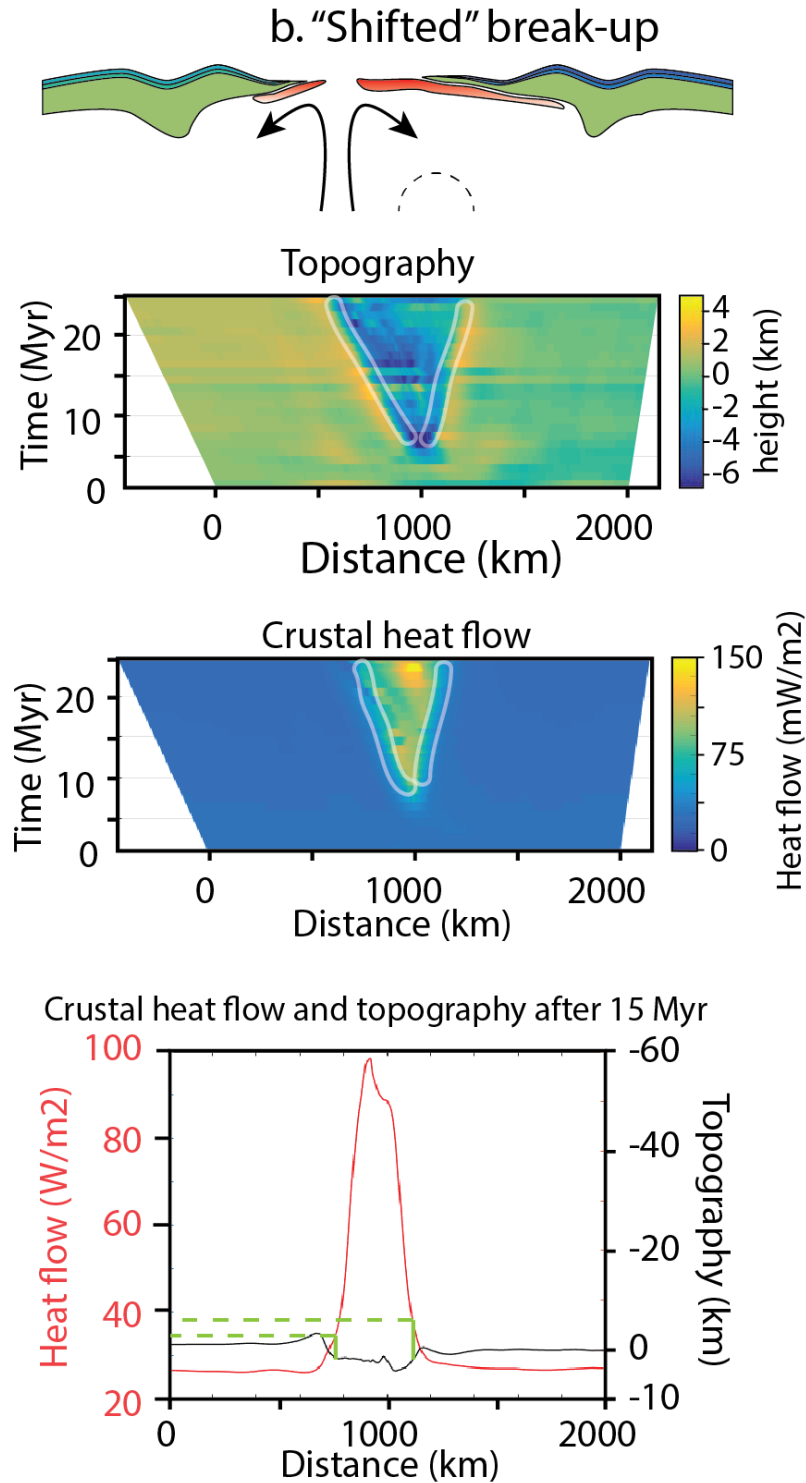


Figure 5.2b. Topographic and heat flow evolution of over time of the 'shifted' break-up mode. The profiles show the topography and heat flow at 15 Myr, during the post-rift phase. The white outline shows the location of the conjugate basins. There is more variation in the topography and heat flow. Topography is higher on the left margin than on the right whereas heat flow is higher on the right margin, especially during the post-rift phase.

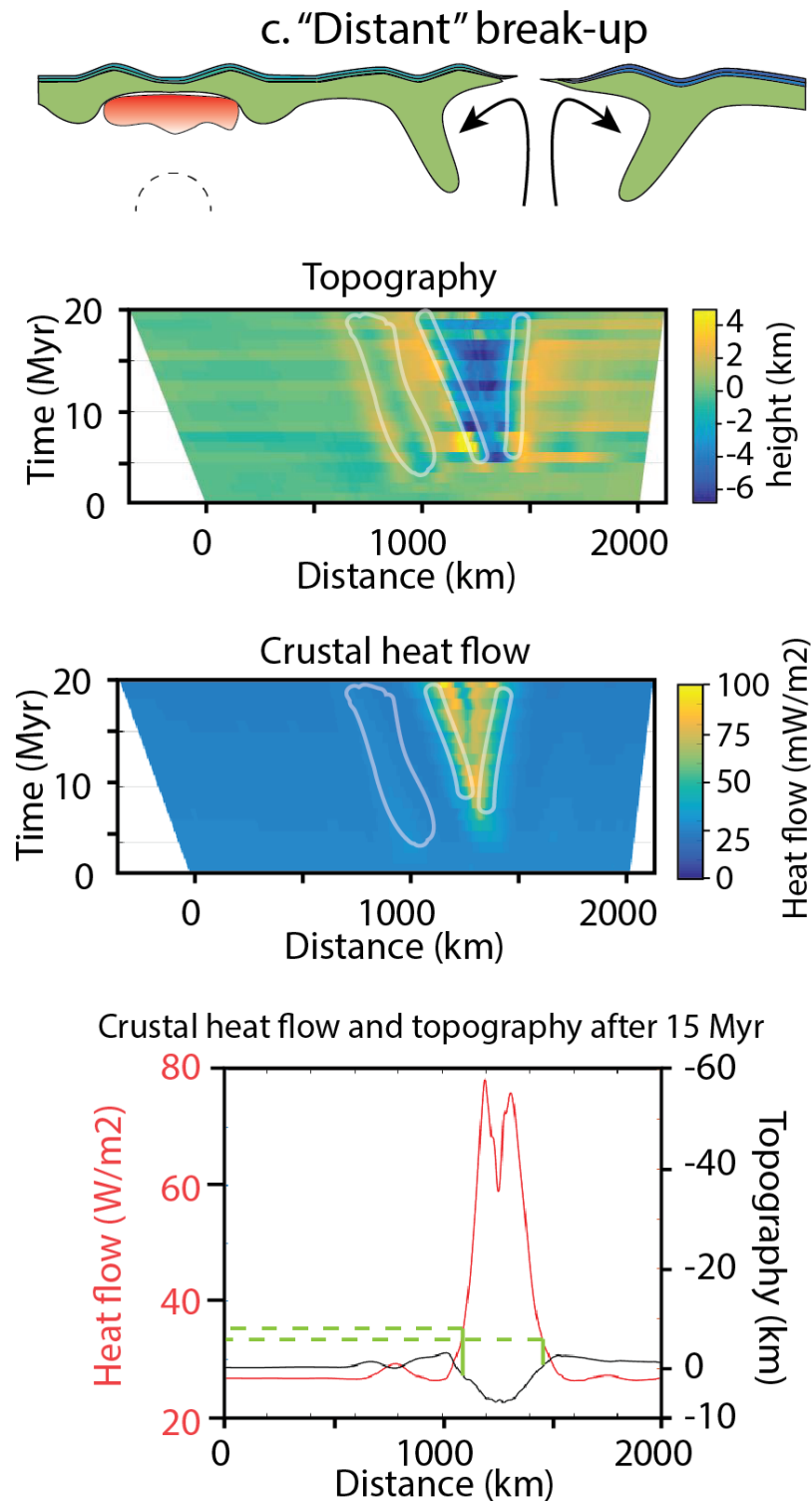


Figure 5.2c. Topographic and heat flow evolution of over time for the 'shifted' mode of break-up. The profiles show the topography and heat flow at 15 Myr, during the post-rift phase. The white outline shows the location of the conjugate basins. Both heat flow and topography show similar values true time along the spreading centre. A second basin develops with slightly heat flow values where the mantle plume remains glued to the lithosphere.

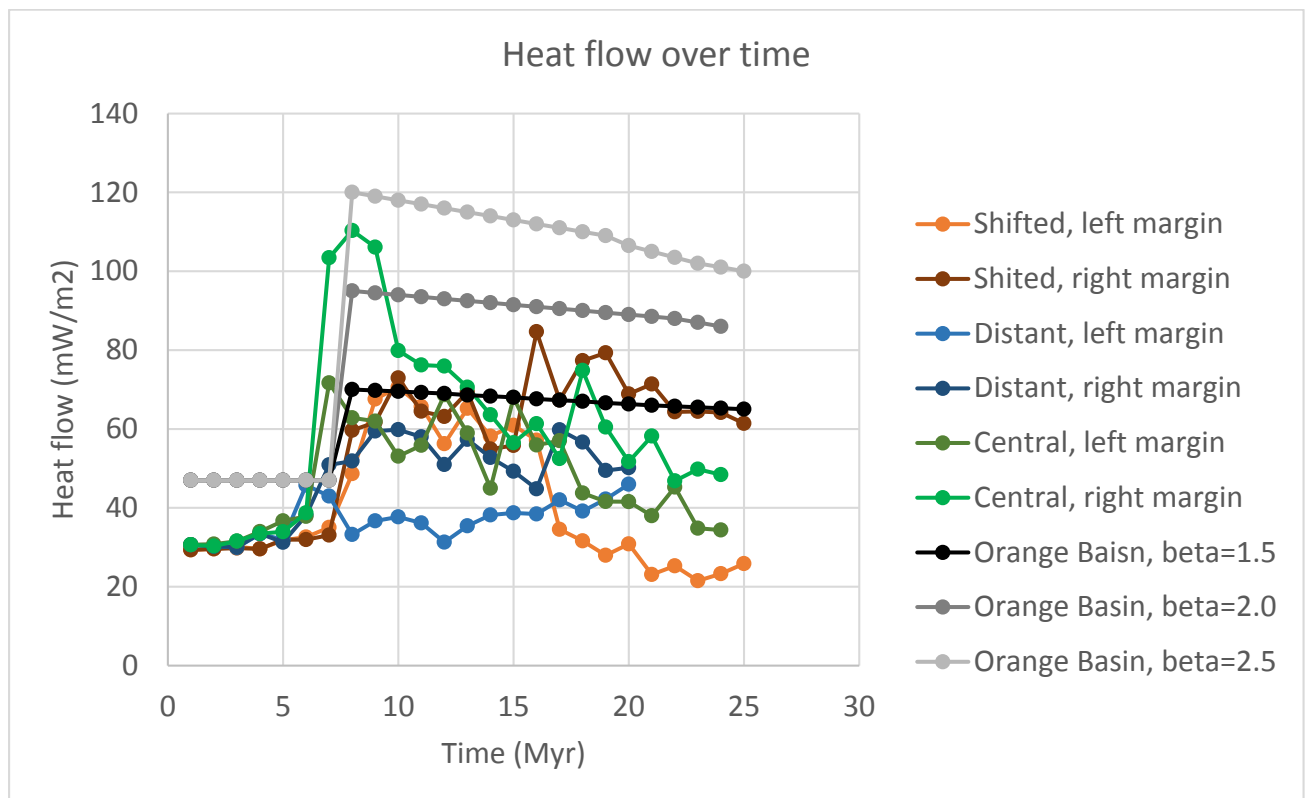


Figure 5.3. 1-D Heat flow calculations over time for the three model systems of rifting. The green curves are values for the central break-up mode, the orange ones the shifted and the blue ones represent the distant break-up mode. The grey and black-lines represent the 'pure-shear' stretching model using a β -factor of 1.5, 2.0 and 2.5 for the case of the Orange basin (Paton et al., 2007).

In basin modelling programs such as TemisFlow™, developed by IFP Energies nouvelles (Burrus et al., 1996; Doligez et al., 1986; Ungerer et al., 1990), many different parameters are taken into account to evaluate the generation and migration of hydrocarbons in sedimentary basins. In petroleum system analysis and modelling, it is important to reduce the uncertainties of these parameters by carefully assembling geological data sets. The first step would be 3D data assemblage of the sedimentary basin geometries. The surface of each stratigraphic interval and its structural elements (basin scale faults) need to be clear. Next, data on the characteristics for each strata have to be identified in terms of lithology (siliciclastic, sand, clay, or carbonate rich marls, limestones etc.) and rock petro-physical properties (porosity-depth, porosity permeability, etc.), their rock geochemical content and their kinetics (Ungerer, 1990), i.e. the richness in terms of total organic matter content (TOC) and type of kerogen (type I, II, IIS or III, most commonly used in literature). Once these elements have been entered as input data for the numerical basin model, its history needs to be reconstructed over geological time. Past geometries, temperatures and the fluid transfers (gas, oil and water) need to be understood. This is established by doing first a sequential restoration of each past geometries using back stripping and decompaction of sedimentary successions, followed by forward modelling of heat transfer, solving the heat equation

taking into account conduction, convection and radiogenic production, and lastly the circulation of each fluid phases (gas, oil and water) using the Darcy's equation. One important question in this itinerary is to set realistic boundary conditions for solving the heat equation (Bethke, 1989). The numerical method used in TemisFlow™ demands to define the temperature or the heat flow along any model's surface boundary (e.g. face if the basin is a cubic shape body). This must be defined in space and over time.

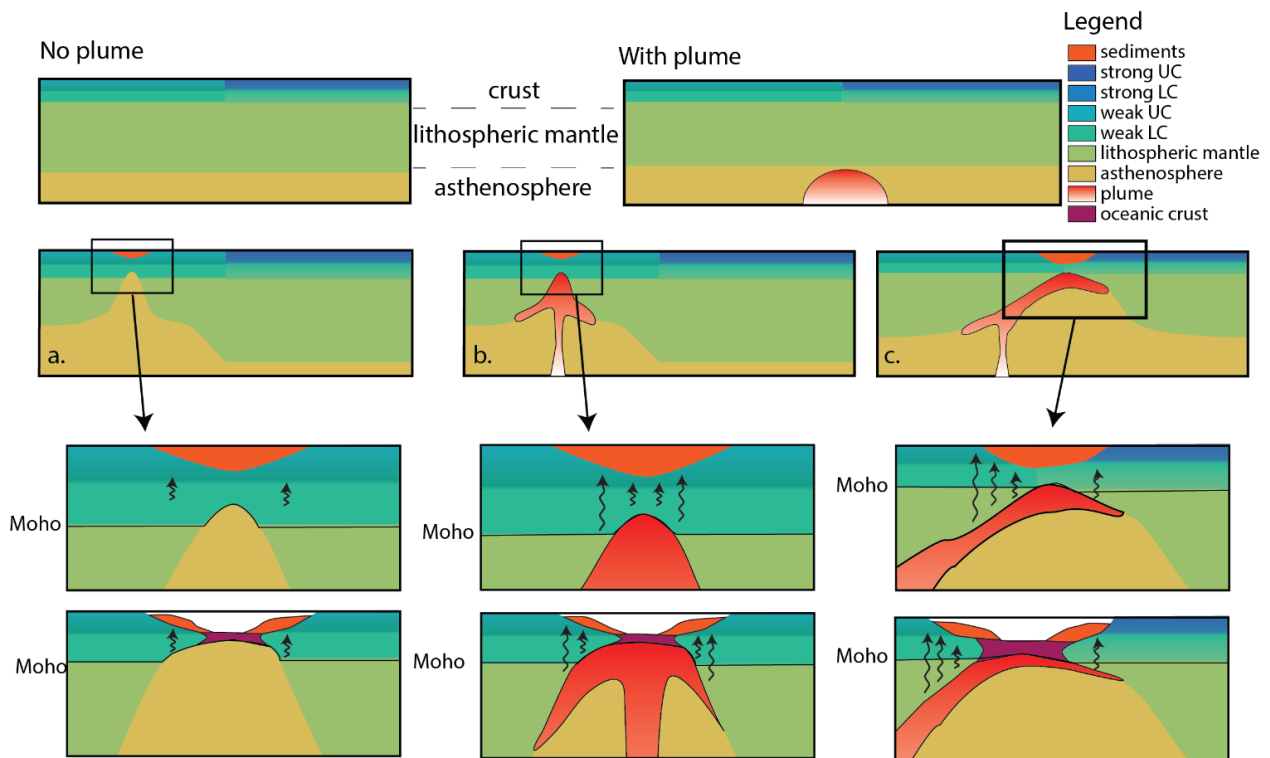


Figure 5.4. Schematic representation of heat flow distribution and intensity in case of a) no mantle plume or 'distant' break-up, b) a mantle plume with central break-up mode and c) a mantle plume and 'shifted' break-up mode. The longer arrows indicate higher intensities, the quantity refers to the distribution.

One of the parameters is the heat flow which can be either chosen as a standard value, taken from a library (Zeinalzadeh et al., 2015), or by implementing manually the heat flow values obtained through e.g. interpolating vitrinite reflection data (Kontorovich et al., 2013) or deriving heat flow from seafloor measurement of bottom simulating reflector mapping (Rousseau et al., 2015).

Thermal simulations show that when lateral variations are taken into account, the thermal regime is best explained (Rousseau et al., 2015). The heat flow calculations provided above are only 1D calculations, not taking into account lateral thermal variations. There is however a spatial and temporal intensity and distribution contrast between the different types of break-up and the margins, that can be taken into account easily in basin modelling programmes, like TemisFlow™.

In addition, with TemisFlow™ it is possible to include crustal structures into its basin model and thus, the geometry change of the crustal structure below the margins over time can also be included to better simulate the hydrocarbon and thermal evolution of the modelled basin.

The basins along the South Atlantic domain do not all have the same hydrocarbon occurrences. For example the Pelotas Basin has six potential petroleum systems (Conti et al., 2016) whereas its conjugate the Walvis basin on the African side has no sign for source rocks, although good reservoir rocks are present (Holtar and Forsberg, 2000). Further south along the margin, the Colorado basin contains source rocks that have matured to Kerogen types I-III during syn-rift and post-rift phase (Marcano et al., 2013) whereas the conjugate Orange Basin contains source rock with Kerogen type I during the syn-rift and type II during the post-rift phase (Marcano et al., 2013). In some cases the presence or absence of hydrocarbon accumulations is due to the lack of essential petroleum system feature, for example source rocks or traps or a cap-rocks, but in other cases it's the physical conditions that decide if hydrocarbons are generated and migrate towards their reservoir.

For the South Atlantic Domain different processes have played a role in the continental break-up, in some cases influenced by deep-rooted thermal anomalies as in the South Segment (Torsvik et al., 2009). This most likely has resulted in high, or maybe even too high heat flows compared to the Central Segment where hydrocarbon occurrences are more abundant. The Campos Basin is the most prolific petroleum-bearing basin of the Brazilian margin (Guardado et al., 2000). Its conjugate the Kwanza and Congo basins also host hydrocarbons, although its occurrences are more modest compares to its Brazilian conjugate (Burwood, 1999).

Highlights:

- The formation of a-symmetric and symmetric conjugate margin geometries depend on the on presence or absence of mantle anomalies in a complex lithosphere setup.
- Heat flow intensities and distribution along conjugate margins may vary depending on the presence or absence of a mantle anomaly
- Time and spatial heat flow boundary conditions for basin models can be constrained by large scale thermo-mechanical modelling.
- Understanding the thermal evolution of conjugate margin systems diminishes uncertainties for basin and petroleum system models and increases our knowledge on geodynamic processes in extensional systems.

Chapter 6: Conclusions

*La vie n'est facile pour aucun de nous, mais quoi,
Il faut avoir de la persévérance et surtout de la confiance en soi.*

*Il faut croire que l'on est doué pour quelque chose
Et que cette chose il faut l'atteindre coûte que coûte.*

~ Marie Curie, Physicist and Chemist

Continental rift initiation and break-up of Gondwanaland to form the South Atlantic domain is a complex process. The amalgamation of different rheological segments that made up Pangea were subjected to amongst others far-field forces and thermal processes in the mantle. The complex initial setup of this domain makes it difficult to quantify the role of every different factor on rift initiation and final break-up.

Analogue modelling has been performed at the Tectonics Laboratory at Utrecht University in the Netherlands to investigate the effect of extensional far-field on an alternative, more complex lithosphere setup, consisting of two segment with different rheological strength. The results show that when the lithosphere consists of two different strengths, e.g. two cratons with vertically contrasting rheological setups, the weaker segment accommodates all the deformation. The strong segment remains intact with its original thickness without showing any signs of crustal thinning or deformation. More importantly, when a strong sub-Moho mantle is present, the rift-evolution happens in two phases. The first phase is a wide-rift phase in the weak segment. As soon as the strong part of the upper mantle loses its strength, the rift localizes into a narrow rift. If extension would continue the crust would break at this point. Eventually, asymmetric margins would form weak with thin crust on either side. The thin margin that forms on the part glued to the strong segment has an asymmetric thickness distribution. The strong part would be thick, whereas the weak part would be thin, giving this margin a ‘hyperextended’ character. Also the basins that develop during the first, wide rift phase, can be unequally distributed on either side. These results can thus explain conjugate margin asymmetry without the use of a mantle anomaly. They also resemble the present-day geometry of the South Segment of the South Atlantic where the South American crust is thinner and shows less variation than the African crust which is thicker and more ‘extended’. Also the unequal distribution of basins, the South American margins have more basins than the African margins, is coherent with the expected evolution if extension would have continued in the analogue model.

However, in the South Segment of the South Atlantic Ocean, the only deep-rooted mantle anomaly, the Tristan Plume, is located below the oceanic crust, slightly to the right of the Mid Oceanic Ridge. Hotspot tracks and extensive volcanism point to some influence of this mantle anomaly during the rift and spreading phase. The analogue models do not take into account thermal processes and thus 2D thermo-mechanical modelling, using the FLAMAR and I3ELVIS codes, is performed to add the effect of mantle plumes to the rift initiation and continental break-up of a complex lithosphere consisting of two segments.

The numerical setup allows more variation in terms of thickness of the layers, geometry of the contact between the structures, initial plume location and extension rates. The results show that there is not just one way of continental break-up when a plume is involved. The ‘classical’ (or ‘central’) plume-induced break-up mode (Fig. 6.1b), where the lithosphere will break directly above the plume impingement point and the margins evolve rather symmetrically, is only one form of continental break-up. Another type would be the ‘shifted’ break-up mode (Fig. 6c), where, after plume impingement, mantle plume material

migrates below the base of the lithosphere to the contact between the two segments where break-up would eventually take place. The results even show that it is possible to have a ‘distant’ mode of break-up (Fig. 6d), where the plume does not reach the spreading centre at all and rifting initiates at a large distance from the mantle plume and the anomaly itself remains glued to the base of the lithosphere. At this point, where the plume impinged the lithosphere, topography develops and higher heat flows are calculated, although no break-up occurs. For the South Atlantic, the ‘shifted’ mode of break-up shows the most similarities to geological and geophysical observations. There is an asymmetry between the margins in terms of thickness and hyperextension and also the plume material that remains at lower crustal depths can be compared with Seaward Dipping Reflectors and/or high velocity/high density bodies at depth.

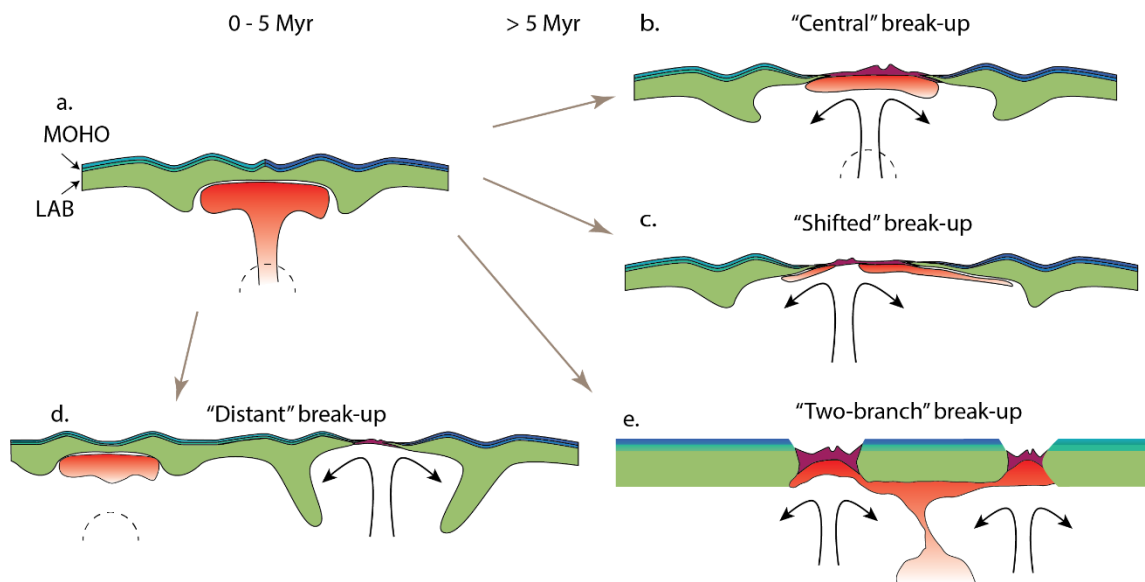


Figure 6.1. Four different ways of plume-induced continental break-up. a) All modes initiate similarly with plume-impingement at the base of the lithosphere and development of topography. Next, different modes can form b) ‘central’ break-up, c) ‘shifted’ break-up, d) ‘distant’ break-up and e) ‘two’-branch break-up.

This exercise, of testing the effect of mantle plume locations on complex lithospheric setups, does unfortunately not allow to qualitatively investigate the effect of plume emplacement in extensional numerical models. Therefore, a new exercise was designed, where the plume was positioned systematically further away from the centre of the model where the contact between two rheological segments is located. The results are in agreement with the previous exercise and multiple types of continental break-up are simulated. Again, the ‘classical’ or ‘central’ or ‘plume-induced’ mode, where break-up occurs directly above the plume impingement point is only one mode. Also the ‘shifted’ or ‘structural inherited’ mode is modelled in which case plume material migrates along the base of the lithosphere and break-up occurs at the contact between the segments. This exercise reveals a third mode of break-up, where plume material of one mantle plume reaches two spreading centres. In this case,

depending on the extension rate and the plume location, both 'plume-centred' and 'structural inherited' break-up develop. There is only a small window in which this 'two-branch' mode forms and depending on the location of the plume, first 'plume-induced' and then 'structural-inherited' break-up forms or vice-versa. When extension rates are too low, in this case 5 mm/yr half-rate, only 'structural-inherited' break-up forms. This 'two-branch' mode (Fig. 6.1e) is thus very sensitive to extension rate, plume location and the rheological setup and can explain complicated rift and spreading systems where aborted arms or failed rifts are present, for example in the North Atlantic domain.

Both the analogue and numerical models are capable of reproducing geological and geophysical observations. For asymmetric conjugate margin development, a complex lithosphere with multiple rheological segments and some extensional forces acting on the system are sufficient to produce this asymmetry. However, when a mantle anomaly is known to be present, the situation becomes more complicated and more than one type of break-up can result in asymmetric margins. Features observed at the surface and at depth that cannot be explained without thermal processes taken into account, can be explained when taking a plume into account. The models have shown though that more than one plume-induced rift-to-break-up evolution is possible and care should therefore be taken when including these anomalous features in thermo-mechanical modelling.

The thermal evolution of the conjugate margins that results from thermo-mechanical modelling varies in terms of intensity and distribution. These trends can be used in basin and petroleum system modelling to diminish the uncertainties for the thermal evolution included in these kind of models.

Chapter 7: Future work and perspectives

A ship in a port is safe, but that's not what ships are for.

Sail out on sea and do new things.

~ Grace Hopper, U.S. Navy Rear Admiral & Computer Scientist

Testing heat flow trends on natural cases

This study has shown that heat flow trends that result from numerical models differ from the heat flow trends used in the industry for spreaded systems. There is more variation in heat flow values and also margins do not necessarily suffer similar heat flow evolutions. These different heat flow trends should be tested on natural systems to see what the quantitative impact is on hydrocarbon maturation and generation. This can be done with petroleum system models, such as TemisFlow™, where it is possible to use more complex thermal histories as boundary conditions as well as more complex lithosphere geometries.

Increasing the complexity of analogue and numerical models

Numerical models become more complex and capable of calculating multiple processes. Developing more complex setups, for example including more than two rheological segments, or playing with non-linear extension velocities will be better suitable for specific regions on earth. Also reproducing numerical models in an analogue fashion or recalculating the analogue models in a numerical way will give insights in the limits of either method. A very challenging follow-up would be the development of an analogue modelling machine that can include thermal processes. These more complex analogue and numerical models come one step closer to reproducing tectonic processes. The results can then be used for models at a smaller scale, for example basin models, to receive better estimations of hydrocarbon reserves or geothermal potential of a basin.

Predicting initiating rift systems

The analogue modelling exercise provides a framework for rift initiation without the implication of mantle plumes. When a strong sub-Moho mantle is present, the two phase rift evolution starts with a wide rift until the sub-Moho mantle has lost its strength and rifting localizes. During this first rift phase the sub-Moho mantle is actively under extension and if it behaves in a brittle fashion it might produce earthquakes at depths below the Moho. It would be interesting to investigate if seismic activity at sub-Moho depths in a continental setting are an indication for continent rift initiation. Also the earthquake magnitudes associated with this type of tectonic activity is worth investigating to understand the risk of hazards. A recent earthquake (6.4 on the scale of Richter) in Botswana occurred at lower crustal levels and is situated in an extensional setting and could provide a natural laboratory to test this hypothesis.

References

- Abdelmalak, M.M., Planke, S., Faleide, J.I., Jerram, D.A., Zastrozhnov, D., Eide, S., Myklebust, R., 2016. The development of volcanic sequences at rifted margins: new insights from the structure and morphology of the Vøring Escarpment, mid-Norwegian Margin. *J. Geophys. Res. Solid Earth* 121, 5212–5236. doi:10.1002/2015JB012788
- Allemand, P., Brun, J.-P., 1991. Width of continental rifts and rheological layering of the lithosphere. *Tectonophysics* 188, 63–69.
- Allen, P.A., Allen, J.R., 2013. *Basin analysis: principles and application to petroleum play assessment*. John Wiley & Sons.
- Antonio, L., Gamboa, L.A.P., Rabinowitz, P.D., 1981. The Rio Grande Fracture Zone in the Western South Atlantic and Its Tectonic Implications. *Earth Planet. Sci. Lett.* 52, 410–418. doi:10.1016/0012-821X(81)90193-X
- Artemieva, I.M., Mooney, W.D., 2001. Thermal thickness and evolution of Precambrian lithosphere: A global study. *J. Geophys. Res.* 106, 16387–16414. doi:10.1029/2000JB900439
- Aslanian, D., Moulin, M., Olivet, J.L., Unternehr, P., Matias, L., Bache, F., Rabineau, M., Nouzé, H., Klingelhoefer, F., Contrucci, I., Labails, C., 2009. Brazilian and African passive margins of the Central Segment of the South Atlantic Ocean: Kinematic constraints. *Tectonophysics* 468, 98–112. doi:10.1016/j.tecto.2008.12.016
- Asmus, H.E., Baisch, P.R., 1983. Geological evolution of the Brazilian continental margin. *Episodes* 4, 3–9.
- Autin, J., Scheck-Wenderoth, M., Loegering, M.J., Anka, Z., Vallejo, E., Rodriguez, J.F., Dominguez, F., Marchal, D., Reichert, C., di Primio, R., Götze, H.-J., 2013. Colorado Basin 3D structure and evolution, Argentine passive margin. *Tectonophysics* 604, 264–279. doi:10.1016/j.tecto.2013.05.019
- Averbuch, O., Piromallo, C., 2012. Is there a remnant Variscan subducted slab in the mantle beneath the Paris basin? Implications for the late Variscan lithospheric delamination process and the Paris basin formation. *Tectonophysics* 558–559, 70–83. doi:10.1016/j.tecto.2012.06.032
- Balázs, A., Burov, E., Matenco, L., Vogt, K., Francois, T., 2017. Symmetry during the syn- and post-rift evolution of extensional back-arc basins: The role of inherited orogenic structures. *Earth Planet. Sci. Lett.* 462, 86–98. doi:10.1016/j.epsl.2017.01.015
- Bauer, K., Neben, S., Schreckenberger, B., Emmerman, R., Hinz, K., Fechner, N., Gohl, K., Schulze, A., Trumbull, R.B., Weber, K., 2000. Deep structure of the Namibia continental margin as derived from integrated geophysical studies. *J. Geophys. Res.* 105, 25,829–25,853.
- Bellahsen, N., Faccenna, C., Funicello, F., Daniel, J.M., Jolivet, L., 2003. Why did Arabia separate from Africa? Insights from 3-D laboratory experiments. *Earth Planet. Sci. Lett.* 216, 365–381. doi:10.1016/S0012-821X(03)00516-8
- Ben-Avraham, Z., Hartnady, C.J.H., Kitchin, K.A., 1997. Structure and tectonics of the Agulhas-Falkland fracture zone. *Tectonophysics* 282, 83–98. doi:10.1016/S0040-1951(97)00213-8
- Beniest, A., Koptev, A., Burov, E., 2017a. Numerical models for continental break-up: Implications for the South Atlantic. *Earth Planet. Sci. Lett.* 461, 176–189. doi:10.1016/j.epsl.2016.12.034
- Beniest, A., Koptev, A., Leroy, S., Sassi, W., Guichet, X., 2017b. Two-branch break-up systems by a single mantle plume: Insights from numerical modelling. *Geophys. Res. Lett.* 44, 1–9. doi:10.1002/2017GL074866
- Bethke, C.M., 1989. Modelling subsurface flow in sedimentary basins. *Geol. Rundschau* 78, 129–154.
- Bittner, D., Schmeling, H., 1995. Numerical modelling of melting processes and induced diapirism in the lower crust. *Geophys. J. Int.* 123, 59–70.
- Blaich, O.A., Faleide, J.I., Tsikalas, F., 2011. Crustal breakup and continent-ocean transition at South Atlantic conjugate margins. *J. Geophys. Res.* 116, 1–38. doi:10.1029/2010JB007686
- Blaich, O.A., Faleide, J.I., Tsikalas, F., Franke, D., León, E., 2009. Crustal-scale architecture and segmentation of the Argentine margin and its conjugate off South Africa. *Geophys. J. Int.* 178, 85–105. doi:10.1111/j.1365-246X.2009.04171.x
- Blaich, O.A., Faleide, J.I., Tsikalas, F., Gordon, A.C., Mohriak, W., 2013. Crustal-scale architecture and segmentation of the South Atlantic volcanic margin. *Geol. Soc. London, Spec. Publ.* 369, 167–183.
- Bonini, M., Corti, G., Ventisette, C., Del, Manetti, P., Mulugeta, G., Sokoutis, D., 2007. Modelling the lithospheric rheology control on the Cretaceous rifting in West Antarctica. doi:10.1111/j.1365-3121.2007.00760.x
- Bott, M.H.P., 1993. Modelling the plate-driving mechanism. *J. Geol. Soc. London* 150, 941–951.
- Bott, M.H.P., Kusznir, N.J., 1979. Stress distributions associated with compensated plateau uplift structures with application to the continental splitting mechanism. *Geophys. J. R. Astron. Soc.* 56, 451–459.
- Brozena, J.M., White, R.S., 1999. Ridge jumps and propagations in the South Atlantic Ocean. *Nature* 348, 149–152.
- Brun, J.-P., 2002. Deformation of the continental lithosphere: Insights from brittle-ductile models. *Geol. Soc. London, Spec. Publ.* 200, 355–370. doi:10.1144/GSL.SP.2001.200.01.20
- Brun, J.-P., Sokoutis, D., Van Den Driessche, J., 1994. Analogue modelling of detachment fault systems and core complexes. *Geology* 22, 319–322.
- Brun, J.P., 1999. Narrow rifts versus wide rifts: inferences for the mechanics of rifting from laboratory experiments [and discussion]. *Philos. Trans. R. Soc. London. Ser. A, Math. Phys. Eng. Sci.* 357, 695–712.
- Brun, J.P., Beslier, M.O., 1996. Mantle exhumation at passive margins. *Earth Planet. Sci. Lett.* 142, 161–173. doi:10.1016/0012-821X(96)00080-5
- Brune, S., Heine, C., Pérez-Gussinyé, M., Sobolev, S. V., 2014. Rift migration explains continental margin asymmetry and crustal hyper-extension. *Nat. Commun.* 5, 1–9. doi:10.1038/ncomms5014
- Brune, S., Popov, A.A., Sobolev, S. V., 2013. Quantifying the thermo-mechanical impact of plume arrival on continental break-up. *Tectonophysics* 604, 51–59. doi:10.1016/j.tecto.2013.02.009
- Brune, S., Williams, S.E., Nathaniel, P., 2016. Abrupt plate accelerations shape rifted continental margins. *Nat. Publ. Gr.* 536, 201–204. doi:10.1038/nature18319
- Buck, W.R., 2007. *Dynamic Processes in Extensional and Compressional Settings: The Dynamics of Continental Breakup and Extension*. *Treatise Geophys.* 6, 335–376. doi:10.1016/B978-044452748-6.00110-3
- Buck, W.R., 1991. Modes of continental lithospheric extension. *J. Geophys. Res.* 96, 20,161–20,178. doi:10.1029/91JB01485

- Buiter, S., Tetreault, J., 2015. The role of structural inheritance in continental rifting, in: EGU General Assembly, 12-17 April, Vienna. p. 1.
- Bull, A.L., Domeier, M., Torsvik, T.H., 2014. The effect of plate motion history on the longevity of deep mantle heterogeneities. *Earth Planet. Sci. Lett.* 401, 172–182. doi:10.1016/j.epsl.2014.06.008
- Bullard, E., Everett, J.E., Smith, A.G., 1965. The fit of the continents around the Atlantic. *Philos. Trans. R. Soc. London. Ser. A, Math. Phys. Sci.* 258, 41–51.
- Burke, K., 1996. The African Plate. *South African J. Geol.* 99, 341–409.
- Burke, K., 1976. Development of graben associated with the initial ruptures of the Atlantic Ocean. *Tectonophysics* 36, 93–112.
- Burov, E., Cloetingh, S., 2010. Plume-like upper mantle instabilities drive subduction initiation. *Geophys. Res. Lett.* 37, 1–6. doi:10.1029/2009GL041535
- Burov, E., Cloetingh, S., 2009. Controls of mantle plumes and lithospheric folding on modes of intraplate continental tectonics: Differences and similarities. *Geophys. J. Int.* 178, 1691–1722. doi:10.1111/j.1365-246X.2009.04238.x
- Burov, E., Cloetingh, S., 1997. Erosion and rift dynamics: new thermomechanical aspects of post-rift evolution of extensional basins. *Earth Planet. Sci. Lett.* 150, 7–26. doi:10.1016/S0012-821X(97)00069-1
- Burov, E., Gerya, T., 2014. Asymmetric three-dimensional topography over mantle plumes. *Nature* 513, 85–89. doi:10.1038/nature13703
- Burov, E., Guillou-Frottier, L., 2005. The plume head – continental lithosphere interaction using a tectonically realistic formulation for the lithosphere. *Geophys. J. Int.* 161, 469–490. doi:10.1111/j.1365-246X.2005.02588.x
- Burov, E., Guillou-Frottier, L., D'Acromont, E., Le Pourhiet, L., Cloetingh, S., 2007. Plume head-lithosphere interactions near intra-continental plate boundaries. *Tectonophysics* 434, 15–38. doi:10.1016/j.tecto.2007.01.002
- Burov, E., Jolivet, L., Le Pourhiet, L., Poliakov, A., 2001. A thermomechanical model of exhumation of high pressure (HP) and ultra-high pressure (UHP) metamorphic rocks in Alpine-type collision belts. *Tectonophysics* 342, 113–136. doi:10.1016/S0040-1951(01)00158-5
- Burov, E., Poliakov, A., 2001. Erosion and rheology controls on synrift and postrift evolution: Verifying old and new ideas using a fully coupled numerical model. *J. Geophys. Res.* 106, 16461–16481. doi:10.1029/2001JB000433
- Burov, E.B., 2011. Rheology and strength of the lithosphere. *Mar. Pet. Geol.* 28, 1402–1443. doi:10.1016/j.marpetgeo.2011.05.008
- Burov, E.B., Diament, M., 1995. The effective elastic thickness (T_e) of continental lithosphere: What does it really mean? *J. Geophys. Res.* 100, 3905–3927. doi:10.1029/94JB02770
- Burrus, J., Osadetz, K., Wolf, S., Doligez, B., Visser, K., Dearborn, D., 1996. A Two-Dimensional Regional Basin Model of Williston Basin Hydrocarbon Systems. *Am. Assoc. Pet. Geol. Bull.* 80, 265–291.
- Burwood, R., 1999. Angola: source rock control for Lower Congo Coastal and Kwanza Basin petroleum systems. *Geol. Soc. London, Spec. Publ.* 153, 181–194.
- Byerlee, J., 1978. Friction of Rocks. *Pure Appl. Geophys.* 116, 615–626.
- Calignano, E., Sokoutis, D., Willingshofer, E., Gueydan, F., Cloetingh, S., 2015a. Asymmetric vs. symmetric deep lithospheric architecture of intra-plate continental orogens. *Earth Planet. Sci. Lett.* 424, 38–50. doi:10.1016/j.epsl.2015.05.022
- Calignano, E., Sokoutis, D., Willingshofer, E., Gueydan, F., Cloetingh, S., 2015b. Strain localization at the margins of strong lithospheric domains: Insights from analog models. *Tectonics* 34, 396–412. doi:10.1002/2014TC003756. Received
- Cappelletti, A., Tsikalas, F., Nestola, Y., Cavozzi, C., Argnani, A., Meda, M., Salvi, F., 2013. Impact of lithospheric heterogeneities on continental rifting evolution: Constraints from analogue modelling on South Atlantic margins. *Tectonophysics* 608, 30–50. doi:10.1016/j.tecto.2013.09.026
- Carter, N.L., Tsenn, M.C., 1987. Flow properties of continental lithosphere. *Tectonophysics* 136, 27–63. doi:10.1016/0040-1951(87)90333-7
- Cemark, V., Rybach, L., 1982. Thermal conductivity and specific heat of minerals and rocks. *Landolt-Bornstein; Zahlenwerte und Funktionen aus Naturwissenschaften und Tech.* 305–343.
- Chalmers, J.A., Larsen, L.M., Pedersen, A.K., 1995. Widespread Palaeocene volcanism around the northern North Atlantic and Labrador Sea: evidence for a large, hot, early plume head. *J. Geol. Soc. London* 152, 965–969.
- Chang, H.K., Kowsmann, R.O., Figueiredo, A.M.F., Bender, A.A., 1992. Tectonics and stratigraphy of the East Brazil Rift system: an overview. *Tectonophysics* 213, 97–138. doi:10.1016/0040-1951(92)90253-3
- Channell, J.E.T., Erba, E., Nakanishi, M., Tamaki, K., 1995. Late Jurassic-Early Cretaceous time scales and oceanic magnetic anomaly block models. *Spec. Publ. - Soc. Sediment. Geol.* 54, 51–63.
- Chenin, P., Beaumont, C., 2013. Influence of offset weak zones on the development of rift basins: Activation and abandonment during continental extension and breakup. *J. Geophys. Res. Solid Earth* 118, 1698–1720. doi:10.1002/jgrb.50138
- Chester, F.M., 1995. A rheologic model for wet crust applied to strike-slip faults. *J. Geophys. Res.*, 13,033–13,044.
- Clauser, C., Huenges, E., 1995. Thermal Conductivity of Rocks and Minerals. *Rock Phys. Phase Relations A Handb. Phys. Constants* 105–126.
- Clerc, C., Jolivet, L., Ringenbach, J.C., 2015. Ductile extensional shear zones in the lower crust of a passive margin. *Earth Planet. Sci. Lett.* 431, 1–7. doi:10.1016/j.epsl.2015.08.038
- Cloetingh, S., Burov, E., Matenco, L., Beekman, F., Roure, F., Ziegler, P.A., 2013. The Moho in extensional tectonic settings: Insights from thermo-mechanical models. *Tectonophysics* 609, 558–604. doi:10.1016/j.tecto.2013.06.010
- Cloetingh, S., Burov, E., Poliakov, A., 1999. Lithosphere folding: primary response to compression? (from central Asia to Paris basin). *Tectonics* 18, 1064–1083.
- Cobbold, P.R., Gapais, D., Rossello, E.A., Milani, E.J., Szatmari, P., 1992. Permo-Triassic intracontinental deformation in SW Gondwana. Invers. *Tectonics Cape Fold Belt, Karoo Cretac. Basins South. Africa* 23–26.

- Colli, L., Stotz, I., Bunge, H.-P., Smethurst, M., Clark, S., Iaffaldano, G., Tassara, A., Guillocheau, F., Bianchi, M.C., 2014. Rapid South Atlantic spreading changes and coeval vertical motion in surrounding continents: Evidence for temporal changes of pressure-driven upper mantle flow. *Tectonics* 32, 1304–1321. doi:10.1002/2014TC003612. Received
- Connolly, J.A.D., 2005. Computation of phase equilibria by linear programming : A tool for geodynamic modelling and its application to subduction zone decarbonation. *Earth Planet. Sci. Lett.* 236, 524–541. doi:10.1016/j.epsl.2005.04.033
- Conti, B., Perinotto, A., Soto, M., Ana, H.D.S., 2016. Speculative Petroleum Systems of the Southern Pelotas Basin, Offshore Uruguay. *Search Discov.* 10832, 1–14.
- Contrucci, I., Matias, L., Moulin, M., Géli, L., Klingelhofer, F., Nouzé, H., Aslanian, D., Olivet, J.L., Réhault, J.P., Sibuet, J.C., 2004. Deep structure of the West African continental margin (Congo, Zaïre, Angola), between 5°S and 8°S, from reflection/refraction seismics and gravity data. *Geophys. J. Int.* 158, 529–553. doi:10.1111/j.1365-246X.2004.02303.x
- Cornwell, D.G., Mackenzie, G.D., England, R.W., Maguire, P.K.H., Asfaw, L.M., Oluma, B., 2006. Northern Main Ethiopian Rift crustal structure from new high-precision gravity data. *Geol. Soc. London, Spec. Publ.* 259, 307–321. doi:10.1144/GSL.SP.2006.259.01.23
- Corti, G., Bonini, M., Innocenti, F., Manetti, P., Piccardo, G.B., Ranalli, G., 2007. Experimental models of extension of continental lithosphere weakened by percolation of asthenospheric melts. *J. Geodyn.* 43, 465–483. doi:10.1016/j.jog.2006.11.002
- Corti, G., Calignano, E., Petit, C., Sani, F., 2011. Controls of lithospheric structure and plate kinematics on rift architecture and evolution: An experimental modelling of the Baikal rift. *Tectonics* 30, 1–16. doi:10.1029/2011TC002871
- Corti, G., Ranalli, G., Agostini, A., Sokoutis, D., 2013. Inward migration of faulting during continental rifting: Effects of pre-existing lithospheric structure and extension rate. *Tectonophysics* 594, 137–148. doi:10.1016/j.tecto.2013.03.028
- Coulié, E., Quidelleur, X., Gillot, P., Courtillot, V., Lefèvre, J.-C., Chies, S., 2003. Comparative K - Ar and Ar / Ar dating of Ethiopian and Yemenite Oligocene volcanism : implications for timing and duration of the Ethiopian traps. *Earth Planet. Sci. Lett.* 206, 477–492.
- Culling, W.E.H., 1960. Analytical theory of erosion. *J. Geol.* 68, 336–345.
- Cundall, P.A., 1989. Numerical experiments on localization in frictional materials. *Ingenieur-Archiv* 59, 148–159.
- Cundall, P.A., Board, 1988. A microcomputer program for modelling large-strain plasticity problems, in: *Proceedings, 6th International Conference on Numerical Methods in Geomechanics, Innsbruck, Austria*. Edited by G. Swoboda. AA Balkema, Rotterdam. pp. 2101–2108.
- D’Acremont, E., Leroy, S., Burov, E.B., 2003. Numerical modelling of a mantle plume: the plume head–lithosphere interaction in the formation of an oceanic large igneous province. *Earth Planet. Sci. Lett.* 206, 379–396. doi:10.1016/S0012-821X(02)01058-0
- Davaille, A., Stutzmann, E., Silveira, G., Besse, J., Courtillot, V., 2005. Convective patterns under the Indo-Atlantic « box ». *Earth Planet. Sci. Lett.* 239, 233–252. doi:10.1016/j.epsl.2005.07.024
- Davaille, A., Vatteville, J., 2005. On the transient nature of mantle plumes. *Geophys. Res. Lett.* 32, 1–4. doi:10.1029/2005GL023029
- Davies, D.R., Rawlinson, N., Iaffaldano, G., Campbell, I.H., 2015. Lithospheric controls on magma composition along Earth’s longest continental hotspot track. *Nature* 525, 511–514. doi:10.1038/nature14903
- Davies, J.H., 2013. Global map of solid Earth surface heat flow. *Geochemistry, Geophys. Geosystems* 14, 4608–4622. doi:10.1002/ggge.20271
- Davies, J.H., Davies, D.R., 2010. Earth’s surface heat flux. *Solid Earth* 1, 5–24. doi:10.5194/se-1-5-2010
- Davis, M., Kusznir, N.J., 2004. Depth-dependent lithospheric stretching at rifted continental margins. *Proc. NSF Rift. Margins Theor. Inst.* 136, 92–137.
- Debayle, E., Kennett, B.L.N., 2000. Anisotropy in the Australian upper mantle from Love and Rayleigh waveform inversion. *Earth Planet. Sci. Lett.* 184, 339–351.
- Dewey, J.F., Burke, K., 1974. Hot spots and collisional break-up: Implications for collisional orogeny. *Geology* 2, 57–60. doi:10.1130/0091-7613(1974)2<57:HSACBI>2.0.CO;2
- Dietz, R.S., 1961. Continent and Ocean Basin Evolution by Spreading of the Sea Floor. *Nature* 190, 854–857. doi:10.1038/190854a0
- Doligez, B., Bessis, F., Burrus, J., Ungerer, P., Chenet, P.Y., 1986. Integrated numerical simulation of the sedimentation heat transfer, hydrocarbon formation and fluid migration in a sedimentary basin: the THEMIS model. *Collect. Colloq. séminaires-Institut français du pétrole* 40, 173–195.
- Dorfman, S.M., 2016. Phase diagrams and thermodynamics of lower mantle materials. *Geophys. Monogr.* 217, 241–252.
- Dressel, I., Scheck-Wenderoth, M., Cacace, M., Lewerenz, B., Götze, H.-J., Reichert, C., 2015. Reconstruction of the southwestern African continental margin by backward modelling. *Mar. Pet. Geol.* 67, 544–555. doi:10.1016/j.marpetgeo.2015.06.006
- Du Toit, A.L., 1937. Our wandering continents: an hypothesis of continental drifting. *Oliver and Boyd*, p. 366.
- Dupré, S., Bertotti, G., Cloetingh, S., 2007. Tectonic history along the South Gabon Basin: anomalous early post-rift subsidence. *Mar. Pet. Geol.* 24, 151–172. doi:10.1016/j.marpetgeo.2006.11.003
- Eagles, G., 2007. New angles on South Atlantic opening. *Geophys. J. Int.* 168, 353–361. doi:10.1111/j.1365-246X.2006.03206.x
- Eaton, D.W., Darbyshire, F., Evans, R.L., Grütter, H., Jones, A.G., Yuan, X., 2009. The elusive lithosphere-asthenosphere boundary (LAB) beneath cratons. *Lithos* 109, 1–22. doi:10.1016/j.lithos.2008.05.009
- Ebinger, C.J., Casey, M., 2001. Continental breakup in magmatic provinces: An Ethiopian example. *Geology* 29, 527–530. doi:10.1130/0091-7613(2001)029<0527:CBIMPA>2.0.CO;2
- Engelmann de Oliveira, C.H., Jelinek, A.R., Chemale Jr., F., Bernet, M., 2016. Evidence of post-Gondwana breakup in Southern Brazilian Shield : Insights from apatite and zircon fission track thermochronology. *Tectonophysics* 666, 173–187. doi:10.1016/j.tecto.2015.11.005

- Ernesto, M., Marques, L.S., Piccirillo, E.M., Molina, E.C., Ussami, N., Comin-Chiaramonti, P., Bellinie, G., 2002. Paraná Magmatic Province- Tristan da Cunha plume system: fixed versus mobile plume, petrogenetic considerations and alternative heat sources. *J. Volcanol. Geotherm. Res.* 118, 15–36.
- Ernesto, M., Raposo, M.I.B., Marques, L.S., Renne, P.R., Diogo, L.A., De Min, A., 1999. Paleomagnetism, geochemistry and ⁴⁰Ar/³⁹Ar dating of the North-eastern Paraná Magmatic Province: tectonic implications. *J. Geodyn.* 28, 321–340. doi:10.1016/S0264-3707(99)00013-7
- Evans, B.W., Kohlstedt, D.L., 1995. Rheology of rocks. *Rock Phys. Phase Relations A Handb. Phys. Constants* 3, 148–165. doi:10.1029/RF003p0148
- Feighner, M.A., Richards, M.A., 1995. The fluid dynamics of plume-ridge and plume-plate interactions : An experimental investigation. *Earth Planet. Sci. Lett.* 129, 171–182.
- Ferrero, C., Gallagher, K., 2002. Stochastic thermal history modelling. 1. Constraining heat flow histories and their uncertainties. *Mar. Pet. Geol.* 19, 633–648.
- Fishwick, S., 2010. Surface wave tomography: Imaging of the lithosphere – asthenosphere boundary beneath central and southern Africa? *Lithos* 120, 63–73. doi:10.1016/j.lithos.2010.05.011
- Forsyth, D., Uyeda, S., 1975. On the Relative Importance of the Driving Forces of Plate Motion. *Geophys. J. R. Astron. Soc. London* 43, 163–200. doi:10.1111/j.1365-246X.1975.tb00631.x
- Fowler, C.M.R., 1990. *The solid earth: an introduction to global geophysics.* Cambridge University Press, p. 728.
- Franke, D., 2013. Rifting, lithosphere breakup and volcanism : Comparison of magma-poor and volcanic rifted margins. *Mar. Pet. Geol.* 43, 63–87. doi:10.1016/j.marpetgeo.2012.11.003
- Franke, D., Neben, S., Hinz, K., Meyer, H., Schreckenberger, B., 2002. Deep crustal structure of the Argentine continental margin from seismic wide-angle and multichannel reflection seismic data. *AAPG Search Discov. Artic.* 90022, 1–4.
- Franke, D., Neben, S., Schreckenberger, B., Schulze, A., Stiller, M., Krawczyk, C.M., 2006. Crustal structure across the Colorado Basin, offshore Argentina. *Geophys. J. Int.* 165, 850–864. doi:10.1111/j.1365-246X.2006.02907.x
- French, S.W., Romanowicz, B., 2015. Broad plumes rooted at the base of the Earth’s mantle beneath major hotspots. *Nature* 525, 95–99. doi:10.1038/nature14876
- Frimmel, H.E., Basei, M.S., Gaucher, C., 2011. Neoproterozoic geodynamic evolution of SW-Gondwana: a southern African perspective. *Int. J. Earth Sci.* 100, 323–354. doi:10.1007/s00531-010-0571-9
- Furlong, K.P., Chapman, D.S., 2013. Heat Flow, Heat Generation, and the Thermal State of the Lithosphere. *Annu. Rev. Earth Planet. Sci.* 41, 385–410. doi:10.1146/annurev.earth.031208.100051
- Gaherty, J., Jordan, T.H., 1995. Lehmann discontinuity as the base of an anisotropic layer beneath continents. *Science*, 268, 1468–1471.
- Gaina, C., Gernigon, L., Ball, P., 2009. Palaeocene – Recent plate boundaries in the NE Atlantic and the formation of the Jan Mayen microcontinent. *J. Geol. Soc. London* 166, 601–616. doi:10.1144/0016-76492008-112
- Gaina, C., Roest, W.R., Müller, R.D., Symonds, P., 1998. The Opening of the Tasman Sea: a gravity anomaly animation. *Earth Interact.* 2, 1–23.
- Gallagher, K., 1998. Inverse thermal history modelling as a hydrocarbon exploration tool. *Inverse Probl.* 14, 479–497.
- Geoffroy, L., 2005. Volcanic passive margins 337, 1395–1408. doi:10.1016/j.crte.2005.10.006
- Geoffroy, L., Burov, E.B., Werner, P., 2015. Volcanic passive margins: another way to break up continents. *Sci. Rep.* 5, 14828. doi:10.1038/srep14828
- Gerya, T., 2010. Dynamical instability produces transform faults at mid-ocean ridges. *Science*, 329, 1047–1050.
- Gerya, T. V., Yuen, D.A., 2007. Robust characteristics method for modelling multiphase visco-elasto-plastic thermo-mechanical problems. *Phys. Earth Planet. Inter.* 163, 83–105. doi:10.1016/j.pepi.2007.04.015
- Gladchenko, T.P., Hinz, K., Eldholm, O., Meyer, H., Neben, S., Skogseid, J., 1997. South Atlantic volcanic margins. *J. Geol. Soc. London* 154, 465–470.
- Gladchenko, T.P., Skogseid, J., Eldholm, O., 1998. Namibia volcanic margin. *Mar. Geophys. Res.* 20, 313–341.
- Goetze, C., Evans, B., 1979. Stress and temperature in the bending lithosphere as constrained by experimental rock mechanics. *Geophys. J. R. Astron. Soc.* 59, 463–478. doi:10.1111/j.1365-246X.1979.tb02567.x
- Gradstein, F.M., Ogg, J.G., Hilgen, F.J., 2012. On The Geologic Time Scale. *Newsletters Stratigr.* 45, 171–188. doi:10.1127/0078-0421/2012/0020
- Granot, R., Dyment, J., 2015. The Cretaceous opening of the South Atlantic Ocean. *Earth Planet. Sci. Lett.* 414, 156–163. doi:10.1016/j.epsl.2015.01.015
- Greenhalgh, E.E., Kuszniir, N.J., 2007. Evidence for thin oceanic crust on the extinct Aegir Ridge, Norwegian Basin, NE Atlantic derived from satellite gravity inversion. *Geophys. Res. Lett.* 34, 1–5. doi:10.1029/2007GL029440
- Guardado, L.R., Spadini, A.R., Brandão, J.S.L., Mello, M.R., 2000. Petroleum System of the Campos Basin, Brazil. *AAPG Mem.* 73, 317–324.
- Guillou-Frottier, L., Burov, E., Nehlig, P., Wyns, R., 2007. Deciphering plume-lithosphere interactions beneath Europe from topographic signatures. *Glob. Planet. Change* 58, 119–140. doi:10.1016/j.gloplacha.2006.10.003
- Guiraud, R., Maurin, J.-C., 1992. Early Cretaceous rifts of Western and Central Africa: an overview. *Tectonophysics* 213, 153–168. doi:10.1016/0040-1951(92)90256-6
- Hager, B.H., Richards, M.A., 1989. Long-wavelength variations in Earth’s geoid: physical models and dynamical implications. *Philos. Trans. R. Soc. London. Ser. A, Math. Phys. Sci.* 328, 309–327.
- Hassan, R., Flament, N., Gurnis, M., Bower, D.J., Müller, M., 2015. Provenance of plumes in global convection models. *Geochemistry Geophys. Geosystems* 18, 1541–1576. doi:10.1002/2014GC005684
- Heezen, B.C., 1956. The Origin of Submarine Canyons. *Sci. Am.* 195, 36–41.
- Heezen, B.C., Tharp, M., Ewing, E., 1959. The floors of the Oceans: I. The North Atlantic. *Geol. Soc. Am. Spec. Pap.* 65, 1–145.
- Heine, C., Zoethout, J., Müller, R.D., 2013. Kinematics of the South Atlantic rift. *Solid Earth* 4, 215–253. doi:10.5194/se-4-

- 215-2013
- Heit, B., Sodoudi, F., Yuan, X., Bianchi, M., Kind, R., 2007. An S receiver function analysis of the lithospheric structure in South America. *Geophys. Res. Lett.* 34, 1–5. doi:10.1029/2007GL030317
- Hess, H.H., 1962. History of Ocean Basins. *Petrol. Stud.* a Vol. to Honor A.F. Buddingt. 599–620.
- Hinz, K., Neben, S., Schreckenberger, B., Roeser, H.A., Block, M., Goncalves de Souza, K., Meyer, H., 1999. The Argentine continental margin north of 48 S: sedimentary successions, volcanic activity during breakup. *Mar. Pet. Geol.* 16, 1–25. doi:10.1016/S0264-8172(98)00060-9
- Hirsch, K.K., Scheck-Wenderoth, M., Wees, J.-D. Van, Kuhlmann, G., Paton, D.A., 2010. Tectonic subsidence history and thermal evolution of the Orange Basin. *Mar. Pet. Geol.* 27, 565–584. doi:10.1016/j.marpetgeo.2009.06.009
- Hirth, G., Kohlstedt, D.L., 1996. Water in the oceanic upper mantle: implications for rheology, melt extraction and the evolution of the lithosphere. *Earth Planet. Sci. Lett.* 144, 93–108.
- Hofmann, C., Courtillot, V., Féraud, G., Rochette, P., Yirgu, G., Ketefo, E., Pik, R., 1997. Timing of the Ethiopian flood basalt event and implications for plume birth and global change. *Nature* 389, 838–841. doi:10.1038/39853
- Holmes, A., 1929. A review of the continental drift hypothesis. *Min. Mag.* 1–15.
- Holtar, E., Forsberg, A.W., 2000. Post-rift development of the Walvis Basin, Namibia: Results from the exploration campaign in quadrant 1911, in: *Petroleum Systems of South Atlantic Margins: AAPG Memoir 73*. pp. 429–446.
- Hubbert, M.K., 1951. Mechanical basis for certain familiar geologic structures. *Bull. Geol. Soc. Am.* 62, 355–372.
- Huismans, R., Beaumont, C., 2011. Depth-dependent extension, two-stage breakup and cratonic underplating at rifted margins. *Nature* 473, 74–78. doi:10.1038/nature09988
- Huismans, R.S., Beaumont, C., 2008. Complex rifted continental margins explained by dynamical models of depth-dependent lithospheric extension. *Geology* 36, 163–166. doi:10.1130/G24231A.1
- Huismans, R.S., Beaumont, C., 2007. Roles of lithospheric strain softening and heterogeneity in determining the geometry of rifts and continental margins. *Geol. Soc. London, Spec. Publ.* 282, 111–138. doi:10.1144/SP282.6
- Huismans, R.S., Beaumont, C., 2003. Symmetric and asymmetric lithospheric extension: Relative effects of frictional-plastic and viscous strain softening. *J. Geophys. Res.* 108, 1–22. doi:10.1029/2002JB002026
- Huismans, R.S., Beaumont, C., 2002. Asymmetric lithospheric extension: The role of frictional plastic strain softening inferred from numerical experiments. *Geology* 30, 211–214.
- Huismans, R.S., Podladchikov, Y.Y., Cloetingh, S., 2001. Transition from passive to active rifting: relative importance of asthenospheric doming and passive extension of the lithosphere. *J. Geophys. Res.* 106, 11271–1191.
- Husson, L., Conrad, C.P., Faccenna, C., 2012. Plate motions, Andean orogeny, and volcanism above the South Atlantic convection cell. *Earth Planet. Sci. Lett.* 317–318, 126–135.
- Ito, G., Lin, J., Gable, C.W., 1996. Dynamics of mantle flow and melting at a ridge-centred hotspot: Iceland and the Mid-Atlantic Ridge. *Earth Planet. Sci. Lett.* 144, 53–74. doi:10.1016/0012-821X(96)00151-3
- Jackson, J., 2002. Strength of the lithosphere: time to abandon the jelly sandwich? *GSA Today* 2, 1–11. doi:10.1130/1052-5173(2002)012<0004:SOTCLT>2.0.CO;2
- Jackson, M.P.A., Cramez, C., Fonck, J.M., 2000. Role of subaerial volcanic rocks and mantle plumes in creation of South Atlantic margins: Implications for salt tectonics and source rocks. *Mar. Pet. Geol.* 17, 477–498. doi:10.1016/S0264-8172(00)00006-4
- Janssen, M.E., Stephenson, R.A., Cloetingh, S., 1995. Temporal and spatial correlations between changes in plate motions and the evolution of rifted basins in Africa. *Geol. Soc. Am. Bull.* 107, 1317–1332. doi:10.1130/0016-7606(1995)107<1317:TASCBC>2.3.CO;2
- Japsen, P., Chalmers, J.A., Green, P.F., Bonow, J.M., 2012. Elevated, passive continental margins: Not rift shoulders, but expressions of episodic, post-rift burial and exhumation. *Glob. Planet. Change* 90–91, 73–86. doi:10.1016/j.gloplacha.2011.05.004
- Jaupart, C., Mareschal, J.-C., 2010. *Heat generation and transport in the Earth*. Cambridge University Press, p. 476.
- Jolivet, L., Menant, A., Sternai, P., Rabillard, A., Arbaret, L., Augier, R., Laurent, V., Beaudoin, A., Grasemann, B., Huet, B., Labrousse, L., Le, L., 2015. The geological signature of a slab tear below the Aegean. *Tectonophysics* 659, 166–182. doi:10.1016/j.tecto.2015.08.004
- Keefner, J.W., Mackwell, S.J., Kohlstedt, D.L., Heidelbach, F., 2011. Dependence of dislocation creep of dunite on oxygen fugacity: Implications for viscosity variations in Earth's mantle. *J. Geophys. Res.* 116, B05201. doi:10.1029/2010JB007748
- Keeley, M., Light, M., 1993. Basin evolution and prospectivity of the Argentine continental margin. *J. Pet. Geol.* 16, 451–464.
- Kerr, A., Hall, J., Wardle, R.J., Gower, C.F., Ryan, B., 1997. New reflections on the structure and evolution of the Makkovikian - Ketilidian Orogen in Labrador and southern Greenland. *Tectonics* 16, 942–965.
- Kirby, S.H., Stein, S., Okal, E.A., Rubie, D.C., 1996. Metastable mantle phase transformations and deep earthquakes in subducting oceanic lithosphere. *Rev. Geophys.* 34, 261–306. doi:10.1029/96RG01050
- Kohlstedt, D.L., Evans, B., Mackwell, S.J., 1995. Strength of the lithosphere: constraints imposed by laboratory experiments. *J. Geophys. Res.* 100, 17,587–17,602.
- Konopásek, J., Sláma, J., Kosler, J., 2016. Linking the basement geology along the Africa-South America coasts in the South Atlantic. *Precambrian Res.* 280, 221–230. doi:10.1016/j.precamres.2016.05.011
- Kontorovich, A.E., Burshtein, L.M., Malyshev, N.A., Safronov, P.I., Gus'kov, S.A., Ershov, S. V., Kazanenkov, V.A., Kim, N.S., Kontorovich, V.A., Kostyreva, E.A., Melenevskiy, V.N., Livshits, V.R., Polyakov, A.A., Skvortsov, M.B., 2013. Historical-geological modelling of hydrocarbon generation in the Mesozoic – Cenozoic sedimentary basin of the Kara Sea (basin modelling). *Russ. Geol. Geophys.* 54, 917–957. doi:10.1016/j.rgg.2013.07.011
- Koptev, A., Burov, E., Calais, E., Leroy, S., Gerya, T., Guillou-Frotier, L., Cloetingh, S., 2016. Contrasted continental rifting via plume-craton interaction: Applications to Central East African Rift. *Geosci. Front.* 7, 221–236.

- doi:10.1016/j.gsf.2015.11.002
- Koptev, A., Burov, E., Gerya, T., Le, L., Leroy, S., Calais, E., Jolivet, L., 2017. Plume-induced continental rifting and break-up in ultra-slow extension context: Insights from 3D numerical modelling. *Tectonophysics* 1–17. doi:10.1016/j.tecto.2017.03.025
- Koptev, A., Calais, E., Burov, E., Leroy, S., Gerya, T., 2015. Dual continental rift systems generated by plume – lithosphere interaction. *Nat. Geosci.* 8, 388–392. doi:10.1038/NGEO2401
- Kuszniir, N.J., Marsden, G., Egan, S.S., 1991. A flexural-cantilever simple-shear/pure-shear model of continental lithosphere extension: applications to the Jeanne d’Arc Basin, Grand Banks and Viking Graben, North Sea. *Geol. Soc. London, Spec. Publ.* 56, 41–60.
- Kuszniir, N.J., Ziegler, P.A., 1992. The mechanics of continental extension and sedimentary basin formation: A simple-shear/pure-shear flexural cantilever model. *Tectonophysics* 215, 117–131. doi:10.1016/0040-1951(92)90077-J
- Larsen, H.C., Saunders, A.D., 1998. Tectonism and volcanism at the southeast Greenland rifted margin: a record of plume impact and later continental rupture. *Proc. Ocean Drill. Progr. Sci. Results* 152, 503–533. doi:10.2973/odp.proc.sr.152.1998
- Lavecchia, A., Thieulot, C., Beekman, F., Cloetingh, S., Clark, S., 2017. Lithosphere erosion and continental breakup: Interaction of extension, plume upwelling and melting. *Earth Planet. Sci. Lett.* 467, 89–98. doi:10.1016/j.epsl.2017.03.028
- Lavier, L.L., Manatschal, G., 2006. A mechanism to thin the continental lithosphere at magma-poor margins. *Nature* 440, 324–328. doi:10.1038/nature04608
- Le Pourhiet, L., 2004. Modélisation thermo-mécanique de l’extension continentale: développements théoriques et applications au golfe de Corinthe.
- Le Pourhiet, L., Burov, E., Moretti, I., 2004. Rifting through a stack of inhomogeneous thrusts (the dipping pie concept). *Tectonics* 23, 1–14. doi:10.1029/2003TC001584
- Lee, C.A., Leeman, W.P., Canil, D., Li, Z.A., 2005. Similar V / Sc Systematics in MORB and Arc Basalts : Implications for the Oxygen Fugacities of their Mantle Source Regions. *J. f Petrol.* 46, 2313–2336. doi:10.1093/petrology/egi056
- Lister, G.S., Etheridge, M.A., Symonds, P.A., 1986. Detachment faulting and the evolution of passive continental margins. *Geology* 14, 246–250.
- Lithgow-Bertelloni, C., Silver, P., 1998. Dynamic topography, plate driving forces and the African superswell. *Nature* 395, 345–348. doi:10.1038/26212
- Lundin, E., Doré, A.G., 2002. Mid-Cenozoic post-breakup deformation in the “passive” margins bordering the Norwegian - Greenland Sea. *Mar. Pet. Geol.* 19, 79–93.
- Lustrino, M., 2016. (More than) fifty shades of plumes.
- Macdonald, D., Gomez-Perez, I., Franzese, J., Spalletti, L., Lawver, L., Gahagan, L., Dalziel, I., Thomas, C., Trewin, N., Hole, M., Paton, D., 2003. Mesozoic break-up of SW Gondwana: Implications for regional hydrocarbon potential of the southern South Atlantic. *Mar. Pet. Geol.* 20, 287–308. doi:10.1016/S0264-8172(03)00045-X
- Manatschal, G., Lavier, L., Chenin, P., 2015. The role of inheritance in structuring hyperextended rift systems: Some considerations based on observations and numerical modelling. *Gondwana Res.* 27, 140–164. doi:10.1016/j.gr.2014.08.006
- Marcano, G., Anka, Z., di Primio, R., 2013. Major controlling factors on hydrocarbon generation and leakage in South Atlantic conjugate margins: A comparative study of Colorado, Orange, Campos and Lower Congo basins. *Tectonophysics* 604, 172–190. doi:10.1016/j.tecto.2013.02.004
- Marti, J., Cundall, P., 1982. Mixed discretization procedure for accurate modelling of plastic collapse. *Int. J. Numer. Anal. Methods Geomech.* 6, 129–139.
- Martin, A.K., Hartnady, C.J.H., 1986. Plate tectonic development of the South West Indian Ocean: a revised reconstruction of East Antarctica and Africa. *J. Geophys. Res.* 91, 4767–4786.
- Martin, K.A., Hartnady, C.J.H., Goodlad, S.W., 1981. A revised fit of South America and South Central Africa. *Earth Planet. Sci. Lett.* 54, 293–305. doi:10.1016/0012-821X(81)90012-1
- Maystrenko, Y.P., Scheck-Wenderoth, M., Hartwig, A., Anka, Z., Watts, A.B., Hirsch, K.K., Fishwick, S., 2013a. Structural features of the Southwest African continental margin according to results of lithosphere-scale 3D gravity and thermal modelling. *Tectonophysics* 604, 104–121. doi:10.1016/j.tecto.2013.04.014
- Maystrenko, Y.P., Scheck-Wenderoth, M., Hartwig, A., Anka, Z., Watts, A.B., Hirsch, K.K., Fishwick, S., 2013b. Structural features of the Southwest African continental margin according to results of lithosphere-scale 3D gravity and thermal modelling. *Tectonophysics* 604, 104–121. doi:10.1016/j.tecto.2013.04.014
- McClusky, S., Reilinger, R., Ogubazghi, G., Amleson, A., Healeb, B., Vernant, P., Sholan, J., Fisseha, S., Asfaw, L., Bendick, R., Kogan, L., 2010. Kinematics of the southern Red Sea – Afar Triple Junction and implications for plate dynamics. *Geophys. Res. Lett.* 37, 1–5. doi:10.1029/2009GL041127
- McKenzie, D., 1978a. Active tectonics of the Alpine-Himalayan belt; the Aegean Sea and surrounding regions. *Geophys. J. R. Astron. Soc.* 55, 217.
- McKenzie, D., 1978b. Some remarks on the development of sedimentary basins. *Earth Planet. Sci. Lett.* 40, 25–32. doi:10.1016/0012-821X(78)90071-7
- Meisling, K.E., Cobbold, P.R., Mount, V.S., 2001. Segmentation of an obliquely rifted margin, Campos and Santos basins, southeastern Brazil. *Am. Assoc. Pet. Geol. Bull.* 85, 1903–1924. doi:10.1306/8626D0B3-173B-11D7-8645000102C1865D
- Mello, M.R., de Azambuja Filho, N.C., Bender, A.A., Barbanti, S.M., Mohriak, W., Schmitt, P., de Jesus, C.L.C., 2013. The Namibian and Brazilian southern South Atlantic petroleum systems: are they comparable analogues ? *Geol. Soc. London, Spec. Publ.* 369, 249–266.
- Mezri, L., Le Pourhiet, L., Wolf, S., Burov, E., 2015. New parametric implementation of metamorphic reactions limited by

- water content , impact on exhumation along detachment faults. *Lithos* 236–237, 287–298.
doi:10.1016/j.lithos.2015.08.021
- Minelli, L., Faccenna, C., 2010. Evolution of the Calabrian accretionary wedge (central Mediterranean). *Tectonics* 29, 1–21.
doi:10.1029/2009TC002562
- Mittelstaedt, E., Ito, G., Behn, M.D., 2008. Mid-ocean ridge jumps associated with hotspot magmatism. *Earth Planet. Sci. Lett.* 266, 256–270. doi:10.1016/j.epsl.2007.10.055
- Mohriak, W.U., Hobbs, R., Dewey, J.F., 1990. Basin-forming processes and the deep structure of the Campos Basin, offshore Brazil. *Mar. Pet. Geol.* 7, 94–122. doi:10.1016/0264-8172(90)90035-F
- Mohriak, W.U., Mello, M.R., Vieira, I.S., Bassetto, M., Koutsoukos, E.A.M., 2000. Crustal architecture, sedimentation, and petroleum systems in the Sergipe-Alagoas Basin, Northeastern Brazil. *AAPG Spec. Vol.* 273–300.
- Mohriak, W.U., Nóbrega, M., Odegard, M.E., Gomes, B.S., Dickson, W.G., 2010. Geological and geophysical interpretation of the Rio Grande Rise, south-eastern Brazilian margin: extensional tectonics and rifting of continental and oceanic crusts. *Pet. Geosci.* 16, 231–245. doi:10.1144/1354-079309-910
- Morgan, P., 1983. Constraints on rift thermal processes from heat flow and uplift. *Tectonophysics* 94, 277–298.
- Moulin, M., Aslanian, D., Olivet, J.L., Contrucci, I., Matias, L., Géli, L., Klingelhoefer, F., Nouzé, H., Réhault, J.P., Unternehr, P., 2005. Geological constraints on the evolution of the Angolan margin based on reflection and refraction seismic data (ZaiAngo project). *Geophys. J. Int.* 162, 793–810. doi:10.1111/j.1365-246X.2005.02668.x
- Moulin, M., Aslanian, D., Rabineau, M., Patriat, M., Matias, L., 2013. Kinematic keys of the Santos – Namibe basins. *Geol. Soc. London, Spec. Publ.* 369, 91–107.
- Moulin, M., Aslanian, D., Unternehr, P., 2010. A new starting point for the South and Equatorial Atlantic Ocean. *Earth-Science Rev.* 98, 1–37. doi:10.1016/j.earscirev.2009.08.001
- Müller, R.D., Sdrolias, M., Gaina, C., Roest, W.R., 2008. Age, spreading rates, and spreading asymmetry of the world's ocean crust. *Geochemistry, Geophys. Geosystems* 9, 1–19. doi:10.1029/2007GC001743
- Müller, R.D., Roest, W.R., Royer, J.-Y., Gahagan, L.M., Sclater, J.G., 1997. Digital isochrons of the world's ocean floor. *J. Geophys. Res.* 102, 3211–3214.
- Müller, R.D., Sdrolias, M., Gaina, C., Steinberger, B., Heine, C., 2008. Long-term sea-level fluctuations driven by ocean basin dynamics. *Science* 319, 1357–1362. doi:10.1126/science.1151540
- Munteanu, I., Willingshofer, E., Matenco, L., Sokoutis, D., Cloetingh, S., 2014. Far-field contractional polarity changes in models and nature. *Earth Planet. Sci. Lett.* 395, 101–115. doi:10.1016/j.epsl.2014.03.036
- Nemcok, M., Henk, A., Allen, R., Sikora, P.J., Stuart, C., 2013. Continental break-up along strike-slip fault zones ; observations from the Equatorial Atlantic. *Geol. Soc. London, Spec. Publ.* 369, 537–556.
- Nestola, Y., Storti, F., Cavozi, C., 2015. Strain rate-dependent lithosphere rifting and necking architectures in analog experiments. *J. Geophys. Res. Solid Earth* 120, 584–594. doi:10.1002/2014JB011623.Received
- Nürnberg, D., Müller, R.D., 1991. The tectonic evolution of the South Atlantic from Late Jurassic to present. *Tectonophysics* 191, 27–53.
- Nyblade, A.A., Robinson, S.W., 1994. The African Superswell. *Geophys. Res. Lett.* 21, 765–768.
- O'Connor, J.M., Duncan, R.A., 1990. Evolution of the Walvis Ridge-Rio Grande Rise Hot Spot System: Implications for African and South American Plate motions over plumes. *J. Geophys. Res.* 95, 17475. doi:10.1029/JB095iB11p17475
- Okay, A.I., Sengor, A. M.C., Gorur, N., 1994. Kinematic history of the opening of the Black Sea and its effect on the surrounding regions. *Geology*. doi:10.1130/0091-7613(1994)022<0267:khotoo>2.3.co;2
- Olsen, K.H., Morgan, P., 1995. Introduction: Progress in understanding continental rifts. *Dev. Geotecton. Cont. Rift. Evol. Struct. tectonics* 25, 3–26. doi:10.1016/S0419-0254(06)80005-4
- Pángaro, F., Ramos, V.A., 2012. Paleozoic crustal blocks of onshore and offshore central Argentina: New pieces of the southwestern Gondwana collage and their role in the accretion of Patagonia and the evolution of Mesozoic south Atlantic sedimentary basins. *Mar. Pet. Geol.* 37, 162–183. doi:10.1016/j.marpetgeo.2012.05.010
- Passchier, C.J., Trouw, R.A.J., 1996. *Microtectonics*. Springer International Publishing, p. 372.
- Paton, D.A., Primio, R., Kuhlmann, G., Spuy, D. Van Der, Horsfield, B., 2007. Insights into the Petroleum System Evolution of the southern Orange Basin, South Africa. *South African J. Geol.* 110, 261–274. doi:10.2113/gssajg.110.2-3.261
- Peace, A., McCaffrey, K., Imber, J., Phethean, J., Nowell, G., Gerdes, K., Dempsey, E., 2016. An evaluation of Mesozoic rift-related magmatism on the margins of the Labrador Sea: Implications for rifting and passive margin asymmetry. *Geosphere* 12, 1–24. doi:10.1130/GES01341.1
- Pérez-Gussinyé, M., Reston, T.J., 2001. Rheological evolution during the extensional nonvolcanic rifted margins: onset of serpentinization and development of detachments leading to continental breakup. *J. Geophys. Res.* 106, 3961–3975.
- Péron-Pinvidic, G., Manatschal, G., 2009. The final rifting evolution at deep magma-poor passive margins from Iberia-Newfoundland: A new point of view. *Int. J. Earth Sci.* 98, 1581–1597. doi:10.1007/s00531-008-0337-9
- Philippon, M., Brun, J., Gueydan, F., Sokoutis, D., 2014. The interaction between Aegean back-arc extension and Anatolia escape since Middle Miocene. *Tectonophysics* 631, 176–188. doi:10.1016/j.tecto.2014.04.039
- Pindell, J., Graham, R., Horn, B., 2014. Rapid outer marginal collapse at the rift to drift transition of passive margin evolution, with a Gulf of Mexico case study. *Basin Res.* 26, 701–725. doi:10.1111/bre.12059
- Podladchikov, Y.Y., Poliakov, A.N.B., Yuen, D.A., 1994. The effect of lithospheric phase transitions on subsidence of extending continental lithosphere. *Earth Planet. Sci. Lett.* 124, 95–103.
- Poliakov, A., Cundall, P., Podladchikov, Y., Lyakhovsky, V., 1993. An explicit inertial method for the simulation of viscoelastic flow: an evaluation of elastic effects on diapiric flow in two- and three-layer models. *Flow Creep Sol. Syst. Obs. Model. Theory* 175–195. doi:10.1007/978-94-015-8206-3_12
- Poliakov, A., Podladchikov, Y., Talbot, C., 1993. Initiation of salt diapirs with frictional overburdens: numerical experiments. *Tectonophysics* 228, 199–210. doi:10.1016/0040-1951(93)90341-G
- Pollack, H.N., 1986. Cratonization and thermal evolution of the mantle. *Earth Planet. Sci. Lett.* 80, 175–182.

- Pollack, H.N., Hurter, S.J., Johnson, R., 1993. Heat flow from the earth's interior: analysis of the global data set. *Rev. Geophys.* 267–280.
- Popov, A.A., Sobolev, S. V., 2010. SLIM3D : A tool for three-dimensional thermomechanical modelling of lithospheric deformation with elasto-visco-plastic rheology To cite this version : HAL Id : hal-00532141. doi:10.1016/j.pepi.2008.03.007
- Rabinowitz, P.D., Labrecque, J., 1979. The Mesozoic South Atlantic Ocean and Evolution of Its Continental Margins. *J. Geophys. Res.* 84, 5973–6002.
- Ramos, V.A., 2004. La Plataforma Patagónica y sus relaciones con la Plataforma Brasileira. *Geol. do Cont. Sul-Americano, Sao Paulo* 22, 371–381.
- Ramos, V.A., Ramos, V.A., Turic, M.A., 1996. Evolución tectónica de la Plataforma Continental. *Geol. y Recur. Nat. la Plataforma Cont. Argentina (Ramos, VA; Turic, MA)* 385–404.
- Ranalli, G., 1995. Rheology of the Earth, 2nd edition. Chapman and Hall, 413 pp.
- Ranalli, G., Murphy, D.C., 1987. Rheological stratification of the lithosphere. *Tectonophysics* 132, 281–295. doi:10.1016/0040-1951(87)90348-9
- Raposo, M.I.B., Ernesto, M., Renne, P.R., 1998. Paleomagnetism and $40\text{Ar}/^{39}\text{Ar}$ dating of the early Cretaceous Florianópolis dike swarm (Santa Catarina Island), Southern Brazil. *Phys. Earth Planet. Inter.* 108, 275–290.
- Renne, P.R., Deckart, K., Ernesto, M., Féraud, G., Piccirillo, E.M., 1996. Age of the Ponta Grossa dike swarm (Brazil), and implications to Paraná flood volcanism. *Earth Planet. Sci. Lett.* 144, 199–211. doi:10.1016/0012-821X(96)00155-0
- Ribe, N.M., 1996. The dynamics of plume-ridge interaction 2. Off-ridge plumes. *J. Geophys. Res.* 101, 16,195–16,204.
- Ribe, N.M., Christensen, U.R., 1994. Three-dimensional modelling of plume-lithosphere interaction. *J. Geophys. Res.* 99, 669–682.
- Rickers, F., Fichtner, A., Trampert, J., 2013. The Iceland-Jan Mayen plume system and its impact on mantle dynamics in the North Atlantic region: Evidence from full-waveform inversion. *Earth Planet. Sci. Lett.* 367, 39–51. doi:10.1016/j.epsl.2013.02.022
- Ringwood, A.E., 1991. Phase transformations and their bearing on the constitution and dynamics of the mantle. *Geochim. Cosmochim. Acta* 55, 2083–2110. doi:10.1016/0016-7037(91)90090-R
- Rogozhina, I., Petrunin, A.G., Vaughan, A.P.M., Steinberger, B., Johnson, J. V., Kaban, M.K., Calov, R., Rickers, F., Thomas, M., Koulakov, I., 2016. Melting at the base of the Greenland ice sheet explained by Iceland hotspot history. *Nat. Geosci.* 9, 366–369. doi:10.1038/NNGEO2689
- Rosenbaum, G., Weinberg, R.F., Regenauer-Lieb, K., 2008. The geodynamics of lithospheric extension. *Tectonophysics* 458, 1–8. doi:10.1016/j.tecto.2008.07.016
- Rosencrantz, E., Ross, M.I., Sclater, J.G., 1988. Age and spreading history of the Cayman Trough as determined from depth, heat flow, and magnetic anomalies. *J. Geophys. Res.* 93, 2141–2157.
- Rosendahl, B.R., 1987. Architecture of continental rifts with special reference to East Africa. *Annu. Rev. Earth Planet. Sci.* 15, 445–503.
- Rosendahl, B.R., Mohriak, W.U., Odegard, M.E., Turner, J.P., Dickson, W.G., 2005. West African and Brazilian conjugate margins: Crustal types, architecture, and plate configurations, in: *Petroleum Systems of Divergent Continental Margin Basins: Houston, 25th Gulf Coast Section, Society Sedimentary Geology, Bob F. Perkins Research Conference.* pp. 4–7.
- Rousseau, M., Guérin, V., Sapin, F., Restiadi, D., Malla-Meidianna, C., Gaulier, J.-M., 2015. South Makassar Basin: 3D thermal modelling - implication for future exploration. *AAPG database Arch.* 39th Annual.
- Royden, L., Keen, C.E., 1980. Rifting process and thermal evolution of the continental margin of eastern Canada determined from subsidence curves. *Earth Planet. Sci. Lett.* 51, 343–361.
- Ryan, W.B.F., Carbotte, S.M., Coplan, J.O., O'Hara, S., Melkonian, A., Arko, R., Weissel, R.A., Ferrini, V., Goodwillie, A., Nitsche, F., Bonczkowski, J., Zemski, R., 2009. Global Multi-Resolution Topography synthesis. *Geochemistry, Geophys. Geosystems* 10, 1–9. doi:10.1029/2008GC002332
- Sandwell, D.T., Smith, W.H.F., 2009. Global marine gravity from retracked Geosat and ERS-1 altimetry: Ridge segmentation versus spreading rate. *J. Geophys. Res. Solid Earth* 114, 1–18. doi:10.1029/2008JB006008
- Saunders, A.D., Fitton, J.G., Kerr, A.C., Norry, M.J., Kent, R.W., 1997. The North Atlantic igneous province. *Geophys. Monogr.* 100, 45–93.
- Schellart, W.P., 2004. Quantifying the net slab pull force as a driving mechanism for plate tectonics. *Geophys. Res. Lett.* 31, 10–14. doi:10.1029/2004GL019528
- Schellart, W.P., Strak, V., 2016. A review of analogue modelling of geodynamic processes : Approaches, scaling, materials and quantification, with an application to subduction experiments. *J. Geodyn.* 100, 7–32. doi:10.1016/j.jog.2016.03.009
- Schlömer, A., Geissler, W.H., Jokat, W., Jegen, M., 2017. Hunting for the Tristan mantle plume - An upper mantle tomography around the volcanic island of Tristan da Cunha. *Earth Planet. Sci. Lett.* 462, 122–131. doi:10.1016/j.epsl.2016.12.028
- Schnabel, M., Franke, D., Engels, M., Hinz, K., Neben, S., Damm, V., Grassmann, S., Pelliza, H., Dos Santos, P.R., 2008. The structure of the lower crust at the Argentine continental margin, South Atlantic at 44°S. *Tectonophysics* 454, 14–22. doi:10.1016/j.tecto.2008.01.019
- Sengör, C., Burke, K., 1978. Relative timing of rifting and volcanism on earth and its tectonic implications. *Geophys. Res. Lett.* 5, 419–421.
- Simon, N.S.C., Podladchikov, Y.Y., 2008. The effect of mantle composition on density in the extending lithosphere. *Earth Planet. Sci. Lett.* 272, 148–157. doi:10.1016/j.epsl.2008.04.027
- Skogseid, J., Planke, S., Faleide, J.I., Pedersen, T., Eldholm, O., Neverdal, F., 2000. NE Atlantic continental rifting and volcanic margin formation. *Geol. Soc. London, Spec. Publ.* 167, 295–326.

- Sleep, N.H., 2006. Mantle plumes from top to bottom. *Earth-Science Rev.* 77, 231–271. doi:10.1016/j.earscirev.2006.03.007
- Sleep, N.H., 2005. Evolution of the Continental Lithosphere. *Annu. Rev. Earth Planet. Sci.* 33, 369–393. doi:10.1146/annurev.earth.33.092203.122643
- Sokoutis, D., Corti, G., Bonini, M., Pierre Brun, J., Cloetingh, S., Mauduit, T., Manetti, P., 2007. Modelling the extension of heterogeneous hot lithosphere. *Tectonophysics* 444, 63–79. doi:10.1016/j.tecto.2007.08.012
- Stab, M., Bellahsen, N., Pik, R., Quidelleur, X., Ayalew, D., Leroy, S., 2016. Modes of rifting in magma-rich settings: Tectono-magmatic evolution of Central Afar. *Tectonics* 35, 2–38. doi:10.1002/2015TC003893
- Svartman Dias, A., Lavier, L.L., Hayman, 2015. Conjugate rifted margins width and asymmetry: the interplay between lithospheric strength and thermo-mechanical processes. *J. Geophys. Res.* 120, 8672–8700. doi:10.1002/2015JB012074
- Tackley, P.J., 2002. *Mantle Convection and Plate Tectonics : Toward an Integrated Physical and Chemical Theory* 288, 2002–2007.
- Tackley, P.J., 1998. Self-consistent generation of tectonic plates in three-dimensional mantle convection 157, 9–22.
- Talwani, M., Abreu, V., 2000. Inferences regarding initiation of oceanic crust formation from the U.S. east coast margin and conjugate South Atlantic margins. *Atl. Rift. Cont. margins.* 115, 211–233.
- Talwani, M., Eldholm, O., 1973. Boundary between continental and oceanic crust at the margin of rifted continents. *Nature* 241, 325–330.
- Tange, Y., Takahashi, E., Nishihara, Y., Funakoshi, K.I., Sata, N., 2009. Phase relations in the system MgO-FeO-SiO₂ to 50 GPa and 2000°C: An application of experimental techniques using multianvil apparatus with sintered diamond anvils. *J. Geophys. Res. Solid Earth* 114, 1–12. doi:10.1029/2008JB005891
- Tankard, A.J., Ultiana, M.A., Welsink, H.J., Ramos, V.A., Turic, M., Milani, A.B.F.E.J., de Brito Neves, B.B., Eyles, N., Skarmeta, J., Santa Ana, H., 1995. Structural and tectonic controls of basin evolution in southwestern Gondwana during the Phanerozoic. *AAPG Mem.* 62, 5–52.
- Taylor, B., Goodliffe, A., Martinez, F., Hey, R., 1995. Continental rifting and initial sea-floor spreading in the Woodlark basin. *Nature.* doi:10.1038/374534a0
- ter Voorde, M., Bertotti, G., 1994. Thermal effects of normal faulting during rifted basin formation, 1. A finite difference model. *Tectonophysics* 240, 133–144.
- ter Voorde, M., Cloetingh, S., 1996. Numerical modelling of extension in faulted crust: effects of localized and regional deformation on basin stratigraphy. *Geophys. Soc. London, Spec. Publ.* 99, 283–296.
- Tirel, C., Brun, J.P., Sokoutis, D., 2006. Extension of thickened and hot lithospheres: Inferences from laboratory modelling. *Tectonics* 25, 1–13. doi:10.1029/2005TC001804
- Torsvik, T.H., Amundsen, H.E.F., Trønnes, R.G., Doubrovine, P. V., Gaina, C., Kuznir, N.J., Steinberger, B., Corfu, F., Ashwal, L.D., Griffin, W.L., Werner, S.C., Jamtveit, B., 2015. Continental crust beneath southeast Iceland. *Proc. Natl. Acad. Sci.* 112, E1818–E1827. doi:10.1073/pnas.1423099112
- Torsvik, T.H., Rousse, S., Labails, C., Smethurst, M.A., 2009. A new scheme for the opening of the South Atlantic Ocean and the dissection of an Aptian salt basin. *Geophys. J. Int.* 177, 1315–1333. doi:10.1111/j.1365-246X.2009.04137.x
- Torsvik, T.H., Smethurst, M.A., Burke, K., Steinberger, B., 2006. Large igneous provinces generated from the margins of the large low-velocity provinces in the deep mantle. *Geophys. J. Int.* 167, 1447–1460. doi:10.1111/j.1365-246X.2006.03158.x
- Tsenn, M.C., Carter, N.L., 1987. Upper limits of power law creep of rocks. *Tectonophysics* 136, 1–26. doi:10.1016/0040-1951(87)90332-5
- Tugend, J., Manatschal, G., Gillard, M., Nirrengarten, M., Epin, M.-E., Sauter, D., Autin, J., Harkin, C., Kuznir, N., 2017. Breaking the paradigm of magma-poor and magma-rich rifted margins. *EGU Gen. Assem. Conf. Abstr.* 19.
- Turcotte, D.L., Emerman, S.H., 1983. Mechanisms of active and passive rifting. *Tectonophysics* 94, 39–50.
- Turcotte, D.L., Schubert, G., 2002. *Geodynamics.* Cambridge Univ. Press, Cambridge, UK, p. 863.
- Ungerer, P., 1990. State of the art of research in kinetic modelling of oil formation and expulsion. *Adv. Org. Geochemistry* 16, 1–25.
- Ungerer, P., Burrus, J., Doligez, B., Chénet, P.Y., Bessis, F., 1990. Basin evaluation by integrated two-dimensional modelling of heat transfer, fluid flow, hydrocarbon generation and migration. *Am. Assoc. Pet. Geol. Bull.* 74, 309–335.
- Unternehm, P., Curie, D., Olivet, J.L., Goslin, J., Beuzart, P., 1988. South Atlantic fits and intraplate boundaries in Africa and South America. *Tectonophysics* 155, 169–179. doi:10.1016/0040-1951(88)90264-8
- Unternehm, P., Peron-Pinvidic, G., Manatschal, G., Sutra, E., 2010. Hyper-extended crust in the South Atlantic: in search of a model. *Pet. Geosci.* 16, 207–215. doi:10.1144/1354-079309-904
- Urien, C.M., Zambrano, J.J., 1973. *The geology of the basins of the Argentine continental margin and Malvinas Plateau,* Plenum Press, New York.
- Urien, C.M., Zambrano, J.J., Martins, L.R., 1981. The basins of southeastern South America (southern Brazil, Uruguay, and eastern Argentina), including the Malvinas Plateau and southern South Atlantic paleogeographic evolution. *Cuencas sedimentarias del Jurásico y Cretácico en Am. del Sur Com. Sudam. del Jurásico y Cretácico* 1, 45–126.
- Urien, C.M., Zambrano, J.J., Yrigoyen, M.R., 1995. Petroleum basins of southern South America: an overview. *AAPG Mem.* 62, 63–77.
- Uyeda, S., McCabe, R., 1983. A possible mechanism of episodic spreading of the Philippine Sea. *Accretion tectonics Circum-Pacific Reg.* 291–306.
- van der Beek, P., Cloetingh, S., Andriessen, P., 1994. Mechanisms of extensional basin formation and vertical motions at rift flanks: Constraints from tectonic modelling and fission-track thermochronology. *Earth Planet. Sci. Lett.* 121, 417–433. doi:10.1016/0012-821X(94)90081-7
- Van Der Meijde, M., Julià, J., Assumpção, M., 2013. Gravity derived Moho for South America. *Tectonophysics* 609, 456–467. doi:10.1016/j.tecto.2013.03.023

- Van Wees, J.D., van Bergen, F., David, P., Nepveu, M., Beekman, F., Cloetingh, S., Bonté, D., 2009. Probabilistic tectonic heat flow modelling for basin maturation: Assessment method and applications. *Mar. Pet. Geol.* 26, 536–551. doi:10.1016/j.marpetgeo.2009.01.020
- Vine, F.J., Matthews, D.H., 1963. Magnetic Anomalies over Oceanic Ridges. *Nature* 4897, 947–949.
- Vink, G.E., 1982. Continental rifting and the implications for plate tectonic reconstructions. *J. Geophys. Res.* 87, 10677–10688. doi:10.1029/JB087iB13p10677
- von Wegener, A., 1912. Die Entstehung der Kontinente. *Geol. Rundschau* 3, 276–292.
- Wangen, M., 1995. The blanketing effect in sedimentary basins. *Basin Res.* 7, 283–298. doi:10.1111/j.1365-2117.1995.tb00118.x
- Wangen, M., Throndsen, T., Halvorsen, G., 2007. The Paleo Heat Flow Contents in Vitrinite Reflectance Observations. *Math. Geol.* 39, 491–511. doi:10.1007/s11004-007-9110-z
- Waples, D.W., 2001. A new model for heat flow in extensional basins : radiogenic heat, asthenospheric heat, and the McKenzie Model. *Nat. Resour. Res.* 10, 227–238.
- Watts, A.B., 2001. *Isostasy and Flexure of the Lithosphere*, University of Cambridge, Cambridge. Cambridge University Press, p. 458. doi:10.1029/JB084iB10p05599
- Watts, A.B., Stewart, J., 1998. Gravity anomalies and segmentation of the continental margin offshore West Africa. *Earth Planet. Sci. Lett.* 156, 239–252. doi:10.1016/S0012-821X(98)00018-1
- Wernicke, B., 1985. Uniform-sense normal simple shear of the continental lithosphere. *Can. J. Earth Sci.* 22, 108–125.
- Wessel, P., Muller, R.D., 2007. 6.02 Plate Tectonics, in: *Treatise on Geophysics*. pp. 49–98.
- White, R., McKenzie, D., 1989. Magmatism at rift zones : the generation of volcanic continental margins. *J. Geophys. Res.* 94, 7685–7729.
- White, R.S., Smith, L.K., 2009. Crustal structure of the Hatton and the conjugate east Greenland rifted volcanic continental margins, NE Atlantic. *J. Geophys. Res. Solid Earth* 114, 1–28. doi:10.1029/2008JB005856
- White, R.S., Smith, L.K., Roberts, A.W., Christie, P.A.F., Kusznir, N.J., Roberts, a M., Healy, D., Spitzer, R., Chappell, A., Eccles, J.D., Fletcher, R., Hurst, N., Lunnun, Z., Parkin, C.J., Tymms, V.J., 2008. Lower-crustal intrusion on the North Atlantic continental margin. *Nature* 452, 460–464. doi:10.1038/nature06687
- Will, T.M., Frimmel, H.E., 2017. Where does a continent prefer to break up ? Some lessons from the South Atlantic margins. *Gondwana Res.* doi:10.1016/j.gr.2017.04.014
- Willingshofer, E., Sokoutis, D., Burg, J.-P., 2005. Lithospheric-scale analogue modelling of collision zones with a pre-existing weak zone. *Geol. Soc. London, Spec. Publ.* 243, 277–294. doi:10.1144/GSL.SP.2005.243.01.18
- Wilson, J.T., 1966. Did the Atlantic close and then re-open? *Nature* 211, 676–681.
- Wilson, M., Guiraud, R., 1992. Magmatism and rifting in Western and Central Africa, from Late Jurassic to Recent times. *Tectonophysics* 213, 203–225. doi:10.1016/0040-1951(92)90259-9
- Withjack, M.O., Jamison, W.R., 1986. Deformation produced by oblique rifting. *Tectonophysics* 126, 99–124.
- Yamasaki, T., Nakada, M., 1997. The effects of the spinel-garnet phase transition on the formation of rifted sedimentary basins. *Geophys. J. Int.* 130, 681–692.
- Yamato, P., 2006. Des contraintes pour les zones de convergence: Confrontation des données du métamorphisme et des modélisations numériques thermomécaniques - Application aux Alpes et à l’Oman.
- Yamato, P., Burov, E., Agard, P., Le Pourhiet, L., Jolivet, L., 2008. HP-UHP exhumation during slow continental subduction: Self-consistent thermodynamically and thermomechanically coupled model with application to the Western Alps. *Earth Planet. Sci. Lett.* 271, 63–74. doi:10.1016/j.epsl.2008.03.049
- Yamazaki, D., Ito, E., Yoshino, T., Tsujino, N., Yoneda, A., Guo, X., Xu, F., Higo, Y., Funakoshi, K., 2014. Over 1Mbar generation in the Kawai-type multianvil apparatus and its application to compression of (Mg_{0.92}Fe_{0.08})SiO₃ perovskite and stishovite. *Phys. Earth Planet. Inter.* 228, 262–267. doi:10.1016/j.pepi.2014.01.013
- Younes, A.I., McClay, K., 2002. Development of accommodation zones in the Gulf of Suez-Red Sea rift, Egypt. *Am. Assoc. Pet. Geol. Bull.* 86, 1003–1026.
- Zeinalzadeh, A., Moussavi-Harami, R., Mahboubi, A., Sajjadian, V.A., 2015. Basin and petroleum system modelling of the Cretaceous and Jurassic source rocks of the gas and oil reservoirs in Darquain field, south west Iran. *J. Nat. Gas Sci. Eng.* 26, 419–426. doi:10.1016/j.jngse.2015.05.041
- Zhao, D., 2007. Seismic images under 60 hotspots: Search for mantle plumes. *Gondwana Res.* 12, 335–355. doi:10.1016/j.gr.2007.03.001
- Ziegler, P.A., 1993. Plate-moving mechanisms: their relative importance: William Smith Lecture 1992. *J. Geol. Soc. London.* 150, 927–940. doi:10.1144/gsjgs.150.5.0927
- Ziegler, P.A., Cloetingh, S., 2004. Dynamic processes controlling evolution of rifted basins. *Earth-Science Rev.* 64, 1–50. doi:10.1016/S0012-8252(03)00041-2
- Ziegler, P.A., Cloetingh, S., Guiraud, R., Stampfli, G.M., 2001. Peri-Tethyan platforms: constraints on dynamics of rifting and basin inversion. *Mémoires du Muséum Natl. d’histoire Nat.* 186, 9–49.
- Ziegler, P. A., Cloetingh, S., van Wees, J.-D., 1995. Dynamics of intra-plate compressional deformation: the Alpine foreland and other examples. *Tectonophysics* 252, 7–59. doi:10.1016/0040-1951(95)00102-6
- Zwaan, F., Schreurs, G., Naliboff, J., Buitert, S.J.H., 2016. Insights into the effects of oblique extension on continental rift interaction from 3D analogue and numerical models. *Tectonophysics* 693, 239–260. doi:10.1016/j.tecto.2016.02.036

APPENDICES

Appendix I Numerical code FLAMAR

The FLAMAR code (Burov et al., 2001), used for chapter 2 and 5 of this manuscript, is based on the F.L.A.C. (Fast Lagrangian Analysis of Continua) algorithm developed by Cundall and Board (1988) and Cundall (1989). It is modified after the PARA(O)VOZ code from Poliakov et al. (1993) by several other PhD studies such as Le Pourhiet (2004) and Yamato (2006).

The model solves for several coupled physical equations, the first one being Newton's second law of motion (eq. 3.1) to account for pressure-dependant deformation and free upper surface. This law is coupled with constitutive equations for visco-elasto-plasticity (eq. 3.2) accounting for realistic visco-elasto-plastic rheologies. Both eq. 3.1 and eq. 3.2 are coupled with the heat equation (eq. 3.3). The model also takes into account erosion processes by using a diffusion equation for transport (eq. 3.4) (Burov and Poliakov, 2001), which is based on the classical model of Culling (Culling, 1960). The model can perform calculations by assuming either a Boussinesq adiabatic thermal dependence (eq. 3.5a) or a thermodynamic dependence for the density (eq. 3.5b). Our calculation assume a Boussinesq adiabatic thermal dependence.

$$\text{Eq. 3.1} \quad \rho_{eff} g_i + \frac{\partial \sigma_{ij}}{\partial x_j} = \rho_i \frac{\partial V_i}{\partial t}$$

$$\text{Eq. 3.2} \quad \frac{D\sigma}{Dt} = F(\sigma, \mathbf{u}, \mathbf{V}, \nabla \mathbf{V}, \dots, T, \dots)$$

$$3.2a \quad \text{Elastic:} \quad \sigma_{ij} = \lambda \cdot \delta_{ij} \cdot \sum_k \varepsilon_{kk} + 2\mu \varepsilon_{ij}$$

$$3.2b \quad \text{Plastic:} \quad \tau = (\tan \varphi) \cdot \sigma_n + C_0$$

$$3.2c \quad \text{Viscous:} \quad \tau_{ij} = 2 \cdot \eta_{eff} \cdot \dot{\varepsilon}_{ij}^d$$

$$\eta_{eff} = \dot{\varepsilon}_{II}^{d(1-n)/n} \cdot (A)^{-1/n} \cdot \exp\left(\frac{H}{nRT}\right)$$

$$\dot{\varepsilon}_{II}^d = \left(Inv_{II}(\dot{\varepsilon}_{ij}^d)\right)^{1/2}$$

(the maximum effective deformation)

$$n \text{ and } A^* = \frac{1}{2} \cdot A \cdot 3^{(n+1)/2}$$

(material constants)

$$\text{Eq. 3.3} \quad \frac{\partial T}{\partial t} = \frac{\partial}{\partial x_i} \left(X \frac{\partial T}{\partial x_i} \right) + \frac{H_r}{\rho_{eff} C_p} - V_i \frac{\partial T}{\partial x_i}$$

$$\text{Eq. 3.4} \quad \frac{\partial h}{\partial t} = k_{erosion} \frac{\partial^2 h}{\partial x^2}$$

$$\text{Eq. 3.5a} \quad \rho_{eff} = \rho_0 (1 - \alpha \cdot \Delta T)$$

$$\text{Eq. 3.5b} \quad \rho_{\text{eff}} = \rho(G(P, T))$$

where V is the velocity; σ_{ij} the stress tensor; g the gravity; u the displacement; ρ_{eff} the effective density; ρ_i the initial density; λ and μ the Lamé coefficients; δ_{ij} the Kronecker delta; ϕ the friction angle, C_0 the cohesion factor; H the activation enthalpy; R the gas constant; T the temperature; k_{erosion} the diffusion coefficient for erosion; t the time; α the thermal expansion coefficient; G the Gibbs free energy; $P = 1/3$ of the pressure.

The code is written explicitly and discretises two finite-element grids, both consisting of two triangular elements (Fig. 1). This is done to avoid ‘mesh-locking’ problems (Marti and Cundall, 1982). Due to this numerical setup, the elastically compressible code independently calculates the temperature, gravity and pressure-dependant body-forces. The algorithm also explicitly solves elastic-brittle-ductile properties of the mantle, crust and lithosphere. Brittle and ductile strain localization are calculated, allowing the formation and visualisation of brittle faults and ductile shearzones. A satisfactory deformation of the lithosphere is realized by the free upper surface boundary condition.

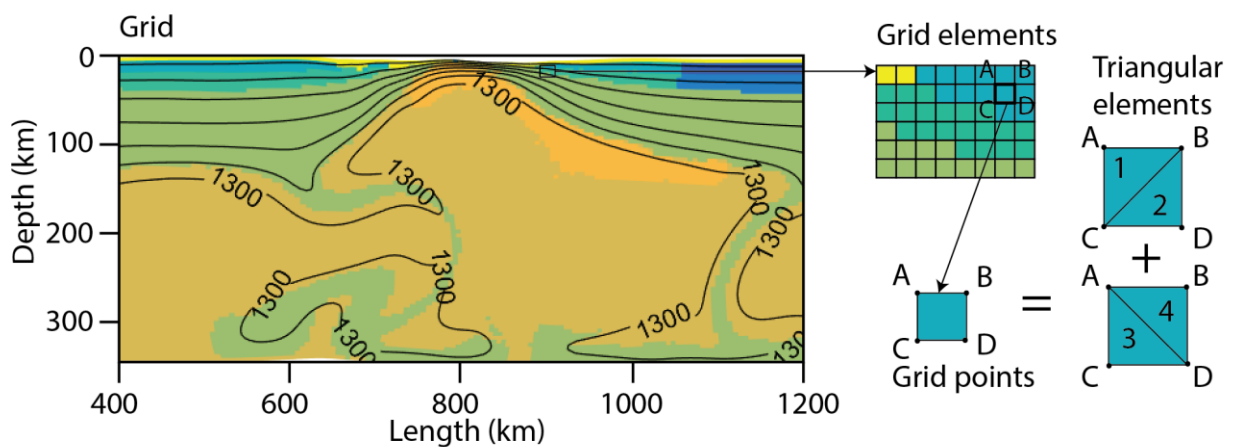


Figure 1. Schematic visualisation of discretisation of the grid. Every grid element consists of four grid points that make up four triangular elements. On the grid points, the velocity, resulting from extensional forces are calculated. The deformation constraints are calculated with the triangular elements, in which markers are placed (Yamato, 2006).

The calculations are using time steps given by the numerical time of the model. After the Courant criteria, the time steps have to be smaller than the time it takes for the slowest physical process to happen. Different calculations need a different times span to propagate from one cell to the next. The algorithm calculates the critical time step for every process occurring in the model (thermal, elastic perturbations etc.). Then it selects a time step that is lower than the lowest critical time it needs for a calculation. On the other side of the duration of a time step the fastest processes are the non-elastic processes, like

viscous and plastic deformation. The maximum time-step for viscous deformation is limited by the time of the viscous-elastic relaxation that needs to be bigger than the time step. Other calculations for other mechanical phenomena like material diffusion and surface processes are also taken into account. As a result, the algorithm will choose a time step that is lower than the shortest critical time-step. To increase the time steps and speed up the calculation, the fastest process needs to be slowed down. The fast process in the model is by far, the speed of propagated, elastic waves through a known medium. By increasing the inertial mass of a near-static system artificially, like geological deformations, the forces of inertia remain negligible (Cundall, 1989). The time for elastic waves to pass through the medium will therefore increase, hence, increasing the time steps.

The PARA(O)VOZ algorithm allows for large scale deformation simulations thanks to the automatic correction of the components of the stress tensor after rotation of the stress axes. Also the automatic procedure for remeshing the grid whenever it gets too distorted, helps in performing large-scale numerical calculations. This remeshing uses a critical angle that cannot be lower than 10° when using the double triangular grids that give a better precision than a single grid. In addition, numerical diffusion due to remeshing is limited due to the use of an interpolation procedure by passive markers, developed by Yamato (2006).

After the theses of Le Pourhiet (2004) and Yamato (2006) and publications that describe the code in full detail (Burov et al., 2001; Burov and Guillou-Frottier, 2005; Burov and Poliakov, 2001).

Appendix II Numerical model I3ELVIS and supplementary material chapter 4

Introduction

This supplementary material provides background information about the modelling procedure including a description of the code, model parameters, setup and a full list of performed experiments. In addition, figures showing the results of the complementary models that test the sensitivity of the model to the variations of such parameters as grid cell size, initial temperature at Moho interface, plume radius and temperature, and geometries of lithospheric mantle are also included. Lastly, viscosity, temperature and strain rate plots are added to accompany Fig. 2 of the main text, highlighting the evolution of these parameters over time.

Supplementary material 2.1.

Numerical methods

1.1. Governing equations.

The 2D version of thermo-mechanical coupled numerical code I3ELVIS (Gerya, 2010; Gerya and Yuen, 2007) is used to solve momentum, continuity and heat conservation equations in the Eulerian frame. The physical properties are transported by Lagrangian markers that move according to the velocity field interpolated from the fixed grid. The multitudinous markers are initially distributed on a fine regular marker mesh with a small ($\leq 1/2$ of marker grid distance) random displacement (see Gerya and Yuen (2007) for more detail).

The momentum equations are solved in the form of Stokes flow approximation:

$$\begin{aligned} \frac{\partial \sigma'_{xx}}{\partial x} + \frac{\partial \sigma'_{xy}}{\partial y} &= \frac{\partial P}{\partial x}, \\ \frac{\partial \sigma'_{yx}}{\partial x} + \frac{\partial \sigma'_{yy}}{\partial y} &= \frac{\partial P}{\partial y} - g\rho, \end{aligned} \quad (1)$$

where σ'_{ij} are the components of the viscous deviatoric stress tensor, ρ is the density (supplementary table 2.1) dependent on rock composition, temperature (T) and pressure (P), and g is the acceleration due to gravity.

Conservation of mass is approximated by the continuity equation, as follows:

$$\frac{\partial V_x}{\partial x} + \frac{\partial V_y}{\partial y} = 0, \quad (2)$$

where V_x and V_y are the components of velocity vector.

The components of the deviatoric stress tensor are calculated using the viscous constitutive relationship between stress and strain rate for a compressible fluid:

$$\sigma'_{ij} = 2\eta\dot{\epsilon}_{ij}, \quad (3)$$

where $\dot{\epsilon}_{ij}$ are the components of strain rate tensor:

$$\dot{\epsilon}_{ij} = 1/2 \left(\frac{\partial V_i}{\partial x_j} + \frac{\partial V_j}{\partial x_i} \right). \quad (4)$$

The model uses non-Newtonian visco-plastic rheologies where the viscosity for dislocation creep is defined, as follow [Ranalli, 1995]:

$$\eta = 1/2 \left(A_D \exp \left(\frac{E+PV}{RT} \right) \right)^{\frac{1}{n}} \dot{\epsilon}_{II}^{\frac{1-n}{n}}, \quad (5)$$

where T is temperature, $\dot{\epsilon}_{II} = \sqrt{1/2 \dot{\epsilon}_{ij} \dot{\epsilon}_{ij}}$ is the second invariant of the strain rate tensor and A_D, E, V, n and R are the material constant, the activation energy, the activation volume, the stress exponent and the gas constant respectively (supplementary table 1).

Plasticity is implemented using the Drucker-Prager yield criterion (Ranalli, 1995):

$$\sigma_{yield} = C + P \sin(\varphi), \quad (6)$$

where C and φ the residual rock strength and the internal frictional angle respectively that depend on the total plastic strain:

$$C = C_0, \quad \epsilon < \epsilon_0,$$

$$C = C_1, \quad \epsilon > \epsilon_1,$$

$$C = C_0 + (C_1 - C_0) \frac{\epsilon - \epsilon_0}{\epsilon_1 - \epsilon_0}, \quad \epsilon_0 < \epsilon < \epsilon_1, \quad (7)$$

$$\sin(\varphi) = b_0, \quad \epsilon < \epsilon_0,$$

$$\sin(\varphi) = b_1, \quad \epsilon > \epsilon_1,$$

$$\sin(\varphi) = b_0 + (b_1 - b_0) \frac{\epsilon - \epsilon_0}{\epsilon_1 - \epsilon_0}, \quad \epsilon_0 < \epsilon < \epsilon_1, \quad (8)$$

where ϵ is the second invariant of plastic strain and $C_0, C_1, b_0, b_1, \epsilon_0$ and ϵ_1 are plastic strain softening parameters (supplementary table 1).

The mechanical equations are coupled with heat conservation equations:

$$\rho C_p \left(\frac{\partial T}{\partial t} \right) = - \frac{\partial q_x}{\partial x} - \frac{\partial q_y}{\partial y} + H_r + H_a + H_s,$$

$$q_x = -k \frac{\partial T}{\partial x}, \quad (7)$$

$$q_y = -k \frac{\partial T}{\partial y},$$

where C_p is the heat capacity; k is the thermal conductivity, H_r is the radiogenic heat production and H_a and H_s are the contributions due to isothermal (de)compression (i.e., adiabatic heating/cooling) and the shear heating, respectively.

Partial melting is introduced using the most common parameterization of hydrous mantle melting processes. Melt is assumed to be transported together with the mineral matrix. Thermo-mechanical effects of melt percolation through the matrix are neglected. The effect of latent heating is included implicitly by increasing the effective heat capacity (C_{Peff}) and thermal expansion (α_{eff}) of the melting/crystallizing rocks:

$$C_{Peff} = C_p + H_L \left(\frac{\partial M}{\partial T} \right)_{P=const}, \quad (8)$$

$$\alpha_{eff} = \alpha + \rho \frac{H_L}{T} H_L \left(\frac{\partial M}{\partial T} \right)_{T=const} \quad (9)$$

where H_L is the latent heat of melting of rock (supplementary table 1) and M is volumetric degree of melting.

Mineralogical phase changes have been taken into account by thermodynamic solution for density, $\rho = f(P, T)$ obtained from optimization of Gibbs free energy for a typical mineralogical composition of the mantle, plume and lithosphere material (Connolly, 2005). For crustal rocks a simple Boussinesq approximation has been used since phase transformations in these rocks are of minor importance for the geodynamic settings explored here.

Full details of used here method, allowing for its reproduction, are provided in *Gerya* [2010].

1.2. 2D model design: Spatial dimensions and resolution

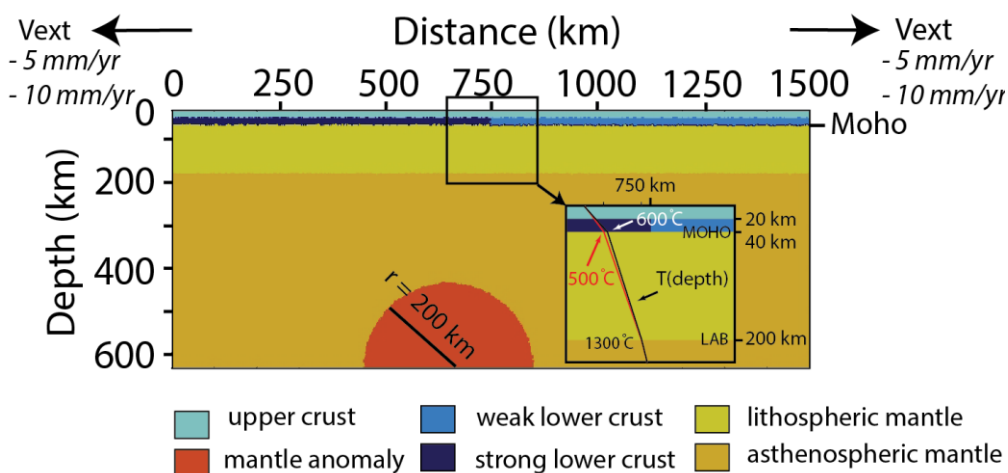
The regular rectangular model box used in this study consists of 297×133 nodes that corresponds to dimensions of 1500×635 km and offers spatial resolution of ca. 5×5 km per grid cell (supplementary Fig. 1.1). At each time step, the code advects about five million Lagrangian markers and solves a system of algebraic equations that comprises more than one million degree of freedom. The total model time of experiments varies between 5 and 25 Myr, representing 10,000 time steps in average. Simulations were run on a SGI shared (NUMA) fat-node cluster with 2.8 Ghz Intel Xeon CPU cores.

We have performed numerical resolution test for the “best-fit” model 7 to assess the robustness of our results. The results presented on supplementary Fig. 4.1 (model 28) show that a notable increase

in the resolution (up to 2.5 km per grid cell) does not change considerably the main features of the system evolution - compare “high-resolution” experiment 28 (supplementary Fig. 4.1b) with “normal-resolution” case of the model 7 (supplementary Fig. 4.1a). We conclude that a development of multi-branch rift system is a robust model feature appearing independently of the size of the grid cell. Therefore, the grid resolution of 5 km adopted in presented experiments is optimal and its further increasing does not change significantly our principal findings.

The free surface topography is reproduced using the ‘sticky air’ technique enhanced by the introduction of a high-density marker distribution in the upper part of the model domain. The viscosity of this 30 km-thick ‘sticky air’ layer added on the top of the upper crust is 10^{18} Pa s and the density is 1 kg/m^3 , according to previously derived optimal parameters.

Further information on model structure, initial temperature distribution and boundary conditions can be found in the main text of the manuscript.



Supplementary figure 1.1. Numerical model setup. Three-layered lithosphere with a weak crustal rheology on the right side of the box and a strong crustal rheology on the left side of the box. The mantle anomaly has a 200 kilometer radius. Extension velocities (V_{ext}) are 5 mm/yr or 10 mm/yr. The Moho temperature is 600°C or 500°C .

Supplementary material 2.2.

Supplementary table 2.1. Rheological and material properties.

Material	ρ_0 (kg/m ³)	Rheological parameters										Thermal parameters			
		Flow law	Ductile			Brittle			k (W/(m×K))	H_r (μ W/ m ³)	H_L (kJ/kg)				
			E kJ/mol	n	A_D (Pa ⁿ × s)	V J/(MPa × mol)	C (MPa)	$\sin(\phi)$				ε			
Upper crust	2750	Wet quartzite (WetQz)	154	2.3	1.97×10^{17}	0	C_0 10	C_1 3	b_0 0.6	b_1 0.3	ε_0 0.0	ε_1 0.25	$0.64 + 807 / (T + 77)$	2.00	300
Lower crust	2950	Wet quartzite (WetQz)	154	2.3	1.97×10^{17}	0	10	3	0.6	0.3	0.0	0.25	-//-	1.00	300
	3000	Plagioclase (An75)	238	3.2	4.80×10^{22}	0	10	3	0.6	0.3	0.0	0.25	$1.18 + 474 / (T + 77)$	0.25	380
Lithosphere- sub-lithosphere mantle	3300	Dry olivine	532	3.5	3.98×10^{16}	1.6	10	3	0.6	0.3	0.0	0.25	$0.73 + 1293 / (T + 77)$	0.022	380
Plume mantle	3200	Wet olivine	470	4.0	5.01×10^{20}	1.6	3	3	0.1	0.0	0.0	0.25	-//-	0.024	300
Reference*	1,2												6	1	1,2

Rheological and material property parameters, where ρ_0 is reference density (at $P_0 = 0.1$ MPa and $T_0 = 298$ K), E is activation energy, n is power law exponent, A_D is material constant, V is activation volume, C is cohesion, φ is friction angle, ε is strain, C_0 , C_1 are maximal and minimal cohesion (linear softening law), b_0 , b_1 are maximal and minimal sines of frictional angle (linear softening law), ε_0 , ε_1 are minimal and maximal strains (linear softening law), k is thermal conductivity, H_r is radiogenic heat production, H_L is the latent heat of melting of rock.

*1 – Turcotte and Schubert (2002); 2 – Bittner and Schmeling (1995); 3 – Ranalli (1995); 4 – Kohlstedt et al. (1995); 5 – (Burov, 2011); 6 – Clauser et al. (1995).

**Mantle densities, thermal expansion, adiabatic compressibility, and heat capacity are computed as function of pressure and temperature in accord with a thermodynamic petrology model *Perple_X* by Connolly (2005). For the crustal rocks we used simple Boussinesq approximation

$\rho = \rho_0 [1 - \alpha(T - T_0)] [1 + \beta(P - P_0)]$, where $\alpha = 3 \times 10^{-5} \text{ K}^{-1}$ is thermal expansion coefficient, $\beta = 1 \times 10^{-3} \text{ Mpa}^{-1}$ is adiabatic compressibility

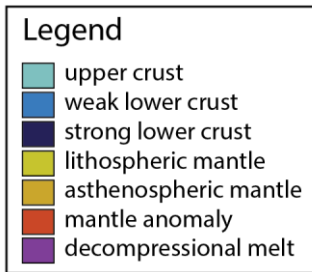
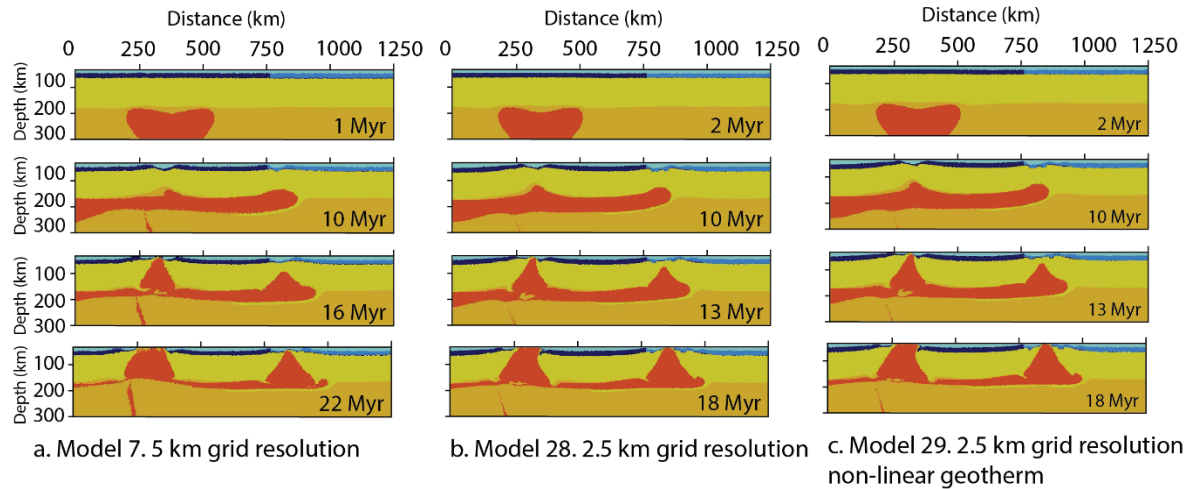
Exp. Nr.	Variable Parameters			Results
	Location plume	Moho Temp (C)	Ext. rate (mm/yr)	Break-up mode
1	0	500	10	structural inherited
2	100	500	10	structural inherited
3	200	500	10	structural inherited
4	250	500	10	structural inherited
5	300	500	10	structural inherited
6	350	500	10	two branches (left first)
7	375	500	10	two branches (right first)
8	400	500	10	plume-centred
9	450	500	10	plume-centred
10	0	600	10	structural inherited
11	100	600	10	structural inherited
12	200	600	10	structural inherited
13	250	600	10	structural inherited
14	300	600	10	two branches
15	350	600	10	plume-centred
16	375	600	10	plume-centred
17	400	600	10	plume-centred
18	450	600	10	plume-centred
19	0	500	5	structural inherited
20	100	500	5	structural inherited
21	200	500	5	structural inherited
22	250	500	5	structural inherited
23	300	500	5	structural inherited
24	350	500	5	structural inherited
25	375	500	5	structural inherited
26	400	500	5	structural inherited
27	450	500	5	structural inherited

Supplementary table 3.1. Key variable parameters and break-up modes of main model series

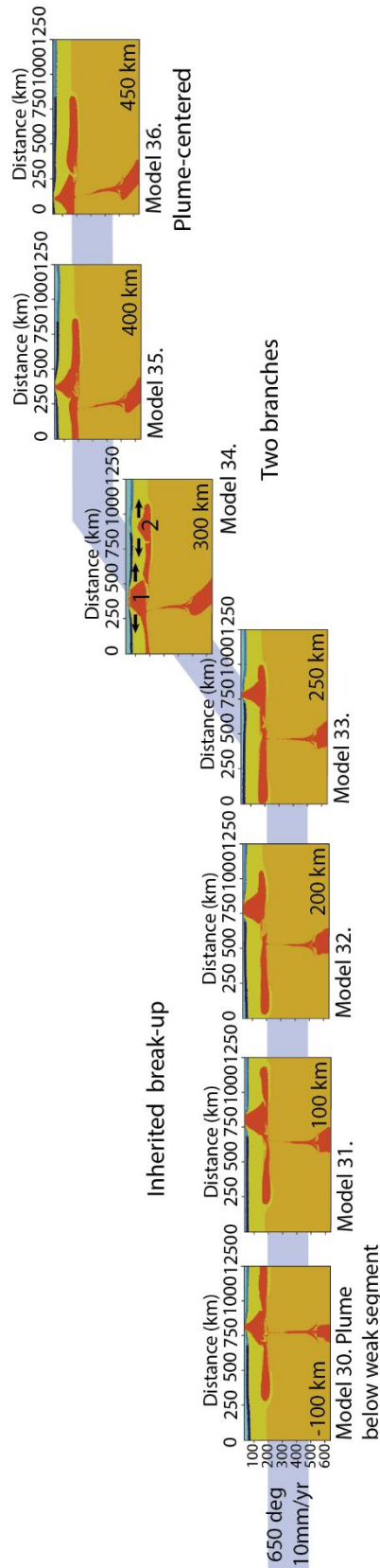
Supplementary table 3.2. Key variable parameters and break-up modes of supplementary model series

Exp. Nr.	Parameters							Results	
	Plume location (km)	Moho temp (°C)	Crustal geotherm	Ext. rate (mm/yr)	Grid cell size (km)	Plume radius (km)	Plume temp. (°C)		Structure of lithosphere mantle
28	375	500	linear	10	2,5	200	2000	homogeneous	two branches
29	375	500	non-linear	10	2,5	200	2000	homogeneous	two branches
30	-100	650	linear	10	5	200	2000	homogeneous	plume-centered
31	100	650	linear	10	5	200	2000	homogeneous	structural inherited
32	200	650	linear	10	5	200	2000	homogeneous	structural inherited
33	250	650	linear	10	5	200	2000	homogeneous	structural inherited
34	300	650	linear	10	5	200	2000	homogeneous	two branches
35	400	650	linear	10	5	200	2000	homogeneous	plume-centered
36	450	650	linear	10	5	200	2000	homogeneous	plume-centered
37	375	500	linear	10	5	250	2000	homogeneous	plume-centered
38	375	500	linear	10	5	300	2000	homogeneous	structural inherited
39	100	600	linear	10	5	200	1900	homogeneous	structural inherited
40	200	600	linear	10	5	200	1900	homogeneous	structural inherited
41	300	600	linear	10	5	200	1900	homogeneous	structural inherited
42	375	500	linear	10	5	200	1900	homogeneous	structural inherited <i>passive regime</i>
43	100	500	linear	10	5	200	2000	heterogeneous: vertical contact	structural inherited
44	300	500	linear	10	5	200	2000	heterogeneous: vertical contact	structural inherited
45	350	500	linear	10	5	200	2000	heterogeneous: vertical contact	structural inherited
46	300	500	linear	10	5	200	2000	heterogeneous: slope contact	structural inherited

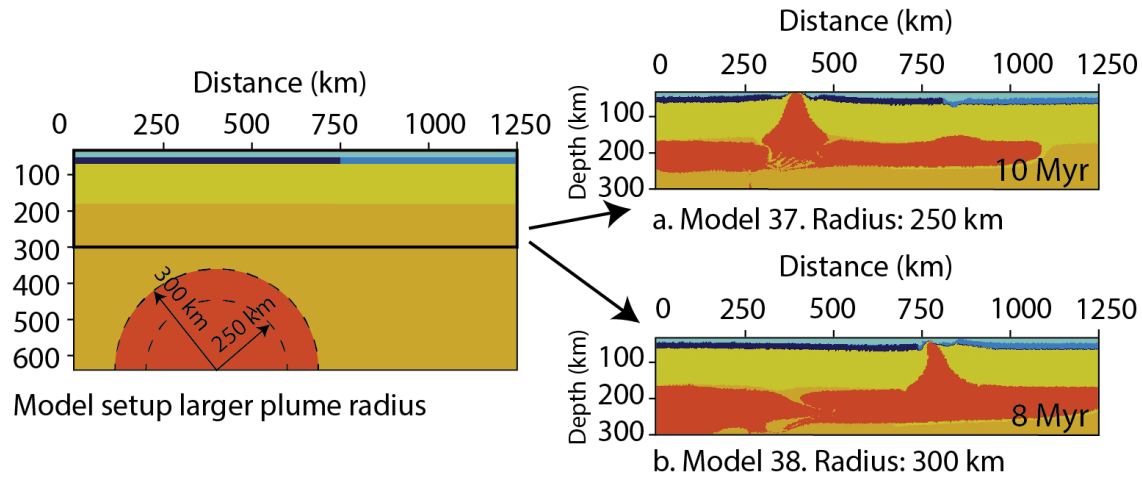
Supplementary material 2.4.



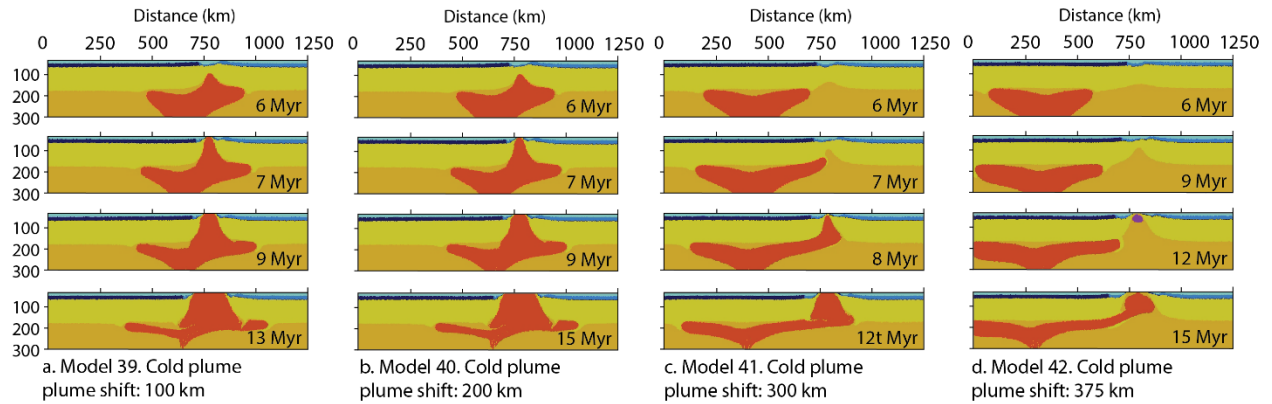
Supplementary figure 4.1. Our “best fit” experiment of the main model series (model 7 (a); 5 km per grid cell) is compared with complementary models 28 (b) and 29 (c) with a higher resolution grid (2.5 km per grid cell). Model 29 has a non-linear crustal geotherm that takes into account radiogenic heat production (supplementary table 2.1). Independent of the grid cell size and the type of crustal geotherm all three models show a similar system evolution resulting in ‘two-branch’ break-up mode.



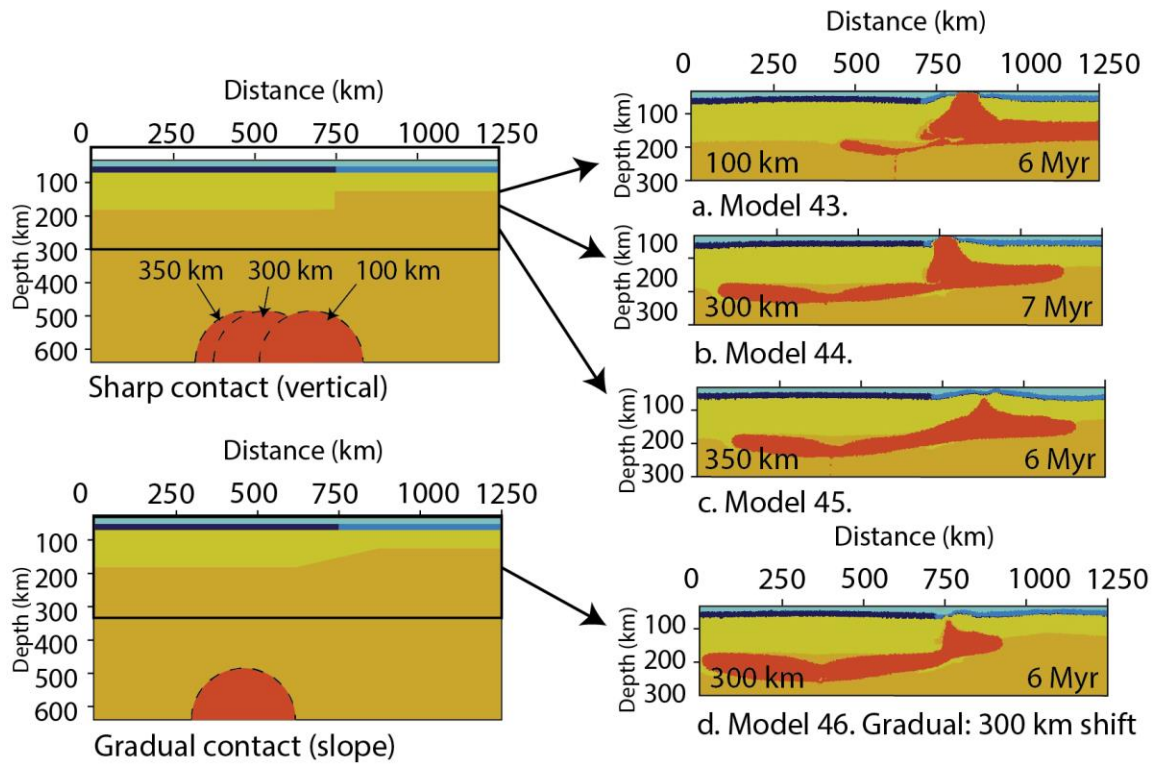
Supplementary figure 4.2. Graph showing the results of the complementary models with a warmer Moho temperature of 650 °C and extension rate of 10 mm/yr (models 30-36). The results are very similar to that of the models 10-18 (Fig. 3b, main text) with the same far-field extension rate and a lower Moho temperature (600 °C). The critical distance between the plume location and the lithosphere inhomogeneity for which a two-branch system develops is again around 300 km (model 34). Model 30 has a shift of 100 km towards the weak segment and in this case, the system expectedly evolves according to “plume-centred” break-up mode, despite close distance between mantle plume and pre-defined zone of rheological contact.



Supplementary figure 4.3. Complementary models 37 (a) and 38 (b) testing the impact of the size of the mantle anomaly. A slightly bigger plume radius (250 km instead of 200 km used in the main model series) expectedly leads to more profound penetration of hot plume material into lithosphere thus favoring “plume-induced” break-up. In contrast, further increasing the mantle plume’s size (300 km-radius) results in long-distance lateral spreading of plume material at the base of the lithosphere leading to “structural inherited” break-up.



Supplementary figure 4.4. Complementary models 39 – 42 (a-d) with relatively cold mantle anomaly (1900 °C instead of 2000 °C used in the main model series) at several locations below the stronger lithospheric segment. In all models, the break-up mode is “structural inherited”. Only in model 42, continental break-up occurs in a quasi-passive regime without direct implication of the mantle anomaly due to lithospheric thinning and associated decompressional melting. Plume material arrives at the break-up centre only at a later stage when oceanic spreading has already been established. Similar system behavior is presented in the models by Lavecchia et al. [2017]. In contrast, when the plume is located closer to zone of “structural inherited” deformation (shift of 100 and 200 km; models 39 and 40, respectively), break-up occurs in the “plume-induced” way, typical for our study. Model 41 demonstrate intermediate behavior: “structural inherited” lithospheric thinning starts in “passive” regime (i.e. without direct implication of the mantle plume), but final break-up stage is achieved in the presence of the plume material.

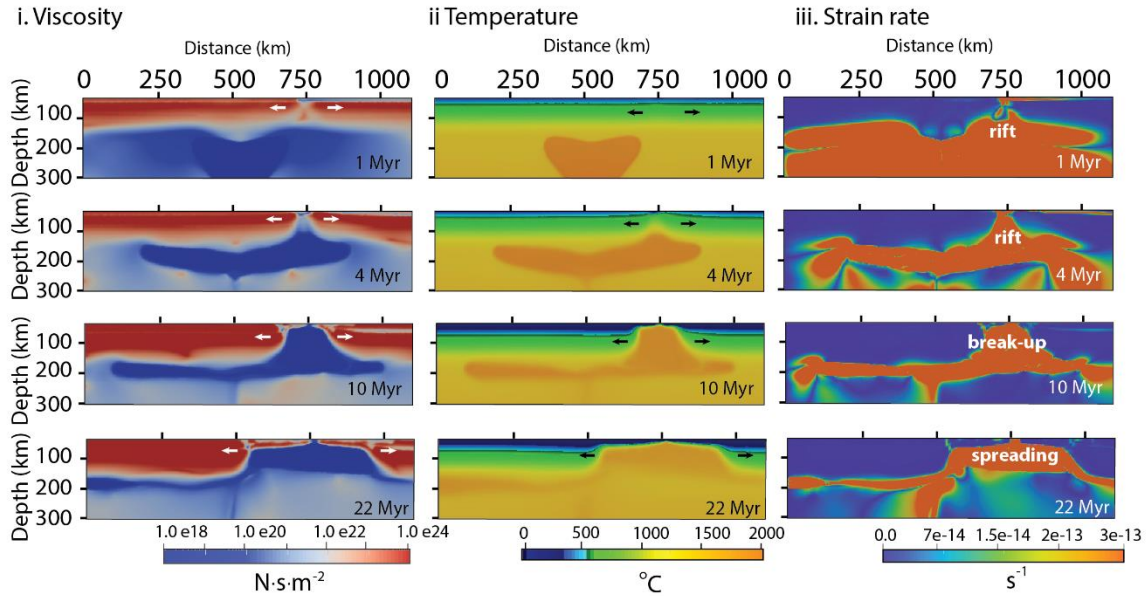


Supplementary figure 4.5. Complementary models with more complex initial geometries: lithospheric thickness within the “stronger” segment is 150 km whereas it is only 100 km in the “weaker” one. The contact between the two segments is either sharp (or vertical, models 43-45 (a-c)) or gradual (with a slope, model 46 (d)). All models result in “structural inherited” break-up regardless of the plume position or the type of transitional zone.

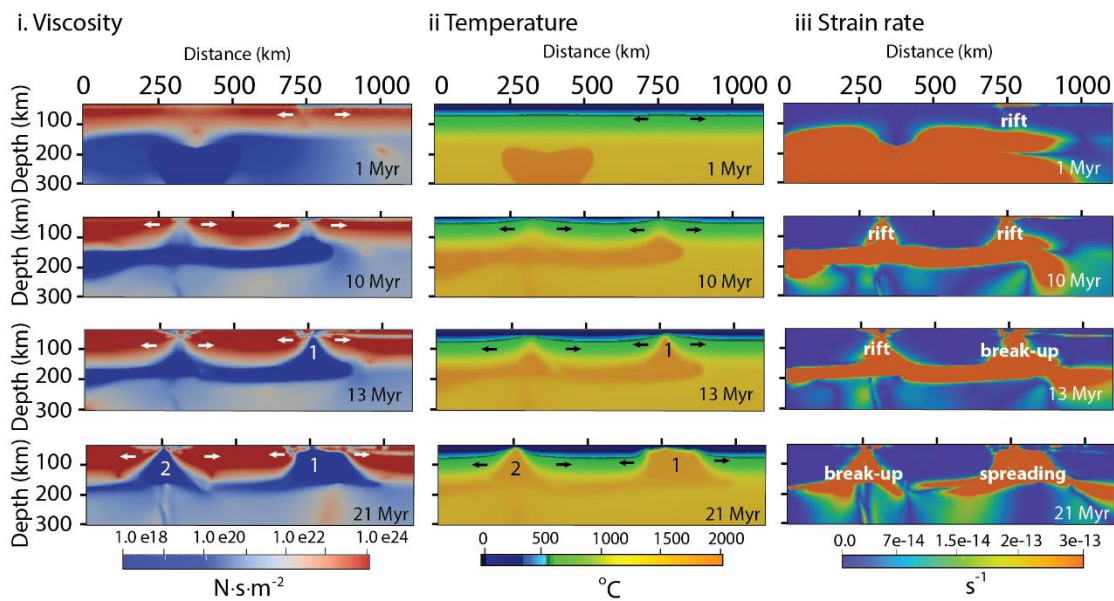
Supplementary material 2.5.

Supplementary figure 5.1. The images display the viscosity, temperature and strain plots of the experiments shown in Fig. 2: a) model 3; b) model 6; c) model 7; d) model 8. See “Experimental results” of the main text for more details.

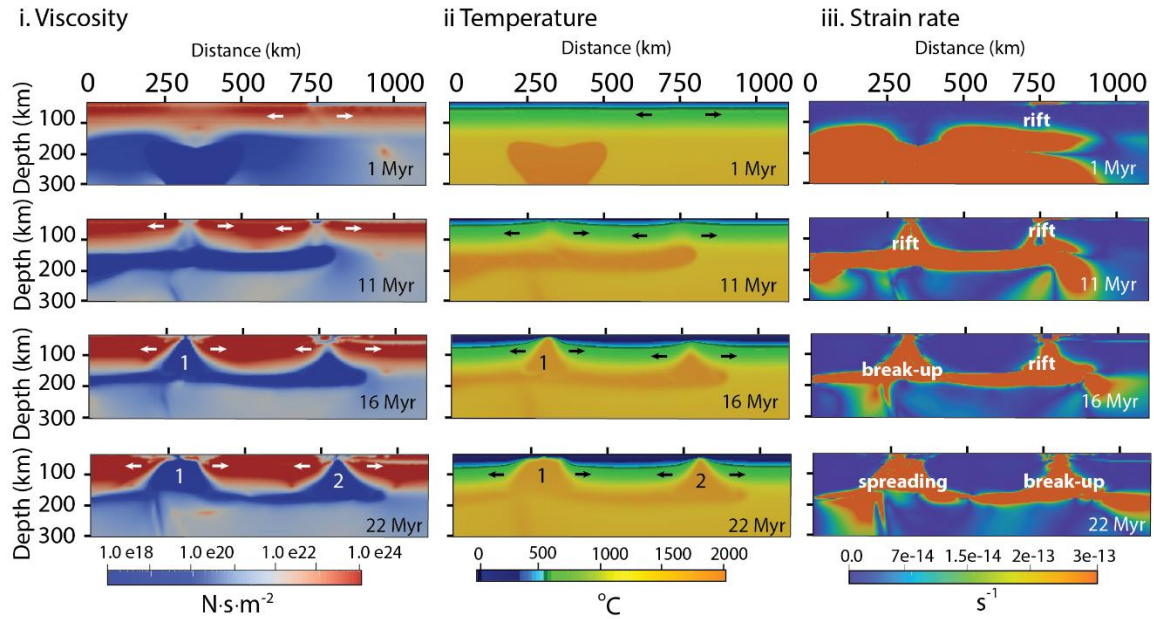
a. Model 4. 200 km displacement



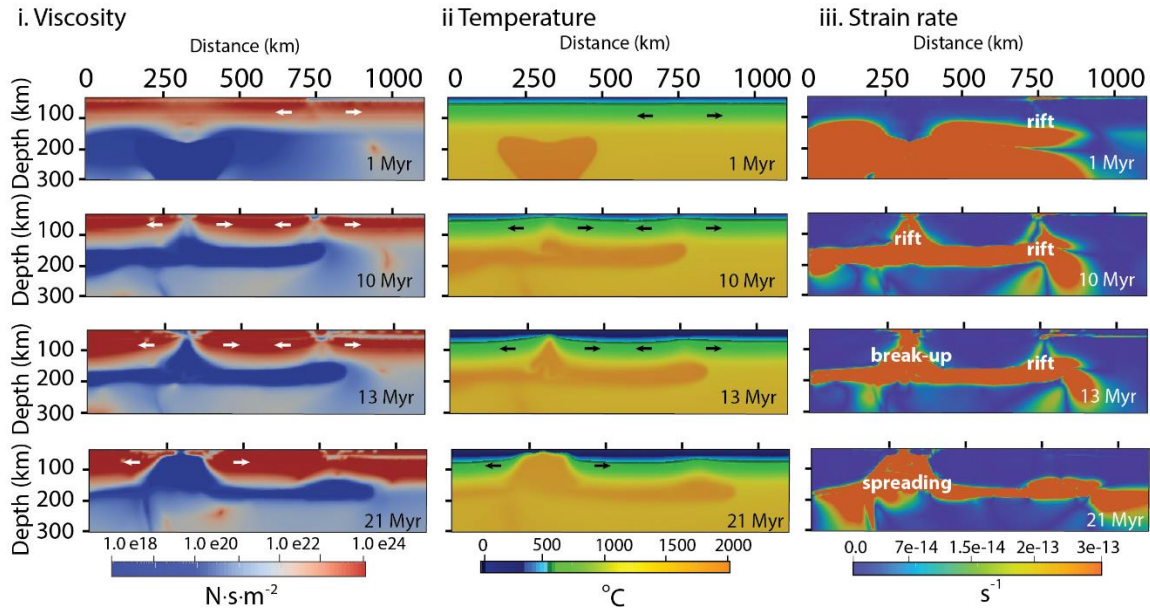
b. Model 6. 350 km displacement



c. Model 7 375 km displacement



d. Model 8. 400 km displacement



Appendix III Report scientific cruise INGON

Polar research on the equator: tracking India's escape from Antarctica by ship

GPS location: 0° 000,000' S; 81° 000,000' E

By Anouk Beniest

Published as blogpost on: www.travellinggeology.com

A warm, blue ocean stretches as far as the eye can see in all directions. The water is over 4000 meters deep, too deep for swimming. The weather is calm now, even for monsoon times, which is a good thing because I can adapt easily to the ocean's motions. I am standing on the Monkey Island of a German research vessel, Sonne. The vessel left from the harbour of Colombo, Sri Lanka, and traces the 81° E longitude southwards. The empty quarter of the Indian Ocean lies right in front of me. The southern-most point of this trip is 11° 30' S. The cruise will take me back and forth between the northern and southern hemispheres several times. On the other side of the ocean lies Antarctica that was once connected to India and Sri Lanka. The aim of the cruise is to understand more about the break-up history of Antarctica and so we trace back how India fled from Antarctica by gathering all types of geophysical data. As soon as we pass the nautical highway in front of Colombo deployment of the first equipment begins. The first acquisition instruments that need to be put into place are the magnetometer and the hydro-acoustic equipment.



Photo 1. Deploying the magnetometer. A magnetometer measures the intensity of the magnetic particles in the rocks. Whenever there is a change in intensity, we have found an anomaly. There is a variety of reasons for magnetic anomalies to exist. They could be due to crustal features such as faults, or as a result of a change in chemical composition, for example an elevated amount of magnetite. Here, we are interested in the magnetic minerals in the oceanic crust that have captured polarity changes of the Earth's magnetic field. (Photo by Konrad Behnke, 2017)

While the magnetometer is recording and the hydro acoustic equipment produces high-frequency beeps, the ship is heading further south. We reach the equator and the weather is about to change. I am standing again on the Monkey Island, the highest deck on the ship where scientists are allowed to come. Dark clouds are rolling in and the wind is blowing so strong that I have the impression my eyelashes are blowing away. Despite the dark sky, the ocean still has its dark blue colour and suddenly a group of spinner dolphins turns up out of nowhere. There at least 30 of them as they jump out of the water, doing little tricks.



Photo 2. Spinner dolphins speeding our way. There are three marine mammal observers on board. During day-time they watch for whales, dolphins, turtles and other wildlife. Once the airguns are working for seismic data acquisition, the observers have to watch that no marine mammal comes too close to the vessel as it might damage their hearing and the orientation. Once a marine mammal is observed, a shutdown of the airguns is being requested by the observers until the animals are gone. (Photo by Marcus Bridge, 2017)

Clouds are covering the sky now and the waves have reached heights of over 5 meters. When on deck, the waves sometimes reach above me, which is very impressive. In the eating room the salt and pepper has been removed from the table as they wouldn't stand straight anymore. In the lab everything rolls from left and right and front to back. It is time to learn some knots and secure all the equipment. The storm remains for a couple of days but there is no time to lose and so I prepare my first Ocean Bottom Seismometer (OBS) station while the ship is dancing with the waves. While I am testing my balancing skills I somehow manage to attach the different OBS equipment items to the brightly coloured floating devices. From time to time a wave floods the deck, making the whole scene quite dynamic. My fellow scientist colleagues prepare the streamer and the airguns. The OBS stations and streamer will be deployed as soon as the longest magnetic profile is finished.



Photo 3. Preparing the OBS stations on deck. Releaser, flash light, radio beacon, pressure tube, hydrophone and geophone are all attached to the floating device that is again attached to an anchor, before deployment. (Photo by Mareen Lösing, 2017)

When the first OBS station, #301, is being assigned to the ocean bottom, all hands are on deck. Everybody is curious about the deployment procedure. To me, it is completely alien to throw heavily coloured equipment overboard and hope that they will surface again, but apparently this works. For two days and two nights I work my shifts to deploy all the stations. In the early morning of the second night, the last station is thrown into ocean. We watch a beautiful sunrise and treat ourselves on a well-earned cold drink. Then I go back to my cabin and dream about oceans full of floating OBS stations.

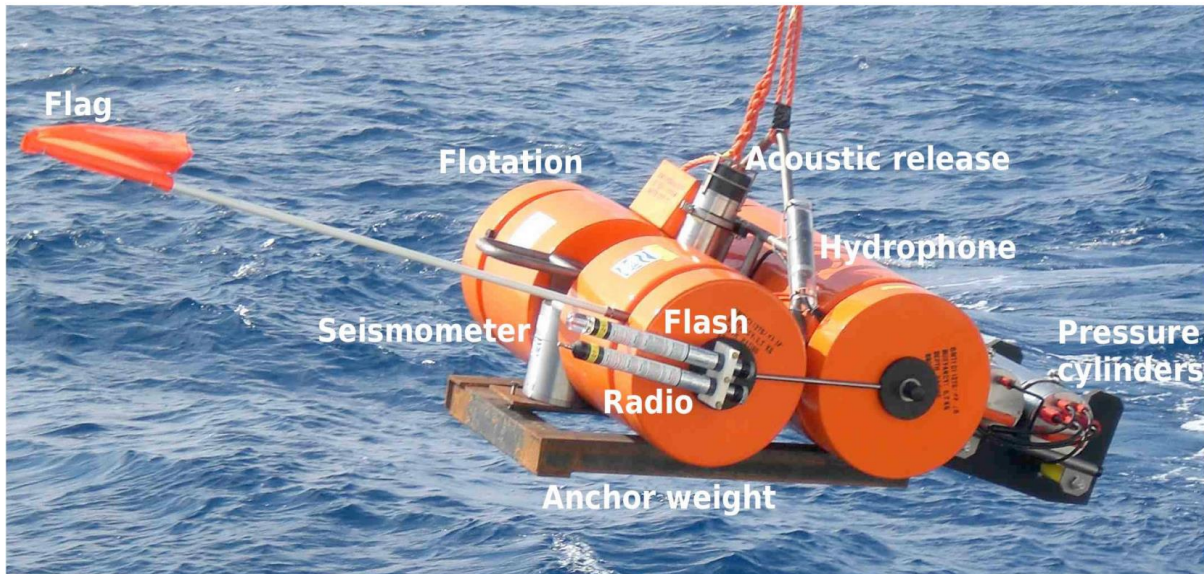


Photo 4. An OBS system consists of many parts. First, a recording system is needed inside a pressure tube. For this cruise, it needs to hold pressures up to 4500 m depth, the maximum depth we expect for this cruise. The recorder records hydrostatic pressure changes with a hydrophone and records refracted and reflected seismic waves through a geophone or seismometer. These are all attached to a floating device that should bring the whole system back up after the seismic profile has been shot. To bring the system down, the OBS is attached to an anchor with a releaser. A releaser is the only connection between the OBS and the anchor and replies to high-frequency sounds as sound is the only way to communicate through water. When the correct frequency is heard by the releaser, it will let go of the anchor and the OBS makes its way back to the surface. (Photo by Tabea Altenbernd, 2017)



Photo 5. Deploying OBS stations. Every 12-15 kilometres an OBS station is thrown overboard. With the anchor positioned correctly, they should reach the bottom in little time. It is important that the anchor sinks well into the sediments, because only then will the geophone record the refracted and reflected waves produced by the airguns. (Photo by Menaka Goonewardena, 2017)

The morning shift deploys the airguns into the water. It is quite a violent business as they are very heavy and bump against the back of the boat. The first seismic profile runs north-south and starts on the platform with only 400 meters water depth, close to the continent. It crosses the shelf to the deep ocean with roughly 4500 meters water depth. The shelf is the perfect area for marine wildlife and so the whale watchers have an intensive look-out to make sure no sea mammals are in the vicinity of the ship before the soft-start of the airguns begins. The shelf is also the perfect place to investigate how India broke apart from Antarctica as it records the whole break-up to spreading history.

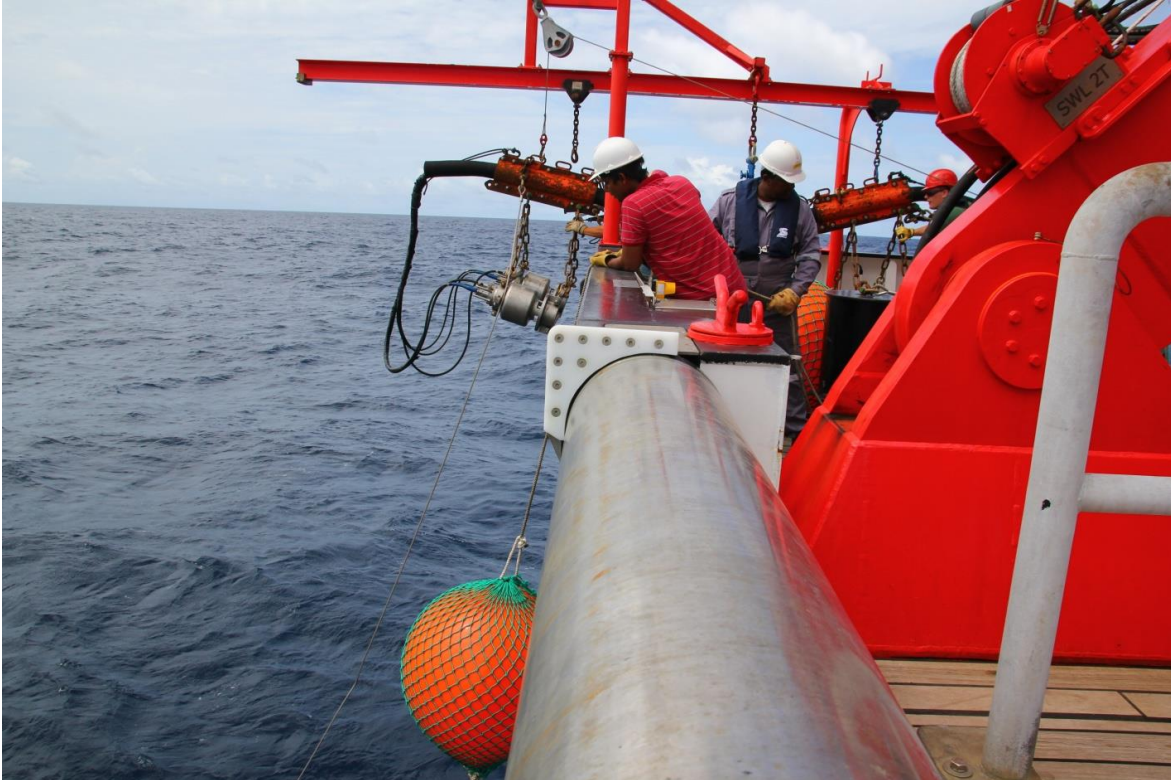


Photo 6. Deployment of the airguns. The seismic installation has 8 airguns, 4 on each side. They are programmed to release high air pressure every minute. Air-pressure will rise to 200 bar before discharging. This produces a seismic signal that the geophones and hydrophones can record. The orange balloons are connected to the airguns so they remain close to the surface and to show where they are located in the water. (Photo by Konrad Behnke, 2017)

The scientific team counts 26 people and during the data acquisition there are 4 hour watches day and night. Per watch, three people take care of quality control and airgun performance. In the meantime, we also prepare OBS recovery and the next seismic profile. But it's not only work on the ship. There is some free time on board. For the sportive ones there is a gym, a table tennis table and a football table. There is also a library and a large television screen to watch movies. Even a sauna is installed complete with relaxing chairs on the sun deck. Every now and then there are events such as seminars given by the scientists, poker evenings, movie nights and birthday parties. Everybody is invited, both crew and scientists.



Photo 7. Football table competition during OBS deployment. It takes roughly one hour between the OBS drop-off locations and so we try the football table to kill some time (Photo by Konrad Behnke, 2017)

With five knots per hour, the vessel sails along the profile. At the end, it makes a turn and the recovery of the OBS stations starts. The whole OBS team is restless. Will the releaser pick up the signal and let go of the anchor? We wait for a long time, but then the bridge relieves us from our worries, the radio picked up a signal! The OBS station surfaced! The watchman has already spotted the device and the vessel heads towards the yellow, floating unit. On the deck the crew-members are ready to rescue the OBS station from the water using hooks and ropes. The recovery also continues night and day. My cabin is located on the second deck, close to the surface of the sea. I have bull's eye windows and during the night I can see the OBS stations flashing by.



Photo 8. OBS recovery. The OBS rises with 0.9 m/s to the surface. With a depth of over 4300 meters, the ascent takes roughly 80 minutes. When there are strong currents, heavy waves or bad weather they are not so easy to spot. Luckily the OBS station is equipped with a radio beacon and when they reach the surface the radio picks up the signal. They also have a flash light so it can be easily spotted at night (Photo by Mareen Lösing, 2017)

The recovery is going according to plan. OBS after OBS surfaces and gets safely back on the deck. The ocean remains blue and wavy. There is not much to disturb that few. Every now and then a lonely fisherman's boat passes the ship, but other than it is quiet empty on this side of the world. The weeks pass by quickly. In total, we measured two seismic lines with OBS's and streamer. We acquire 10 magnetic profiles and cover whatever we have sailed with bathymetry. Processing the data would be the logical next step, but most of this will be done back in our labs. The RV Sonne is used for many different research purposes and so the boat is not permanently equipped with OBS stations or a streamer. Packing all the equipment in containers, so the next cruise starts with a clean ship, is our last task before we get back to harbour of Colombo.



Photo 9. A fisherman boat on the Indian Ocean. Men on boats like these are often at sea for over a month. They only come back ashore when they caught some fish. Sometimes these boats have some places to store fish, but often this is lacking. There is not much luxury on these kinds of boat. (Photo by Marc Hiller, 2017)

The weeks pass by quickly. We shoot two seismic lines with OBS's and streamer. We acquire 8 magnetic profiles and covered the whole sailed ground with bathymetry. What remains is processing the data and packing all the equipment in containers, so the next cruise starts with a clean ship. The main processing will be done back in Germany.

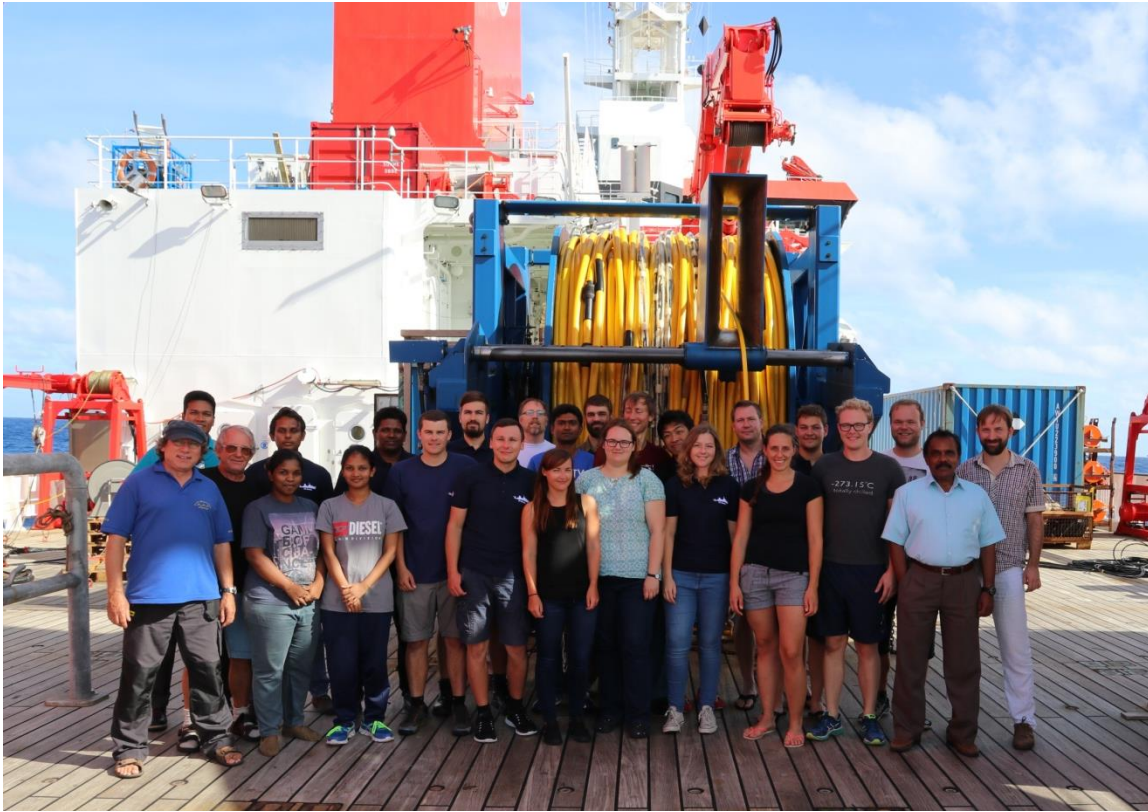


Photo 10. The science party of the INGON cruise Leg 258b. We left Colombo Harbour with the RV Sonne on the 12th of July 2017. The aim of the cruise was to gather more subsurface data along the Sri Lankan continental margin. Once, India and Sri Lanka were attached to Antarctica. The break-up to spreading history is recorded on the margins of the continent and in the oceanic crust. With the magnetic data acquired during this cruise, we investigate the magnetic pattern and thus the age of the oceanic crust and the timing of the spreading history. The OBS stations record both reflected and refracted waves, giving inside in the crustal structure of the margin. Do the margins contain volcanic material? Where does the continental crust change to oceanic crust? The hydro-acoustic data provided information on the ocean floor, which in this case was quite flat except for one deep-sea channel. On the 17th of August 2017 the vessel docked again in the harbour of Colombo. (Photo by Wolfgang Borchert, 2017)

Acknowledgments

The awesome in me bows

To the awesome in you.

~ Adriene Mishler, Actor, Yoga Teacher & Entrepreneur

The most difficult part to write and the most read part of a PhD manuscript are the acknowledgments, or ‘les remerciements’, or ‘het dankwoord’.

Very grateful am I towards two people who helped building the project from the beginning and for various reasons are not around anymore, at the end. *Evgueni, your decease came as a shock, for everyone. During the nine months we worked together, you relied on my independence, but you were always available for questions. I would have loved to learn more from your knowledge, but I am already very grateful for the basics of thermo-mechanical modelling that you gave me and that served me during the rest of my PhD. François, même si vous n'étiez pas officiellement dans l'encadrement de ma thèse, vous aviez toujours eu du temps pour parler de mon projet, merci beaucoup pour la confiance que vous avez toujours eu.*

Next, I have to thank William and Xavier who gave me the chance to start this project and had confidence in me, even though my background was quite different. *William, je vous remercie pour tous les conversations et discussions scientifiques que nous avons eu et qui ont intensifié pendant la dernière phase de la thèse. Xavier, merci pour tes conseils et surtout pour ton regard critique qui a bien aider à avancer les choses.* In the same breath I need to thank Sylvie, who even though she knew she was going to be director of the department, became co-director of my thesis after Evgueni passed away. *Sylvie, j'ai apprécié beaucoup votre efficacité, la communication claire et l'appréciation pour un travail indépendant.*

There is one person to whom I dedicate a whole paragraph. *Alexander, if it wasn't for you, I might not have reached the same scientific level I have today. Your motivation, accuracy, optimism and efficiency were very compatible with my drive to make something out of the model results that I did shortly after Evgueni passed away. We published two very nice papers and I truly hope we will collaborate again in the future. Thank you very much for everything.*

At Utrecht University I got the chance to work in Tectonics lab and translated my numerical models into analogue versions. *Sierd, dankjewel voor je doorzettingsvermogen om mij te overtuigen een beurs voor Parijs aan te vragen na mijn master (in 2013) en dankjewel voor de support op alle fronten gedurende mijn PhD. Ernst and Dimi, thank you very much for giving me the chance to work in the lab and make me understand the nuances of analogue modelling. I also appreciated the smooth communication and the fun we had in the lab and in the snow. Antoine, as of January 2017, you are my favorite Frenchman. Keep your charm, sense of humor and love for life and hopefully we can dance again in the lab one day. Yola, you are the most enthusiastic, optimistic and power-lab assistant I have seen in my life, thank you for that! Also the other colleagues from the TecLab, Liviu, Fred, Jeroen, Taco, Attila, Jon, Eszter, Kristopher, Nevana,*

Katharina, Inge, Derya, Lukman, Esmee, Tessa, Iverna. Thank you all very much for being around, drinking beers and going bouldering. Thanks to you I felt very much at home.

The summer of 2017 I spent on RV Sonne on the Indian Ocean for a scientific campaign on sea. *Wolfram, the intriguing stories about Arctic research you shared with me during a workshop in Monschau, have not disappointed me during the cruise. I am very grateful that you gave me the opportunity and the chance to participate. Tabea, I have a lot of admiration for you as the senior scientist on the ship. You know exactly what to do, you're strong, and no caveman can ever bring you down. Patrick, many thanks for adopting me in your OBS team, I am the happiest 'cheffin' in the world. Andreas, thank you for sharing your adventurous spirit with us, I am sure it will bring you to many more awesome places. Mareen, muchas gracias for your sharp comments and thoughtful thinking. Marc and Max, it was a pleasure to hang around with you, 'your dirty minds, will be a joy forever'. Menaka, many thanks for the funny jokes, good mood and of course inviting us over to your place and meeting your family. Isuri, thank you so much for the interesting conversations we had during the cruise and letting me experience Sri Lanka at your families place. Last but not least, Crew and scientists from the INGON cruise LEG 258b, thank you all very much for this unforgettable experience.*

Over the last three years I met so many wonderful, interesting, powerful and inspiring people, not only during the numerous conferences and workshops, but also closer-by at the UPMC and IFPEN. I would like to thank you all by name, but I am afraid of forgetting people. But hey, that is the risk, so here we go.

Camille, ma biche, merci pour tous les moments qu'on a passé ensemble. Les weekends dans les provinces, les fêtes dans ton jardin, les cafés, les bières, les soirées. Tu m'as fait apprécier la vie française. Reste comme tu es, grande, forte et Parisienne. Gros bisous !

Virginie, tu es une des premières copines françaises, que j'ai rencontrée même bien avant le début de la thèse. Ça m'a fait beaucoup de plaisir de prendre les responsabilités du bureau de l'ADIFP. J'adore ton esprit optimiste et ta gentillesse. Merci beaucoup pour tout!

Rachael, thank you so much for the lunches, thanksgivings, beers in the park and the interesting discussions about world politics, science and society that inevitably happen when we are all together. Thank you for your energy, honesty and openness.

Vasilis, μαλακά, we survived three years in Paris! It was a pleasure to chat with you over a cup of tea (or beer) at the kitchen table whenever I was in Paris. Your laidback and chilled out lifestyle makes you the perfect flat mate and I am very happy you're staying a bit longer. Thanks for all the good moments, Για μας!

Nikos, my soulmate, many thanks for all the late night drinking events at home, in the bar, or along the Seine. Your logical way of thinking makes you the perfect person to discuss difficult situations with. Thank you too for all the good moments!

Alberto, many thanks for being my first office mate at UPMC and introducing me to the parties at la Cité Université. I like your optimism and chilled out attitude. I really hope we stay in touch and get the opportunity to drink a beer in Brazil. Obrigado!

Manfred, Andrew, Leila, Paul, Marianne, Chloé, Aïda, Marine, Emanuel, Alexis, Lorella, Quentin, Marie, Benjamin, Juliana, Ella, Guillaume, Francesca, Pauline, Matthieu, Vincent, Camille, Elodie, Maxim, Io, merci pour tous les déjeunées, petits terrains de l'ED, cafés et soirées à l'Inévitable. Sans vous, l'ISTeP ne serait pas le même.

Aussi un grand merci pour tous les autres collègues de l'UPMC, aux 2ièmes, 3ièmes, 4ièmes et 5ièmes étages, merci à Dovy, Sandrine, Gitane, Marie-José et Philippe pour tous votre aide bureaucratique et informatique. Merci François et Loïc pour tout l'aide avec de l'ED. Merci Christian, pour toujours être là and thank you Bilal for your poetic inspiration.

Erica, Zsuzsanna, Lucas, Julia, Isabelle, Thomas, Omar, Zady, Nicolas, Chahir, Bertrand, Arthur, Thibaut, Raphaëlle, Christopher, Ivana, Chakib, Pauline, Xavier, Mona, Julie, Marion, Kévin, Svetan, Mamady, Martien, Wei, Charlotte, Robin, Michel, Katreine, Stephan, Marianne, Estelle, Sophie, Pauline, Claire, Erica, Esther, Etienne, Pedro, Ana-Sofia, Venkat, Hamza, Ramadan, Antoine and all the other colleagues from IFPE in Laurier and Tilleuls, many thanks for the lunches, coffees, excursions and IFP Trainings ! Un grand merci spécial pour Djaméla, merci pour ta bonne esprit et efficacité !

Paris is a great city, and so I explored and explored and along the way I met even more wonderful, interesting, powerful and inspiring people, often with no relation to my field. You opened my eyes and let me experience a different world. Here's to you.

Inge, Noemie, Dana en Valerie. Mijn lieve, fantastische, gekke, Nederlandse energie bommetjes. Jullie zijn mijn lichtpuntjes in de stad Parijs, ook al zijn jullie allang vertrokken. Nooit zal ik de etentjes in 'Huize colocanation' vergeten, de avonden in Corcoran's, illegale feestjes in Saint-Denis, picknicken langs de Seine of in het park. Jullie zijn altijd welkom, waar ik ook uithang. Jullie zijn pareltjes, stuk voor stuk.

Martha, jouw vrolijke hoofd maakt mijn dag altijd goed! Jouw rationele kijk op de wereld was zo eye-opening de afgelopen vier jaar. Dankjewel voor jouw vrolijkheid, energie en doorzettingsvermogen. Dat er nog vele vakanties, weekendjes en avondjes in Parijs of ergens anders mogen komen.

Jasmijn, jouw energie, optimisme en FOMO maken jou de grootste power-vrouw die ik ken. Dankjewel voor alle fantastische ontspan-weekendjes in Parijs, Marrakesh, Rotterdam en Amsterdam en voor alle keren dat ik bij je kon crashen in Rotterdam, in wat voor toestand ik ook was. You're awesome!

Eva, Amanda and Alison, even though I am the Benjamin of the four of us, I never feel like one. I so much enjoy the little city trips we do every year, the kirrs we drink wherever we go (let it be Paris, or in an emergency situation when there is no chance escaping the island), and the fancy wine bars and pub-crawls we explored in Paris. I truly hope we can do this until we're 80 and then still complain about the good, old times in Paris.

Christa, I am so happy I helped you moving that day from Rueil-Malmaison to Neuilly. For me, that's where it all started. I was captured by your stories and decided you are a really cool, awesome and most of all fun person to hang around with. I truly hope we can make more stories together and that we'll stay friends, even after my time in Paris has run out.

Merel, dankjewel voor de happy-hour borrels, de kopjes thee in de Marrais, de bioscoop, de musea en jouw oprechte interesse in alles waar ik het ook maar over had.

Kattalin, many thanks for the coffees, lunches and beers every now and then and I am happy we stayed in touch! I have always very much appreciated your optimism and positive view on the world.

Eveline, dankjewel voor de motiverende woorden over een carrière in de wetenschap. Jij weet als geen ander hoe het is om daarmee te beginnen en die succesvol op te zetten. Jouw energie, optimisme en doorzettingsvermogen zijn een voorbeeld voor mij.

Leonie, Ina, Jenny et Vicky. Qui aura su qu'en 2017, dix ans après qu'on s'est rencontrée à Nice, on se retrouvait ? On a toujours dit qu'on se revoyait, sans doute. Le weekend de réunion qu'on a fait à Nice était comme à l'époque. Je l'ai adoré. Et de vous recevoir chez moi (et Léonie) à Paris était la cerise sur le gâteau. Même si on ne se voit pas tous les jours, vous restez mes filles de Nice pour toujours.

Dan zijn er natuurlijk nog de meiden van Paris by Bike. Yvonne, dankjewel dat je me in 2015 toch nog hebt aangenomen als gids. Ik heb ontzettend genoten van de tripjes door de stad op de fiets en daarbij ook ontzettend veel geleerd over de stad zelf. Dankjewel voor de gezelligheid, de gekkigheid, de borrels en de vakanties. Britt, Barbara, Rachella, Lisa, Iris, Myron, Anouk en Fenne, dankjulliewel voor jullie vrolijkheid en geklets over van alles en nog wat voor en na de tours, bij de fietsen of op een terras. Jullie zijn een heerlijk stel en weten hoe het werkt met de Franse 'joie de vivre'.

And of course there are many more people that I met in Paris. Gino, Thijs, Antoinette, Dilruba, Mathijs, Mirja, Paolo, John, Suzanne, Claire, Diane, Jelle and Missy and all the others that I have forgotten but who made my time in Paris unforgettable. Thank you all very much for the talking, the relaxing and the soirées along the Seine, in bars or at home.

Also the girls from the I Scientist meeting in Berlin, Katharina, Pranoti, Lucia, Bianca and Clara, it was amazing to meet such energetic and inspiring women! Thank you so much for your critical opinions on social issues and gender equality that go across fields. The world needs you.

En dan iedereen die langs is geweest in Parijs! Al dan niet in huize Beniest-Wessels. De moeite om een berichtje te sturen, 'hey ik ben in de buurt!' heb ik altijd enorm gewaardeerd.

Yvonne, Anke, Laura, Joke en Renate. Eerst verhuisde ik naar Utrecht, daarna naar Parijs. Ik kwam niet dichterbij, maar we hebben elkaar afgelopen paar jaar wel vaak gezien. Een bruiloft hier, een babyborrel daar, wat spontane verjaardagen en niet te vergeten een weekje naar Kroatië! Al meer dan 25 jaar komen we bij elkaar over de vloer. Dat ik vind dat best wel bijzonder en ik heb goeie hoop dat we dat tot aan het bejaardentehuis aan toe, ook nog blijven doen. Dankjulliewel voor al dat oude en vertrouwde.

Meisjes '07, Janneke, Lydian, Marily, Janja, Agnes, Nienke en Dineke, we zijn in alle windrichtingen vertrokken wat betreft onze carrière, maar ondanks dat lukt het toch steeds om te borrelen hier of op weekend te gaan daar. Ik vind het echt geweldig dat jullie iedere keer weer tijd vinden om even een kopje koffie te doen, even snel te lunchen of naar een restaurant te gaan ergens in Nederland als ik opeens weer

op de stoep sta. Waar ik ook heel erg van geniet is de grote variatie aan sterke karakters binnen Meisjes '07. Dit zorgt altijd zorgt voor leven in de brouwerij, goeie discussies en mooie initiatieven zoals YAFS. Ik ben erg blij met jullie als vriendinnen en ik ben heel benieuwd waar we over vijf jaar zijn met zijn allen. Eén ding is zeker, we laten ons niet tegenhouden door lange afstanden!

Annique, dankjewel voor alle virtuele communicatie momenten. Jouw energie om wetenschap te bedrijven is onuitputbaar en ik heb daar heel veel inspiratie uit gehaald. Dankjewel voor alle random vakanties, veldwerken en logeerpartijtjes in Utrecht en in Parijs.

Geertje, ook al wonen we nu 1000-en km's uit elkaar, dankjewel voor jouw lezend oog, opbeurende woorden en de occasional appjes 'hoe is het er nu mee?'. Als geen ander begrijp je hoe het is om te emigreren. Dankjewel voor de knusse avondjes op de bank in Trondheim en de gezelligheid in Parijs en Utrecht.

Saxi-dames, Suzanne, Gitte, Chantal, Maartje, Anne S., Karla, Anne P., Anja, Lisanne, Sabine en Nina, te pas en te onpas kom ik jullie tegen, in Utrecht, Parijs, Groningen, Athene en Wenen, het maakt niet uit waar. Ongeacht waar we uiteindelijk belanden, ik ben blij dat ik deel uitmaak van dit fantastische netwerk van sterke geo-vrouwen. Jullie zijn fantastisch en de wereld heeft ons nodig!

Alex, jij bent het verste weg gaan wonen van iedereen die ik ken. Dankjewel dat er nog steeds ruimte is om zo nu en dan te skypen. Dankjewel dat je zoveel initiatief neemt, dankjewel voor je optimisme en dankjewel voor het langskomen in Parijs.

Alannah, ik wist al dat je van Parijs hield voordat ik hierheen vertrok, maar dat je zo vaak zou langs komen had ik niet verwacht! Dankjewel voor alle chill-weekendjes in Parijs, aan de Seine, gekke musea bezoeken die we allebei nog niet hebben gehad. Dankjewel dat ik altijd in jouw huis mag komen crashen, zelfs al laat ik je dat één dag van tevoren weten. You're the best.

Suus, dankjewel voor je vrolijkheid, humor en het rijden van de auto naar wedstrijden op zaterdagmiddag zodat ik op de achterbank kon slapen, zelfs in januari 2017 heb ik daar nog van kunnen profiteren. We gaan snel weer een keer naar de McDonalds, big mac's eten en klagen over de tegenstanders.

De meiden van SVE. Sas, Mel, Berber, Irene, Laura, Anne, Evelien, Yusra, Nena, Amber, Daphne, Stephanie, Judith en Tanja. Dankjulliewel voor alle Uteregse gezelligheid tijdens het voorjaarsseizoen in

2017. Ik vond het zo leuk dat ik meteen weer mee kon doen met trainingen, competities en avondjes in de Derrick! Jullie zijn een heerlijk stel en ik hoop dat ik me op een dag weer bij jullie aan kan sluiten.

And all the other people who visited me in Paris over the last four years or who came all the way to Paris for this defense, Gerrit, Jan, Martin, Cora, Laurine, Selma, Fanny, Kerwin, Jeffrey, Peter, Bas, Inge, Iris, Tawny, Collin, Ronald, Anne, Freek, Jort, Lot, Simon, Lore, Nienke, Koen, Shannon, Fay, Linda, Juliette, Martha, Yvonne, Kris, Paul, Luuk, Stephanie, Simon, Dahnja, Ellen, Nina, Paul and Michael thank you all very much, because of you I have appreciated the city Paris so much more! Dank jullie wel!

I also would like to thank the people that let me crash at their place or had time to go for a drink or dinner whenever I was in the neighborhood Wouter and Eva in London, Korien and Quintijn in Kuala Lumpur, Inge in the Americas (zo zie je elkaar nooit, dank kom je elkaar binnen 1 maand op 2 continenten tegen!), Laurine en Maarten in Gent, Rachael and her family in Connecticut and Vermont, Robert and Susan in New York, Anne in Oslo, Sara and CheeKok in Singapore, Tim and Lidiya in Sofia, Jeroen and Wieke in Milaan, many thanks to all of you for opening your house to me. You are always welcome at my place too!

Jeanne en Marly, dankjulliewel voor jullie steun, flexibiliteit en warme welkom iedere keer als ik weer in Nederland ben. Het is iedere keer erg gezellig om met jullie rond de tafel te zitten. En dankjewel mam, voor jouw onverwachte verschijning voor mijn 30^e verjaardag, dat vond ik echt geweldig!

Ivo, Ik vond het heel fijn dat we elkaar in de winter van 2017 wat vaker gezien hebben. Dankjewel voor de updates, de verjaardag berichtjes en de gezellige avondjes uit in Tilburg, Lissabon en met mam. Ook al hebben we allebei ons eigen leventje, ik ben toch blij dat jij mijn bro bent.

Richard, dankjewel. Dankjewel voor alle avonturen die we al hebben meegemaakt, het zijn er zoveel! Dankjewel dat je zo relaxed bent, voor je humor, voor je vertrouwen. Ik vind het fantastisch dat je er nog steeds bent en dat we ons eerste lustrum al hebben mogen vieren. Rich, jij en ik, we zijn onoverwinbaar. Laten we alles eruit halen wat erin zit, ik ben klaar voor het volgende avontuur!

Curriculum Vitae

Anouk Beniést was born on the 5th of October 1987 in Sittard, in the South of the Netherlands. She grew up in Nieuwstadt, a small village in ‘de taillie van Limburg’. She completed her Gymnasium degree at the Trevianum, in Sittard in 2006. In October 2006 she went to France for a year as a ‘jeune fille au-pair’, to learn French and discover the world. She started her BSc studies in Earth Sciences at Utrecht University in September 2007 which she completed in 2010. Next, she backpacked for 10 months in Asia and Australia, after which she came back to Utrecht University in 2011 to finish her MSc degree in Earth Structures and Dynamics in 2013. She then went on a six-month journey where she drove from Utrecht to South Africa by car. A scholarship ‘Bourse d’Excellence de Descartes’ was her gateway to Paris where she first obtained a ‘Diplôme d’Études Supérieures’ in December 2014. In January 2015 she started her PhD of which this thesis is the result.



Peer-reviewed articles

Published

Beniest, A., Koptev, A., Leroy, S., Guichet, X., Sassi, W., 2017. Two-branch rift system by a sole mantle plume: insights from numerical modelling. *Geophysical Research Letters*, 44, doi:10.1002/2017GL074866.

Beniest, A., Koptev, A., Burov, E., 2017. Numerical models for continental break-up: implications for the South Atlantic. *Earth and Planetary Science Letters*, 461, 176-189, doi : 10.1016/j.epsl.2016.12.034

Beniest, A., Brun, J.-P., Gorini, C., Crombez, V., Deschamps, R., Hamon, Y., Smit, J., 2016. Interaction between trench retreat and Anatolian escape as recorded by Neogene basins in the northern Aegean Sea. *Marine and Petroleum Geology*, 77, 30-42, doi:10.1016/j.marpetgeo.2016.05.011

Van Gelder, I.E., Matenco, L., Willingshofer, E., Tomljenovic, B., Adriessen, P.A.M., Ducea, M.N., Beniest, A., Gruic, A., 2015. The tectonic evolution of a critical segment of the Dinarides-Alps connection: kinematic and geochronological inferences from the Medvednica Mountains, NE Croatia. *Tectonics*, 34, 1952-1978, doi:10.1002/2015TC003937

Hüsing, S.K., Beniest, A., van der Boon, A., Abels, H.A., Deenen, M.H.L., Ruhl, M., Krijgsman, W., 2014. Astronomically-calibrated magnetostratigraphy of the Lower Jurassic marine successions at St. Audrie's Bay and East Quantoxhead (Hettangian – Sinemurian; Somerset, UK). *Palaeogeography, Palaeoclimatology, Palaeoecology*. 403, 43-56. doi:10.1016/j.palaeo.2014.03.022

Submitted

Van der Boon, Beniest, A., Ciurej, A., Gaździcka, E., Grothe, A., Sachsenhofer, R., Langereis, C., Krijgsman, W. The Eocene-Oligocene transition in the North Alpine Foreland Basin and subsequent closure of a Paratethys gateway. *Global and Planetary Change*, *accepted*.

Beniest, A., Willingshofer, E., Sokoutis, D., Sassi, W. Extending the continental lithosphere: influence of lateral strength variations on deformation mode and geometry. *Geology*, *in review*.

*...For knowing yourself gives you the wings
to fly unshackled of your chains.*

~ Bilal Haq, Scientist